A novel gold nanoparticle-based approach for the rapid diagnosis of meningococcal infection

A thesis submitted in fulfillment of the requirements for
the degree of Doctor of Philosophy

By

Basi Reddy. Sreenivasulu Reddy

M.Sc., Biochemistry

Biotechnology and Environmental Biology
School of Applied Science
RMIT University
Melbourne, Victoria, Australia.

January 2008

Declaration

I hereby declare that except where due acknowledgement has been made; the work is that of my own; and the work has not been submitted previously, in whole or in part, to qualify for any other academic award. The content of the thesis is the result of work which has been carried out since the official commencement date of the approved research program; and, any editorial work, paid or unpaid, carried out by a third party is acknowledged.

Basi Reddy. Sreenivasulu Reddy

4th January 2008

Dedication

I dedicate this thesis to my loving parents and sisters, for their support, understanding and encouragement throughout the years of my study.

Acknowledgements

I would like to take this opportunity to thank everyone who helped me to complete this research project. In spite of the difficulties entailed by the scope and duration of this project, there was always somebody to help me out when needed.

Firstly, I would like to acknowledge the tireless support, guidance, encouragement and insights of my supervisor, *Dr*. John V Fecondo, who also became both friend and mentor to me; and who taught me appreciate real Scotch whisky. My thanks also to my other supervisor, *Prof.* David Mainwaring, for his generous help at all stages of the project. I would also like to thank Edward Grixti and Sapna George Thoduka for all their help and cooperation as well as their friendship and advice. My thanks also go to Nanovic for the funding that made such a groundbreaking project possible.

A special vote of thanks is due to *Dr.* Peter Smooker and to *Dr.* George Moutafis for providing the Omp85 clone; to Stewart Nuttall and Julie Angerosa for the CSIRO-IgNAR work; to Mohammad and Prashanth in the Quartz Crystal Microbalance lab in the city campus; and to Celia McKenzie and Taghrid Istivan for their invaluable work in growing different strains of bacteria to facilitate cross-reactivity studies.

I would also like to thank my parents and my family, who despite being on the other side of the world, were always there to lend support and encouragement. And last but not least, I would also like to thank my many friends for all the moral, emotional and mental support during the many stressful and demanding times. To Amit, Ashish, Dilip, Krutika, Harsha, Harshit, Hashmath, Luke, Nalin, Nitin, Rajesh,

Siddesh, Sethu, Tomy and Veera go all my thanks and love for everything they did for me and also for their invaluable friendship.

Table of Contents

List of Figures

List of Tables

List of Abbreviations

ACN	Acetonitrile
AFM	Atomic force microscopy
Amp	Ampicillin
Amp/glc/YT	Ampicillin/glucose/yeast extract-tryptone
Au	Gold
AuNP	Gold nanoparticle
BBB	Blood-brain barrier
CDR	Complimentarity-determining region
CFA	Freund's complete adjuvant
CFC	Critical flocculation concentration
CPS	Capsular Polysaccharide
CSF	Cerebrospinal fluid
CTAB	Cetyl trimethylammoniumbromide
Ctr	Capsule transfer gene
DCM	Dichloromethane
DIEA	*N, N*-Diisopropylethylamine
DMF	Dimethyl formamide
DNP	Dinitrophenol
DSC	Differential scanning calorimetry
DTT	Dithiothreitol
E. Coli	*Escherichia coli*
EDX	Energy Dispersive X- ray microanalysis
ELISA	Enzyme-linked immunoSorbant assay
EXAFS	Extended X-ray absorption fine structure
F-moc	9-fluorenylmethoxycarbonyl group
FR	Frame work
Gu.HCl	Guanidine hydrogen chloride
HBTU	2-(1H-benzotriazol-1-yl)-1,1,3,3-tetramethyluronium hexafluorophosphate
HCl	Hydrogen chloride

HEL	Hen egg-white lysozyme
HF	Hydrogen fluoride
HOBT	1-hydroxybenzotriazole
HPLC	High Performance Liquid Chromatography
HRP	horsh raddish peroxidase
HRTEM	High-resolution transmission electron microscopy
ICG	International Coordinating Group
IFA	Freund's incomplete adjuvant
Ig	Immunoglobulins
IgNAR	Immunoglobulin-like new antigen receptor
IMVS	Institute of Medical and Veterinary Science
IPTG	*Isopropyl β-D-1-thiogalactopyranoside*
IR	Infrared
KCN	Potassium cyanide
KLH	Keyhole limpet Haemocyanin
LB	Luria-Bertani
LDI-MS	Laser desorption ionisation mass spectrometry
LOS	Lipo-oligosaccharide
LPS	Lipopolysaccharides
MALDI-TOF	Matrix assisted laser desorption/ionisation-time of flight
Man- NAc	*N*-acetylmannosamine
mBHA	4-methylbenzhydrylamine
$MgCl_2$	Magnesium chloride
MIC	Minimum inhibitory concentration
mM	Milli Molar
MPBS	Milk powder dissolved in PBS
MPC	Monolayer protected clusters
N. meningitides	*Neisseria meningitidis*
NaAOT	Sodium bis (2-ethylhexyl) sulphosuccinate
NaCl	Sodium chloride
NANA	N-acetyl neuraminic acid
NaOH	Sodium hydroxide

NeuNAc	*N*-acetylneuraminic acid
NIBSC	National Institute for Biological Standards and Control
Ni-NTA	Nickel- Nitrilotriacetic acid
NM	*Neisseria meningitidis*
NMR	Nuclear magnetic resonance
NP	Nanoparticle
OD	Optical density
OMP	Outer membrane protein
PAGE	Polyacrylamide gel electrophoresis
PAMAM	Polyamidoamine
PBS	Phosphate buffer saline
PCR	Polymerase chain reaction
PEG	Polyethylene glycol
PEP	Phosphoenolpyruvate
PFGE	Pulsed-field gel electrophoresis
PMN	Polymorphonuclear leukocytes
PMSF	Phenylmethanesulphonylfluoride
PVDF	Polyvinylidene Difluoride
PVP	Polyvinyl pyrollidine
QCM	Quartz crystal microbalance
rec.	Recombinant
RFLP	Restriction fragment length polymorphism
RP-HPLC	Reverse-phase High performance liquid chromatography
RT	Room temperature.
SAXS	Small-angle X-ray scattering
SDS	Sodium dodecyl sulphate
SEM	Scanning electron microscopy
SERS	Surface-enhanced Raman scattering
SMAD	Solvated metal atom dispersion
SMCC	Sulfosuccinimidyl 4-N-maleimidomethyl cyclohexane-1-carboxylate
SPB	Surface plasmon band

SPPS	Solid phase peptide synthesis
SPR	Surface plasmon resonance
STM	Scanning tunneling microscopy
t-Boc	Nα-*t*-butyloxy carbonyl group
TBS	Tris buffer saline
TCR	T cell receptors
TFA	Trifluoroacetic acid
TFMSA	Trifluromethanesulphonic acid
TGA	Thermogravimetric analysis
TOABr	Tetraoctyl ammonium bromide
T-SPR	Transmission surface plasmon resonance
UV-Vis	UV-Visible spectroscopy
V_H	Variable heavy chain
V_L	Variable light chain
WHO	World health organisation
XPS	X-ray photoelectron spectroscopy
XRD	X-ray diffraction
YT media	Yeast extract-tryptone media

Abstract

The bacterial meningitis caused by *Neisseria meningitidis* is responsible for considerable morbidity and mortality throughout the world. Given the limitations of existing diagnostic tests and the severity of the illness associated with the disease, there is a clear requirement for a rapid and specific diagnostic assay. This thesis describes the development of nanoparticle based tests for the detection of *Neisseria meningitidis* specific cell surface markers.

The highly conserved outer membrane protein 85 (OMP85) antigen was selected as initial target antigen for the development of the diagnostic assays. A recombinant form of OMP85 with an attached hexa his-tag was cloned and expressed in *E. coli* and purified successfully by the use of various methods including Ni-NTA metal affinity column chromatography and a sonic gel extraction method. Within the OMP85 protein sequence, a predicted antigenic sequence between residues 720 and 745 was identified and found to be unique to this organism. This amino acid sequence was synthesised as peptide (SR1) with a gly-gly-cysteine spacer sequence at the N-terminus using t-boc chemistry. Also, the major virulence factor, capsular polysaccharide of *N. meningitidis* serogroup B bacteria was purified by a simple procedure developed during the course of this work.

Polyclonal antibodies were raised against purified OMP85 antigen in rabbits and against SR1 peptide and also against formalin inactivated *N. meningitidis* serogroup B whole cell bacteria in sheep. Commercial anti-capsular monoclonal antibodies were shown to be equally reactive both with the bacteria and the purified capsular

polysaccharide. In addition, screening of an Immunoglobulin New Antigen Receptor (IgNAR) library was attempted to identify novel receptors against OMP85 and other antigens for use in the diagnostic tests. This panel of different antibodies were examined for cross reactivity against a range of closely related Gram negative bacteria. Based on these cross-reactivity studies, a highly specific anti-NM antibody was developed following purification of the anti-SR1 antiserum by immuno-affinity chromatography.

Monodisperse 13 nm gold nanoparticles were synthesised by the Turkevich citrate reduction method. Larger particles (30nm, 40 nm, 50 nm and 60 nm) were purchased from British Biocell, UK for use in these studies. Coupling of the gold nanoparticles results in a shift of the the respective surface plasmon peak toward longer wavelengths resulting in a change of the colour of the colloidal suspension from red to purple to blue. Purified OMP85 antigen and protein A purified anti-OMP85 antibody were successfully conjugated on 13, 30, 40, 50 and 60 nm gold nanoparticles by an electrostatic adsorption method.

An attempt was made to develop a rapid diagnostic assay based on gold nanoparticle induced colour shift assay for *N. meningitidis* by utilising the specific interaction of OMP85 and anti-OMP85 antibody conjugated to gold nanoparticles as a model system. This interaction between 50 nm gold nanoparticles conjugated with OMP85 and anti-OMP85 antibody resulted in an increase in absorbance in the range of 600-800 nm, with a resulting colour shift. However, this system was not

reproducible and is likely to be due to problems with stability of gold nanoparticles during the conjugation process.

As an alternative approach, a highly selective quartz crystal microbalance (QCM)-based immunosensor was designed using the OMP85/anti-OMP85 antibody system as a model diagnostic test for meningococcal infection. Following initial attempts with self-assembled monolayer model experiments, a method was developed using polyvinylidene fluoride (PVDF) coated QCM crystals with protein A for for the directional orientation of the antibodies. The resonant frequency of the sensor decreased over time due to the binding of OMP85 antigen onto the immobilised antibodies, within a time frame of 5 to 10 minutes.

To further enhance the sensitivity of the test, OMP85-conjugated gold nanoparticles were used as signal amplification probes for the reproducible detection of the target down to 300 ng/mL, corresponding to a five fold increase in sensitivity compared to detection of OMP85 antigen alone. In addition, the immunosensor was successfully regenerated using glycine-HCl solution pH 3.0 to release antigen–antibody complexes from the protein A layer, thus enabling the immunosensor to be used multiple times. Also, this sensor has successfully been employed to detect whole cell bacteria at a concentration as low as 100 cfu/mL. Thus, in this study using the real-time QCM measurements, a novel strategy has been developed for the sensitive detection of both *N. meningitidis* bacteria and the protein antigen at very low concentrations, using gold nanoparticles as signal amplification probes. This work

advances the design and evaluation of a QCM based model biosensor for the rapid diagnosis of meningococcal meningitidis.

Chapter 1

Introduction and Review of Literature

1.1. *Neisseria meningitidis* – A role in meningococcal disease

The meninges, the membranes that line the brain and the spinal cord can become inflamed leading to the potentially fatal disease known as meningitis (Rosenstein, Perkins *et al.* 2001). Most cases of meningitis are due to bacterial infections that start elsewhere in the body and spread to the brain or spinal cord via the bloodstream. Bacterial pathogens that may cause meningitis include *Haemophilus influenzae* (Hubert, Watier *et al.* 1992), *Escherichia coli* (Glode, Sutton *et al.* 1977; Yang, Lu *et al.* 2005), *Streptococcus pneumoniae* (Hirst, Gosai *et al.* 2003) and *Neisseria meningitidis* (Nadel and Kroll 2007). Other types of meningitis which occur less commonly include cryptococcal meningitis (Bicanic and Harrison 2004), syphilitic meningitis (Hsieh, Hung *et al.* 1996), pneumococcal meningitis (Wasier, Chevret *et al.* 2005), staphylococcal meningitis (Perez-Camarero, Escalante-Boleas *et al.* 2000), tuberculous meningitis (Theron, Andronikou *et al.* 2006) and aseptic meningitis (Lee and Davies 2007). Meningitis can also be caused by a number of other factors including viruses (Chadwick 2005), chemical irritation (Marinac 1992), or tumors (Lee, Cromwell *et al.* 2005). Although, different cocci cause meningitis, the term *meningococcus* is retained for the *Neisseria meningitidis* (*N. meningitidis*), a Gram-negative, diplococcus bean-shaped bacterium.

Reports of illness resembling meningococcal infection dates back to the 16th century. Vieusseux in 1805, described an outbreak of meningococcal disease which caused 33

deaths in the vicinity of Geneva, Switzerland (Rosenstein, Perkins *et al.* 2001). The Italian pathologists Marchiafava and Celli (1884) first described the presence of intracellular oval micrococci in a sample of cerebrospinal fluid (CSF) (Marchiafava and Celli 1884). However, the first bacterium known to cause meningococcal disease was first identified in CSF by Anton Weichselbaum in 1887, which he detected in six out of eight patients suffering from bacterial meningitis and this bacterium was named *Neisseria intracellularis* (Manchanda, Gupta *et al.* 2006). It was later named as *Neisseria meningitidis*.

1.1.1. Structure and Classification

Based on genome sequencing studies, *Neisseria meningitidis* is categorised as belonging to the family *Neisseriaceae* and class α-proteobacteria related to the genera *Bordetella, Moraxella, Burkoholderia, Kingella* and *Methylomonas* and more distantly related to *Vibrio, Haemophilus* and *Escherichia coli* (Manchanda, Gupta *et al.* 2006). The genus *Neisseria* includes two important human pathogens, *N. gonorrhoeae* which causes gonorrhoea and *N. meningitidis* (Todar 2006), which is responsible for acute bacterial meningitis. These are Gram-negative, bean-shaped aerobic diplococci are isolated on chocolate/blood agar and infect humans exclusively. Like most other members of its genus *Neisseriae*, these organisms are aerobic, non-motile, produce catalase, oxidase positive, susceptible to drying while their growth is stimulated by CO_2 and humidity and their growth is inhibited by free fatty acids (Platt and Snell 1976; Manchanda, Gupta *et al.* 2006). *N. meningitidis* is surrounded by an outer membrane composed of lipids, outer membrane proteins (OMPs) and

lipopolysaccharides. Pathogenic meningococci bacteria are enveloped by a polysaccharide capsule attached to this outer membrane.

The capsular polysaccharide (CPS), lipo-oligosaccharide (LOS) and outer membrane proteins (OMPs) are considered as important virulence factors in meningitis. The main distinguishing structural feature between *N. meningitidis* and *N. gonorrhoeae* is the presence of an anti-phagocytic polysaccharide capsule in the former (Spinosa, Prodiga *et al.* 2007). As the name suggests, the anti-phagocytic capsular polysaccharide helps in evading phagocytosis as well as providing the basis for grouping of the organism. The chemical composition of these capsular polysaccharide types is known. Based on this capsular structure, 13 serogroups in total have been identified and designated as serogroups A, B, C, H, I, K, L, M, X, Y, Z, 29E, and W135 (Sippel 1981; Frasch, Zollinger *et al.* 1985). The most important serogroups associated with the disease in humans are A, B, C, Y, and W135. Meningococci reveal more genetic diversity than most other pathogenic human bacteria and this is explained partly by horizontal intra-species recombination and incorporation from closely related *Neisseria* species (Caugant 1998).

Meningococci are further subdivided (Table 1) into 20 serotypes (on the basis of class 2 or class 3 OMP antigens), 10 subtypes (based on class 1 OMP antigen differences) and 13 immunotypes (based on differences in lipooligosaccharide antigens) (Mandrell and Zollinger 1977; Frasch, Zollinger *et al.* 1985; Scholten, Kuipers *et al.* 1994).

Component	Function	Classification System	Number of Groups	Names
Capsule	Protects against complement dependent bacteriolysis and phagocytosis	Serogroups	13	A, B, C, E-29, K, I, K, L, M, W-135, X, Y, Z
Outer membrane proteins (Porins)	Creates pores through which small hydrophilic solute pass, cation selective or anion selective			
Por A (Class1 OMP)		Subserotypes	10	P1.1, P1.2, P1.3……P1.10
Por B (Class 2/3 OMP)		Serotypes	20	1, 2a, 2b, ….2l
Lipooligosaccharide (LOS)	Has potent immunotoxic activity	Immunotypes	13	L1, L2,…..L13
Pili	Promotes initial adherence to epithelial/ehdothelial cells and red blood cells		2	I, II

Table 1.1.: Classification based on outer-membrane components of *N. meningitidis* (Manchanda, Gupta *et al.* 2006)

The bacterial outer membrane proteins of *N. meningitidis* have been classified from class 1 to class 5 proteins. Although meningococcal outer membranes contain as many as five major proteins, much of the observed serotype specificity can be attributed to class 2 and class 3 proteins, both of which are mutually exclusive within different meningococcal strains (Frasch, Zollinger *et al.* 1985). The class 2 and 3 proteins function as porins, which function as molecular sieves in Gram-negative bacteria where they mediate the aqueous diffusion of solutes through the water-filled channels derived from their unique folding assembly (Nikaido 1994; Minetti, Tai *et al.* 1997). Serogroups B and C meningococci have been further subdivided on the basis of subtype determinants located on the class 2 and 3 porin proteins. Most of the known serogroup A strains have the same protein serotype antigens in the outer membrane. Another serotyping system exists based on the antigenic diversity of meningococcal lipo-oligosaccharide (LOS) (Tsang, Law *et al.* 2001).

1.1.2. Incidence and risk factors

Viral meningitis is a mild form of meningitis and occurs more commonly than bacterial meningitis. It usually develops in the winter and affects people under 30 (Durand, Calderwood *et al.* 1993) with 70% of the infections occurring in children under the age of 5 years.

In the case of bacterial meningitis caused by *N. meningitidis,* the meningococcus organism usually inhabits the human nasopharynx resulting in an asymptomatic carrier state, prior to invasion of the central nervous system via the bloodstream with a rapid onset of signs and symptoms at this stage (Nowak, Boehmer *et al.* 2003). Most individuals in close contact with a person suffering from meningococcal meningitis become carriers of the organism. This carrier state, which may last from a few days to months is important because it not only provides a reservoir for meningococcal infection but also stimulates host immunity and leads to exposure to asymptomatic carriers and is responsible for 10-25% of infections (Manchanda, Gupta *et al.* 2006). This carrier rate may reach 20% of the total population before the first case is recognized, and may reach up to 80% at the height of an epidemic. Transmission rate is 500- to 800- fold greater among household contacts than among the general population due to their close association with infected individuals. Between 5% and 30% of normal individuals are carriers at any given time, yet few develop meningococcal disease. Attack rates are highest in infants, usually less than one year old while carriage rates are highest in older children and young adults. The infection typically occurs in winter or spring, and may cause local epidemics at, for example

boarding schools or military bases. Meningococci spread via respiratory droplets, and transmission requires aspiration of infective particles.

1.1.3. Virulence Factors

Meningococci are diverse organisms and are usually commensal bacteria present in the nasopharynx of humans with only a minority of the nasopharyngeal isolates causing invasive disease. Studies on strains from African epidemic outbreaks show that clonal characteristics of carrier and disease isolates are similar (Greenwood, Bradley *et al.* 1985). For a time, the virulence of *Neisseria meningitidis* was attributed to the production of an exotoxin that was later found out to be the released parts of their cell walls in a soluble form. Hence, a major factor in the virulence of the organism is the release of outer-membrane vesicles that consist of lipooligosaccharide (endotoxin), outer-membrane proteins, phospholipids and capsular polysaccharides (Rosenstein, Perkins *et al.* 2001).

The endotoxin of *N. meningitidis* is structurally different from the lipooligosaccharide of enteric Gram negative bacteria. Lipid A molecules of lipooligosaccharide (LOS) act as endotoxins and their effects are due to the interaction with innate immune receptors (Manchanda, Gupta *et al.* 2006). Purified meningococcal LOS is found to be highly toxic and lethal for mice similar to the LOS of *E. coli* and *Salmonella typhimurium*. However, meningococcal LOS is 5 to 10 times more effective than enteric LPS in eliciting dermal haemorrhages due to endothelial damage and haemorrhages and microthrombi in small vessels (Sanarelli-Shwartzman reaction) in rabbits (Quakyi, Hochstein *et al.* 1997). The lesions are a reflection of the endotoxin

mediated upregulation of activated neutrophils (van Deuren, Brandtzaeg *et al.* 2000). Also, up to 16% of the cells present in the nasal mucosa are monocytes and inflammation increases polymorpho nuclear (PMN) leukocyte infiltration. Meningococcal LOS has also been shown to suppress leukotriene B4 synthesis in human polymorphonuclear (PMN) leukocytes (Salari, DeVoe *et al.* 1982). The loss of leukotriene B4 deprives the leukocytes of a strong chemokinetic and chemotactic factor (Virji 1996). The other important determinants of virulence of *N. meningitidis* include its antiphagocytic polysaccharide capsule, pili , IgA protease and opacity proteins (Opa and Opc) (Virji, Kayhty *et al.* 1991; Lorenzen, Dux *et al.* 1999).

N. meningitidis associated with invasive disease has a capsule, which provides protection from desiccation during transmission and aids in the evasion of host immune mechanisms. The capsule and sialylated lipopolysaccharides (LPS) are expressed in disseminated isolates and are believed to protect the organism against antibody/complement and phagocytic killing (Vogel, Hammerschmidt *et al.* 1996). The LPS of carrier strains tend to be structurally different and often asialylated but, sialylation of LPS has functional consequences similar to the capsule as it imparts resistance to immune mechanisms of the host and in doing so, masks the functions of many outer membrane proteins (Estabrook, Christopher *et al.* 1992). The relationship between surface polysaccharides and various adhesins and invasins is a complex area of investigation, while other components like antigenicity and phase variation adds further complexity (Virji, Makepeace *et al.* 1995).

In studies to determine bacterial factors that increase phagocyte interactions, it was shown that capsulate bacteria resist phagocytosis in the absence of opsonins, but acapsulate bacteria are internalized and the bacterial opacity proteins Opa and Opc mediate bacterial uptake (Ward, Fleer *et al.* 1987). Pili proteins which are involved in adhesion to glycoconjugate structures in the host epithelial cells, were ineffective in mediating interactions with phagocytic cells (McNeil and Virji 1997). Meningococcal phase variable opacity proteins (Opc, Opa) and pili are widely expressed in case isolates (McNeil, Virji *et al.* 1994; McNeil and Virji 1997). Bacterial components that mediate cellular interactions in the absence of added opsonins are of importance from the point of view that immunocompromised phagocytes acts as potential 'Trojan Horse' carriers of bacteria (Gagnon, Duclos *et al.* 2002).

Pili also may target the CD46 receptor, a host cell membrane cofactor protein and subsequently the opacity-associated proteins, Opa and Opc, bind to CD66 and heparan sulphate proteoglycan receptors respectively (Rosenstein, Perkins *et al.* 2001). Other differences may include the expression of distinct porins (class 1 / 2 / 3) which have been implicated in impairment of host cell functions (Wetzler, Ho *et al.* 1996). Putative toxic factors (e.g. RTX-like proteins) have been reported in some meningococcal strains (Osicka, Kalmusova *et al.* 2001). These are environmentally regulated and their expression could also increase the pathogenic potential of a strain.

Invitro investigations on the toxicity of carrier and case isolates indicate that both possess the capacity to damage human endothelial cells. In addition, specific

nutrient-acquisition factors, especially mechanisms for acquiring iron from human lactoferrin, transferrin and hemoglobin, enhance their pathogenic potential (Rosenstein, Perkins *et al.* 2001; Donna, Melanie *et al.* 2004). Multiple meningococcal components (pili and LPS) act together to destroy endothelial integrity characteristic of meningococcal septicemia (Virji, Makepeace *et al.* 1995). Finally, the expression of pili, class 5 OMPs, capsule and LOS is highly variable and subject to phase switching (on/off) and antigenic variation (van Deuren, Brandtzaeg *et al.* 2000) and this means can be used by the bacterium to circumvent host immunity.

1.1.4. Host factors and Pathogenesis of meningitis

In the case of invasive meningococcal disease, although the majority will recover fully, 10-15% of those infected will die, and around 20% will have permanent disabilities, ranging from learning difficulties, sight and hearing problems, to liver and kidney failure, scarring caused by skin grafts as well as loss of fingers, toes and limbs (Maiden 2004). Various pathological outcomes associated with the meningitis are influenced by different factors like type of bacteria, environmental and social conditions, preceding or concomitant to viral infections as well as the immune status of the person (Manchanda, Gupta *et al.* 2006).

The integrity of the nasopharyngeal epithelium appears is important in protection against invasive disease. Any factors that cause damage to mucosa such as chronic irritation of the mucosa due to dust or low humidity, a concurrent upper respiratory infection (*Mycoplasma pneumoniae* or influenza A virus), smoking (active or passive), chronic underlying illness such as hepatic failure, systemic lupus erythematosis,

multiple myeloma and prior infection of the host etc. may be predisposing factors for invasive disease and increased host susceptibility (Kleemola and Kayhty 1982; 2000; Booy, Iskander *et al.* 2007). For nasopharyngeal colonization of bacteria, it requires equilibrium between the host and bacteria and in most individuals; it results in acquisition of serum bactericidal antibodies (Goldschneider, Gotschlich *et al.* 1969; Stephens 1999). At the age of 6 to 24 months, the incidence of meningococcal disease is highest due to the disappearance of maternal antibodies (Goldschneider, Gotschlich *et al.* 1969; Moore, Reeves *et al.* 1989).

Because of the shared antigenic determinants, individuals who are infected with non-groupable strains (without a capsule) also develop high titres of antibody against groupable strains (Goldschneider, Gotschlich *et al.* 1969; Gold 1983; Moore, Reeves *et al.* 1989). For example, *Bacillus pumilus* and *Escherichia coli* K1 possess the capsule that is structurally and immunologically identical to the capsule of serogroup A and serogroup B meningococci respectively (Grados and Ewing 1970; Vann, Liu *et al.* 1976). This type of response does not necessarily eliminate the carrier state, but it may protect them from obvious disease by the induction of cross-reacting antibodies (Vann, Liu *et al.* 1976). The time of exposure to meningococci and cross reacting enteric bacteria may be critical in determining the fate of disease in each individual. Despite having the protective antibody response, persons with complement deficiencies (C5, C6, C7, or C8) may also develop meningococcaemia (Mandrell, Azmi *et al.* 1995; Borrow, Balmer *et al.* 2005).

Meningococci overcome host defences and attach by fimbriae to the microvillous surface of non-ciliated columnar mucosal epithelial cells of the nasopharynx, where they colonise (Stephens, Hoffman *et al.* 1983). Events involved after bloodstream invasion and how the meningococcus enters the central nervous system are not clear. The brain capillary endothelial cells (ECs) which make the blood-brain barrier (BBB), limits the paracellular flux by the formation of the tight junctions. It was suggested that, the possible routes for bacteria to traverse this barrier include, a transcytosis event and the bacteria may undergo fimbrial phase variation and cross the blood brain barrier (Collier, Balows *et al.* 1996).

Others have reported that, the bacteria cross the blood brain barrier by internalising themselves in phagocytes (Nassif, Bourdoulous *et al.* 2002). The subarachnoid space in phagocytic cells lacks the principal humoral and cellular host defense mechanisms. It was suggested that, bacteria may gain access to this subarachnoid space, where an uncontrolled proliferation of meningococci may occur (Collier, Balows *et al.* 1996). This in turn elicits compartmentalised activation of proinflammatory cytokines (Waage, Halstensen *et al.* 1989), which ultimately contributes to the development of clinically overt meningitis. The functional ability of a phagocyte to deal with internalised bacteria may also depend on the number of bacteria engulfed (Ison, Heyderman *et al.* 1995). Studies on the infant rat model of *Haemophilus influenzae*, have shown that bacteraemia may arise due to the survival of even a single organism in the blood stream (Moxon and Murphy 1978). Meningeal infection, resulting from haematogenous route, occurs in about 50 to 55% percent of patients and in about 75%

of the patients *N. meningitidis* was be isolated from the bloodstream (Connolly and Noah 1999).

Different bacterial strains vary in their capacity to invade the nasopharynx. Serogroups A, B and C are more invasive than other serogroups of meningococci. However, experimental problems in determining the intracellular survival of meningococci are considerable since they often grow more rapidly extracellularly (Spinosa, Progida *et al.* 2007). Another characteristic of human pathogenic *Neisseriae* is the production of an immunoglobulin IgA1-specific protease that cleaves preferentially human IgA1 and thus helps in survival in epithelial cells (Lorenzen, Dux *et al.* 1999; Rosenstein, Perkins *et al.* 2001).

Other factors responsible for increased risk of sporadic meningococcal disease include infection with the human immunodeficiency virus and *Streptococcus pneumoniae* (Rosenstein, Perkins *et al.* 2001). Also, any genetic immune defects including, polymorphisms in the genes encoding mannose-binding lectin and tumor necrosis factor-alpha, may also affect the susceptibility to meningococcal disease (Rosenstein, Perkins *et al.* 2001). Factors influencing the outcome of the disease depend on the duration of disease before treatment; the site, severity and the prognosis.

1.1.5. Clinical manifestations of *N. meningitidis* infection

During meningococcal infection, the patients can be classified into one of following clinically recognisable groups (i) bacteraemia without shock (acute mild

meningococcaemia), (ii) bacteraemia with shock but no meningitis (fulminant meningococcaemia), (iii) shock and meningitis, (iv) meningitis alone and (v) chronic benign meningococcemia (D'Alessandro 2006; Manchanda, Gupta *et al.* 2006). After tolerating the potentially lethal bacteria for several weeks in the bloodstream, about 20% will later develop meningitis.

Infection with *N. meningitidis* may result in meningitis or as septicaemia (blood poisoning), or as a combination of both, depending on which part of the body the bacteria invade (Riordan, Marzouk *et al.* 1995). The mildest form of the disease is characterised by transient bacteraemic illness with fever and malaise and symptoms resolve spontaneously in 1 to 2 days. Meningococcaemia is characterised by skin lesions, which may appear more prominently in areas of the skin subjected to pressure, such as the axillary folds, the belt line, or the back (Beek, Gans *et al.* 2004).

The most serious form is the fulminant disease complicated further by meningitis. Fulminant meningicoccaemia disease (with or without meningitis) is characterised by multisystem involvement and high mortality (Edwards 1971). Fulminant meningococcaemia which occurs in 5 to 15% of patients, begins abruptly (Singh and Arrieta 2004). Typically, signs of meningitis may not be present. Pulmonary insufficiency develops within a few hours, and septicaemia can lead to death within 24 hours of being hospitalized despite giving appropriate antibiotic therapy (Devoe 1982; Hameed and Riordan 2002). Sometimes the disease is responsible for permanent neurological damage in the event of late diagnosis. Increasing antibiotic

resistance, which is being observed worldwide, further adds grounds to the concern (Quagliarello and Scheld 1997).

The rapid symptoms of meningococcal meningitis in children include irritability and refusal to take food and vomiting leading to dehydration (Augustine 2005). Fever may not be observed in children younger than 2 months of age, but hypothermia is more common in neonates. In 30 to 60% of patients with meningococcal disease, with or without meningitis, the appearance of petechiae or purpura occurs from the first to the third day of illness. As the disease progresses, symptoms like high fever, severe headache, nausea and vomiting, sensitivity to light (photophobia), altered mental status, apnoea, seizures and coma due to disturbances in motor tone may develop (Beek, Gans *et al.* 2004; Milonovich 2007). In older children and adults, chronic benign meningococcaemia with one or more specific symptoms and signs, with spiking fever and altered mental status, arthralgia, or arthritis and a recurrent rash may occur (van Deuren, Brandtzaeg *et al.* 2000).

The examination of CSF may show normal chemistry and cell counts but signs of meningeal irritation such as spinal rigidity, hamstring spasms and exaggerated reflexes are commonly observed (Goldschneider, Gotschlich *et al.* 1969). Additional symptoms that may be associated with this disease are: speech impairment, stiff neck, muscle pain, hallucinations, facial paralysis, brain damage, eye lid drooping, drowsiness, consciousness decreased, rapid breathing, agitation, positive Babinski's reflex (occurs when the great toe flexes toward the top of the foot and the other toes fan out after the sole of the foot has been firmly stroked (Milonovich 2007). In

addition, bulging of the fontanelles, opisthotonos (a condition of abnormal posturing characterised by rigidity and severe arching of the back, with the head thrown backward), deafness, paralysis of various muscles, and loss of vision may be seen (Voss, Lennon *et al.* 1989; Milonovich 2007).

1.1.6. Complications associated with *N. meningitidis* infection

Complications such as arthritis or pericarditis, cellulitis and endophthalmitis can develop (Blaser, Reingold *et al.* 1984; Lin, Parekh *et al.* 1995; Wells and Gibbons 1997). Other complications associated with meningococcal infection include multiple organ damage due to insufficient blood flow (shock), increased intracerebral pressure, myocarditis and hydrocephalus. Additionally, primary meningococcal conjunctivitis, pneumonia, adnexitis, or pelvic inflammatory disease may be seen (Lin, Parekh *et al.* 1995). Meningococcal pneumonia is generally uncommon and may occur in immunocompromised or elderly patients (Stephens, Hajjeh *et al.* 1995).

1.1.7. Treatment and Prognosis

The symptoms of disease caused by *N. meningitis* ranges from occult bacteremia, which clears spontaneously, to fulminant sepsis resulting in serious complication which may lead to death within a few hours after the first symptoms, occur. This latter occurrence explains much of the challenge and anxiety surrounding the diagnosis, since early symptoms may be difficult to distinguish clinically from more common but less serious illnesses (Wang, Malley *et al.* 2000). Before the 1920s, meningococcal disease was fatal in up to 70 percent of cases (Flexner 1913).

In the case of bacterial meningitis, due to the high risk of complications involved, anti-microbial therapy must be started immediately (Wang, Malley *et al.* 2000). Therapy with horse serum containing anti-NM antibodies, introduced at the beginning of this century by Jochmann in Germany and Flexner in the United States, reduced the mortality rate from nearly 100% to 30% (Jochmann 1906; Flexner 1913). Antibiotics are prescribed for bacterial meningitis and the type varies depending on the infecting organism (Fitch and Beek 2007). Penicillin is the drug of choice in the treatment of meningococcaemia and meningococcal meningitis (Wang, Malley *et al.* 2000). Under normal conditions, penicillin does not penetrate the normal blood-brain barrier, but it readily penetrates the blood-brain barrier when the meninges are acutely inflamed.

The discovery of sulphonamides and other antimicrobial agents led to a further decline in fatality rates (Suntur, Yurtseven *et al.* 2005). Sulphonamides were the chemoprophylactic agent of choice until the emergence of sulphonamide-resistant meningococci (Moore, Reeves *et al.* 1989; Paap and Bosso 1992). Nearly 25% of clinical isolates of *N. meningitidis* in the United States appear to be resistant to sulphonamides. Either chloramphenicol or third-generation cephalosporins such as cefotaxime, ceftriaxone or rifampin are used in patients allergic to penicillins (Smith and Ryan 1987; Paap and Bosso 1992). Intravenous mannitol administration can be used to treat the complications arising from the increased intracerebral pressure. Sometimes systemic corticosteroids are also used.

Viral meningitis is usually not serious and symptoms disappear within 2 weeks with no residual complications. Antibiotics are ineffective in viral meningitis but the treatment of secondary symptoms including brain swelling, shock, and seizures will require other medications and intravenous fluids (Chitkara, Ryan *et al.* 2002). Hospitalisation may be needed depending on the severity of the illness.

1.1.8. Prevention of meningitis

The transmission of meningitis from one person to another occurs by direct contact or via inhalation of respiratory droplets (van Deuren, Brandtzaeg *et al.* 2000). Apart from avoiding the direct contact with infected people, other preventive measures may be taken to avoid serious infection.

N. meningitidis serogroups A, C, Y, and W135 capsular polysaccharide vaccines are available (Robbins, Schneerson *et al.* 2003). However, these vaccines are ineffective in very young children (under 1 year old) since antibody levels decline rapidly after immunisation. Also, it has been shown that the duration of protection is limited in children vaccinated at 1 to 4 years of age (Ramsay, Andrews *et al.* 2001). As the risk of infection is low in this age group, routine vaccination is not currently recommended before the age of 5. Also, these meningococcal capsular polysaccharide vaccines are not effective against group B (the most common isolate) because of its poor immunogenic profile. The group B capsular polysaccharide is a homopolymer of sialic acid and is not immunogenic in humans due to the antigenic mimicry with the polysialosyl gangliosides and glycoproteins in fetal and adult neural and extra-neural tissues (Park, Choi *et al.* 2004). A group B meningococcal vaccine consisting of outer membrane protein antigens has recently been developed

(Boslego, Garcia *et al.* 1995). Though, an overall efficacy of 51% was observed, a substantial drop in the antibody levels was observed by 6 months time.

1.1.9. Epidemiology

Meningococcal infections occur worldwide as an endemic disease with mortality rate at times reaching upto 85% (Moore, Reeves *et al.* 1989; Schwartz, Moore *et al.* 1989; Caugant 1998). Epidemiological studies by modern molecular methods have revealed a multifaceted picture of pathogenic meningococcal clones spreading worldwide. Of the five common serogroups (A, B, C, Y and W135) responsible for about 90% of infections caused by *N. meningitidis,* serogroups A, B and C are more often associated with disease than other serogroups or acapsulate bacteria. With the highest incidence during late winter and early spring, *N. meningitidis* infections occur both sporadically (serogroups B and C) and in epidemics (mainly serogroup A). For the past 200 years, epidemics of meningococcal infection have been occurred in Europe, Africa, Asia, the United States, and New Zealand. In USA alone, about 5000 cases of new bacterial meningitis occur each year, a 50% increase in incidence compared to the number of cases recorded in the last decade. Although, it is classed as a rare disease in Australia, 700 people are affected each year approximately, (Jelfs and Munro 2001; Rosenstein, Perkins *et al.* 2001; Skull and Butler 2001).

Serogroup A and C predominate throughout Asia and Africa and are responsible for epidemic spread, whereas serogroups B and C prevail in the Europe and West (Caugant, Kristiansen *et al.* 1988; Schwartz, Moore *et al.* 1989; Rosenstein, Perkins *et al.* 1999; Pollard 2004). Serogroup B strains related infections are common in developing countries (Caugant 1998). In recent years (1996-98), one third of reported

infections in United States were due to serogroup Y (Rosenstein, Perkins *et al.* 1999). Israel and Sweden are the other countries that have reported an increase in serogroup Y disease (ET-508) (Connolly and Noah 1999). The serogroup W-135 infections were reduced from 15-20% between 1978 and 1980 to only 4% of currect cases in the United States (Band, Chamberland *et al.* 1983). During 2002-2003, serogroup W135 has been associated with a large epidemic in Burkina Faso (Vogel 2003).

In the last 30 years, major epidemics of meningococcal disease have occurred through out Asia (China 1979 and 1980, Vietnam 1977, Mongolia 1973-1974 and 1994-1995, Saudi Arabia 1987, Yemen 1988) (van Deuren, Brandtzaeg *et al.* 2000). One of the largest outbreaks, which originated in China and later became global, was caused by two clones of serogroup A (Schwartz, Moore *et al.* 1989; Caugant 1998; van Deuren, Brandtzaeg *et al.* 2000). One of these clones, after causing an outbreak in the Indian subcontinent during 1983 to 1987, reached African countries through the Middle East between 1987 to 1996, causing epidemic among pilgrims during the Haj in Mecca (Schwartz, Moore *et al.* 1989; Caugant 1998; van Deuren, Brandtzaeg *et al.* 2000). Between September 1985 and March 1986, Bhutan was also hit by meningitis with 247 cases and 41 deaths (WHO 2005). In the Kathmandu valley in Nepal, 1475 cases occurred during 1982-1984, especially in children less than one year of age (Caugant 1998).

The semi-arid area of sub-Saharan Africa has a special epidemiological pattern. A region of savannah that extends from Ethiopia in the east to Senegal in the west,

designated the "meningitis belt", was first described by Lapeyssonnie in 1963 and comprised of 10 countries i.e., Burkina Faso, Ghana, Togo, Benin, Niger, Nigeria, Chad, Cameroon, Central African Republic, and The Sudan (Lapeyssonnie 1963). The "expanded meningitis belt" includes three more countries, Ethiopia, Mali, Guinea, Senegal, and the Gambia (Riedo, Plikaytis *et al.* 1995). Over 100 years, serogroup A meningococcal disease had been a continuous threat to public health in this region (Greenwood, Bradley *et al.* 1985). In 1996, the largest outbreak ever reported occurred with a total number of cases 152,813 was reported, with 15,783 deaths (WHO 1997). Following these large outbreak in Africa, the International Coordinating Group (ICG) for Vaccine Provision for Epidemic Meningitis Control was established in 1997, to ensure rapid and equal access to vaccines and antibiotics. The ICG was established by partners from the UN, including WHO, non-governmental organisations and the private sector.

Epidemic rates of meningococcal disease vary between different nations and the precise bacterial factors responsible for these geographic differences are not clear (Stephens 1999; van Deuren, Brandtzaeg *et al.* 2000). Despite the development of the vaccines for serogroups A and C) and appropriate treatment available, the overall case fatality rates have remained relatively stable over the past 20 years, at 9 to 12%, while the rate rises up to 40 % among patients with meningococcal sepsis (Rosenstein and Perkins 2000).

1.1.10. Methods for Diagnosis of meningococcal infection

Current methods of diagnosis of meningococcal infection in patients with

meningococcal disease include Gram staining of a CSF sample, direct antigen detection using latex agglutination, CSF smear or bacteriological culture of CSF and blood growing meningococci culture. In addition, molecular diagnostic methods are available including amplification of a meningococcal serotype specific gene by polymerase chain reaction (PCR) and CSF serology to detect meningococci antigen. Radiological examination including X-ray of the skull, sinuses, chest and head CT scan can detect abscess or swelling (Daoud, Omari *et al.* 1998; De Gaspari 2000; Berry, Boese *et al.* 2005; Fernandez-Rodriguez, Vazquez *et al.* 2005; Martin, McCallum *et al.* 2005; Bronska, Kalmusova *et al.* 2006; Jolley, Brehony *et al.* 2007).

N. meningitidis are oxidase-positive, Gram-negative diplococci. These are fastidious and fragile bacteria and the clinical material must be examined as soon as possible after collection to increase the isolation rates (CDCP 1998; WHO 1998). Gram staining is still considered as an important method for rapid detection of *N. meningitidis*. Direct examination of the CSF or a skin lesion biopsy specimen reveals the presence of Gram-negative diplococci both inside and outside of polymorphonuclear cells (Dunbar, Eason *et al.* 1998). Heavily capsulated strains may be seen with a distinct pink halo around the cells.

Meningococcal capsular polysaccharide in CSF, serum or urine may be detected using specific antibodies. This method is rapid and can provide a serogroup-specific diagnosis. However, false negative results are common, especially in cases of serogroup B disease due to the shared structural similarity with the host tissues as described previously (Zollinger and Boslego 1997). Antigen tests of urine or serum

are found to be less reliable for the diagnosis of meningococcal disease. Negative Gram staining or antigen detection does not necessarily rule out the meningococcal disease and so confirmation of meningococcal infection requires bacteriologic culture.

N. meningitidis may be recovered from CSF, blood and aspirates and may be cultured on a selective Thayer-Martin agar or in a peptone-blood base medium or other suitable non-selective media like chocolate agar and sheep blood agar with incubation in 5-10% CO_2 at 37 ^oC for 48-72 hours (Zollinger and Boslego 1997). Positive colonies of *N. meningitidis* appear as gray coloured, low convex colonies, with entire smooth moist edge and glistening surface with a size of approximately 1mm in diameter. However, prior antibiotic therapy reduces the sensitivity and jeopardises the recovery of bacteria from cultures of blood and CSF but not from skin biopsy specimens (van Deuren, van Dijke *et al.* 1993). Following initiation of antibiotic therapy, analysis of blood or CSF samples by PCR is performed as it is not affected by prior antibiotic therapy (Fernandez-Rodriguez, Vazquez *et al.* 2005).

Molecular diagnosis of *N. meningitidis* specific DNA by PCR analysis offers the advantages such as serogroup-specific detection and may not require live organisms. A study comparing the results of Gram staining and culture of CSF with a rapid PCR assay (2 hours) of 281 cases of suspected showed that PCR had a sensitivity of 97% compared to a 55 % sensitivity for culture (Richardson, Louie *et al.* 2003). PCR for the identification of *N. meningitidis*, based on various primers encoding *ctr A*, *por A*, *crgA*, 16S rRNA, *siaD* and *nsp A* genes have been developed (Mothershed, Sacchi *et al.* 2004;

de Filippis, do Nascimento *et al.* 2005; Fernandez-Rodriguez, Vazquez *et al.* 2005; Jordens and Heckels 2005; Taha, Alonso *et al.* 2005). Real-time PCR analysis of the capsule transfer gene (*ctrA*) has also been reported, but fails to detect non-capsular strains associated with nasopharyngeal carriage (Jordens and Heckels 2005). The same authors have developed a novel porA-based TaqMan assay that is more sensitive than the *ctrA* assay for detecting meningococcal carriage (Jordens and Heckels 2005). A multiplex PCR assay for the simultaneous detection of *N. meningitidis, Streptococcus pneumoniae* and *Haemophilus influenzae* type B, has also been developed based on the *ctrA*, *ply* and *bex* gene targets respectively, and this has enabled the detection of 5-10 pg bacterial DNA (Tzanakaki, Tsopanomichalou *et al.* 2005).

Other molecular typing techniques that may be used for detection include Restriction fragment length polymorphism (RFLP), rRNA probe technology (ribotyping), PCR amplification and restriction endonuclease analysis of chromosomal *dhps* (dihydropteroate synthase), *pil A, pil B* and *porA* genes of *N. meningitidis,* repetitive sequence-based PCR and pulsed-field gel electrophoresis (PFGE) (Janda and Knapp 2003; Healy, Huong *et al.* 2005). Antimicrobial susceptibility testing using minimum inhibitory concentration (MIC) determination is also the method of choice in case the patient doesn't demonstrate an appropriate response to the antimicrobial agents (Hughes, Biedenbach *et al.* 1993; Institute 2005; Vazquez 2007).

This disease may also alter CSF glucose levels and CSF cell count. *N. gonorrhoeae* oxidises glucose only whereas *N. meningitidis* oxidises both glucose and maltose and

tests may be performed to analyse these levels (Fox, Taha *et al.* 2007). Thus, carbohydrate utilisation tests may be used for confirmation of isolates as *N. meningitidis.* Also, Kovac's oxidase test may be performed on the growth of a blood agar plate and then the serogroup may be identified (Prevention 1998).

Skin lesions and blood cultures may not always be revealing but CSF samples are generally positive (van Deuren, Brandtzaeg *et al.* 2000; Arend, Lavrijsen *et al.* 2006). In summary, the current methods of diagnosis used to identify the causative organism rely upon time consuming methods such as culture of organisms from cerebrospinal fluid (CSF) (Olcen, Kjellander *et al.* 1979) and blood samples followed by confirmation using techniques such as PCR for meningococcal serotype specific gene (Taha 2000; Freeman, Mai *et al.* 2004). These are rather time-consuming relative to the rapid pathogenesis of the disease itself. Although the introduction of antibiotics made it curable, morbidity and mortality rates from the disease remain unacceptably high.

CSF culture will definitely identify the bacteria involved, but it is a very time consuming test indicating the need for a rapid, accurate and uncomplicated detection technique. The key to successful treatment of bacterial meningitis is rapid diagnosis followed by appropriate antibiotic therapy (Chanteau, Dartevelle *et al.* 2006). In light of the rapid onset of the disease and its devastating effects, it is critical to diagnose and implement appropriate treatment as soon as possible to monitor and control the disease. Early detection, and prompt treatment with antibiotics is essential to prevent permanent neurological damage, and it can mean the difference between life and

death (Brennan, Somerset *et al.* 2003). Thus there is a need for a rapid (in minutes), sensitive and accurate diagnostic technique to detect the presence of meningococci in patients.

The main objective of this research project is to develop a rapid but simple, sensitive and highly specific diagnostic test for the detection of *Neisseria meningitidis*, the most common causative pathogen of meningitis. The proposed research plan involved a combination of techniques spanning biotechnology, chemistry and nanotechnology to develop novel detection systems involving nanoparticles and binding through specific biomolecular interactions between bacterial cell surface antigens and cognate receptors.

1.2. A History of Colloidal Gold Nanoparticles

Gold is a rare metallic element with a melting point of 1064 °C and a boiling point of 2808 °C. Several properties of gold such as its excellent conductive properties and its inability to react with water or oxygen, have made it very useful to mankind over time. During the 5th millennium B.C., the extraction of gold started near Varna (Bulgaria) and it is believed that "soluble" gold appeared around the 5th or 4th century B.C. in Egypt and China. The marvellous statue of Touthankamon, which was constructed around that time stands as proof. It was referred with different names such as soluble gold and drinkable gold, before the term "colloid" (from the French word, colle) was coined by Graham in 1861 (Graham 1861).

Colloidal gold and its beautiful ruby-red colour has fascinated people for many centuries, that can be traced back to ancient times. It was used extensively for cosmetic, decorative as well as for medicinal purposes (Kunckels 1676; Zsigmondy 1926; Savage 1973). In the Middle Ages, "Aurum potabile" or "drinkable gold" was used to cure diseases like arthritis and heart problems, venereal diseases, dysentery, epilepsy and tumours and also for the diagnosis of syphilis, a method which remained in use until the 20th century (Kahn 1928; Hauser 1952; Brown and Smith 1980; Daniel and Astruc 2004).

The use of colloidal gold as the name of soluble gold for therapeutic purposes was well detailed in a book on soluble gold, published by the philosopher and medical doctor Francisci Antonii in 1618 (Francisci 1618). The authour had briefly described the formation of colloidal gold suspensions and their medical uses, including

successful practical cases. By the end of 16th century, colloidal gold was routinely used to make ruby glass and for colouring ceramics, methods that are still in use now. The most famous examples of the use of colloidal gold in ruby glass are the Lycurgus Cup that was manufactured in the 5th to 4th century B.C. and the "Purple of Cassius", that has been known since the 17th century (Savage 1973). The Lycurgus Cup appears ruby red in transmitted light and turns green in reflected light, due to the presence of gold colloids. In 1794, Mrs. Fuhlame reported that she had used colloidal gold to dye silk (Fulhame 1794). Thus it appears that, these kinds of ideas about colloidal gold were common in the 18th century.

Ostwald carried out several studies on metal colloids and subsequently wrote a book titled "The World of Neglected Dimensions" (Ostwald 1915). Nearly half a century later, Feynman visualised the field of nanotechnology quoted that "There's plenty of room at the bottom" (Feynman 1959). Since then, with availability of several sophisticated tools, this area of research has shown tremendous progress (Cushing, Kolesnichenko *et al.* 2004; Daniel and Astruc 2004; Burda, Chen *et al.* 2005; Love, Estroff *et al.* 2005).

Being the subject of one of the most ancient themes of investigation in science, gold and its past glory now leads to an exponentially increasing number of applications, especially in the context of emerging nanoscience and nanotechnology. Metallic gold can be reduced to gold nanoparticles by a variety of reducing agents. By definition, nanoparticles can range in size from 1 to 100 nanometers (Cervellino, Giannini *et al.* 2005). The nanoparticles have highly interesting optical, electronic, and catalytic

properties, which are very different from those of the corresponding bulk materials (Zharov, Galitovsky *et al.* 2003).

Colloidal gold nanoparticles present interesting aspects such as, the behavior of the individual particles, size-related electronic and optical properties, and their applications to catalysis and biology. The possibility to control and tune these unique optical and electronic properties, can allow these gold nanoparticles to be used as versatile analytical probes. Due to the promises offered by the nanotechnology, these nanoparticles are becoming key materials and building blocks in the 21st century.

1.2.1. Synthesis of gold nanoparticles

Nanoparticles from various materials can be prepared by relatively simple methods. During the past few decades, a variety of different methods have been reported and reviewed for synthesizing gold colloids of monodisperse and uniform sizes particles (Turkevich, Stevenson *et al.* 1951; Frens 1973; Hayat 1991; Schmid 1992; Watson, Zhu *et al.* 1999). Currently, there are two kinds of approaches generally carried out to prepare nanoparticles, (a) The "*top down approach*", which involves the constant division of bulk metals into nanoparticles and (b) The "*bottom-up approach*", which involves the building up of nanoparticles from the atomic level.

1.2.1.1. Top- Down Approach

This method is based on dissolution of metallic gold and various methods included in the "top- down" approach are laser ablation methods, evaporation under high vacuum (Aiyer, Vijayakrishnan *et al.* 1994), solvated metal atom dispersion (SMAD) methods (Lin, Franklin *et al.* 1986; Smetana, Klabunde *et al.* 2005), an electric arc

reduction method (Bradley, Schmid *et al.* 2005) and electrochemical reduction methods (Reetz and Helbig 1994).

In the SMAD method (Lin, Franklin *et al.* 1986), the gold suspension is vapourised under vacuum and the metal atoms are co-deposited with a vapour such as acetone on the walls of a reactor. This method helps to stabilise the particles sterically as well as electrostatically. Using this method, silver and copper nanoparticles have also been prepared (Smetana, Klabunde *et al.* 2005). Gold and siver nanoparticles have also been prepared by electric arc reduction of metal filings (Bradley, Schmid *et al.* 2005). Reetz and Helbig (Reetz and Helbig 1994) have described the preparation of palladium nanoparticles by an electrochemical reduction method. Sibbald *et al.*. reported about the laser ablation method to generate silver nanoparticles (Sibbald, Chumanov *et al.* 1996).

1.2.1.2. Bottom- Up Approach

This method is based on preparation of colloid particles from gold halides such as tetrachloroauric acid, $HAuCl_4$ (Dykman, Lyakhov *et al.* 1998). The bottom- up approach of preparing nanoparticles has become very popular, because one can have a good control on size and monodispersity of the nanoparticles (Toshima and Yonezawab 1998). Cushing and co- workers published a review in which they discussed about various preparative strategies in detail (Cushing, Kolesnichenko *et al.* 2004). In this approach, different reducing agents such as sodium borohydride, trisodium citrate, tannic acid, hydrazine, ascorbic acid and tartaric acid are used to reduce the metal ions into nanoparticles (Cushing, Kolesnichenko *et al.* 2004). Nanoparticles from metals such as Au, Ag, Pt, Pd and Rh, having high positive redox

potentials (E_0>0.7V) can be prepared using mild reducing agents under ordinary conditions, whereas electronegative metals (E0< -0.2V) requires strong reducing agents with extreme reaction conditions (Goia and Matijevi 1998). Daniel and Astruc have reviewed the methods available for the preparation of Au nanoparticles (Daniel and Astruc 2004).

1.2.1.2.1. Citrate Reduction

For many biological applications, it is desirable to have the nanoparticles suspended in water with no loss of physical and chemical properties (Lewis 1993). At first, Faraday prepared aqueous colloidal Au suspensions using phosphorous vapour as the reducing agent (Faraday 1857) and stated that these suspensions contained metallic particles in a "*highly divided state*". The Austrian Nobel laureate Zsigmondy said that *"A colloidal mixture may sometimes behave like a chemical compound and has frequently simulated one"* (Zsigmondy 1926). Initially, Zsigmondy described about the colloidal gold synthesis methods with different particle size using H_2O_2, formalin and white phosphorus as the reducing agents.

Among the various methods described, the trisodium citrate reduction method at elevated temperatures, initiated by Turkevich and co-workers (Turkevich, Stevenson *et al.* 1951), is the most widely method. They have proposed the mechanism of synthesis of monodisperse colloidal gold hydrosols by the controlled reduction of an aqueous solution of tetrachloroauric acid. The Au^{3+} ions are reduced by the multidentate chelating agent (trisodium citrate) to produce clusters of supersaturated Au^0 nuclei. As the Au^0 concentration increases, they form seeds of nuclei and the

particle growth occurs by further deposition of metallic gold upon the nuclei. Small metal particles with a negative charge are formed in which case; the negative charge is believed to arise from dichlorogold (I) ions on their outer surface. Here, the citrate anion acts both as a capping as well as reducing agent. This technique leads to gold nanoparticles of an average core size of 20 nm.

The paticle size obtained by this method is inversely proportional to the ratio between citrate: tetrachloroauric acid, resulting in particles in the range, 20 to 100 nm (Englebienne 1999). In 1973, Frens reported that, pre-selected size between 16 and 147 nm were obtained via controlled formation, by varying the ratio between the reducing/stabilising agents (the trisodium citrate-to gold ratio) (Frens 1973). The sodium citrate reduction method produces a uniform size distribution of nanoparticles but with a slightly different mean size with every synthesis (Link, Wang *et al.* 1999).

Synthesis of smaller particles requires the use of strong reductants such as white phosphorus or sodium borohydride. They produce a great number of nuclei and hence the small particles with average diameter of 2 to 10 nm are produced depending on the synthetic conditions (Hyning and Zukoski 1998). Gold, silver and platinum nanoparticles have been prepared using this method (Turkevich, Stevenson *et al.* 1951; Frens 1973; Lewis 1993; Chow and Zukoski 1994; Henglein 1997). Additives, such as tannic acid, may be used to stabilise and to control their size.

1.2.1.2.2. Two-Phase Synthesis and Stabilisation by Thiols

The two-phase procedure that has revolutionised the field of nanoparticle synthesis involves the phase transfer of metal ions from water into an organic toluene medium using phase transfer reagents such as tetraoctyl ammonium bromide (TOABr) (Brust, Walker *et al.* 1994). Subsequently, the metal ions are reduced using reducing agents such as $NaBH_4$, in the presence of capping agents such as dodecanethiols (Brust, Walker *et al.* 1994) and amines (Leff, Brandt *et al.* 1996) that have great affinity for noble metal surfaces. Once the organic phase changes colour from orange to deep brown, the solvent is evaporated to yield particles. These particles can be made soluble in different solvents depending on the polarity of the capping agent. The advantage of this procedure is that the method yields highly stable and capped nanoparticles which can be repeatedly isolated and re-dissolved in common organic solvents without irreversible aggregation or decomposition.

The above synthesis technique was inspired by Faraday's two-phase system and uses the thiol ligands as capping agents that strongly bind gold due to the soft character of both Au and S (Faraday 1857; Brust, Fink *et al.* 1995). Brust *et al.*. extended this synthesis to *p*-mercaptophenol-stabilised gold nanoparticles in a single phase system, which opened an avenue to the synthesis of monolayer protected clusters (MPCs) of gold nanoparticles stabilised by a variety of functional thiol ligands (Brust, Fink *et al.* 1995; Kang and Kim 1998; Chen 1999). The synthetic procedures have been further refined to obtain highly monodisperse nanoparticles (Hicks, Miles *et al.* 2002).

Nanoparticles are generally better dispersed in organic solvents than aqueous solvents. Giersig and Mulvaney converted the citrate- capped gold nanoparticle sols

into thiol- capped particles by substitution in a phase transfer experiment from aqueous to organic phase (Giersig and Mulvaney 1993). These thiol- capped particles were subsequently redispersed in non-polar solvents. Schmid and co- workers (Schmid, Lehnert *et al.* 1991) have prepared Au clusters capped with triphenylphosphine derivatives and due to the polar nature of the capping agent, these particles can be redispersed in aqueous solutions. Methods to transfer the nanoparticles from organic to aqueous media were also reported which is of particular interest for biological applications (Gittins and Caruso 2002). Superhydride and hexadecylaniline have been used as alternative reagents to $NaBH_4$ for the reduction of gold (III) in the synthesis of thiol-stabilised gold nanoparticles (Yee, Jordan *et al.* 1999; Selvakannan, Mandal *et al.* 2002).

1.2.1.2.3. Seeding Growth and Other methods

Although the seeding-growth procedure is an age old technique, recent studies have successfully led to control of the particle size distribution, by manipulating the ratio of seed to metal salt (Jana, Gearheart *et al.* 2001; Meltzer, Resch *et al.* 2001). Nanoparticles in the size range of 5-40 nm were successfully prepared using this method. It was reported that, step-by-step particle enlargement is more effective than a one-step seeding method since it avoids secondary nucleation (Carrot, Valmalette *et al.* 1998).

The use of microemulsions (Aliotta, Arcoleo *et al.* 1995; Chen, Xu *et al.* 2003) copolymer micelles (Carrot, Valmalette *et al.* 1998; Bronstein, Chernyshov *et al.* 1999) reverse micelles (Lisiecki and Piled 1995), surfactants adsorbed (Markowitz, Dunn *et al.* 1999; Aslan and Perez-Luna 2002), membranes and other amphiphile based

techniques for the synthesis of stabilised nanoparticles in the presence or in the absence of thiol ligands has been reported. The syntheses involve a two-phase system with a surfactant that causes the formation of the microemulsion or the micelle maintaining a favorable microenvironment, and the thiols that interact with nanoparticles surface and stabilise the particles. This provides an advantage over the conventional two-phase systems that control both the growth and stabilisation of the gold nanoparticles.

Common surfactants such as cetyl trimethylammoniumbromide (CTAB) and sodium bis (2-ethylhexyl) sulphosuccinate (NaAOT) are used to form reverse micelles (Chen, Xu *et al.* 2003). The metal salts are dissolved in the water and volume of the water pool inside a reverse micelle can be carefully controlled. The addition of a second reverse micelle containing a suitable reducing agent causes the reduction of metal ions to nanoparticles and their size is predetermined by the micellar core where the water is trapped. Phospholipids were also used in particular as dispersants, for the preparation of gold nanoparticles (Chow, Markowitz *et al.* 1996; Bhattacharya and Srivastava 2003).

Colloidal dispersions of noble metals have been prepared by reducing the metal ions under reflux conditions in methanol/water in the presence of polyvinyl pyrollidine (Hirai, Nakao *et al.* 1978). The sol- gel processing of materials, where the metallic particles can be stabilised in both liquid and solid matrices (Epifani, Giannini *et al.* 2000), is a versatile method for making particles at room temperatures. Very stable dispersions of the Au, Ag, Pd and Pt nanoparticles were synthesised in the form of

sols, gels and monoliths in a single step by a sol-gel process (Bharathi, Fishelson *et al.* 1999).

Spontaneous formation of gold nanoparticles have been observed in aqueous suspensions of sugar-persubstituted PAMAM dendrimers without the addition of additional reductant (Esumi, Hosoya *et al.* 2000). Gold nanoparticles were prepared in both aqueous and organic systems by reducing $HAuCl_4$ with *o*-anisidine in the presence of 1:1 *N*-methyl-2-pyrrolidone/toluene (Dai, Tan *et al.* 2002).

Metal nanoparticles have also been synthesised by techniques such as sonochemical (Pol, Gedanken *et al.* 2003), radiolytic, UV irradiation, Near-IR laser irradiation (Mallick, Wang *et al.* 2001), γ-irradiation (Dawson and Kamat 2000), laser photolysis (Sau, Pal *et al.* 2001), electrochemistry and microwave reduction methods in the presence of suitable stabilisers. Radiolysis has been used to synthesise and to control the size of gold nanoparticle. Irradiation by UV light in conjuction with seed growth method was shown to improve the quality of the gold nanoparticles (Meltzer, Resch *et al.* 2001; Sau, Pal *et al.* 2001). Sonochemistry has also been also used for the synthesis of gold nanoparticles and Au/Pd bimetallic particles within the pores of silica substrate. Laser ablation is another technique of gold nanoparticle synthesis, wherein size can be controlled by the laser (Mafune, Kohno *et al.* 2002).

1.2.1.2.4. Gold nanoparticle biosynthesis

Since there is a growing need to develop non-toxic, environment friendly synthetic procedures, biochemical preparation methods of gold nanoparticles have been reported whereby biological organisms play the roles of reductant, protecting agent,

and precipitating agent (Li, Chung *et al.* 2003). Microorganisms like bacteria and fungi as well as plant extracts, have been successfully employed to stabilise Au nanoparticles (Torresdey, Tiemann *et al.* 1999; Hillyer and Albrecht 2001; Mukherjee, Ahmad *et al.* 2001; Torresdey, Parsons *et al.* 2002).

Reaction of $AuCl4^-$ ions with the extract of geranium leaves and an endophytic fungus, *Colletotrichum* sp., present in the leaves, leads to the formation of gold nanoparticles (Ascencio, Mejia *et al.* 2003; ShivShankar, Ahmad *et al.* 2003). This is described as sort of biomineralisation process, in which protein components control the formation of nanoparticles by specifically interacting with the growing particles.

1.2.1.2.5. Bimetallic Nanoparticles

Bimetallic nanoparticles containing gold as one of the elements have been synthesised in a variety of ways. Bimetallic gold nanoparticles have been reported with Ag, Pd, Pt, Ti, Fe, Zn, Cu, Zr, CdS and Eu (Schmid, Lehnert *et al.* 1991; Vacassy, Valmalette *et al.* 1998; Cao, Jin *et al.* 2001; Kolny, Kornowski *et al.* 2002; Moskovits, Sloufova *et al.* 2002; Ravel, Carpenter *et al.* 2002; Schierhorn and Marzan 2002; Shibata, Bunker *et al.* 2002; Shon, Dawson *et al.* 2002; Mandal, Selvakannan *et al.* 2003; Yang, Shi *et al.* 2003). The molar ratios of metals both in and on the surface of the bimetallic cores differed significantly from the metal: salt ratio used in the bimetallic particle synthesis (Hunter 1993).

1.2.2. Control of size of metal nanoparticles

Almost all properties of nanoparticles are dependent on shape and size (Burda, Chen *et al.* 2005) and nucleation and growth are two closely inter-linked processes that

manage the size and shape of controlled synthesis of metal nanoparticles (Turkevich, Stevenson *et al.* 1951; Toshima and Yonezawab 1998) The size of the nanoparticles is generally governed by factors such as the ratio of the capping agent to the reductant (Frens 1973; Brust, Fink *et al.* 1995), the nature of the reducing and capping agents (Chow and Zukoski 1994), temperature (Hostetler, Wingate *et al.* 1998) and the rate of addition of the reducing agent (Tsai and Dye 1991). Strong reducing agents such as alkali metal anions (alkalides) (Brust, Walker *et al.* 1994; Brust, Fink *et al.* 1995), borohydrides and superhydrides (Yee, Jordan *et al.* 1999) induce the formation of nucleation centres which then grow into small clusters whose final size is determined by the nature of the capping agent. In the case of weak reducing agents such as hydrazine (Nickel, Castell *et al.* 2000), ascorbic acid (Sau, Pal *et al.* 2001), tartarate (Tan, Dai *et al.* 2003) and trisodium citrate (Turkevich, Stevenson *et al.* 1951), the rate of reduction is slow. Hence, it is growth of the particle and not the nucleation process that dominates, resulting in large-sized particles. Methods used to prepare large particles of size 50 nm and above directly, result in high polydispersity and varied shapes (Brown, Walter *et al.* 2000). Methods such as 'seed growth' have the advantage of eliminating nucleation and promoting only the growth process and is used to increase particle size in a uniform manner (Brown, Walter *et al.* 2000).

1.2.3. Stability of gold nanoparticles

As noted, nanoparticles prepared by aqueous chemistry techniques, are often formed in the presence of a surface-capping/stabilising ligand that also control the final dimensions of the nanoparticles. In the absence of suitable stabilising agents, colloidal particles would be attracted to each other by van der Waals forces, ultimately resulting in the aggregation and precipitation of the particles (Brust, Fink

et al. 1995). This is prevented by this use of a stabiliser/ capping agent, (Templeton, Chen *et al.* 1999; Yao, Momozawa *et al.* 2001) which establishes a repulsive barrier between the approaching particles. Many capping systems are available which includes, hydrophobic monolayers, (Miyazaki and Nakano 2000), hydrophilic monolayers (Bradley 1994), which provide electrostatic stabilisation and polymer layers which provide steric stabilisation (Figure 1.2) (Bradley 1994).

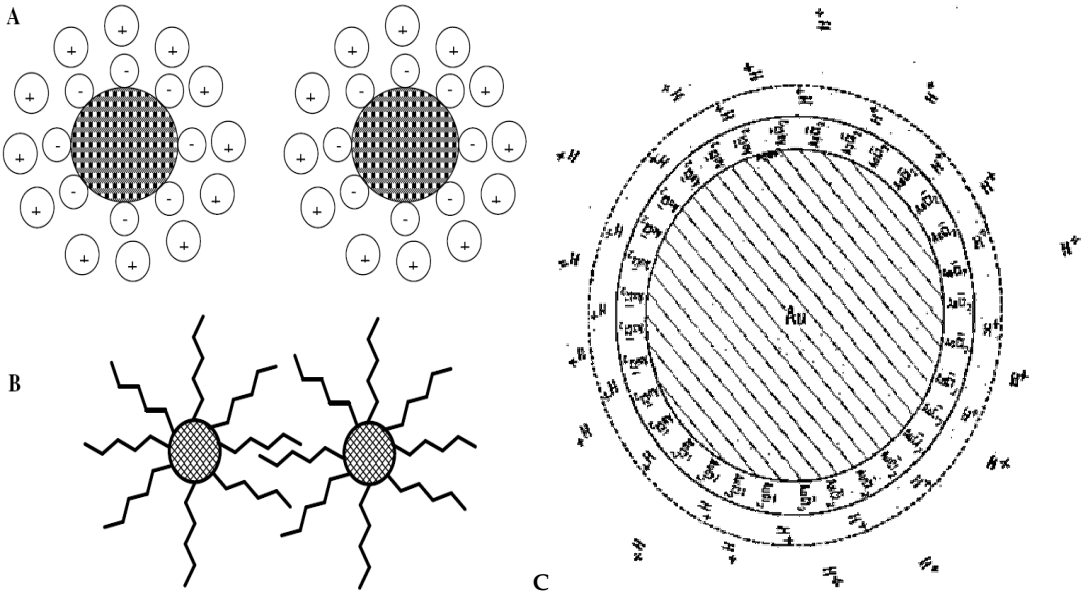

Figure 1.1. Schematic representation of the stabilisation forces in colloidal particles (A) Electrostatic (B) Steric (Bradley 1994) and (C) Citrate reduced colloidal gold particle ("Inorganic Colloid Chemistry;" by Weiser, H. B) (Reyerson 1939).

The electrostatic stabilisation involves the use of charged capping agents such as sodium citrate, where the negatively charged citrate-capped nanoparticles attract positively charged counter-cations from the surrounding solution. This results in the formation of a diffuse electrical double layer, which creates a Coulombic repulsion between the particles. This electrostatic repulsion between the particles will prevent

aggregation, as long as the electric potential associated with the double layer is sufficiently high (Figure 1.1.). However, the double layer is very sensitive to changes in ionic strength of the solution. An increase in the ionic strength by the addition of a salt which causes a compression of the double layer and displacement of the adsorbed citrate anions on the colloid by the addition of a strongly binding adsorbate, would result in aggregation (Brust, Walker *et al.* 1994; Brust, Fink *et al.* 1995).

Large molecules or ligands like polymers (Schmid 1992; Bradley 1994) and long chain thiols (Schmid 1992; Bradley 1994) provides steric stabilisation to the nanoparticles. When particles adsorbed with such molecules approach each other, a reduction in the conformational freedom of the adsorbate molecules occurs due to the interpenetration of the ligand chains. As the local concentration of the the adsorbate increases, the solvent tries to counteract this effect by diluting the concentration of the adsorbate and thereby causes the particles to move apart (Bradley 1994). This is especially useful in organic solvents, where electrostatic effects are small. Thus, a highly monodisperse and uniform sized particles can be synthesised in organic solvents and can be stabilised at relatively high concentrations.

1.2.3.1. Stabilisation by Sulfur and Non-Sulfur Ligands

Sulphur-containing ligands, such as xanthates (Tzhayik, Sawant *et al.* 2002), disulphides (Porter, Ji *et al.* 1998; Tan, Li *et al.* 2002), di- and trithiols (Tan, Li *et al.* 2002) and resorcinarene tetrathiols (Balasubramanian, Kim *et al.* 2002), have also been used to stabilise gold nanoparticles. Thiols are better stabilising agents than disulfides and thioethers (Shelley, Ryan *et al.* 2002), whereas the use of polythioethers

circumvented this problem (Maye, Chun *et al.* 2002). Other gold complexes, in particular gold(I) amine complexes, have been used as precursors for the synthesis of amine-stabilised gold nanoparticles (Leff, Brandt *et al.* 1996). Microemulsions, micelles and reverse micelles have been used to trap and stabilise the nanoparticles (Niemeyer 2001; Sohn, Choi *et al.* 2003).

1.2.3.2. Stabilisation by using Polymers

In 1718, Hans Heinrich Helcher, stated that the use of boiled starch in drinkable gold preparations noticeably enhanced its stability (Helcher 1718). Two centuries later, such materials were recognised as polymers, since then there has been a revival of activity in the field of polymer-stabilised gold nanoparticles (Napper 1983; Hayat 1991; Tuzar and Kratochvil 1993; Schulz, Schulz *et al.* 2002). Poly (*N*-vinyl-2-pyrrolidone) (PVP) is one of the most commonly used polymers for the stabilisation of gold nanoparticles in water. The greatest stability is obtained with polymers possessing hydrophobic backbones and side groups, allowing interactions with the $AuCl_4^-$ ion (Mayer and Mark 1998).

Functionalised polymers such as poly(ethylene glycol)-based polymer have also been used as stabilisers (Otsuka, Akiyama *et al.* 2001). Hollow polymer spheres have been synthesised with movable gold nanoparticles at their core interiors (Kamata, Lu *et al.* 2003). An amine functionalised polymer was used to simultaneously assemble carboxylic acid functionalised gold and silica naoparticles into extended aggregates (Chechik and Crooks 1999; Wang, Neoh *et al.* 2001). Mangeney *et al.*. reported that, disulphide-bearing polymers have shown only a slightly larger affinity for the gold

surface than those that do not have the disulphide groups (Mangeney, Ferrage *et al.* 2002).

1.2.3.3. Stabilisation by using Dendrimers

Gold nanoparticles have been stabilised in the presence of excess polyamidoamine (PAMAM) dendrimers in solution. Thiol functionalized PAMAM dendrimers acted as both a stabiliser and a ligand (Chechik and Crooks 1999). PAMAM dendrimers were also functionalised with hydrophobic groups for solubilisation of the gold nanoparticles in organic solvents (Esumi, Hosoya *et al.* 2000). These dendrimer-gold nanoparticle assemblies have been deposited as films on sensor surfaces (Krasteva, Krustev *et al.* 2003). Another important observation was the use of that PAMAM dendrimers to stabilise gold nanoparticles allowed the control of the interparticle distance (Frankamp, Boal *et al.* 2002).

1.2.4. Characterisation of gold nanoparticles

The most common technique for characterisation of gold nanoparticles is high-resolution transmission electron microscopy (HRTEM), which generates a photomicrograph of the gold core of the gold nanoparticles, providing the size distribution and dispersity of the sample. The mean number of gold atoms can be calculated form the mean diameter, d, of the cores. The core dimensions of the metallic nanoparticles have also been characterised using alternative techniques based on microscopy (scanning electron microscopy-SEM, scanning tunneling microscopy-STM, atomic force microscopy-AFM), X-ray methods (small-angle X-ray scattering-SAXS, Extended X-ray absorption fine structure-EXAFS, X-ray photoelectron spectroscopy- XPS, X-ray diffraction- XRD), optical spectroscopy (UV-

Visible spectroscopy), electrochemistry, infrared (IR), Raman and nuclear magnetic resonance (NMR), thermogravimetric analysis (TGA), laser desorption ionisation mass spectrometry (LDI-MS), or high-resolution time-of-flight mass spectroscopy analysis. (Toshima and Yonezawab 1998).

The localised elemental composition on the nanoparticles can be obtained from Energy Dispersive X- ray microanalysis (EDX) in conjunction with TEM. However, the disadvantage associated with TEM, is that the high energy of the beam can cause phase transitions and desorption of the protective ligands (Bovin and Malm 1991). Scanning tunneling microscopy (STM) is a useful technique for determining particle size, which also includes the size of the ligand shell as well (Reetz, Helbig *et al.* 1995).

UV-Visible spectroscopy is used for analysis of the intensely coloured colloidal dispersions having characteristic surface plasmon absorption. In a given preparation of gold nanoparticles, there is usually a mixture of different size nanoparticles. Different size nanoparticles have characteristic surface plasmon resonance peaks and thus the UV-Visible spectra of the different nanoparticles are also usually significantly different, which may also helps in determining the particle size. The UV-Visible together with infrared (IR) spectra provides an identification of the ligand that is also confirmed by nuclear magnetic resonance (NMR) spectroscopy. The detection of order-disorder transitions in gold nanoparticles in the solid state has ben achieved using by IR and NMR spectroscopy techniques together with differential scanning calorimetry (DSC). The results suggested that the energetic states and the

dimensions of the gold nanoparticles are influenced by both the radii and concentrations of the stabilising groups.

The information on the inter-atomic distances and coordination numbers of the metal atom in colloids can be obtained using Extended X-ray Absorption Fine Structure (EXAFS) sprecroscopy and thus allowing investigation of the size-dependent distance contraction in thiol-stabilised gold nanoparticles. X- ray diffraction is used to investigate the structure and size of metal nanoparticles. Surface-enhanced Raman scattering (SERS) and X-ray photoelectron spectroscopy (XPS) are used to determine the chemisorptive properties of tetrathiol ligands and the oxidation states of metallic nanoparticles. The oxidation state of the gold atoms and the interaction of thiols with gold have been studied by Brust *et al.*. and confirmed using ^{1}H NMR measurements (Brust, Walker *et al.* 1994). Capillary zone electrophoresis has also been used to determine the core radius and size of the nanoparticles based on the mobility of gold nanoparticles in acetate buffer (Hwang, Lee *et al.* 2003).

1.2.5. Optical Properties of gold nanoparticles

Gold nanoparticles have a remarkably low melting temperature (300 - 400°C), compared to that of bulk gold (1064 °C). During the reduction process, the properties of the bulk metal begin to change dramatically because more of inner atoms move to the surface and the electrons begin to suffer the quantum effects. The resulting physical properties are neither those of bulk metal nor those of molecular compounds, but they strongly depend on the factors such as particle size, shape, interparticle distance and nature of the protecting group. This makes nanoparticles different from bulk gold as well as the atomic state of the metal (Katz and Willner

2004). Thus the properties of nanoparticles such as optical, electronic, chemical, magnetic and mechanical are affected by these factors (Hövel, Fritz *et al.* 1993). The optical properties of nanoparticles such as surface plasmon resonance, are strikingly different from that of bulk gold. This section details only about the surface plasmon resonance (SPR) property (Underwood and Mulvaney 1994; Link and El-Sayed 1999) since it is relevant to the present study.

1.2.5.1. Surface Plasmon Resonance

Certain metal colloids like Au, Ag and Cu, exhibit strong absorption bands in the visible region and are therefore intensely coloured. Gustav Mie (Mie 1908) determined that these intense colours associated with metal colloids is a consequence of the absorption and scattering of light and described a theoretical explanation for the colour of the colloidal gold. He solved Maxwell's equations for the absorption and scattering of electromagnetic radiation by spherical particles and proposed an equation (Mie 1908) to calculate the extinction spectra of the particles. Later, Mie's theory was extended by Gans to prolate and oblate spheroidal particles averaged over all orientations (Gans 1915). However, all subsequent reports that describe the spectroscopic behavior of gold nanoparticles continued to correlate with the Mie theory.

An absorption band of metallic nanoparticles induced by an interacting electromagnetic field, is referred as the "surface plasmon band", (Kreibig and Vollmer 1995). This phenomenon appears in the absorption spectrum of the nanoparticles due to the collective coherent oscillation of the free conduction band electrons occupying energy states just above the Fermi level. In the case of gold

nanoparticles, it is due to plasmon oscillation of 6s electrons of the conduction band. The deep-red colour of gold nanoparticles in water and glasses reflects the surface plasmon band (SPB), a broad absorption band in the visible region around 520 nm. In general, the surface plasmon values of gold, silver and copper nanoparticles with a diameter below 20 nm, lie close to 520 nm, 400 nm and 570 nm respectively (Creighton and Eadon 1991) and for larger particles, the peak shifts to longer wavelength (e.g., 529 nm for 50 nm nanoparticles). Thus, the SPB provides information on the development of the band structure in specific metals and has been the subject of extensive study.

The position of the surface plasmon depends on and is sensitive to several factors such as particle size, shape, stabilising agent and temperature as well as nature of the surrounding medium (Hövel, Fritz *et al.* 1993; Underwood and Mulvaney 1994; Kreibig and Vollmer 1995; Link, Wang *et al.* 1999). Kreibig and Fragstein (Kreibig and Fragstein 1969) and several other groups have shown, that the plasmon bandwidth is proportional to 1/R, where R refers to the radius of the particle. When the diameter of the particle becomes smaller than the mean free path of the conduction electrons (approximately 3 nm) electron scattering occurs at the particle boundaries resulting in broadening and damping of the surface plasmons. That is the reason why SPB is absent for gold nanoparticles with core diameter less than 2 nm, as well as for bulk gold.

The plasmon bandwidth increases with decreasing size in the intrinsic size region (mean diameter smaller than 25 nm) (Link, Wang *et al.* 1999), and also increases with

increasing size in the extrinsic size region (mean diameter larger than 25 nm) (Link, Wang *et al.* 1999) and is found to follow the predicted behavior of quantum size effects. The surface plasmon resonance shows a red- shift in the extrinsic size region and as the particle size increases, the gold nanoparticles colour changes from ruby red to purple and finally blue. However, in the intrinsic size region, the changes in surface plasmon position are not very clear (Link, Wang *et al.* 1999). It has been found that the plasmon resonance absorption obtained often deviate from the predictions of the Mie theory, and the discrepancies are attributed to the complex physical and chemical influences of the capping agent.

As the particle shape changes from a sphere to a spheroid, ellipse or a rod, a significant change in the absorption spectrum is observed (Link, Wang *et al.* 1999). With elliptical particles, the SPB is shifted to higher wavelength as the spacing between particles is reduced, and this shift is well described as an exponential function of the gap between the two particles (Blatchford, Campbell *et al.* 1982). A similar phenomenon is observed in the case of particles that are in close contact with each other. This is due to coupling between the plasmon modes of the individual particles (Blatchford, Campbell *et al.* 1982). Gans (Gans 1915; Link, Wang *et al.* 1999) has calculated the extinction coefficient of nanorods and good agreement between theoretical and experimental data has been observed. For rod like particles, the extinction maximum polarised along the long axis occurs at a longer wavelength than the SPB maximum for polarisation along the particle radius.

The presence of a ligand shell or group alters the refractive index and causes either a red or blue shift, so that the spectroscopic data obtained often deviate from the prediction of Mie theory that deals with naked nanoparticles. The agreement with Mie theory is obtained only when the shift induced by this ligand shell is taken into account. Another influential parameter is the core charge. Excess electronic charge causes shifts to higher energies, whereas electron deficiency causes a corresponding shift to lower energy. The effect of temperature was also found to have a smaller effect.

The refractive index of the solvent has been shown to induce a shift of the SPB, as predicted by the Mie theory. For instance, suspensions of dodecanethiolate capped gold nanoparticles of 5.2 nm average diameter reveal an 8-nm shift in SPB as the solvent refractive index is varied from 1.33 to 1.55. Therefore, impurities in the system can be easily detected since the refractive index of gold nanoparticles greatly differs from that of gold oxide or gold chloride. The SPR wavelength and width of nanoparticles also depend on the dielectric constant of the surrounding medium and hence on their average diameter. Underwood and Mulvaney (Underwood and Mulvaney 1994) have demonstrated that, an increase in the refractive index of the gold nanoparticle suspension leads to a corresponding red-shift of the surface plasmon peak. A red shift was also observed with an increase of the solvent dielectric constant with solvents that do not coordinate the gold core, but the SPB is unaffected in polar solvents that do not bind to the core.

The SPB was used to study the degree of dispersion of gold nanoparticles in a variety of solvents. Formation of large aggregates caused a reversible change in colour of the gold nanoparticle suspension from red to violet due to coupling to surface plasmons in aggregated colloids. Apart from colloidal suspensions of Au, Ag and Cu, alkali and alkaline earth metals such as, cadmium and thallium also exhibit distinct absorption bands. Most other metal colloidal suspensions are usually brown in colour, do not show strong absorption bands in the visible region, and the absorption spectra appear flat and featureless (Creighton and Eadon 1991).

1.2.6. Biological Applications of gold nanoparticles

1.2.6.1. Biomolecule-directed nanoparticle organisation - Nanoparticles as biolabels

The dimensions of the metal nanoparticles are similar to those of biomolecules such as proteins (enzymes, antigens, antibodies) or DNA whose dimensions are in the range of 2-20 nm (Service 1997; Mirkin and Taton 2000; Niemeyer 2001). Immibilisation of biomolecules onto nanoparticles to yield novel hybrid nano-biomolecules, has been achieved by a variety of techniques including physical adsorption, electrostatic binding, specific recognition, and covalent coupling (Katz and Willner 2004). Under appropriate conditions, noncovalent bonding is a general strategy to bind colloidal gold and macromolecules, with little or no change in the specific activity of the bound macromolecule. This interaction is influenced by a number of factors including ionic concentration, pH conditions (in correlation with the protein pI values) and protein/DNA stabilising levels.

In the case of citrate capped nanoparticles, biomolecules can be linked directly by exchange reactions with stronger binding ligands (Niemeyer 2001). For example, the coating of colloidal gold with proteins such as immunoglobulins and serum albumin, which have cysteine residues. If the native proteins doesn't have the cysteine residues, thiol groups can be incorporated by chemical modification (Tarentino, Phelan *et al.* 1993) or by genetic engineering. DNA molecules can also be synthesised with alkylthiol groups at either the 3'- or 5'-end to facilitate binding to gold nanoparticles (Tarentino, Phelan *et al.* 1993).

By utilising the advantage of specific receptor-ligand ineractions, various nanoparticle assemblies have been generated. Analogous to the interactions between the amino acid side chains and the metal atoms in many reaction centres of enzymes, the interaction between biomelcules and the surface of an inorganic nanoparticle provides the way for the coupling of biomolecular recognition systems to generate novel materials. The two sets of nanoparticles are functionalised with individual recognition groups that are either directly complementary to each other, or else are complementary to a molecular linker (Niemeyer 2001). The bio-recognition elements such as proteins/enzymes, antigens/antibodies, and DNA/oligonucleotides, in conjunction with nanoparticles, have been used for various biotechnological applications including, affinity separations, biosensing, bioreactors, and the construction of biofuel cells.

1.2.6.2. DNA-gold nanoparticles assemblies and sensors

Negatively charged DNA was found to substitute citrate ions around gold nanoparticles to form a DNA-nanoparticle probe, which was confirmed by

electrophoresis and fluorescence (Cushing, Kolesnichenko *et al.* 2004). DNA functionalised gold and semiconductor nanoparticles have been prepared using the n-alkylthiolated DNA and also using DNA containing several adenosyl phosphothioate residues at their ends (Niemeyer 2001). Nucleic acids are superior for the functionalisation of nanoparticles, since the possible programmability of DNA base-pairing to organise nanoparticles in space and the range of techniques available for the detection of precise DNA sequences (Castaneda, Merkoci *et al.* 2007).

DNA conjugated to the nanoparticles is able to hybridise with complementary DNA and is thermally reversible (Mirkin, Letsinger *et al.* 1996). In the presence of complementary strands, the coupled nanoparticles are released at high temperatures due to the "melting" transition of the complementary DNA strand (Qin and Yung 2007).

In recent times, the fabrications of DNA-driven assemblies of two-dimensional arrays and three-dimensional networks of gold and silver nanoparticles have indeed attracted considerable interest. The Mirkin group have used DNA as a linker to form macroscopic assemblies of 13-nm gold nanoparticles (Mirkin, Letsinger *et al.* 1996). Alivisatos *et al.*. have used DNA as a template to prepare nanocrystal chains consisting of two or three 1.4 nm particles on a single oligonucleotides strand (Alivisatos, Johnsson *et al.* 1996).

Conjugates of gold nanoparticles-oligonucleotides are of great interest for detection of DNA hybridisation, because of its application in the diagnosis of pathogenic and

genetic diseases (Castaneda, Merkoci *et al.* 2007). Most of the DNA hybridisation techniques utilize fluorescent, chemiluminescent, or radioactively labelled probes or requiring special instrumentation or both (Kim, Rajamohan *et al.* 2006). A significant enhancement of the shift (40 nm) of the transmission surface plasmon resonance (T-SPR) absorption band of the gold nanoislands, was observed, when a self assembled monolayer of a single-stranded DNA deposited onto a glass microscopic slide is hybridised by its complementary DNA functionalised to gold nanoparticles (Garcia and Garcia 2000; Hutter and Pileni 2003). The sensitivity of SPR biosensing of DNA hybridisation on continuous Au film was greatly enhanced by using Au nanoparticles (Hutter and Pileni 2003). Indeed, conductivity changes in gold nanoparticle labelled DNA arrays have recently been employed for selective molecular recognition of targets present in low concentration (Tirelli 2006).

The SPB phenomenon has led to the development of a highly selective diagnostic method for DNA, based on the distance-related properties of gold nanoparticles. Aggregation of gold nanoparticles linked by the oligonucleotides mediates a red-to-blue colour change (red shift from 520 to 620 nm of the SPB) and this property is utilised in the DNA-sensing method. The effect of the length of the DNA strands that control the interparticle distance has been studied, and it was found that the SPB frequency changes are inversely dependent on the oligonucleotides linker length (Fischler and Simon 2007). A new colorimetric technique based on the sensitivity of the surface plasmon band (SPB) has been designed to monitor the sequence specific DNA modifications (Li, Chu *et al.* 2005).

Stable, water-soluble, hydroxycapped quantum dots-oligonucleotide conjugates have been used as labels in fluorescence *in situ* hybridization (FISH) studies (Wu, Zhao *et al.* 2006). Biosensors based on gold nanoparticle-DNA interactions have enabled detection within minutes, and quantitative data obtained (Yáñez-Sedeño and Pingarrón 2005). Thus, applications in the fields of biosensors, disease diagnosis, and gene expression using gold nanoparticle-DNA conjugate probes are clearly called for.

1.2.6.3. Protein-based recognition systems: Enhanced immuno sensing

Biomolecules and inorganic nanoparticles are conjugated by means of various conjugation methods that allow the preparation of well-defined bioconjugate hybrid nanoparticles (Niemeyer 2001). Though, a large number of complementary binding pairs are available, nucleic acid based conjugation might offer advantages over protein based assembly, since the physicochemical properties of a single 20-mer oligonucleotide represents 4^{20} (=10^{12}) different recognition elements (Mann, Shenton *et al.* 2000). However, it was suggested that extensive use of protein-based assembly may lead to a "factory of the future", directed by multiple highly specific biomolecular recognition elements such as, antibodies that are specific against various antigens (Mann, Shenton *et al.* 2000). These biomolecule based coupling systems were useful in various diagnostic applications and for generating inorganic nanoparticle networks (Niemeyer 2001).

The conjugation of proteins on colloidal gold nanoparticles is achieved by the electrostatic interactions between negatively charged citrate on surfaces of gold nanoparticles and positively charged groups of the proteins (Xiao, Ju *et al.* 1999). The strong interaction between the protein and the colloidal gold nanoparticle surface

may increase the surface density of the adsorbed protein, and small size of the colloidal gold particles gives the protein molecules more freedom in orientation (Liu, Leech *et al.* 2003). Enzymatic activity of fungal protease-gold nanoparticle bioconjugates was reported (Phadtare, Kausik *et al.* 2004). Assembly of gold nanoparticles on polyurethane spheres were used to immobilise enzymes such as pepsin and these bioconjugate catalysts were reused as free enzymes (Phadtare, Kumar *et al.* 2003).

The conjugation of antigens and antibodies on colloidal gold has been used for the development of immunological detection methods (Lin, Sabri *et al.* 2005). The experimental gold nanoparticle-protein conjugate architectures involves either direct binding of antigen-gold nanoparticle bioconjugates to an antibody modified surface or the exposure of an antibody derived surface to free antigen and then to a secondary antibody-gold nanoparticle conjugate. Recently, a unique, sensitive and highly specific immunoassay system for antibodies using gold nanoparticles has been developed (Thanh and Rosenzweig 2002).

Biosensors for immunoassays in human serum have been developed (Jianrong, Yuqing *et al.* 2004). An electrochemical method to monitor biotin-streptavidin (STV) interactions has been established using colloidal gold as an electrochemical label (Garci, Sanchez *et al.* 2000). The Biotin-STV system is a versatile system for developing novel strategies for assembling nanoparticles in suspension or on a substrate and the conjugates form the basis of many diagnostic and analytical tests (Niemeyer 2001). The STV - biotin interaction was also used to organise gold colloids

that were functionalised by chemisorptive coupling to a disulphide biotin analogue (Connolly and Fitzmaurice 1999). Niemeyer and Ceyhan prepared biofunctionalised nanoparticles by DNA-directed conjugation of proteins (Niemeyer and Ceyhan 2001). These studies demonstrate the emergence of a new field of application for colloidal gold in protein immobilisation and biosensing.

The specific interaction between antibodies and low molecular weight organic compounds, the so-called hapten groups, has been used to cross-link nanoparticles (Shenton, Davis *et al.* 1999). Shenton *et al.* functionalised gold and silver nanoparticles with the immunoglobulins IgG and IgE, which had a specificity directed against either the d-biotin or the dinitrophenyl (DNP) group respectively (Shenton, Davis *et al.* 1999).

Gold nanoparticles have been immobilised in the gaps of microelectrodes through biospecific interactions and then the silver enhancement of gold nanoparticles has been applied for the electrical sensing of biological binding events (Velev and Kaler 1999). These gold colloids serve as catalytic cores for the reductive deposition of a conducting layer of silver, which short circuits the two electrodes. This ultimately resulted in decrease in ohmic resistance which is used as a positive signal for the sensing of the biospecific interactions (Velev and Kaler 1999). Biosensors for the electrocatalytic detection of hydrogen peroxide were prepared by adsorption of the horse-radish peroxidase enzyme onto electrode-immobilised layers of gold colloids (Patolsky, Gabriel *et al.* 1999; Xiao, Ju *et al.* 1999).

In another example, conjugates of nanocrystals with IgG molecules were prepared and subjected to immuno-precipitation by using a complementary antibody with binding specificity for the particle-bound proteins. The widespread aggregation observed in this experiment clearly indicated that the nanocrystals were suitable for the sensitive immunoassays and the attachment of nanocrystals does not interfere with the intrinsic functionality of the biomolecule (Chan and Nie 1998). In continuation to this work, Han *et al.*. tagged the micrometre-sized polymer particles with various quantum dots to achieve an optical barcode for biomolecules (Han, Gao *et al.* 2001).

The great sensitivity of the surface plasmon band (SPB) by gold nanoparticle adsorption has also led to their use in bioassay applications (Daniel and Astruc 2004). Gold nanoparticles were also applied to enhance the detection limits in SPR-based biospecific interaction analysis (Lyon, Musick *et al.* 1998). The dramatic enhancement of SPR biosensing with colloidal Au was observed in a sandwich immunoassay in which Au nanoparticles were coupled to a secondary antibody , thereby allowing picomolar detection of the antigen (Lyon, Musick *et al.* 1998).

1.2.6.4. Drug delivery

Nanoparticles can easily enter cells although the mechanism(s) involved are not well understood. Dai and co-workers (2005) suggested that the nanoparticle influx occurs by endocytosis (Shi Kam, O'Connell *et al.* 2005). In contrast, Bianco *et al.*. suggested that the particles are inserted and diffused through the lipid bilayer of the cell membrane (Bianco, Kostarelos *et al.* 2005). Furthermore, these nanoparticles were shown to be able to enter the cells even after linkage to proteins such as antibodies

(Shi Kam, O'Connell *et al.* 2005). Nanoparticles conjugated with antibodies against exclusive cancer cell surface receptors have been used to specifically bind with cancerous cells (Shi Kam, O'Connell *et al.* 2005).

The functionalised nanoparticles have also been used for targeted entry into cells (Jiang, Kim *et al.* 2007). Phthalocyanine-stabilised gold nanoparticles have ben shown to be a potential delivery vehicle for photodynamic therapy (Hone, Walker *et al.* 2002). gold nanoparticles with a size of 20 nm have been conjugated to various cellular targeting peptides to provide functional nanoparticles that penetrate the biological membrane and target the nucleus (Katz and Willner 2004). Various nanoparticles have also applied as targeted biomarkers and drug-delivery agents for diagnosis and medical treatment of cancers (Katz and Willner 2004).

1.2.6.5. Cytochemical labels and other applications

Colloidal gold nanoparticles prepared in sizes from 1 to 25 nm, are electron dense due to the high atomic number of the gold atoms and, this makes them ideal for electron microscopy. Specific sites in a biological specimen may be visualised by introducing antibody conjugated colloidal gold particles (Hainfeld 1992; Takizawa, Suzuki *et al.* 1998). Small gold clusters with a diameter of 0.8 or 1.4 nm, stabilised with arylphosphanes have been routeinly used as probes for the site-specific labeling of biological macromolecules in histological applications (Hainfeld and Furuya 1992).

Colloidal gold nanoparticles are also used as cytochemical labels for the study of macromolecules with transmission and scanning electron microscopy (Garcia and Garcia 2000), light microscopy (Csaki, Moller *et al.* 2002) and freeze-etch electron

microscopy (Garcia and Garcia 2000) and to enhance the signals of both surface enhanced Raman spectroscopy (Manimaran and Jana 2007) and surface plasmon resonance (Lyon, Musick *et al.* 1999).

Specific binding of mannose-encapsulated gold nanoparticles to FimH adhesin of bacterial type 1 pili in *Escherichia coli*, have been shown by TEM (Lin, Yeh *et al.* 2002). The method used in these studies labelled specific proteins on the cell surface using carbohydrate-conjugated gold nanoparticles, and the visualisation of the target receptor was easily accomplished with an electron microscope.

Colloidal gold, with an indirect digoxigenin-tagged nucleotide and an anti-digoxigenin probe, was used for *in situ* hybridisation studies using an electron microscope (Jin and Lloyd 1997). Both a gold nanoparticle label and a fluorescein tag are attached to an antibody to yield a single probe for imaging a specimen both by fluorescence and electron microscopy (Thompson and Swanson 1998). A further advantage of using the colloidal gold marker is that the colloidal gold nanoparticles can be easily be counted and thus the cytochemical signal may be evaluated quantitatively. Several procedures such as silver enhancement have been developed to amplify the final signal which makes the techniques more sensitive.

Separation of acidic and basic proteins was achieved by nanoparticle-filled capillary electrophoresis (Yu, Su *et al.* 2006). gold nanoparticles have been used to manipulate the selectivity between solutes in capillary electrophoresis (Neiman, Grushka *et al.* 2001). Thus, gold nanoparticles serve as large surface area platforms for organo-

functional groups that interact with the capillary surface, the analytes, or both. The use of gold nanoparticles in conjunction with chip-based capillary electrophoresis to improve the selectivities between solutes and to increase the efficiency of the separation has been reported (Pumera, Wang *et al.* 2001). In summary, gold nanoparticles that are functionalised with proteins have long been used as tools in the biosciences. Moreover, the synthesis of well defined nanoparticle-biomolecule complexes is particularly important to generate well defined nanoarchitectures.

The primary aim of this project is to design and develop a rapid, specific and highly sensitive diagnostic assay for *Neisseria meningitidis* using OMP85 and anti-OMP85 antibody as a model system. In the following chapters, details about the preparation of different target antigens including expression and purification of the recombinant OMP85 antigen are discussed. Polyclonal antibodies were raised against these antigens. Methods were optimised for successful conjugation of both antigens and antibodies to gold nanoparticles. Gold nanoparticles were utilised both as colour reporting agents and also as the signal amplification probes for the detection of the antigen.

Chapter 2

The detection system - Potential biomarker targets and receptors

2.1. Potential biomarkers and target antigens

There are several target antigen molecules on the surface of *Neisseria meningitidis* including the bacterial outer membrane proteins (OMP's) such as OMP85, anti-phagocytic polysaccharide capsule and lipo-oligosaccharides, which are being used for immunodiagnostic and therapeutic purposes (Figure 2.1. and 2.2.) (Granoff, Bartoloni *et al.* 1998; Vipond, Suker *et al.* 2006).

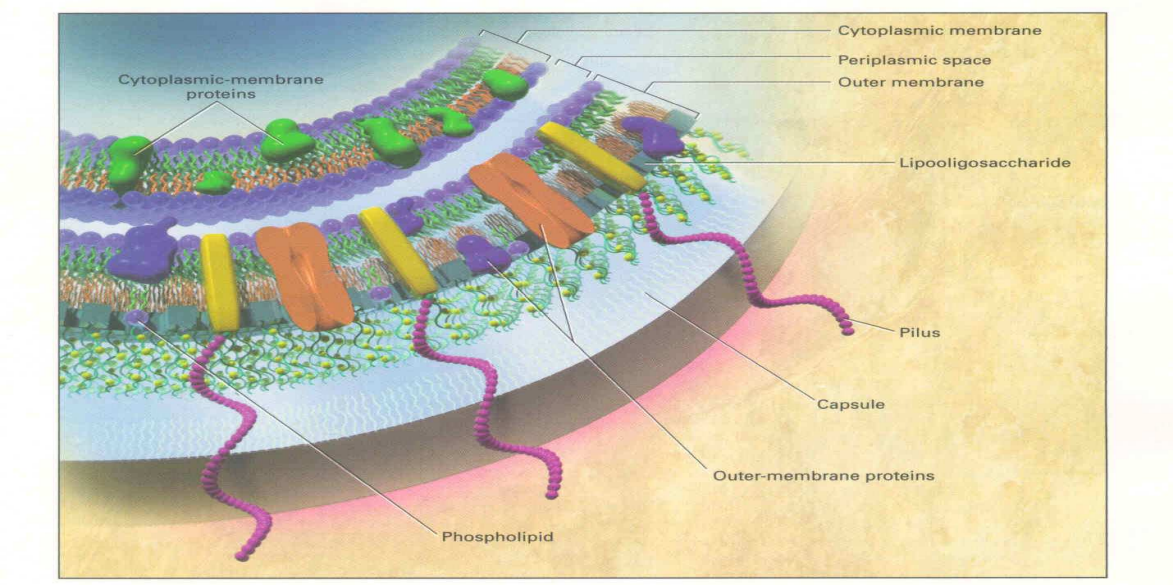

Figure 2.1. Cross-sectional view of the Meningococcal Cell Membrane (Rosenstein, Perkins *et al.* 2001)

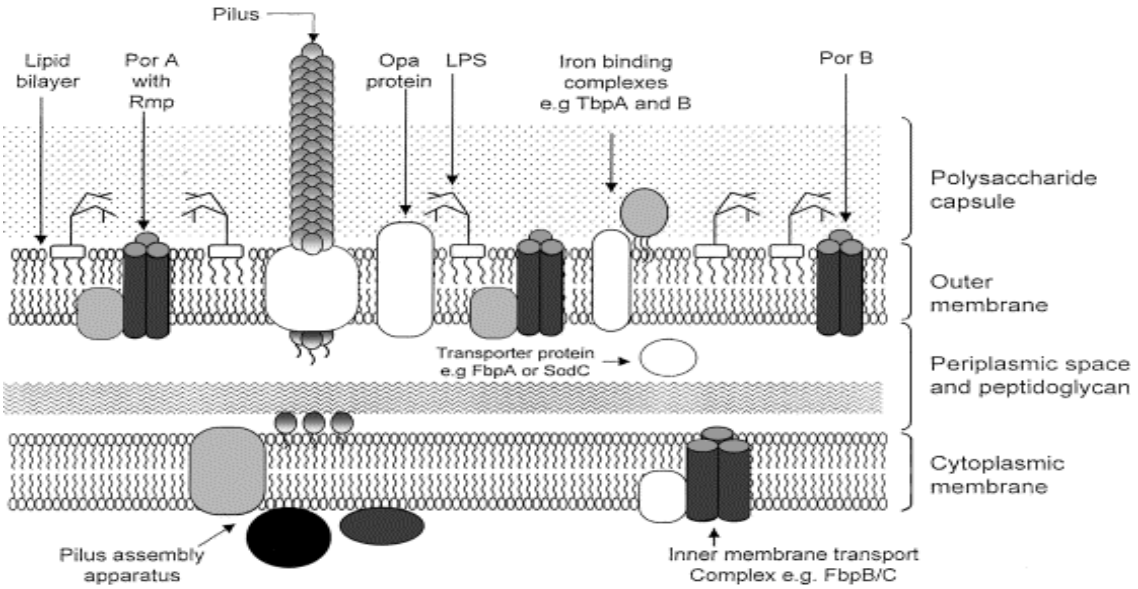

Figure 2.2. Structural representation of meningococcal cell envelope (Morley and Pollard 2001).

2.1.1. *Neisseria meningitidis* OMP85

The cell membrane of Gram negative bacteria consists of an outer membrane and an inner membrane, separated by the periplasm. The inner membrane is a phospholipid bilayer, whereas the outer membrane is an asymmetric structure which consists of phospholipids and lipopolysaccharides (LPS) in its inner and outer leaflets, respectively (Voulhoux, Bos *et al.* 2003). Even though the integral proteins are present in both the outer and inner membranes, the main structural difference between the two membranes is that the integral proteins of inner membrane are mostly α-helical and that of outer membrane proteins (OMPs) are the β-barrel proteins.

OMPs with an NH_2-terminal signal sequence are synthesised in the cytoplasm. After inner membrane translocation (Voulhoux, Bos *et al.* 2003), the signal sequence is cleaved off, releasing the mature OMP protein into the periplasm. In the periplasm,

LPS stimulates the OMP's to fold into their native tertiary conformation and then inserted into the outer membrane (Voulhoux and Tommassen 2004). There have been reports that describe other factors which also mediate OMP folding, such as the periplasmic chaperones SurA and Skp proteins (Voulhoux, Bos *et al.* 2003). Very little information is available about the subsequent steps in OMP biogenesis (Gentle, Gabriel *et al.* 2004).

Meningococcal OMP85 which fulfill the above criteria to some extent, is a highly conserved protein amongst Gram-negative bacteria, and sequence analysis reveals that it has close similarities with other OMP's from other bacteria including OMP 85 protein of *Neisseria gonorrhoeae* (95% sequence identity), *Haemophilus influenzae* D-15-Ag (31.5% sequence identity) and *Pasteurella multocida* Oma87 (31.6% sequence identity) (Manning, Reschke *et al.* 1998). Several hypothetical proteins similar to OMP85 have also been identified (Fitzpatrick and McInerney 2005). Southern blot analysis has shown that omp85 is present as a single copy both in *N. gonorrhoeae* and *N. meningitidis* (Bronska, Kalmusova *et al.* 2006). The gene in *N. meningitidis* encodes a 797 amino acid OMP85 protein with a predicted molecular weight. of 88.5 kDa and NH_2- terminal signal peptide. After cleaving the signal peptide, it yields a mature protein with 85.8 kDa predicted molecular weight. A carboxy-terminal phenylalanine residue is also present in the mature protein, which is characteristic of Gram negative bacterial outer membrane proteins (Judd and Manning 2003).

OMP85 of *N. meningitidis* is an essential protein for growth and also for various other functions such as outer membrane protein assembly (Gentle, Gabriel *et al.*

2004), host-pathogen interactions and lipid transport from the inner membrane to the outer membrane (Genevrois, Steeghs *et al.* 2003). Unsuccessful attempts by Voulhoux *et al.*. to delete the structural gene for the homologous protein in *Haemophilus ducreyi* and *Synechocystis* sp., indicates that OMP85 is an essential protein (Voulhoux, Bos *et al.* 2003). The same authors reported that deletion of the omp85 homologoue gene resulted in the accumulation of various outer membrane proteins in the periplasm, suggesting that OMP85 is also essential for translocation into the outer membrane (Voulhoux, Bos *et al.* 2003).

To demonstrate that the presence of OMP85 is essential for viability, Gentle *et al.*. constructed a meningococcal strain in which OMP85 expression could be switched on or off through a tac promoter-controlled OMP85 gene, (Gentle, Gabriel *et al.* 2004). This experiment also proved that the absence of OMP85 expression leads to the accumulation of electron-dense amorphous material and some vesicular structures in the periplasm.

Another essential function of the OMP85 protein is the lipid transport from the inner membrane to the outer membrane (Genevrois, Steeghs *et al.* 2003). However, it is still not clear how the lipopolysaccharides and phospholipids synthesised at the inner membrane are subsequently transported to the outer membrane. A possible explanation for the role of OMP85 in this regard is that both the omp85 gene and the genes involved in lipid biosynthesis are co-transcribed and thus may be involved in the lipid transport (Genevrois, Steeghs *et al.* 2003). Another interesting observation was that upon depletion of OMP85 expression, the lipopolysaccharide and phospholipids

mostly disappeared from the outer membrane and they were not transported from the inner membrane (Genevrois, Steeghs *et al.* 2003). These results explain the role for OMP85 in lipid transport to the outer membrane and thus in outer membrane protein assembly.

Sequence analysis reveals that proteins homologous to OMP85 are found in other Gram negative bacteria and also in the outer membrane of mitochondria in eukaryotes from plants to humans (Gentle, Gabriel *et al.* 2004). The outer membrane protein, Toc75, a plastid protein translocator of the chloroplast protein-import machinery is a plant homologue of the OMP85 protein (Gentle, Burri *et al.* 2005). Toc75 is involved in protein transportation into chloroplasts and this suggests a common evolutionary origin (Surana, Grass *et al.* 2004).

In eukaryotes, OMP85 is present in the mitochondrial outer membrane is essential for outer membrane biogenesis (Gentle, Gabriel *et al.* 2004) including protein transport and mitochondrial fission. In metazoans, OMP85 is also involved in mitochondrial aspects of programmed cell death (Leuenberger, Curran *et al.* 2005). Antibodies against yeast recombinant OMP85 were conjugated to gold nanoparticles and used to decorate thin sections of cryo-preserved yeast cells (Gentle, Burri *et al.* 2005). Accumulation of the gold nanoparticles indicate the presence of OMP85 on the surface of mitochondria (Gentle, Burri *et al.* 2005).

Bacterial outer membrane proteins (OMP's) can be used as targets for immunodiagnostic and therapeutic purposes because of their easy access and they

perform a variety of different functions. Antibodies to these outer membrane proteins (D-15-Ag and Oma87) have been shown to be protective against infectious challenge in animal models (Manning, Reschke *et al.* 1998), which in turn suggests that these proteins play an important role in host-pathogen interactions and thus in pathogenesis (Judd and Manning 2003). Thus OMP85 protein has been selected as the initial target antigen in the first phase of this project.

2.1.2. Identification of a specific peptide sequence in OMP85

The meningococcal omp85 gene was found to encode a 797 amino acid polypeptide (Figure 2.3.) with a predicted molecular weight of 88.5 kDa (Judd and Manning 2002). Meningococcal OMP85 is a highly conserved protein in Gram-negative bacteria and specially the regions between residues 360-395 and 643-662 of the protein sequence (OMP85 2002). Though it is a conserved protein, it can serve as a useful marker since the predicted antigenic sequence between residues 720 and 745 is unique to this organism (Judd and Manning 2003). Also, there are five additional amino acids at the N-terminus which distinguishes it from other related outer membrane proteins (Judd and Manning 2003). A useful approach will be to target these specific sequences as selective epitopes for immunodiagnosis of *Neisseria meningitidis.*

MKLKQIASALMMLGISPLAFADFTIQDIRVEGLQRTEPSTVFNYLPVKVGDTYNDTHGSAIIKSLYAT
GFFDDVRVETADGQLLLTVIERPTIGSLNITGAKMLQNDAIKKNLESFGLAQSQYFNQATLNQAVA
GLKEEYLGRGKLNIQITPKVTKLARNRVDIDITIDEGKSAKITDIEFEGNQVYSDRKLMRQMSLTEGGI
WTWLTRSNQFNEQKFAQDMEKVTDFYQNNGYFDFRILDTDIQTNEDKTKQTIKITVHEGGRFRWG
KVSIEGDTNEVPKAELEKLLTMKPGKWYERQQMTAVLGEIQNRMGSAGYAYSEISVQPLPNAETKT
VDFVLHIEPGRKIYVNEIHITGNNKTRDEVVRRELRQMESAPYDTSKLQRSKERVELLGYFDNVQFD
AVPLAGTPDKVDLNMSLTERSTGSLDLSAGWVQDTGLVMSAGVSQDNLFGTGKSAALRASRSKTT
LNGSLSFTDPYFTADGVSLGYDVYGKAFDPRKASTSIKQYKTTTAGAGIRMSVPVTEYDRVNFGLVA
EHLTVNTYNKAPKHYADFIKKYGKTDGTDGSFKGWLYKGTVGWGRNKTDSALWPTRGYLTGVN
AEIALPGSKLQYYSATHNQTWFFPLSKTFTLMLGGEVGIAGGYGRTKEIPFFENFYGGGLGSVRGYES
GTLGPKVYDEYGEKISYGGNKKANVSAELLFPMPGAKDARTVRLSLFADAGSVWDGKTYDDNSSS
ATGGRVQNIYGAGNTHKSTFTNELRYSAGGAVTWLSPLGPMKFRYAYPLKKKPEDEIQRFQFQLGT
TF

Figure 2.3. OMP85 protein sequence of *Neisseria meningitidis* with the highlighted specific peptide sequence

According to the topology predictions (Voulhoux and Tommassen 2004), the OMP85 protein consist of two domains, the N-terminal periplasmic domain until residue 483 and the C-terminal β-barrel domain, with 12 β-strands in the outer membrane. The specific region between residues, 720-745 is a surface exposed domain which makes it easily accessible (Figure 2.4.).

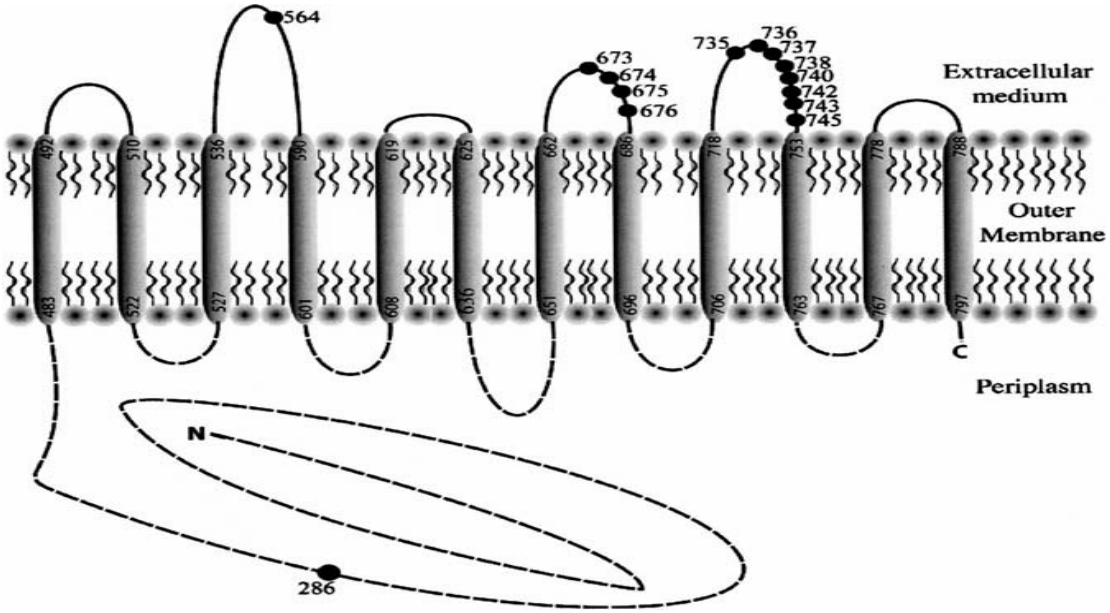

Figure 2.4. Topology prediction of Neisserial OMP85 (Voulhoux, Bos *et al.* 2003; Voulhoux and Tommassen 2004). Periplasmic domains are represented by dashed lines. Exposed domains are represented by solid lines. The first and last amino acids of each β-strand are indicated. The specific peptide region between 720-745 amino acid residues are shown as a surface exposed domain. The amino (N) and carboxy (C) termini of the protein are indicated.

In order to develop *Neisseria meningitidis* specific anti-peptide antibody, the specific region between 720-745 amino acid residues designated as SR1 was synthesized using t-Boc chemistry.

2.1.2A. Peptide Synthesis and Analysis

The first peptide was synthesised by Fischer in the early 1900's by the use of solution phase peptide synthesis (Fischer and Fourneau 1901). Peptide synthesis was revolutionised by Merrifield who introduced solid phase peptide synthesis (SPPS) in 1963 (Merrifield 1963). This technique is less labour intensive, allows the synthesis of much longer peptides and is suitable for automation, considerably reducing the time required for synthesis.

Two main methods are used in which either the acid-labile Nα-*t*-butyloxy carbonyl group (t-Boc) (Merrifield 1963) or the base-labile 9-fluorenylmethoxycarbonyl group (Fmoc) (Atherton, Gait *et al.* 1979) is the protecting group on the α-amino group of the amino acids (Figure 2. 5).

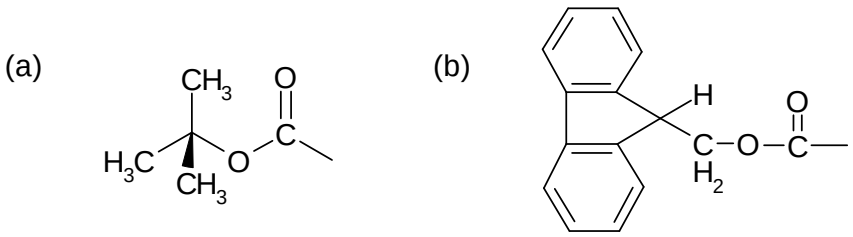

Figure 2.5. Structure of α-amino protecting groups. (a) t-Boc (b) Fmoc

Kent *et al.*. developed a highly optimised form of the t-Boc chemistry (Kent and Clark-Lewis 1985; Schnolzer and Kent 1992). This method increases the coupling of amino acids and reduces the time each cycle takes and later this has been adapted for automation by (Fecondo 1996).

SPPS involves the covalent attachment of the C-terminal amino acid to a solid support and the addition of the following amino acids to assemble the sequence. The main advantage of SPPS is that reactants can be used in excess to drive the reactions forward and can then be separated by simple filtration and washing with respective solvents.

A mBHA resin containing 1% divinyl benzene such as 4-methylbenzhydrylamine (mBHA-HCl) (Figure 2.6) has been used as the solid phase support in t-Boc synthesis.

The synthetic cycle (Figure 2.7) involves the anchorage of the first amino acid to the resin by activating it as an active ester using a reagent such as 2-(1H-benzotriazol-1-yl)-1,1,3,3-tetramethyluronium hexafluorophosphate (HBTU) or a mixture of HBTU and 1-hydroxybenzotriazole (HOBT). The bond is very stable and can only be cleaved using a strong acid such as hydrogen fluoride (HF) or trifluromethanesulphonic acid (TFMSA). The amino acids used have a t-Boc protecting group on the α-amino group, which can be removed with an acid such as trifluoroacetic acid (TFA) and may have side chain protecting groups that are more stable and are removed by only a strong acid. After deprotection by TFA, the peptide resin needs to be neutralised using a tertiary amine, usually *N, N*-diisopropylethylamine (DIEA). Alternatively, the next activated amino acid can be coupled in the presence of DIEA (*in situ* neutralisation) (Schnolzer 1992).

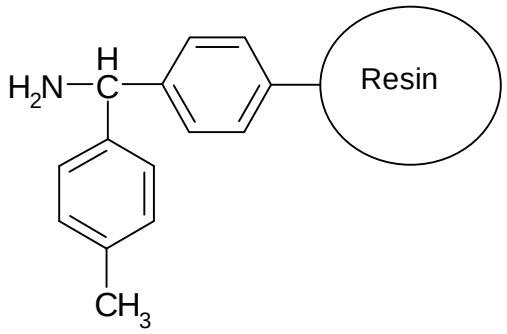

Figure 2.6. Structure of linker on mBHA-HCl resin

This reduces the time required for each cycle of the synthesis. After all the amino acids have been added, the peptide is completely deprotected and cleaved from the resin using anhydrous HF.

The purity of the final product is usually evaluated using reverse-phase high performance liquid chromatography (RP-HPLC) with a C_8 or C_{18} column and with an

acetonitrile gradient. The composition can be analysed using mass spectrometry. Usually analysis by matrix assisted laser desorption/ionisation-time of flight (MALDI-TOF), provides the monoisotopic mass which is sufficient to determine whether the desired peptide has been synthesised.

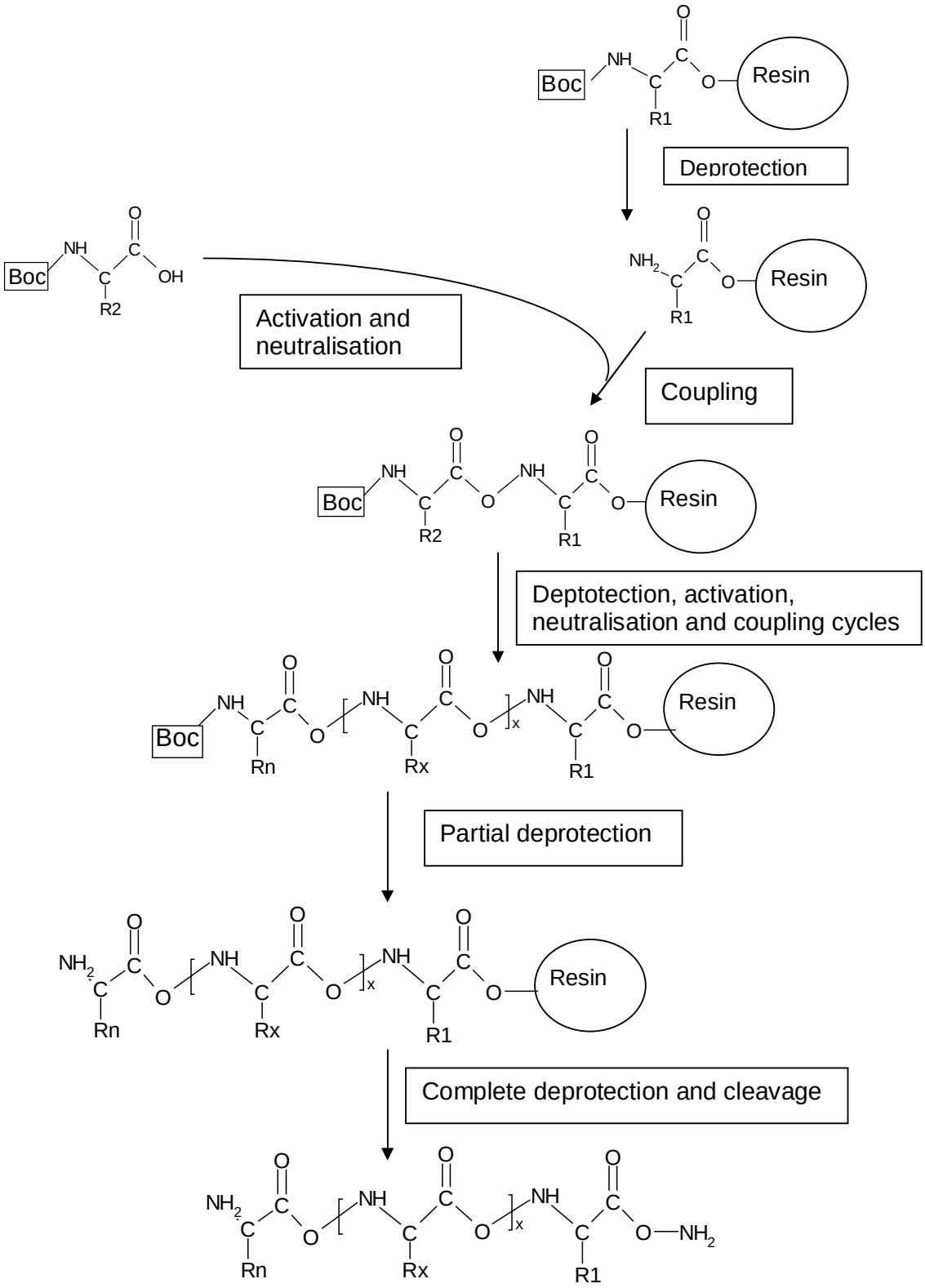

Figure 2.7. Overview of cycle used for peptide synthesis (S. Thoduka, Unpublished).

2.1.3. The Capsule of *Neisseria meningitidis*

In case of certain infectious diseases, especially those caused by some invasive Gram-negative bacteria (Frosch, Gorgen *et al.* 1985), poorly immunogenic bacterial capsules are responsible for the weak humoral immune response. This occurs mainly either because they interfere with cellular events that results in induction of an antibody response (Taylor, Stashak *et al.* 1983) or because of their chemical resemblance to those of host determinants (antigenic mimicry) and as a result they are not recognised as foreign (Mauel 1982). This mechanism results in the ability of bacteria to evade host defences.

The capsular polysaccharide of meningococci is a major virulence factor, consisting of sialic acid derivatives of mono, di, or trisaccharide repeating units as a homopolymer (serogroup B and C) or a heteropolymer (serogroup Y and W135) units (Tone 2005). The serogroup B capsule is composed of (α2→8)-linked N-acetyl neuraminic acid (NANA), whereas the serogroup C capsule composed of partly O-acetylated repeating units of sialic acid, linked with 2-->9 glycosidic bonds, mostly over 100,000 Dalton (100 kDa) in weight (Henriques, Jessouroun *et al.* 2006). The serogroup Y consists of partly O-acetylated alternating units of D-glucose and NANA, linked with 2-->6 and 1-->4 glycosidic bonds and the serogroup W-135 capsule consists of partly O-acetylated alternating units of sialic acid and D-galactose, linked with 2-->6 and 1-->4 glycosidic bonds (Spinosa, Progida *et al.* 2007).

Apart from serogroup A, other serogroup capsules are composed of sialic acid (N-acetyl neuraminic acid, NANA) derivatives (Figure 2.8.). The serogroup A capsule consists of repeating units of *N* -acetyl- O-acetyl mannosamine-1-phosphate (O-

acetylated repeating units of N-acetylmannosamine, linked with 1-->6 phosphodiester bonds) and is encoded by a four gene biosynthesis cassette unique to this group (Spinosa, Progida *et al.* 2007). The differences in sialic acid capsule composition are due to the distinct polysialyl transferases encoded by the fourth gene of the capsule biosynthesis operon and which also forms the basis for capsule specific PCR (Hammerschmidt, Muller *et al.* 1996).

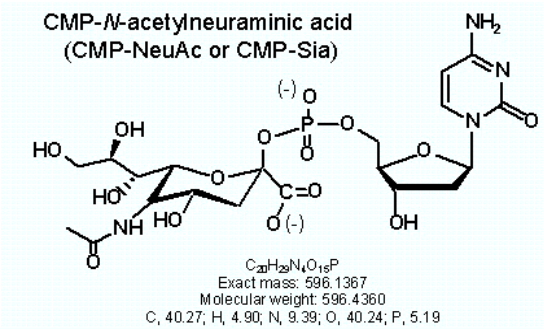

Figure 2.8. N-acetyl neuraminic acid (NANA)

An enzyme, sialic acid synthase NeuB in *N. meningitidis* directly converts phosphoenolpyruvate (PEP) and *N*-acetylmannosamine (Man- NAc) into *N*-acetylneuraminic acid (NeuNAc, or sialic acid) (Masson and Holbein 1983; Gunawan, Simard *et al.* 2005). These nine carbon 3-deoxy-2-keto sugars are found as a series of repeating units on the boundary of the secreted and cell surface glycoproteins and glycolipids on bacterial organisms. The gene *siaD* is responsible for polymerisation of monomers into the homopolymer or heteropolymer to form the capsule (Frosch and Vogel 2006). Several species of pathogenic bacteria, such as *Escherichia coli* and *Neisseria meningitidis*, produce sialylated capsular polysaccharides to avert host defenses and thereby leading to poor antibody responses (Gunawan, Simard *et al.* 2005).

Meningococcal polysaccharide vaccines contain cultured, inactivated, and purified capsular polysaccharides from *N. meningitidis* groups A, C, Y and W-135, respectively, either alone or in combination (Fisseha, Chen *et al.* 2005). The bacterial polysaccharide components, together with calcium ions and residual moisture, account for nearly all of the mass of these vaccines. Immunogenicity of the polysaccharide polymers increases with their molecular weight (Stephens, Gudlavalleti *et al.* 2006). Meningococci also have the capacity to exchange the genetic material responsible for capsule production and thereby switch from serogroup B to C or vice versa (Swartley, Marfin *et al.* 1997). Capsule switching may become an important mechanism of virulence with the widespread use of vaccines that provide serogroup-specific protection (Swartley, Marfin *et al.* 1997). Serotyping is very important for the development of vaccination strategies and the current methods involving the serotyping of meningococcal infection utilise the capsule specific monoclonal antibodies (Popovic, Ajello *et al.* 1999).

2.2. Development of receptors against target antigens

2.2.1. Monoclonal and polyclonal antibodies against target antigens

A range of receptors targeted against the selected antigens from the surface of *Neisseria meningitidis* were developed including polyclonal antibodies against the whole organism, purified OMP85, a 'unique' peptide sequence derived from OMP85 and a polysaccharide capsule component together with commercially available monoclonal antibodies that recognise capsule epitopes on the bacterial cell surface. Rabbit anti-OMP 85 polyclonal antibodies (RMIT University), sheep anti-SR1 peptide

and anti-*N. meningitidis* polyclonal antibodies were made (Institute of Medical and Veterinary Science (IMVS), Australia). Mouse anti-NM type B monoclonal antibodies were purchased from the National Institute for Biological Standards and Control (NIBSC), UK. In addition, attempts were made to define novel and specific receptors known as IgNAR's (immunoglobulin-like new antigen receptors) by screening recombinant antibody fragment libraries in collaboration with Dr Stewart Nuttall's group at CSIRO Molecular and Health Technologies in Parkville. These IgNAR receptors were considered to be the smallest antibody fragment capable of full antigen-binding capacity and specificity but with greater thermal stability and production efficiency.

2.2.2. Immunoglobulin New Antigen Receptors (IgNAR's) as novel receptors

In the adaptive immune system, the antigen receptors, Immunoglobulins (Igs) and T cell receptors (TCRs) are generated for the recognition of pathogens (Roux, Greenberg *et al.* 1998). The typical immunoglobulin receptor is composed of two heavy (H) and two light (L) polypeptide chains. Each chain, in turn, is composed of a single, variable (V) domain at the N-terminal end followed by one to seven constant (C) domains (Roux, Greenberg *et al.* 1998). Normally, constant domains define the effector functions characteristic of a given class of Ig whereas V domains each display a unique sequence and structure defining antigen specificity. Igs can be subdivided further into Fab and Fc fragments, responsible for antigen binding and effector functions (Roux, Greenberg *et al.* 1998). The V region contains frame work (FR) regions and hypervariable sequences known as complimentarity-determining regions (CDR's). FR's are responsible for protein folding and CDR's are responsible

for antigen interactions. The evolutionary origin of antigen receptors is unknown, but the first indication of their emergence phylogenetically is in cartilaginous fish (sharks, skates, and rays), where at least three types of Ig (Greenberg, Avila *et al.* 1995) and four TCR isotypes are found (Rast and Litman 1994; Rast, Anderson *et al.* 1997).

One of the goals of antibody engineering has been to reduce the size of the minimum antibody fragment whilst retaining binding affinity and specificity (Nuttall, Krishnan *et al.* 2001). Until recently Fv fragments, composed of only the heavy and light chain variable (V_H and V_L) domains were considered to be the smallest antibody fragment capable of full antigen-binding capacity. Recently, an alternate type of antigen receptor in nurse sharks *(Orectolobus maculates* and *Ginglymostoma cirratum),* called IgNAR (Immunoglobulin-like New Antigen Receptor) (Roux, Greenberg *et al.* 1998; Nuttall, Krishnan *et al.* 2001) that is secreted by splenocytes but does not associate with Ig light (L) chains had been identified (Greenberg, Avila *et al.* 1995).

The IgNAR protein has been shown to be a homodimeric heavy-chain complex with each chain composed of one V and five C domains (Greenberg, Avila *et al.* 1995). IgNAR's V region undergoes high levels of somatic mutation and is equally divergent from both Ig and T cell receptors and thus may be an evolutionary intermediate (Diaz, Greenberg *et al.* 1998). The NAR V region conforms to the model of prototypic Ig super family domains with an exceptionally small CDR2 region (Williams and Barclay 1988; Greenberg, Avila *et al.* 1995). By electron microscopy, it was shown that NAR V regions, unlike those of conventional Ig and TCR, do not

form dimers but rather are independent, flexible domains function as a bivalent antigen-binding site (Roux, Greenberg *et al.* 1998). This unusual feature is analogous to bona fide camelid IgG in which modifications of Ig heavy chain V (VH) sequences prevent dimer formation with L chains (Roux, Greenberg *et al.* 1998). In camelid species (camels and llamas), a significant proportion of the serum immunoglobulin consists of antibodies naturally devoid of light chains (Casterman, Atarhouch *et al.* 1993) and the unassociated VH domains interact with antigen as monomers (Spinelli, Frenken *et al.* 1996).

The development of phage display has allowed the generation of libraries of Fv fragments and engineered derivatives such as scFv, dsFv from which many antigen specific binders have been isolated (Winter, Griffiths *et al.* 1994; Hoogenboom and Chames 2000). To decrease the size of the minimal binding unit below that of the Fv, it was generally accepted that the antibody fragment must be composed of a single domain.

Based on this IgNAR variable domain region, a single domain library has been created by the successful cloning and generation of a bacterial phage-display library in *E. coli* (Nuttall, Krishnan *et al.* 2001). This library was based upon the antibody fragments V region sequence from the wobbegong shark *(Orectolobus maculates*) which, like the nurse shark, is a member of the shark family Orectolobidae. The library was constructed so as to incorporate a randomised, synthetic CDR3 of either 16 or 18 aa. Selection on a number of proteinaceous antigens resulted in the selection

of anti-Kgp protease clones which were able to bind both specifically and with good affinity (Nuttall, Krishnan *et al.* 2001; Nuttall, Krishnan *et al.* 2002).

Screening of such a library generated from nurse sharks (*Ginglymostoma cirratum*) immunised with the model antigen hen egg-white lysozyme (HEL) facilitated the successful isolation of intact antigen-specific binders matured *in vivo* (Dooley, Flajnik *et al.* 2003). The selected variable domains were shown to be functionally expressed in *Escherichia coli*, selection from this library resulted in the isolation of clones highly specific for antigen, binding with nanomolar affinity and showing great resistance to irreversible thermal denaturation (Dooley, Flajnik *et al.* 2003). This approach can therefore be considered as an alternative route for the isolation of minimal antigen-binding fragments with favourable characteristics.

This chapter mainly delas with the preparation of various *Neisseria meningitidis* cell surface antigens and generation respective monoclonal and polyclonal antibodies. These reagents were utilized for designing a model immuassay for *N. meningitidis*.

2.3. Materials and Methods

All chemicals used were of analytical grade laboratory reagents. All solutions were prepared with deionised water obtained from a Millipore Milli-Q water system excluding media, which was prepared with distilled water (dH_2O). All glassware was washed with Proneg detergent (Diversey-Lever, Pty. Ltd., Australia), rinsed in tap water and then in deionised water.

Finnpipette pipetters (Thermo Labsystems) were used for dispensing all solutions. Volumes of 1.5 mL or less were centrifuged with the Eppendorf microcentrifuge 5415C. Larger volumes upto 50 mL were centrifuged in the Beckman J2-21 M/E centrifuge. For high-speed centrifugation, Beckman Allgra 21R and Beckman J2-21 M/E Super model centrifuges, both from Beckman Coulter, USA were used. Sartorius analytical top-loading balance was used for weighing the reagents.

Materials

Neisseria meningitides, Escherichia coli and other bacteria were obtained from RMIT microorganisms stock. *E. coli* TG1 bacteria were obtained from Stratagene, USA. Luria-Bertani (LB) media, 2 YT (Yeast extract-tryptone) media, ampicillin/glucose/yeast extract-tryptone (Amp/glc/YT) plates were prepared according to the standard microbiology protocols. Nickel-nitrilotriacetic acid (Ni-NTA) sepharose resin, protein A sepharose and protein G Sepharose Fast Flow resin were obtained from Amersham Biosciences Ltd. UK. Sodium dodecyl sulphate (SDS) and dithiothreitol were purchased from Bio-Rad, USA. Also, 0.22 μm and 0.45 μm

pore size polypropylene membrane filters and Centricon 4.0 mL 30 kDa cut-off concentrators were purchased from Millipore, USA.

Isopropyl β-D-1-thiogalactopyranoside (IPTG), phenylmethanesulphonylfluoride (PMSF), sulfosuccinimidyl 4-N-maleimidomethyl cyclohexane-1-carboxylate (SMCC), polyethylene glycol 8000, triton X 100, tween-20, DNAse, RNAse, reduced glutathione, oxidised glutathione, glycerol, lysozyme, tricine, thimerosal, proteinase K, cyanuric chloride, phenolphthalein indicator, poly-L-lysine (type VIII; mol. Wt. 30,000-70,000), ampicillin, kanamycin, chloramphenicol, Freund's complete/incomplete adjuvant, Keyhole limpet haemocyanin, urea, *p*-cresol, *p*-thiocresol and triethylamine were purchased from Sigma-Aldrich Ltd., USA. Anti-rabbit, anti-mice and anti-sheep IgG-HRP (horsh raddish peroxidase) antibodies was obtained from Millipore, USA, where as HRP substrate, BD OPTia TMB substrate reagent was purchased from BD Biosciences, USA. India ink stain was purchased from Pro Art, USA.

The resin used for the synthesis of the peptides was 4-methylbenzylhydrylamine (p-mBHA), with a substitution level of 0. 89 meq/g and was obtained from Peptide Institute Inc, Osaka, Japan. All the amino acids used were Boc protected with benzyl-based side chain protection. The aspartic acid (Boc-Butyloxycarbonyl- L- Aspartic Acid b- Benzyl Ester), arginine (N^{α}- Boc- N^{g}- Tosyl- L- Arginine), glutamic acid (Boc-L- Glutamic Acid g- Benzyl Ester) and cysteine (t- Boc- *S*- Benzyl- L- Cysteine) were obtained from Peptide Institute Inc, Osaka, Japan. The histidine (Boc-L-His (Dnp)-

OH.isopropanol) was obtained from Auspep, Melbourne. All other amino acids used were obtained from Bachem Inc, California.

Solvents including N,N-dimethyl formamide (DMF), trifluoroacetic acid (TFA), ninhydrin reagent, O-benzotriazole-N,N,N',N'-tetramethyl-uronium-hexafluoro-phosphate (HBTU), N-hydroxybenzotriazole (HOBT) and (N, N-diisopropylethylamine (DIEA), which were peptide synthesis grade, were obtained together with HBTU from Auspep. Hydrogen fluoride (HF) was obtained from Matheson Gases, USA. HPLC grade dicholoromethane (DCM) and far UV grade acetonitrile (ACN), were obtained from Mallickrodt. Other reagents were analytical grade unless otherwise stated.

Equipment:

HF manifold reaction vessel	Peptide Institute Inc, Japan
Heto cold trap	Thermo Electron Corporation, USA
Javac DDL 300 vacuum pump	Javac, Australia
Perkin Elmer Series 200 HPLC pump	PerkinElmer, USA
C_{18} column 4.6x30 mm	Applied Biosystems, USA
785A Programmable Absorbance Detector with a PE Nelson 900 Series Interface	Applied Biosystems, USA
Voyager-DE RP mass spectrometer	Applied Biosystems, USA
Ultrasonicator	Branson Sonic Power Co., USA
Rotary shaker	Ratek, Australia

Analytical Balance	Sartorius, Germany
Bio-Rad Model 680XR Microplate reader	Bio-Rad Laboratories, USA
Eppendorf 5414C bench top centrifuge	Eppendorf, Germany
Beckman Allegra 21R centrifuge	Beckman Coulter, USA
Beckman J2-21 M/E Super centrifuge	Beckman Coulter, USA
Electrophoresis PowerPac 300	Bio-Rad Laboratories, USA
Bio-Rad mini-PROTEAN III system	Bio-Rad Laboratories, USA
Bio-Rad PROTEAN II xi cell apparatus	Bio-Rad Laboratories, USA
Electro elution chamber	Bio-Rad Laboratories, USA
Western blot module	Bio-Rad Laboratories, USA
Hitachi U2000 UV-visible absorption spectrophotometer	Hitachi Ltd., Japan
PhilipsEM400 Transmission electron microscopy	Philips, Netherlands

2.3.1. Expression and purification of the recombinant OMP85 antigen in *E. Coli*

Recombinant OMP85 was expressed and extracted from *E. coli*, and purified by Ni-NTA chromatography and sonic extraction (Takahashi, Sandberg *et al.* 1997; Qiagen 2000).

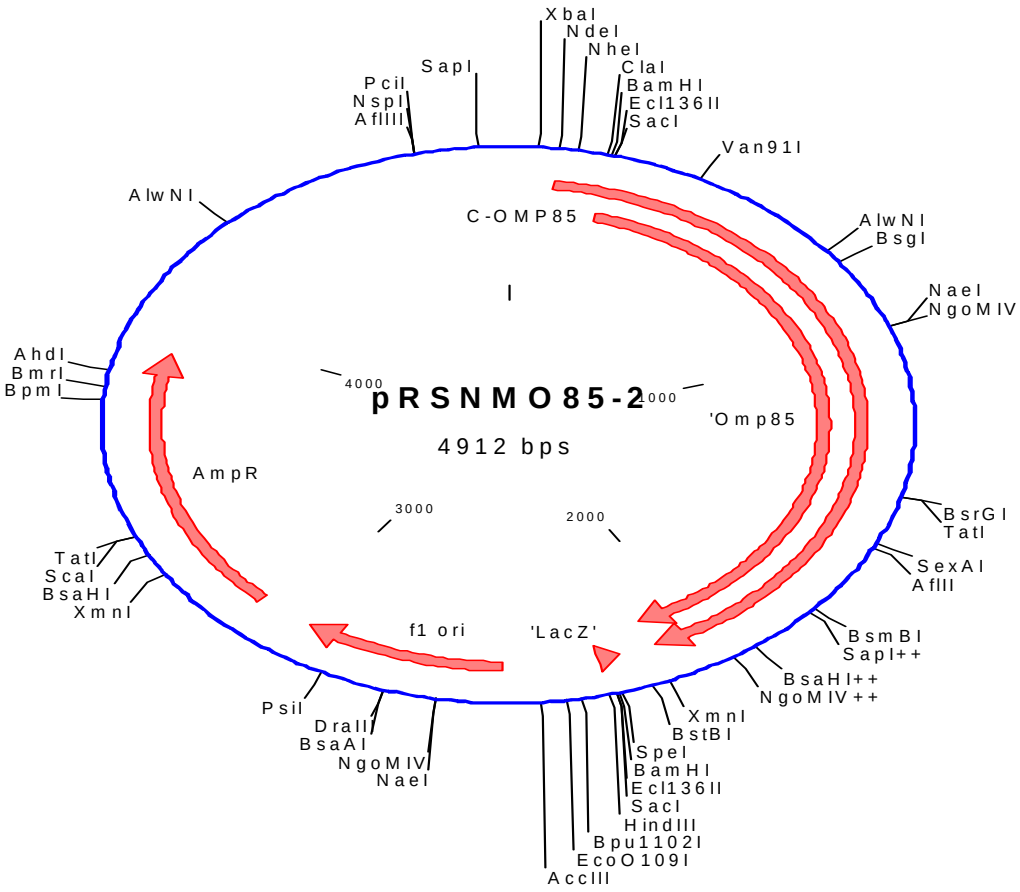

Figure 2.9. Map of pRSNMO85-2

2.3.1A. Recombinant OMP 85 protein expression

A single colony of *E. coli* cells containing pRSNMO87 plasmid with omp85 gene and hexa histidine tag gene inserts (Figure 2.9.) was inoculated in 10 mL LB medium containing 100 µg/mL ampicillin in a 50 mL flask. Cultures were grown overnight at 37°C with shaking. 200 mL of pre-warmed media (with antibiotics) was inoculated with 10.0 mL of the overnight cultures and incubated at 37°C, with vigorous shaking (300 rpm). Incubation was continued until the OD at 600nm reached 0.5-0.7 (approximately 4 hours). To induce protein expression, IPTG to a final concentration of 1 mM was added. Cultures were grown for an additional 4 hours at 37°C. Then the cells were harvested by centrifuging at 5,000 x g for 15 min and the pellet was weighed. The cell pellet was stored at -20°C overnight.

2.3.1B. Protein Extraction and purification

Cell pellet was subjected to freeze/thaw cycles 4 times to improve the lysis efficiency. Then the cell pellet was resuspended in 10 mL of chilled lysis buffer (20 mM Tris-HCl pH 8.0 containing 200 mM NaCl, 5mM DTT, 5% (v/v) Glycerol, 0.35mg/mL lysozyme and 1% (w/v) Triton X-100). 1mM PMSF was added just before experiment.

The cell lysis suspension was incubated for 15 minutes at room temperature, with gentle shaking. It was then subjected to ultrasonication at 250 W with 6X10s with intervals of 30 sec for cooling. The suspension was then cooled on ice for 10 minutes Then, 5 µl of 1M $MgCl_2$ and 1 µl DNase solution (1 mg/mL) per mL of the lysate was added and incubated for 30 min at room temperature.

The cell debris was removed by centrifugation at 30,000 xg for 25 minutes at 4 °C. The supernatant fluid was removed and then 5 µl of 2x SDS-PAGE sample buffer was added to 20 µl supernatant and stored at –20°C for SDS-PAGE analysis. The pellet was retained and thoroughly washed twice by spinning at 30 000 xg for 30min at 4°C with TBS or PBS containing 1% triton X 100.

The pellet was then solubilized in 2 mL of solubilisation/extraction buffer (50 mM Tris-HCl pH 7.5 containing 8 M urea, 1 mM DTT, 2 mM reduced glutathione, 0.2 mM oxidised glutathione, 1 mM PMSF) by incubating for 1h at room temperature. Once the pellet was dissolved, an equal amount of sterile deionised water was added, and mixed gently by vortexing.

Insoluble material that may clog the Ni-NTA column (45-165 µm) was removed by centrifugation at 100,000g for 30 minutes. Then the protein sample was filtered through a 0.45 µm filter). The protein concentration was determined by Bradford assay and adjusted to 1mg/mL using solubilisation buffer. It was followed by Ni-NTA column (45-165 µm) purification. Alternatively, the supernatant was stored at 4°C overnight.

2.3.1C. Ni-NTA Chromatography

Extracted recombinant OMP85 protein was loaded on to a Ni-NTA column for purification. After a number of trials, protein elution conditions were optimised to achieve a >70% reasonable purity. Aliquots (1.0 mL) were collected and the aliquots containing the desired His-tagged protein were determined by using Bradford assay (Bradford 1976).

For analysis of the protein profile, 5.0 µl of SDS-PAGE sample buffer was added to 20 µl of purified OMP85 protein and heated for 10 min at 95°C, followed by loading of the protein samples onto an 8% SDS-PAGE gel (0.75 mm and 1.0 mm thick gels). Electrophoresis was performed using Bio-Rad mini-PROTEAN III electrophoresis system at 80/120 V for 3 hours. It was followed by Coomassie blue staining to check the purity of the protein of interest.

2.3.2. Extraction of protein bands from polyacrylamide gels

As the protein purified by Ni-NTA column chromatography was not pure, two different approaches (1) sonic gel extraction and (2) electro elution were used to

further increase the purity the OMP 85 protein. A slightly modified sonic extraction method was followed (Takahashi, Sandberg *et al*. 1997).

2.3.2.1. Identifying and excising the band of interest

Maxi-gels (16 x 16 cm) were made and run using Bio-Rad PROTEAN II xi cell apparatus to maximise the yield of pure protein. After gel electrophoresis (at 120 V overnight with central cooling core's recirculation ports connected to a refrigerated water bath), a strip containing the protein band was excised from the gel using a scalpel. The cut strip of gel was stained using Coomassie Blue R-250 to identify the portion of the protein band.

The stained gel strip was aligned with the unstained gel portion and the band of gel just above and below the region presumed to contain the protein of interest was also excised and processed. The remaining portion of the gel after excising the protein band was stained with Coomassie blue staining to determine the accuracy of excision. Then the protein of interest was eluted from the gel matrix either by sonic extraction or electro elution methods.

2.3.2.2. Elution of the protein from the gel matrix

2.3.2.2A. Passive elution of proteins by sonic extraction

The excised gel pieces were placed in a clean screw-cap culture or microcentrifuge tube and washed three times for 5 mins with 2.0 mL of 250 mM Tris buffer containing 250 mM EDTA, pH 7.4, followed by three washes for 5 minutes each with distilled water.

After removing the distilled water with a pasteur pipette, elution buffer (50 mM Tris-HCl, 150 mM NaCl and 0.1 mM EDTA; pH 7.5) containing 0.1% (v/v) SDS was added, so that the gel pieces were completely immersed (approx. 2:1 ratio of buffer and gel pieces) .

The sample was then kept in an ice bath and sonicated for 3 min (6 passes of 30 secs) with a 3.0 mm probe sonicator (high-intensity ultrasonic processor, 50-W model). It was followed by mixing of the sample overnight, on a rotary shaker at room temperature.

The extract was centrifuged at 7,500 Xg for 10 minutes and the supernatant fluid was pipetted into a new microcentrifuge tube. An aliquot of the supernatant was tested for the presence of protein by SDS-PAGE (Tris buffer with or without SDS) and for quantitation. Finally, the purified protein samples were stored at -20 °C.

2.3.2.2B. Electro elution of proteins from polyacrylamide gel pieces

In this technique, protein containing gel pieces were placed in an electro elution chamber (Bio-Rad), where the proteins were eluted from the gel matrix into a buffer solution using an electrical field and captured against a dialysis membrane with a 12 kDa molecular weight cut off.

2.3.3. Rabbit anti-OMP85 polyclonal antibodies

To assess the immunogenicity of the purified OMP85 antigen, polyclonal antibodies were raised in rabbit. Antigen was injected at regular intervals (Table 1) and antibody titre was estimated using ELISA method.

The Rabbit antiserum was produced as follows. Two New Zealand white rabbits were injected with four doses of antigen at 2 week intervals subcutaneously with purified OMP85 antigen (100 μg/0.35 mL), emulsified with an equal volume of Freund's complete adjuvant for the initial dose and with Freund's incomplete adjuvant for the booster doses. At the end of week 12, terminal bleeds were performed on the rabbits (Table 2.1.). Antiserum was separated from the collected blood by centrifugation at 2000 x g for 20 min and stored at -20 °C.

Standard Protocol	
Prebleed	Week 0
Primary Inoculation	Week 0
1st Booster	Week 3
2nd Booster	Week 6
Test Bleed	Week 7.5
3rd Booster	Week 9
Bleed out	Week 12

Table 2.1. Rabbit immunisation schedule for raising polyclonal antibodies

2.3.4. Western blot analysis of anti-OMP85 polyclonal antibodies

The immunogenic specificity of the rabbit anti-OMP85 antibodies against both crude and purified OMP85 antigen were assessed by the western blot analysis. SDS-PAGE gel electrophoresis was performed with purified OMP85 antigen and then transferred onto a nitrocellulose membrane. The membranes were blocked overnight in phosphate-buffered saline (PBS, pH 7.6), 1% (w/v) non-fat dried milk, 0.01% (v/v) Tween-20-PBS. It was followed by incubation for 1 hour with primary antibodies against OMP85 antigen in blocking buffer. The antibody was removed and the

membrane was washed three times with 0.01% (v/v) Tween PBS. The membrane was probed by incubating with anti-Rabbit IgG-HRP (horsh raddish peroxidase) antibodies (1 in 5,000) in blocking buffer, for one hour. Finally, the blot was developed using HRP substrate reagent (BD Biosciences, USA).

2.3.5. Synthesis of SR1 peptide specific to *N. meningitidis* type B

2.3.5A. Resin preparation

The peptides were synthesised at a 0.5 m mol scale. Approximately 0.5 mmol of the p-mBHA-HCl resin with a substitution level of 0. 89 meq/g, was weighed out and placed in the reaction vessel. The resin was prepared by flow washing with DMF for 20 seconds. It was neutralised with 1 mL DIEA for 1 minute and flow washed again with DMF. The neutralisation and the resin flow wash steps were repeated.

2.3.5B. Synthetic cycles

The 2 mmol of the Boc-protected amino acid derivatives were weighed out into clean, glass scintillation vials. It was activated using 4 mL of 0.5 M HBTU dissolved in DMF or, in the case of R, N or Q, 4 mL of 0.5M HBTU and 4 mL of 0.5M HOBT dissolved in DMF. Immediately after addition of the activation agent(s), 470 µL of DIEA was added for *in situ* neutralisation.

The activated amino acid was added to the resin and allowed to couple by mixing for 10-15 minutes. After coupling, ninhydrin analysis was performed to calculate the coupling effeciency. Where the coupling percentage was below 99.0%, a double coupling was done, in which a second 2 mmol aliquot of the same protected amino acid was activated, neutralised and coupled. After double coupling, a ninhydrin

analysis was repeated. The solution was then drained and flow-washed with DMF for 30 sec prior to starting a new synthesis cycle.

While the amino acid was activated, the previous amino acid on resin was deprotected by mixing with 10 mL of anhydrous TFA for 1 minute. The TFA was drained and the deprotection step was repeated for a further minute. After removal of TFA, the reaction vessel was filled with DMF and drained. The resin was vigorously flow washed with DMF for 30 seconds after which the activated amino acid was added for next coupling.

The cycle of deprotection, activation, neutralisation and coupling were followed for each amino acid that was added (GKTYDDNSSSATGGRVQNIYGAGNTH). Double couplings were carried out when required.

2.3.5C. Ninhydrin Analysis

Approximately 5 mg of resin was removed at the end of each coupling to calculate the coupling percentage according to the procedure described by Sarin *et al.*. (Sarin, Kent *et al.* 1981). The resin was washed three times with 50:50 DCM : Methanol mixture and then dried under vacuum. The dried resin was placed in a culture tube and weighed. 2 drops of phenol solution, 4 drops of 20 mM KCN solution and 2 drops of ninhydrin solution were added to the resin prior to heating at 100 °C for 5 minutes together with a reagent blank tube.

After 5 minutes, the tubes were removed from the heating block and 3 mL of 60% ethanol was added. After the resin was allowed to settle at the bottom of the tube, the

absorbance of the solution was measured against the blank at 570 nm. The weight of the resin and absorbance of the solution were entered into Pepmate (Fecondo, unpublished) to determine the coupling percentage.

2.3.5D. Deprotection prior to HF cleavage

Approximately 360 mg of the resin-peptide was weighed out to be deprotected and cleaved. The protecting group on the side chain of Histidine, 2,4-Dinitrophenol (DNP), was removed using 10mL of 20% (v/v) 2-mercaptoethanol : 10% (v/v) DIEA in DMF, which was mixed for 30 minutes. This was repeated three times until the solution was clear. The resin was then washed with DMF.

The N α-terminal Boc protecting group was removed by the addition of 10 mL anhydrous TFA and mixed for 1 minute. The resin was then flow washed with DCM for 30 seconds, followed by a second 10 mL anhydrous TFA deprotection step for 1 minute. Following a further 30 sec flow wash with DMF, the resin was neutralised with approximately 10 mL of 10% (v/v) DIEA in DCM for 1 minute, followed by 1 minute DCM flow wash. The resin was dried under vacuum.

2.3.5E. Hydrogen Fluoride cleavage of the peptide-resin

Aliquots (0.5 mL) of the scavengers' *p*-cresol and *p*-thiocresol were melted and added to the dried peptide-resin in the small reaction vessels of the HF manifold (Peptide Institute Inc) reaction vessel. Vacuum pressure was maintained in the apparatus at -330 mm Hg and about 25 mL of anhydrous HF was released from the cylinder and condensed into the reservoir using liquid nitrogen. Water heated to about 50 ^{o}C was used to evaporate the HF collected, which was allowed to condense into the reaction

vessels. The peptide was completely deprotected and cleaved from the resin by reacting with anhydrous HF, for 1 hour at 0 ^{o}C under vacuum. HF was then removed by aspiration.

2.3.5F. Extraction of the cleaved peptide

The peptide-resin mixture was washed twice with 40 mL of anhydrous ethyl ether to remove the scavengers and all traces of HF. The peptide was extracted with a minimal volume of 10-20% acetic acid (Sigma) and collected into round-bottomed flasks under vacuum. The peptide was lyophilised overnight with a Heto cold trap fitted with a Javac DDL 300 vacuum pump (Javac, Australia). The freeze-dried peptides were stored at –20^{o}C.

2.3.6. Analysis of peptides

2.3.6A. High Performance Liquid Chromatography (HPLC)

Approximately 100 µg of the SR1 peptide was dissolved in 0.5 ml of 0.1% TFA in Milli Q water. A Perkin Elmer Series 200 HPLC pump was used with a C_{18} column 4.6x30 mm (Brownlee Labs, Applied Biosystems, USA) and 20 µl of the peptide solution was injected.

The mobile phase gradient used was 0-60% ACN / 0.1% TFA over 30 minutes with a flow rate of 1 mL/minutes The absorbance was monitored at 214 nm using an Applied Biosystems 785A Programmable Absorbance Detector. The data was acquired using Turbochrom software (Perkin Elmer) with a PE Nelson 900 Series Interface.

2.3.6B. Mass spectrometry

MALDI-TOF was performed in reflector mode using a Voyager-DE RP mass spectrometer with a horizontal tube of 2 m in length. The matrix used was α-cyano-4-hydroxycinnamic acid (10 mg/mL in 60% ACN / 0.3% TFA). Samples were irradiated at 337 nm with 2 nsec pulses from a nitrogen laser at a frequency of 20 Hz. The resultant ions were then accelerated to 20 kV, recorded at a digitisation rate of 500 MHz and reflected to a dual micro channel plate detector. The signal from a minimum of 200 shots was then summed to achieve the reported intensities. The data was examined on Data Explorer 4.0 software.

2.3.7. Keyhole limpet haemocyanin (KLH) – SR1 peptide conjugation

To assess the immunogenic specificity of the SR1 peptide, polyclonal antibodies were raised in sheep. The SR1 peptide was conjugated to keyhole limpet haemocyanin (KLH) prior to immunisation given the relatively low molecular weight of the peptide.

2.3.7A. Column Pre-swelling and Equilibration

Approximately 300mg of Sephadex G10 gel filtration media was weighed out into a small eppendorf tube and added an excess of 2M Gu.HCl in PBS, pH 7.4 for pre-swelling. It was allowed to equilibrate with three buffer changes.

2.3.7B. KLH/SMCC Preparation

While allowing time for the column media to equilibrate in the eppendorf tube, the entire contents of 1 vial of KLH (20mg) was reconstituted in 2mL of milliQ H_2O to obtain a 10 mg/mL solution. An aliquot (600 µL) of this mixture was transferred into

an eppendorf tube. In another eppendorf tube, 0.8mg of SMCC was weighed out and dissolved in 30µL of DMF solvent. Then 400 µL of PBS, pH 7.3 was added to this eppendorf tube and mixed thoroughly. Later, 600mL aliquot of KLH was added to the eppendorf tube containing the SMCC cross linker and mixed gently for 30 min at room temperature.

2.3.7C. Peptide Preparation

Approximately 12 mg of peptide was dissolved in 300 µl of 2 M Gu. HCl in PBS, pH 3-4 solution. Once the crude peptide material was dissolved, an equimolar amount of solid dithiothreitol (7-7.5 mg of DTT) was added and mixed gently until solubilised and allowed to stand for 10 minutes.

2.3.7D. Column arrangement

The top of Bio-rad mini prep column was cut so that the column could fit into a 15mL centrifuge tube and filled with pre-swelled 300mg of Sephadex G10 gel filtration media.

An empty eppendorf tube was wedged (with lid removed and hole pierced on the side) to the tip of the column and placed this apparatus in a 15mL centrifuge tube. Then the column was spun in a centrifuge at 1000 x g for 2 min in order to remove excess buffer.

2.3.7E. Peptide Conjugation to KLH/SMCC Carrier Complex

Once excess buffer had been removed, the wedged eppendorf tube at the tip of the column was replaced with the eppendorf tube containing the KLH/SMCC mixture. A one step gel filtration and coupling was performed by placing the KLH-SMCC

solution to a receiving bottom tube with the peptide solution applied to G-10 centrifuge column (i.e. spin column). The entire column setup was placed in a 15mL centrifuge tube and spun at 4000xg for 3min to allow for the peptide to elute from the column into the receiving bottom tube.

The spin column was rinsed twice with 300 µl 2M PBS-Gu.HCl (pH 3.5) and centrifuged for 3 minutes at 4000 x g in order to recover as much of the peptide as possible. The peptide-KLH conjugate mixture was transferred the entire contents into another sealable eppendorf tube. The pH of the contents was adjusted to 7.5 with 2 M NaOH. The conjugate sample was allowed to mix i.e. end over end mixing for 3 hours at room temperature for complete conjugation. Finally 30 µL of 1% Thimerosal in PBS was added to the conjugate sample and stored at 4 °C until required.

2.3.8. Sheep anti-SR1 and anti-NM serotype B polyclonal antibodies

SR1 peptide conjugated with Keyhole Limpet Haemocyanine (KLH) was used to raise the sheep polyclonal antibodies (Institute of Medical and Veterinary Science (IMVS), Australia). Antibodies were also raised in sheep against the formaldehyde treated whole cell *N. meningitidis* bacteria. A standard immunisation protocol was followed, antigens were injected at regular intervals and antibody titre was estimated as described in table 2.2.

Antigen ID	Amount mg/dose/animal	Details	Number of animals	Species
SR-1 Peptide	2.5 mg (in 0.5 mL KLH-peptide solution) / dose mixed this dose with 0.5 mL CFA/IFA	KLH conjugated Peptide (2.8kD) via SMCC, in PBS	1	Sheep
NM-B	10^9 cells / 0.5 mL of PBS mix this dose with 0.5 mL CFA/IFA	*Neisseria meningitidis* Serogroup B Inactivated by treatment with 2% Formaldehyde , in PBS at 2 x10^9 cfu/mL	1	Sheep

Table 2.2. Sheep immunisation details for raising polyclonal antibodies against the SR1 peptide and *N. meningitidis* bacteria.

2.3.9. Preparation of capsular polysaccharide (CPS) from *Neisseria meningitidis* serotype B

The following steps were followed in the preparation of the capsular polysaccharide from *Neisseria meningitidis* bacteria. A bacterial culture grown overnight was chilled rapidly on ice. The cells were harvested by centrifugation at 13,600 x g for 15 minutes and the pellet was washed 3 times with sterile ice cold saline (pH 7.2).

The supernatant liquid containing the released soft fibrillar capsular material was collected and stored on ice. The bacterial pellet was then suspended in 0.01% (w/v) SDS in PBS at room temperature until the capsule was released as monitored by India ink staining. Bacteria were then pelleted by centrifugation at 13,600 x g for 15 minutes at 4°C. The supernatant was collected and mixed with the initial supernatant collected. The whole supernatant mixture was then filtered through a 0.22 μm pore size membrane filter and kept on ice.

The bacterial pellet from the above separation was resuspended in 500 μl of lysis buffer containing 31.25 mM Tris-HCl (pH 6.8), 4% (w/v) SDS, 20% (v/v) glycerol. Samples were then heated at 100 °C for 5 minutes. The cell debris along with the

remaining capsular material was pelleted by centrifugation at 13, 600 x g for 30 minutes at 4°C.

Proteinase K (15 units/mL) was then added to the filtered capsular material and incubated at 56 °C for 1 hour, followed by addition of 2 volumes of ice cold ethanol to precipitate the carbohydrates. The precipitated capsular material was subsequently washed with a mixture of cold ethanol-saline (3:1). The purified capsule was solubilised in sterile distilled water and NaCl was added to a final concentration of 0.9 % (w/v). Finally, the capsule was treated with DNase and RNase (10 μg/mL) for 2 hours at 37 °C, and the absorbance was measured at 260 and 280 nm. The polysaccharide capsule was then lyophilised and resuspended in Tris buffer (0.01M Tris-HCl, pH 7.5). This solution was lyophilised again and stored at -20 ^{0}C until required.

2.3.10. Analysis of the purity of *N. meningitidis* type B specific capsular polysaccharide

2.3.10A. Gels

The purity of the capsular polysaccharide preparation was visualised by loading onto a Tricine SDS-PAGE gel. A sample of the polysaccharide preparation was dissolved in 2 ml of sample buffer (0.125 M Tris base, 10% (v/v) glycerol, pH 6.8), loaded onto the gel. A running buffer containing 0.1 M Tris, 0.1 M tricine, 0.1% (w/v) SDS, pH 8.25 was used and run at a constant voltage of 120 V. Siver staining was performed to visualise the capsule.

2.3.10B. High Performance Liquid Chromatography (HPLC)

Approximately 100 µg of the polysaccharide capsule was dissolved in 200 µl milli Q water. A Perkin Elmer Series 200 HPLC pump was used with a C_8 column 4.6x30 mm (Applied Biosystems) and 20 µl of the capsule solution was injected.

Analysis was performed using the elution conditions, 0-60% ACN / 0.1% (v/v) TFA over 30 minutes with a flow rate of 1 mL/minutes The absorbance was read at 214 nm using an Applied Biosystems 785A Programmable Absorbance Detector. The data was acquired using Turbochrom software (Perkin Elmer) with a PE Nelson 900 Series Interface.

2.3.11. Anti-NM serotype B capsular monoclonal antibodies

Anti-NM serogroup B Capsular monoclonal antibodies were purchased from National Institute for Biological Standards and Control (NIBSC), UK. These antibodies were tested for the specificity and titre against the whole cell bacteria and the purified capsular preparation by ELISA method.

2.3.12. BLAST search to identify related organisms-cross reactivity

A BLAST search of OMP 85 protein antigen sequence using NCBI/ BLAST/ blastp program (protein-protein BLAST) against 5,815,196 sequences, produced a broad list of different Gram negative bacteria with varying similarity (Table 2.3.). From the list, the bacteria which are more likely to be associated with human infections were short listed. Out of that list, 21 bacteria were available from the RMIT microbiology stocks (Table 2.3.). Cross reactivity experiment was done with the panel of antibodies against the 21 bacteria.

	Sequence Identities	Percentage of identity
➢ **Neisseria meningitidis**	**797/797**	**100%**
➢ **Neisseria meningitidis MC58**	**795/797**	**99%**
➢ **Neisseria gonorrhoeae**	**758/797**	**95%**
➢ **Chromobacterium violaceum ATCC 12472**	**404/800**	**50%**
➢ **Bordetella pertussis**	**285/783**	**36%**
➢ **Acinetobacter sp.**	**283/816**	**34%**
➢ **Escherichia coli**	**273/830**	**33%**
➢ **Pseudomonas fluorescens**	**263/790**	**33%**
➢ **Pseudomonas aeruginosa**	**266/799**	**33%**
➢ **Salmonella Paratyphi**	**276/824**	**33%**
➢ **Salmonella Typhi**	**276/824**	**33%**
➢ **Vibrio alginolyticus**	**275/826**	**33%**
➢ **Vibrio vulnificus**	**273/817**	**33%**
➢ **Shigella dysenteriae**	**273/830**	**32%**
➢ **Vibrio cholerae**	**265/817**	**32%**
➢ **Vibrio parahaemolyticus**	**265/817**	**32%**
➢ **Vibrio sp.**	**267/817**	**32%**
➢ **Haemophilus influenzae**	**261/823**	**31%**
➢ **Legionella pneumophila**	**244/783**	**31%**
➢ **Pasteurella multocida**	**257/813**	**31%**
➢ **Brucella abortus**	**217/821**	**26%**

Table 2.3. List of Bacteria used for cros reactivity study against the panel of prepared antibodies. The sequence identities varied from 26% to 100%.

2.3.13. Purification of polyclonal antibodies

2.3.13.A. Protein A sepharose antibody purification procedure

A five mL column was packed with 1.0 mL of Protein A (Protein G in case of sheep antibodies) Sepharose Fast Flow (Amersham Biosciences) resin. The column was washed 10 column volumes with PBS (binding buffer). An aliquot of anti-serum (1.0 mL) obtained from rabbits was filtered using syringe through a 0.45 µm filter and centrifuged for 5 minutes at 5000 x g. Then the serum was diluted into 5.0 mL PBS and this was then filtered through a 0.45 µ filter.

The diluted anti-serum was loaded onto the column and the flow through was collected. Unbound protein was washed out with 10 column volumes of PBS or until the UV absorption at 280 nm measured reached to near zero. After a flat base line was achieved with binding buffer, antibodies were eluted with 0.1 M glycine pH 3.0 (elution buffer). Eluted antibody was collected in 500 µl aliquots into 1.0 mL eppendorf tubes containing 500 µL of 1.0M Tris-HCl, pH 7.0, to neutralise the acidic elution buffer. All fractions were mixed and kept on ice. The fractions were pooled and concentrated into 0.1 M PBS, pH 7.4, using a Millipore Centricon 4.0 mL 30 kDa cut-off concentrator according to the manufacturer's instructions. Then, UV absorption of each aliquot at 280 nm was measured and the IgG concentration was determined using an absorptivity constant of 1.4 mg^{-1}. mL. cm^{-1}.

The Protein A sepharose was regenerated by washing with additional 3-4 column volumes of elution buffer followed by re-equilibration with 3-4 column volumes of PBS.

2.3.13.B. Protein G sepharose antibody purification procedure-Isolation of sheep antibody

Polyclonal antibody was purified from sheep serum using Protein G sepharose beads (Amersham Biosciences, USA). The pH of the 500µl fractions eluted using 0.1M Glycine (pH 3.0) was raised to 7.4 by mixing each of the fractions with 500µl of 1.0 M Tris-HCl buffer (pH 7.4). All 1.0 mL fractions were pooled together and the protein quantity was estimated.

2.3.14. Monospecificity of anti-SR1 antibodies

The protein G purified sheep anti-SR1 antibody was further purified by affinity purification and then tested for cross reactivity against the previously tested panel of bacteria by ELISA method.

2.3.15. ELISA analysis of bacterial polysaccharide antigens

ELISA with the purified capsule was performed according to the published procedure (Gray 1979). Three glass vails containing, 0.5 mL of 0.01N NaOH with 0.001% phenolphthalein indicator, 0.5 mg of Cyanuric chloride crystals and 0.1 mL of 0.1% poly-L-lysine (type VIII; mol. Wt. 30,000-70,000) were taken. Alkalinisation of polysaccharide antigen was done by adding 0.1mL of capsule antigen (1.0 mg/mL) in distilled water, to the tube containing 0.5 mL of 0.01N NaOH with 0.001% phenolphthalein indicator and mixed for 10 sec (solution was pink at this stage).

The contents of the above vial were pipetted into the vail containg 0.5 mg of cyanuric chloride crystals and mixed for approximately 10 sec, and the solution became colourless as the pH dropped to 8.0 – 8.2 (mixed gently as the vigorous mixing could

release more HCl into solution and pH might drop below 8.0). Then to couple the the polysaccharide antigen to poly-L-lysine, the entire solution was transferred into a vial containing 0.1 mL of 0.1% poly-L-lysine (type VIII; mol. Wt. 30,000-70,000), mixed and refrigerated at 4 °C for 2 hrs.

The protein coujugated polysaccharide antigen was then diluted in 0.01M PBS pH 7.4 to approximately 1.0 μg/mL and coated the ELISA wells overnight. Then, the normal ELISA procedure was followed.

2.3.16. IgNAR's as novel receptors- protocol for phage rescue and panning

Selection from IgNAR library resulted in the isolation of clones highly specific for a range of antigens, binding with nanomolar affinity and showing great resistance to irreversible thermal denaturation. In this project, OMP85 protein (0.156 mg/mL of purified OMP85), SR1 paptide (0.05 mg/mL crude peptide) and 10.0 μg/mL capsular polysaccharide antigens were screened against the IgNAR library to identify suitable IgNAR receptor molecules and to characterise them in terms of binding specificity and affinity for their cognate antigen.

DAY 1

2.3.16.1. Phage rescue from library glycerol stock

All 2 YT media was prewarmed to 37 °C. Each 1mL of library stock (~10^9 cells), was inoculated into 20mL of prewarmed 2YT in a small flask, followed by incubation with shaking at 37°C for 30 minutes Then, another 20mL of 2YT/Amp100 (to a final conc. of Ampicillin 50 μg/mL) was added and incubated with shaking at 37°C for 1 hour.

It was then transferred to a 500mL baffled flask, and added another 40mL of 2YT/Amp 100 and incubated with shaking at 37 °C for 45 minutes. It was followed by further incubated at 37 °C for 15 min without shaking to allow formation of F pili. At this stage, helper phage (MOI phage/*E. coli* = 20:1) was added and incubated the culture for 15 min at 37 °C without shaking. Then, another 90 mL of 2YT/Amp100 was added and incubated with shaking at 37 °C for 2 hours. Finally, Kanamycin (25 µg/mL) was added and incubated overnight at 28 °C with shaking.

2.3.16.2. Coating immunotubes

For each antigen prepared, a pre-absorption of immunotubes was carried out to eliminate non-specific high affinity binders present in the library, which may bind to either the modified polystyrene surface (Maxisorp) of the immunotube or to the blocking reagent.

Approximately 10 µg of each antigen was diluted in appropriate coating buffer (1 x PBS, 0.1 M sodium carbonate) and added to individual immunotubes. Pre-absorption tubes were coated with 2% (w/v) MPBS solution and incubated the tubes at 4°C overnight.

DAY 2

2.3.16.3. Washing and blocking immunotubes

Each immunotube was washed 3 times with 1 x PBS. The tubes were filled with 2% MPBS, capped and then incubated at RT for 2 h to block. Prior to adding precipitated phage, each tube was washed 3 times with 1 x PBS.

2.3.16.4. Rescue and Panning

Overnight cultures were centrifuged at 6500 x g for 10 minutes The supernatant fluid (containing phage) was transferred into an ice-cold 250 mL centrifuge bottle and 1/5 volume of ice cold 20 % (w/v) PEG 8000/15% (w/v) NaCl was added. The phage was incubated on ice for 1 h with intermittent shaking.

The cell pellet was resuspended in a small volume of 2YT and prepared 2-3 glycerol stocks to recover the library at a later stage if necessary. Alternatively, the phagemid was purified and transformed into competent cells for future use.

The phage was centrifuged in 20 % PEG (w/v) 8000 / 15% (w/v) NaCl at 9500 x g for 45 minutes. Supernatant was discarded and the bottle was drained upside down on a tray lined with a Teri wipe. Phage was visible on the side of flasks as a white smear. Then the phage was resuspended in 3 mL of 1 x PBS and transferred to 1.5 mL tubes. It was followed by a centrifugation at 14000 x g for 10 min at 4°C. The phage was filtered through a 0.22 µm filter and then stored at 4°C. This phage stock was used for polyclonal phage ELISAs after the 3^{rd} - 4^{th} panning rounds.

To titre amplified phage, 990 µL of TG1 cells were infected with 10 µL of precipitated phage then incubated at 37 °C without shaking for 15-20 minutes The infected cells were diluted to 10^{-3}, 10^{-5}, 10^{-7} and 10^{-9} then 100 µL of each dilution was plated on YT/Amp/glucose plates.

2.3.16.5. Panning

Two millilitres of precipitated phage was transferred to each (washed) pre-absorption immunotube, then added 2.0 mL of 4 % (w/v) MPBS and incubated for 15-30 min at RT. Following pre-absorption, phage was transferred into immunotubes coated with antigen, then incubated for 30 min at room temperature rotating continuously, and then stood for at least 90 min at room temperature. The pre-absorption tubes were discarded. The immunotubes were washed 3 times with 1 x PBS/ 0.1% (v/v) Tween-20 and then same number of times with 1 x PBS. For second and subsequent panning rounds the number of washes were increased to 4 times.

Excess PBS was drained from immunotubes. The phage was eluted with 1 mL of freshly prepared 100 mM triethylamine by rotating continuously for 10 min, then neutralised with 0.5 mL Tris-HCl pH 7.4 buffer. Aliquotes (100 µL) of Tris-HCl buffer (pH 7.4) was added to each immunotube and all phage samples were stored at 4°C for using in next round of panning. An overnight culture of TG1 from a minimal media plate was set up for the next round of rescue and panning.

DAY 3.

2.3.16.6. Phage rescue

An overnight TG1 culture (1/100) was inoculated into 100 mL of 2YT media and grown until mid log phase. TG1 cells (5.0 mL) along with half of the eluted phage from the previous pan were added to a sterile 50 mL tube. 4.0 mL of the TG1 cells were added to each immunotube (from the previous panning round). Both were incubated at 37°C for 15-20 min without shaking.

Both the cultures from the 50 mL tube and the immunotube were pooled into a 0.5 L flask. 100 µL from this was taken for titration and plated 100 µL of 10^{-1}, 10^{-3}, 10^{-5}, 10^{-7} dilutions on Amp/glc/YT plates and next day, colony count was performed.

Next, 15 mL of 2YT, Amp 40 µg/mL was added into the above flask and incubated for 1 h at 37 °C with shaking. It was followed by addition of 30 mL 2YT, Amp 100 µg/mL into the flask and incubated for 1 h at 37 °C with shaking. Helper phage (MOI = 20:1; phage: *E. coli*) was added, swirled to mix and left in the incubator at 37 °C for 15 min without shaking. Then, 110 mL of 2YT and Amp to 100 µg/mL was added and incubated for 2 h at 30 °C with shaking. Finally, 25 µg/mL of Kanamycin was added and incubated overnight at 28°C.

2.3.16.7. Preparation of DNA for cloning

An overnight TG1 culture was grown and inoculated with a single colony taken from a minimal media plate of less than 1 week old. Then, the overnight TG1 culture was diluted 1/100 into 50 mL of 2YT and grown until mid log growth phase (A_{595} OD 0.2-0.5). This step was followed by incubation at 37 °C for 15-20 min without shaking to allow the formation of F pili. The, 10.0 mL TG1 cells were inoculated with 1 mL eluted phage in a 0.5 L flask and incubated at 37 °C for 15 - 20 min without shaking. 100 µL from this for titration was taken: plated 100 µL each of 10^{-1}, 10^{-3}, and 10^{-5} dilutions on Amp/glc/YT plates. Colonies on these titration plates could be used for monoclonal phage ELISAs.

Then, 10.0 mL of 2YT with Amp 40 µg/mL (8 µL of 100 mg/mL stock) and glucose 2 % (w/v) were added and incubated for 1 h at 37°C with shaking. Then, 100 mL of

2YT and 100 µg/mL Amp and 2 % (w/v) glucose was added and incubated at 37 °C until the end of the day. To prepare glycerol stocks, 20 mL of the culture was separated and incubated overnight at 28°C. To the remaining culture, chloramphenicol was added to a final concentration of 170 µg/mL and the growth continued overnight at 28°C. This latter culture was used for isolation of amplified phagemid.

2.4. Results

2.4.1. Purification of recombinant OMP85 protein

Recombinant OMP85 was expressed and purified to raise anti-OMP85 polyclonal antibodies. Overexpression of recombinant hexa-his tagged OMP85 in bulk quantities in *E. coli*, was achieved. It was difficult to purify the protein using Ni-NTA column chromatography. Many other proteins were eluted along with the OMP85 protein. Electro elution as an additional purification step yielded very low quantities (70% loss) of the protein. Then, the modified sonic extraction method from maxi gels (16 x 16 cm) using Bio-Rad PROTEAN II xi cell apparatus was adopted (Figure 2.10.). The protein was purified to apparent homogeneity as indicated by a single band on the gel by Coomassie blue R-250 staining with increased yield (Figure 2. 11).

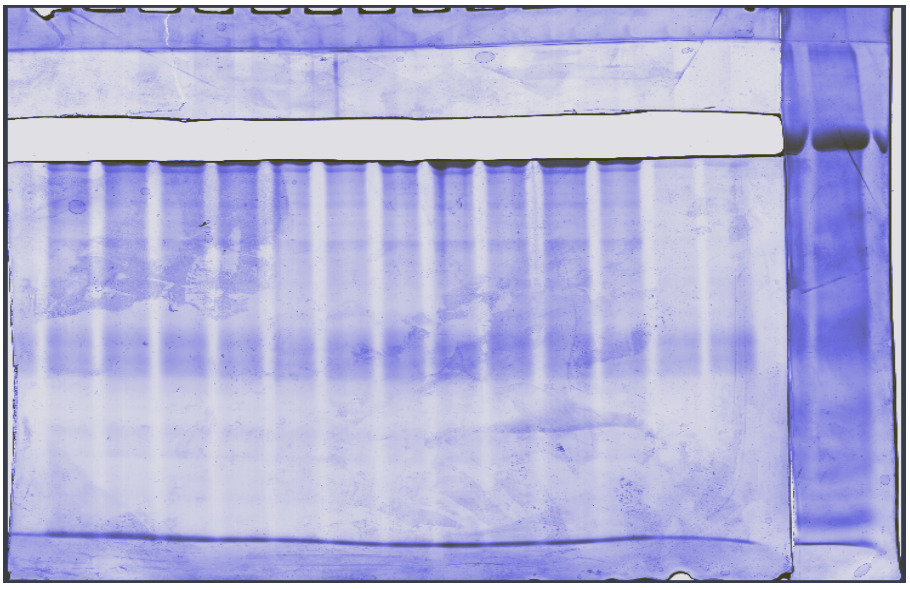

Figure 2.10. A Coomassie blue R-250 stained maxi-gel image showing the excised OMP85 protein band.

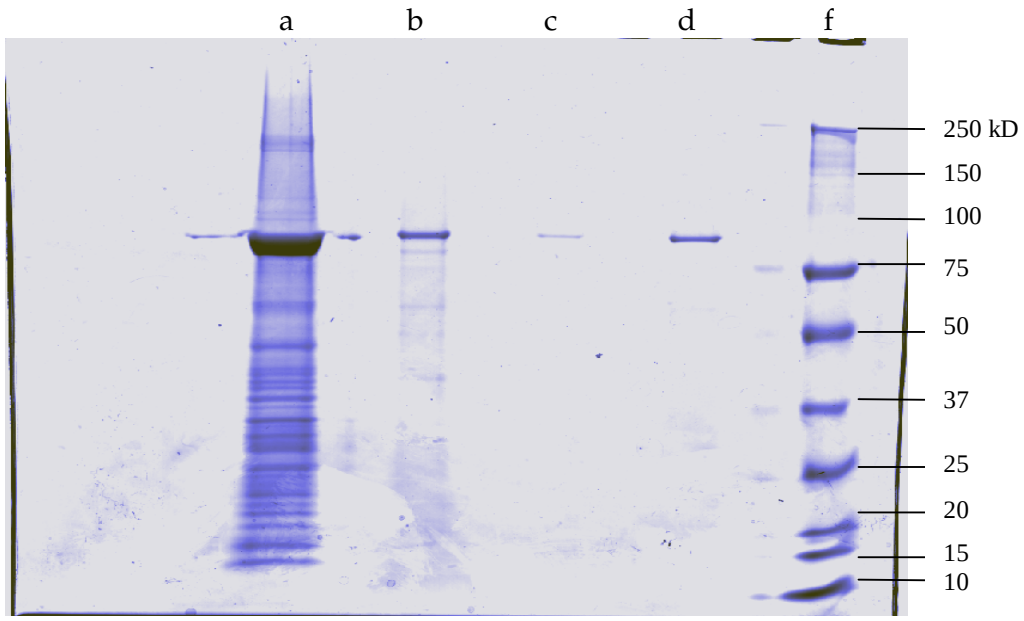

Figure 2.11. **OMP85 Protein purified by sonic extraction Method. (a). Crude OMP85 protein (b). OMP85 by Ni-NTA chromatography, (c). OMP85 by electro elution (d). OMP85 by sonic gel extraction, and (f) Protein marker.**

2.4.2. Titration of rabbit anti-OMP 85 polyclonal antibodies

Rabbit polyclonal antibodies were raised against OMP-85 antigen in the RMIT animal facility. A standard procedure for polyclonal antibody production was followed (Section 2.2.2A.). By serial dilution of serum, between 1/10 and $1/10^{32}$, a sigmoidal curve was plotted with the absorbance on the y-axis against the related titre on the x-axis. The antibody titre for rabbit anti-OMP 85 polyclonal antiserum was determined 1 in 10^{-4} (Figure 2.12. (a)). In ELISA, the anti-OMP85 antiserum recognised the *N. meningitidis* bacteria equally as like sheep anti-NM antisera (Figure 2.12. (b)).

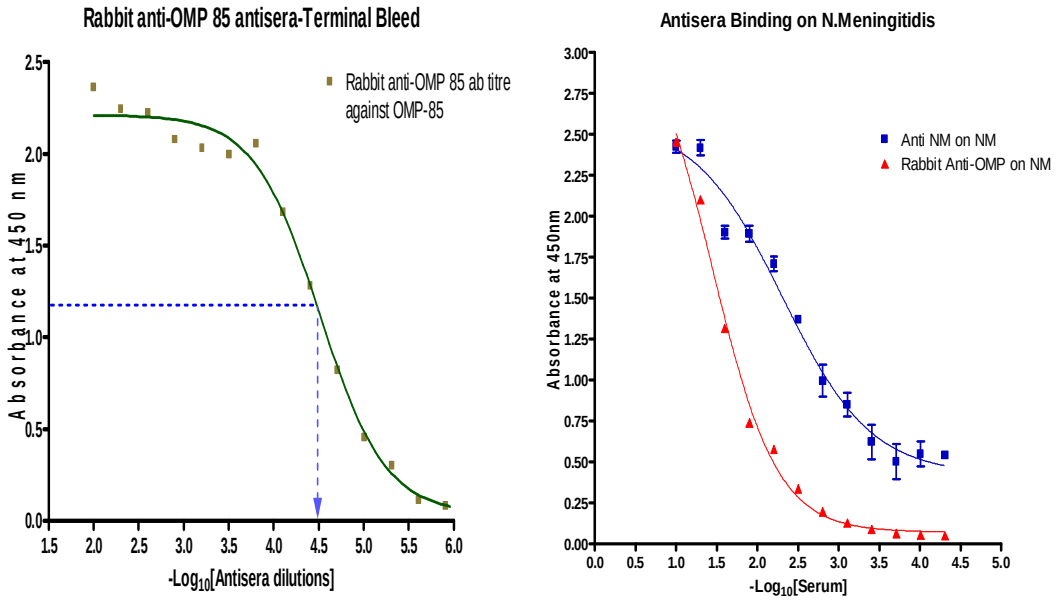

(a) (b)

Figure 2.12. Rabbit anti-OMP85 antisera-Terminal bleed (a). Assay to determine the anti-OMP85 antibody titre (b). Comparison between anti-OMP Ab and anti-NM antibody against whole cells.

2.4.3. Western blot analysis of anti_OMP85 antibodies

The rabbit anti-OMP85 antiserum was used to probe western blots containing protein extracts of from cell lysates of *E. coli* DH5a, *E. coli* DH5a/pOMP85 and the purified OMP85 protein (Figure 2.13.). The anti-OMP85 serum reacted with the recombinant OMP85 protein produced by *E. coli* DH5a/pOMP85 as well as with other proteins due to the polyclonal specificity. The purified protein was equally reactive with the antibodies suggesting that OMP 85 was expressed in its active conformation. These results also suggest that OMP85 is a highly conserved protein. Pre-clearing of the antiserum with *E. coli* removed the majority of cross-reactive antibodies, but complete removal of all reactive antibodies was not possible.

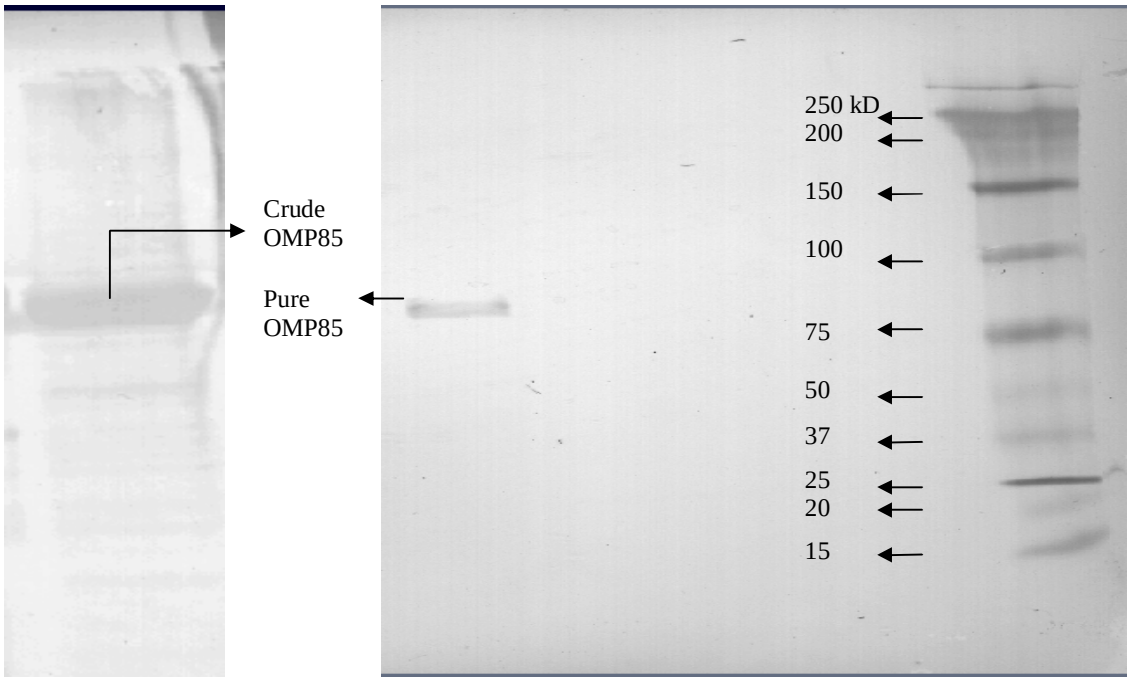

Figure 2.13. Western Blot: Rabbit polyclonal antibodies against crude and purified OMP 85 Protein antigen

2.4.4. Synthesis of the SR1 peptide specific to *N. meningitidis* type B

2.4.4.1. Coupling

The ninhydrin analysis results are shown in Figure 2. 14. The average coupling achieved per residue was 99.33%. The overall theoretical yield was calculated to be 99.34%, which indicates a theoretical yield 719.91 mg of deprotected peptide for each gram of dried peptide-resin used.

Given that the sequence was relatively long (29 aa's), the coupling of a number of residues required double or triple couplings to achieve a coupling efficiency of >99.5%. Out of the 29 amino acids in the complete sequence (including the gly-gly-cys spacer sequence), 15 residues required double coupling. However, as can be seen in Figure 2.14. , the coupling percentage of a number of amino acid residues did not reach the 99.5% coupling. The triple couplings were required for residues 7 (N), 15

(R) and 18 (N) which had a final coupling percentages of 97.83, 98.96 and 97.90% respectively. Although the first cysteine and the two glycine residues were not part of the original sequence, they were added to facilitate binding of the peptide to the gold nanoparticles via the thiol group and also to act as a spacer arm.

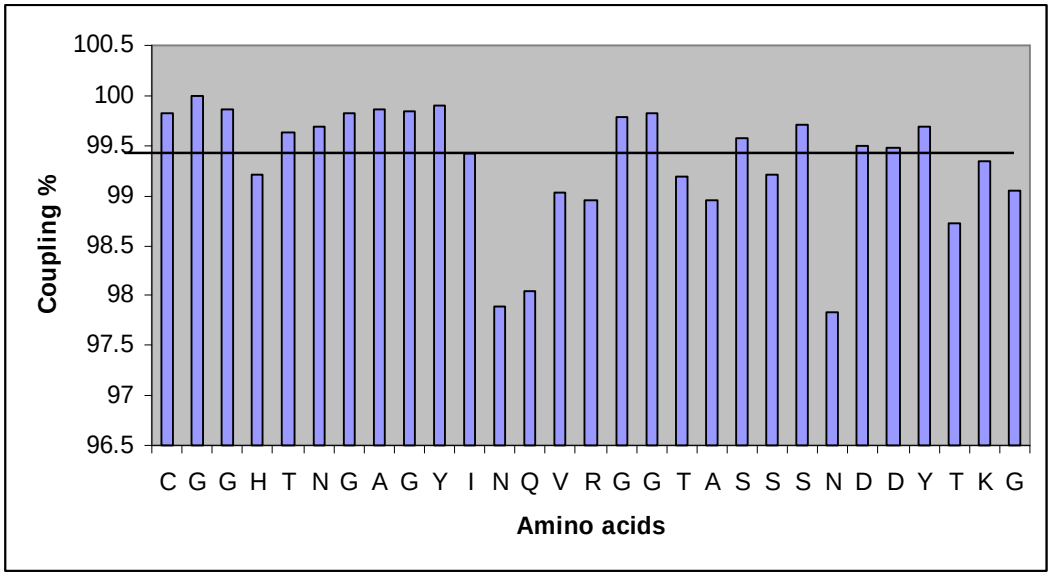

..

Figure 2.14. Coupling efficiency of the synthesis of the SR1 peptide sequence. Ninhydrin analysis data was used to quantify the coupling using the Pepmate program (J. Fecondo, unpublished).

2.4.4.2. Peptide-resin yield

Resin used	559.24 mg
Peptide-resin	2183 mg

Table 2.4. Peptide-resin yield

Peptide-resin used	359.20 mg
Peptide extracted	130.14 mg

Table 2.5. Crude peptide yield from second cleavage

2.4.4.3. HPLC analysis

Figure 2.15. shows the crude peptide chromatogram developed on the analytical HPLC system. The highest peak that is eluted at 13 minutes is the expected peptide.

From the chromatogram, it can be seen that there are impurities in the crude peptide. But this is expected because of the deletion peptides that are formed due to incomplete coupling and also truncated peptides. During extraction of the peptide, not all the scavengers and the protecting groups can be removed and these will also appear on the chromatogram. Although HPLC analysis indicates the purity of the peptide, mass spectrometry is needed to verify if the desired peptide has been synthesised.

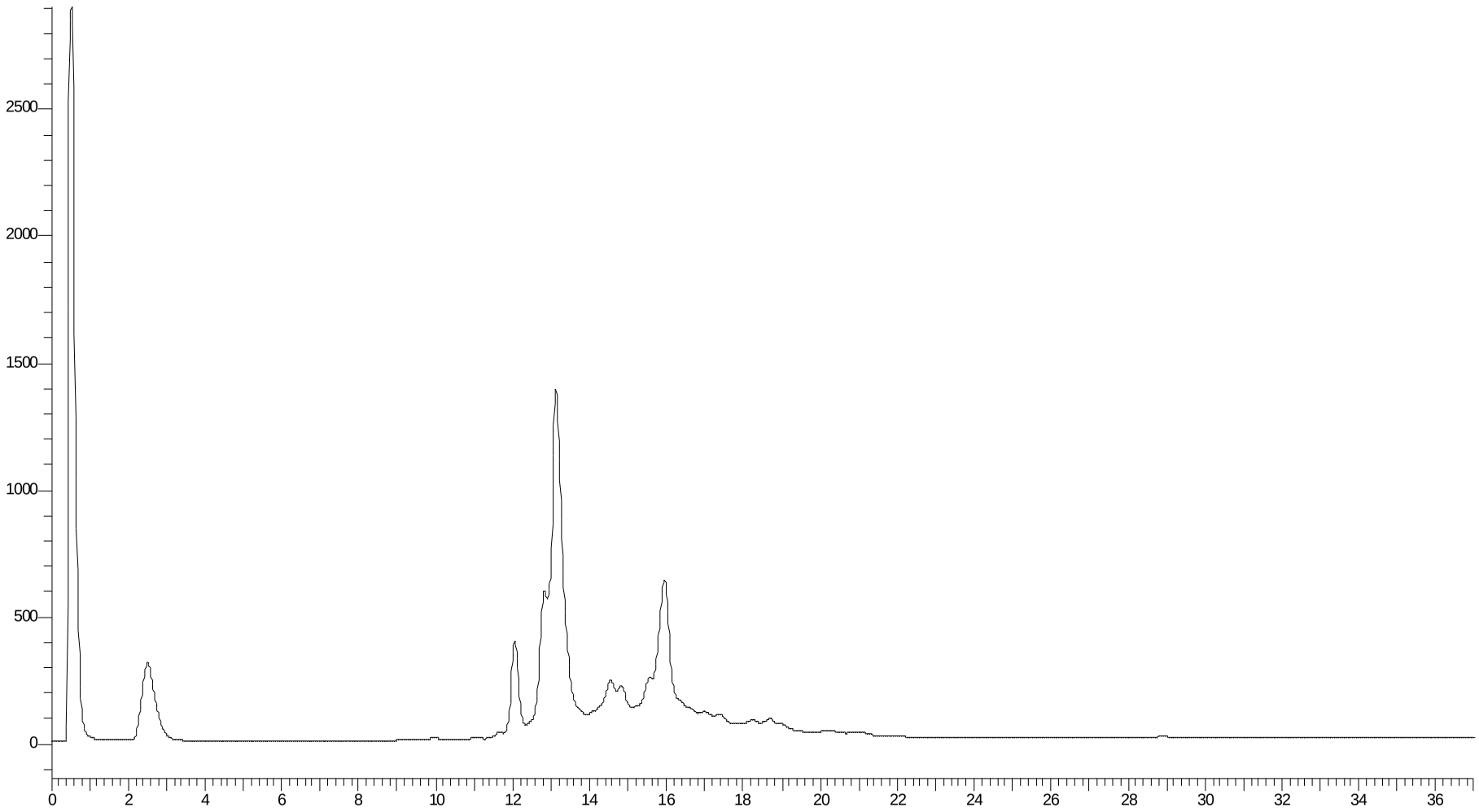

Figure 2.15. HPLC chromatogram of crude SR1. The peak eluted at 13 minutes is the peptide SR1. There is a small shoulder peak adjacent to main peptide peak. This is likely to be due to a deletion peptide or a terminated synthetic peptide analogue generated during synthesis of the peptide.

2.4.4.4. Mass Spectrometry

Figure 2.16. shows the MALDI-TOF analysis of SR1. One of the highest peaks is the most abundant compound the crude peptide and it had a mass, m/z of 2887. The calculated monoisotopic mass of SR1 (Peptide Mass Calculator, PeptideSynthetics, UK) is 2886.248. A second major peak with an m/z of 2993 (+106) was also observed. This peptide derivative is most likely due to a combination of oxidation and formation of a thiocresyl adduct during HF cleavage (ABRF) (Fields, Angeletti *et al.* 1994). It was reported that, during the cleavage and side-chain deprotection of peptide-resins, oxidation and scavenger alkylation of the peptide were primary causes of poor quality products and this can be minimized by optimizing HF concentration and/or temperature during peptide resin cleavage (Feinberg and Merrifield 1975).

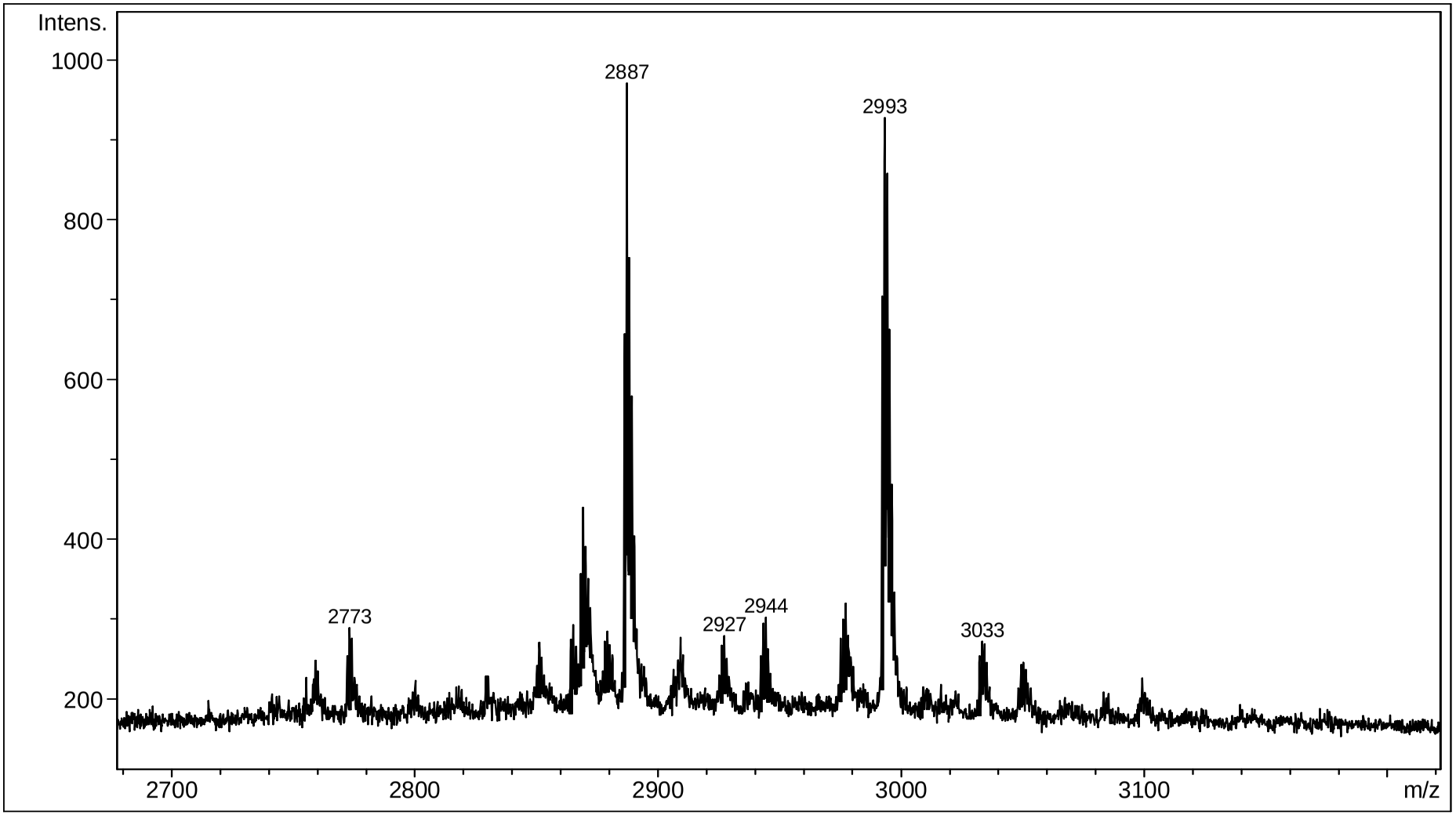

Figure 2.16. MALDI-TOF analysis of SR1. The most abundant component in the peptide mixture has a monoisotopic mass of 2887

2.4.5. Characterisation of sheep anti-SR1 and anti-NM polyclonal antibodies

Sheep polyclonal antibodies were raised against SR1 peptide antigen and the whole cell *N. meningitidis* bacteria. Formalin (2% v/v) treated whole cells and SR1-peptide-KLH conjugate were injected into sheep to raise antibodies against *N. meningitidis* serogroup B bacteria and SR1 peptide respectively. By serial dilution of serum, between 1 in 10 and 1 in 10^{32}, a sigmoidal curve was plotted with the absorbance on the y-axis against the related titre on the x-axis. The antibody titres for both the anti-SR1 and anti-NM polyclonal antisera were turned out to be 1 in 10^{-4}.

Both anti-NM and anti-SR1 polyclonal antisera were tested against SR1 peptide and the whole cell bacteria (Figure 2. 17). Anti-NM and anti-SR1 antisera recognised their respective antigens at a high titre value (1 in 10^{-4}). Interestingly, anti-SR1 antibodies recognised the bacteria (Figure 2. 17. a) more strongly than the anti-NM antibodies with SR1 peptide (Figure 2. 17. b). Rabbit anti-OMP85 antiserum reacted with the SR1 peptide (Figure 2.17. c). Another interesting observation is the anti-SR1 and anti-NM antibodies purified by protein G column chromatography recognised the whole cell bacteria equally (Figure 2. 17. d).

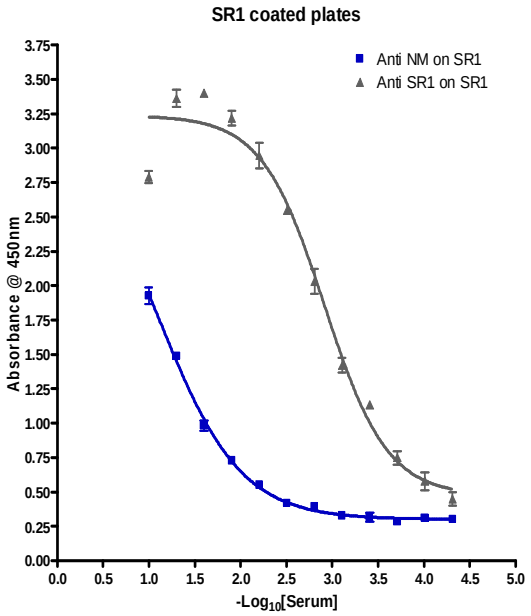

(a)

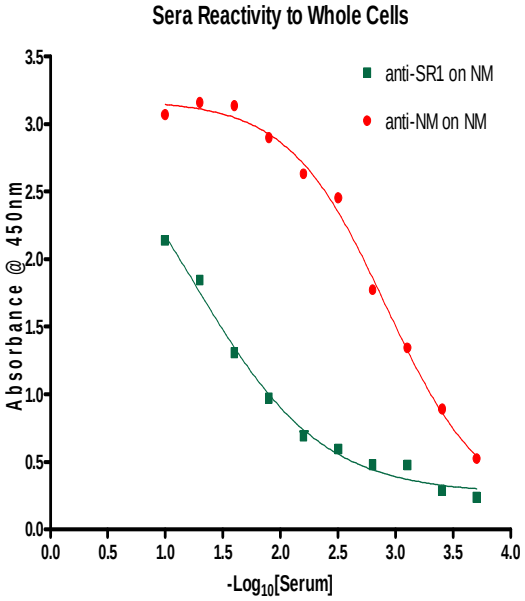

(b)

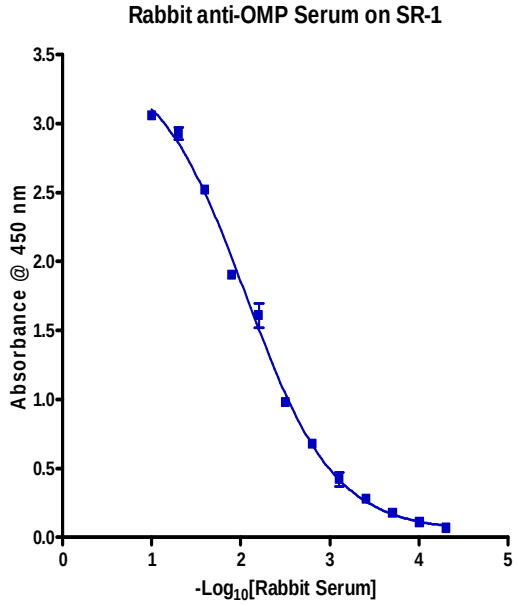

(c)

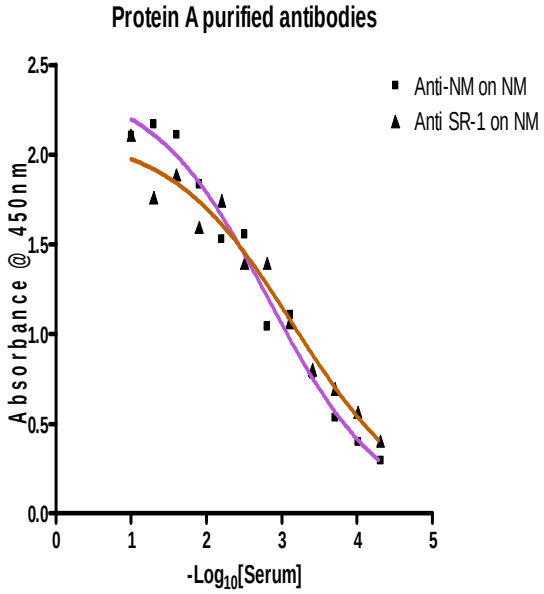

(d)

Figure 2.17. Reaction of antisera against the SR1 peptide and the whole cell *Neisseria* bacteria. (a). anti-SR1 and anti-NM antisera against the SR1 peptide (b). anti-SR1 and anti-NM antisera against the whole cell bacteria antiserum (c). Rabbit anti-OMP85 antiserum against SR1 peptide (d). protein G purified anti-NM and anti-SR1 antibodies against NM.

2.4.6. Capsule purification and Tricine SDS-PAGE analysis

Analysis of the polysaccharide capsule extract from *Neisseria meningitidis* using a Tricine-SDS PAGE gel revealed diffuse bands, commonly observed with polysaccharide analysis in SDS-PAGE gels (Figure 2.18.).

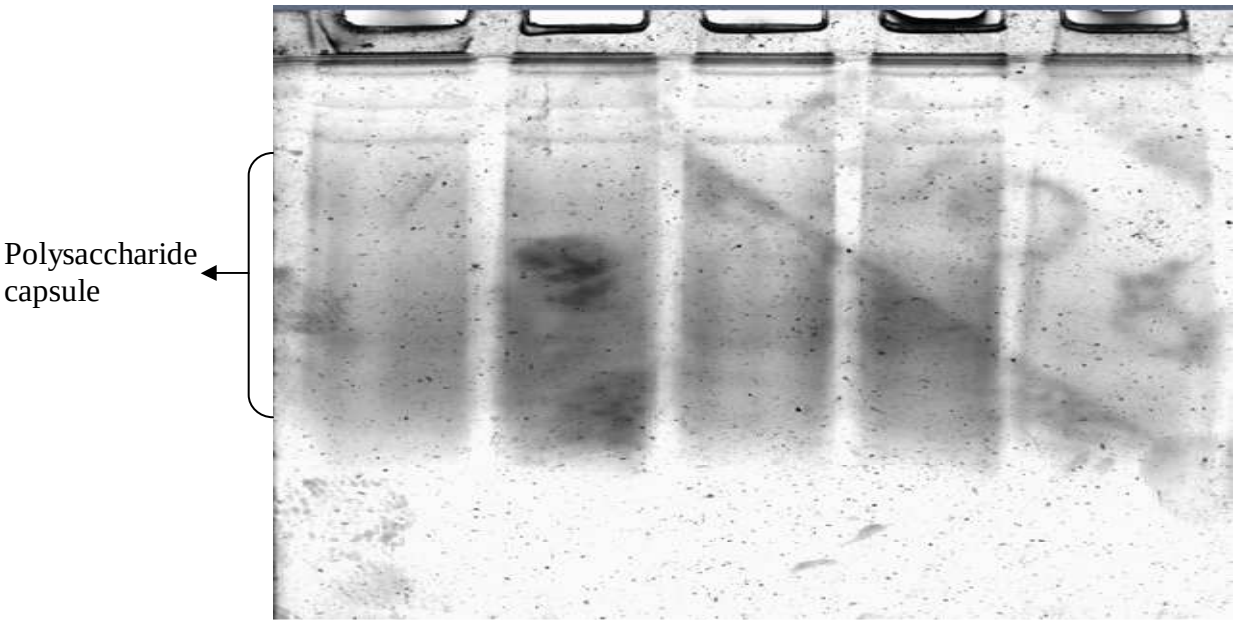

Figure 2.18. Capsular preparation on Tricine SDS-PAGE gel. All of the lanes in the gel were loaded with the same capsular polysaccharide.

2.4.6.1. HPLC analysis of Polysaccharide analysis

Figure 2.19. shows the extracted and purified polysaccharide capsule chromatogram developed on the analytical HPLC system. The highest peak that is eluted at 21 minutes is the expected peak, which indicates that the capsule preparation was pure.

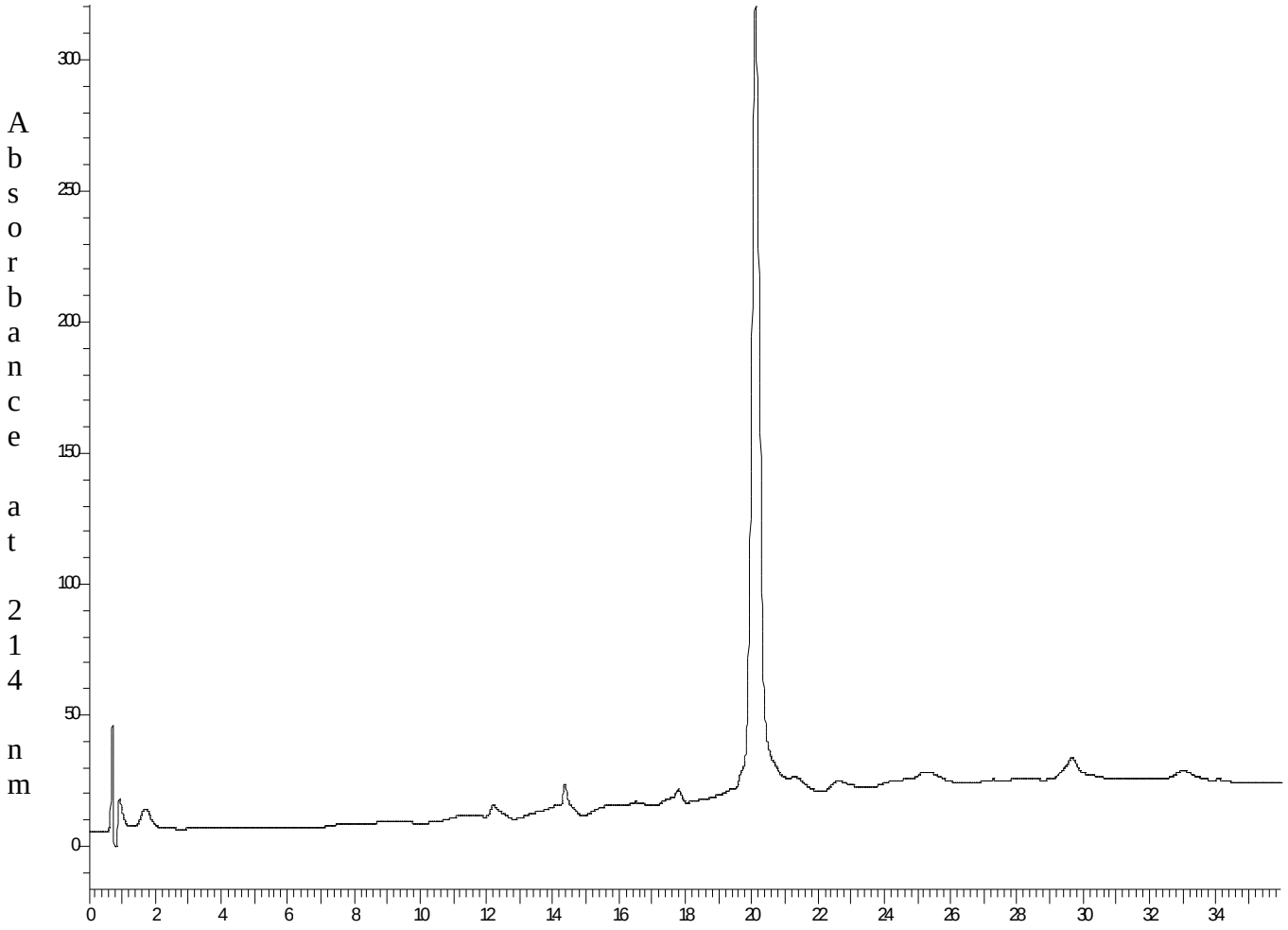

Figure 2.19. HPLC chromatogram of the capsular polysaccharide. The peak eluted at 21 minutes is the extracted capsule.

2.4.7. Anti-NM serotype B capsular specific monoclonal antibodies

N. meningitidis serogroup B capsule specific monoclonal antibodies (MAbs) were purchased from National Institue for Biological Standards and Control (NIBSC), UK. These MAbs were evaluated for their specificity and sensitivity against the whole cell bacteria as well as against the purified capsular preparation by ELISA

method (Figure 2.20.). The monoclonal antibodies recognised the whole cell bacteria with a titre of 1 in 10^{-4} and to a lesser extent with the poly-L-lysine conjugated purified capsular polysaccharide. By serial dilution of the antibody solution, between 1/10 and $1/10^{32}$, a sigmoidal curve was plotted with the absorbance on the y-axis against the related titre on the x-axis.

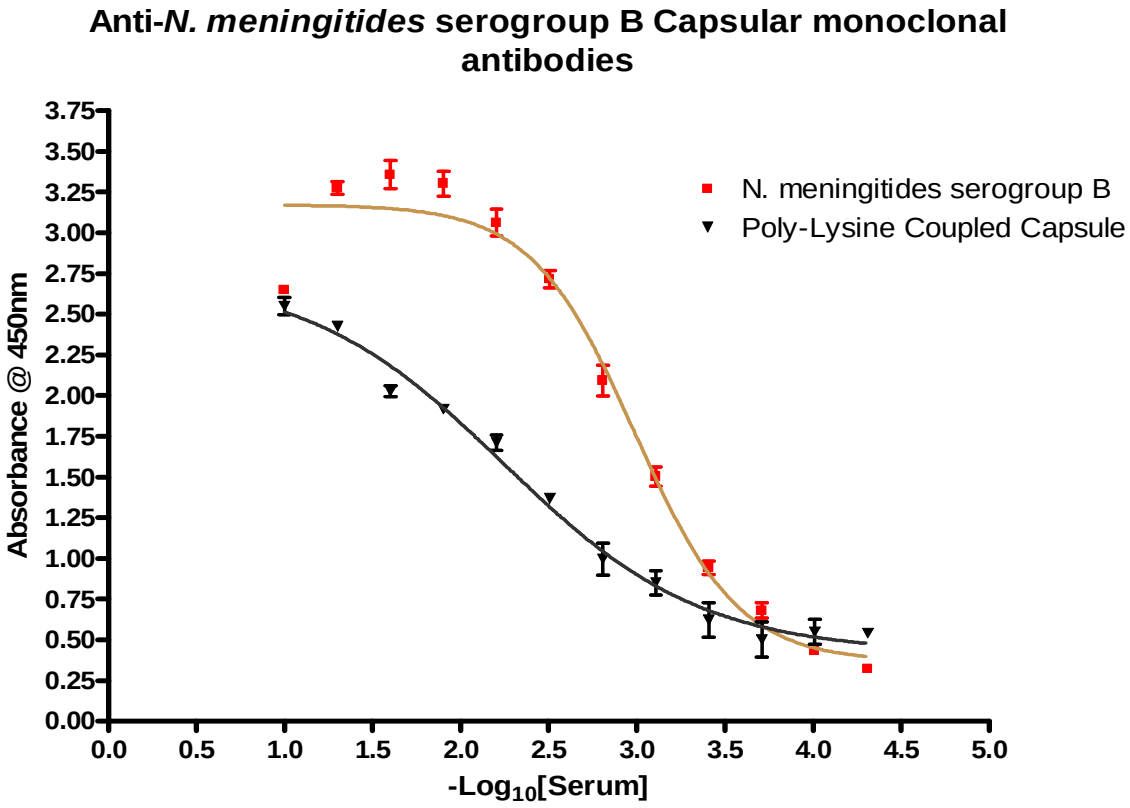

Figure 2.20. Reaction of anti-NM serogroup B capsule specific monoclonal antibodies with the whole cell bacteria and the purified capsule.

2.4.8. Cross reactivity assay against different Gram negative bacteria

The panel of antibodies against the different Gram negative bacteria examined showed varying degree of cross reactivity (Figure 2.21.). Anti-NM capsular monoclonal antibody was highly specific against the *Neisseria meningitidis* serogroup B bacteria. All other polyclonal antibodies including rabbit anti-OMP85 antibody, sheep anti-SR1 antibody and sheep anti-NM antibody were highly cross-reactive against different analysed bacteria. All bacteria except *Legionella pneumophila, Pasteurella multocida, Brucella abortus* had shown varying degree of cross reactivity. The results are summarised in table 2.6., where 4+ indicates the highest reactivity and + indicates least or no reactivity.

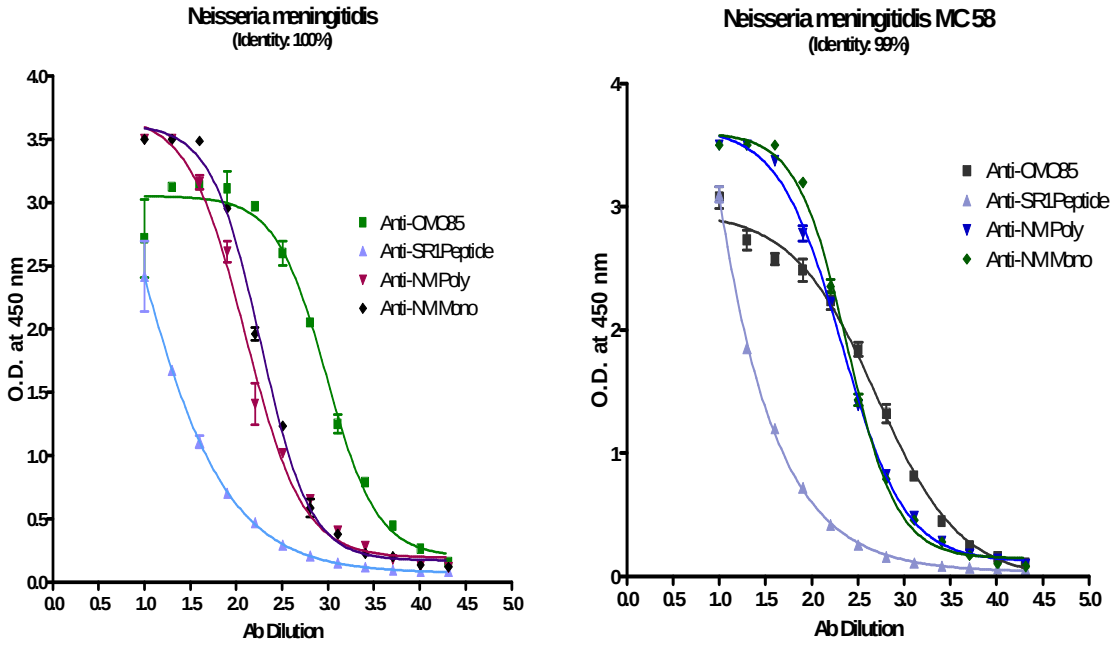

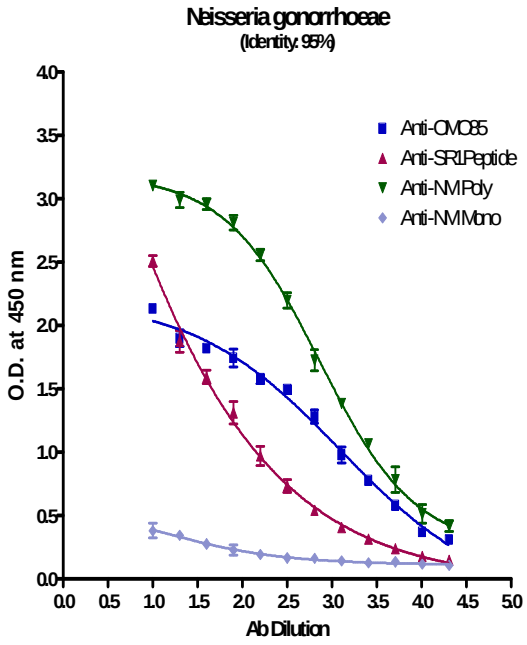
Neisseria gonorrhoeae
(Identity: 95%)
Anti-OMC85
Anti-SR1Peptide
Anti-NM Poly
Anti-NM Mono
O.D. at 450 nm
Ab Dilution

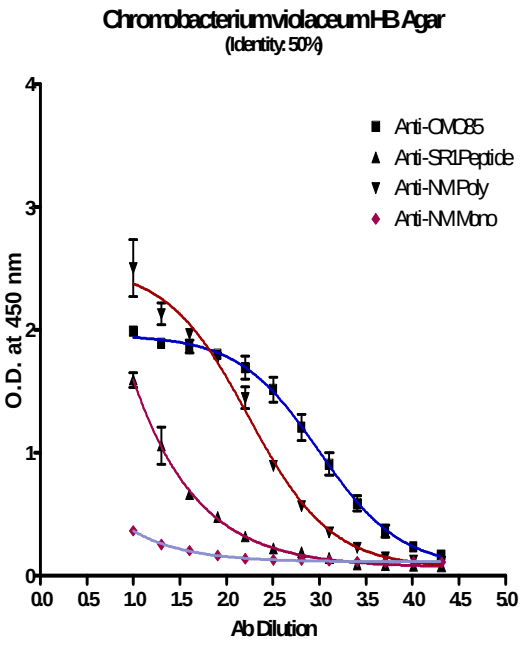
Chromobacterium violaceum HB Agar
(Identity: 50%)
Anti-OMC85
Anti-SR1Peptide
Anti-NM Poly
Anti-NM Mono
O.D. at 450 nm
Ab Dilution

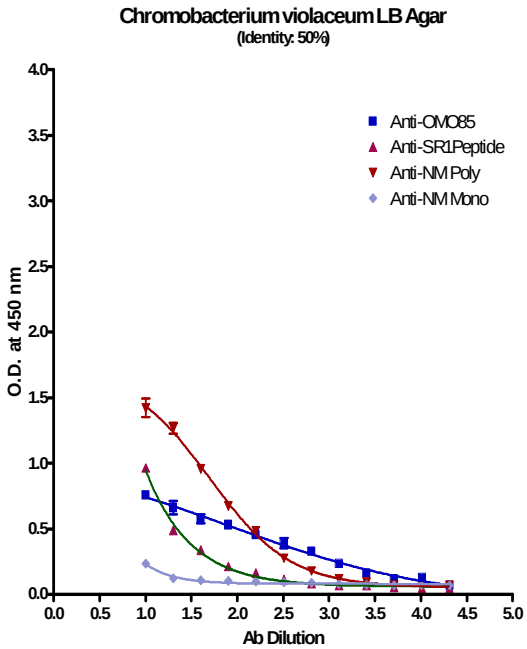
Chromobacterium violaceum LB Agar
(Identity: 50%)
Anti-OMC85
Anti-SR1Peptide
Anti-NM Poly
Anti-NM Mono
O.D. at 450 nm
Ab Dilution

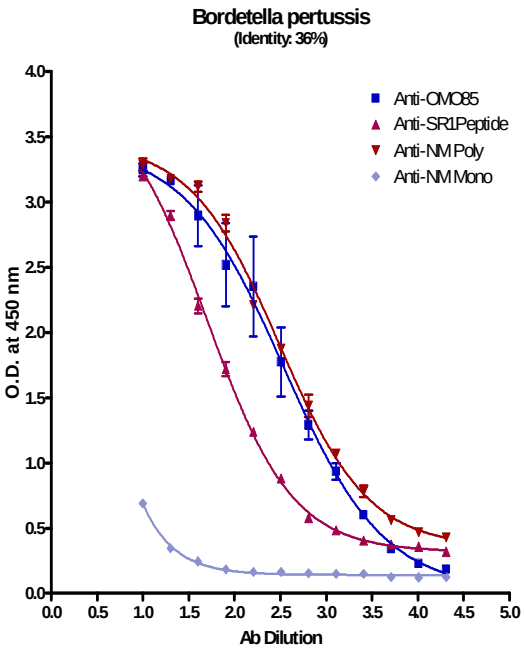
Bordetella pertussis
(Identity: 36%)
Anti-OMC85
Anti-SR1Peptide
Anti-NM Poly
Anti-NM Mono
O.D. at 450 nm
Ab Dilution

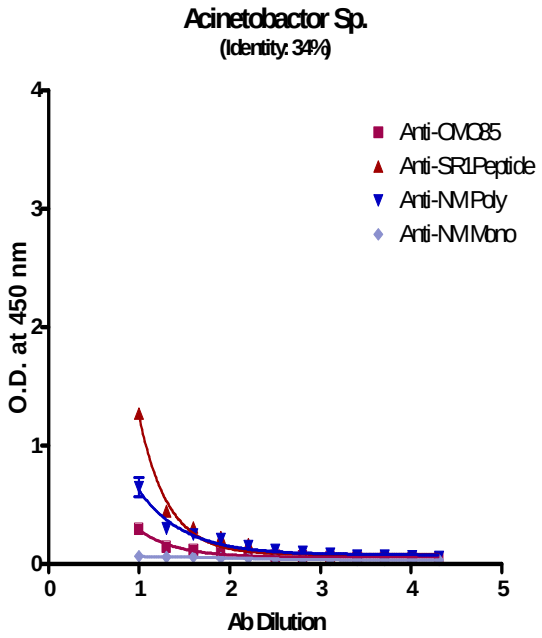
Acinetobactor Sp.
(Identity: 34%)
Anti-OMC85
Anti-SR1Peptide
Anti-NM Poly
Anti-NM Mono
O.D. at 450 nm
Ab Dilution
0
1
2
3
4
5

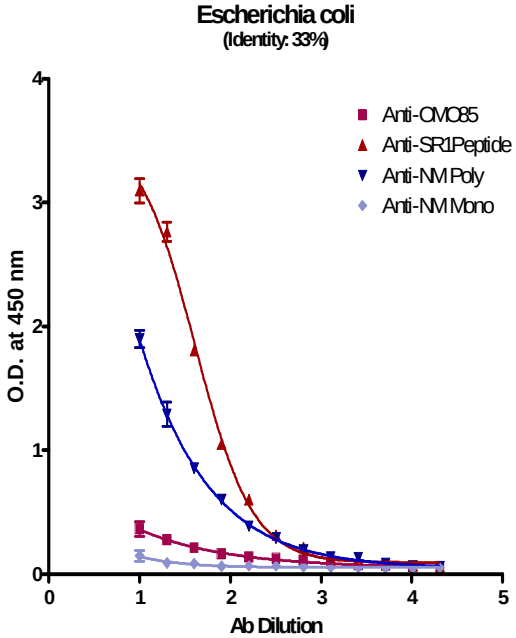
Escherichia coli
(Identity: 33%)
Anti-OMC85
Anti-SR1Peptide
Anti-NM Poly
Anti-NM Mono
O.D. at 450 nm
Ab Dilution
0
1
2
3
4
5

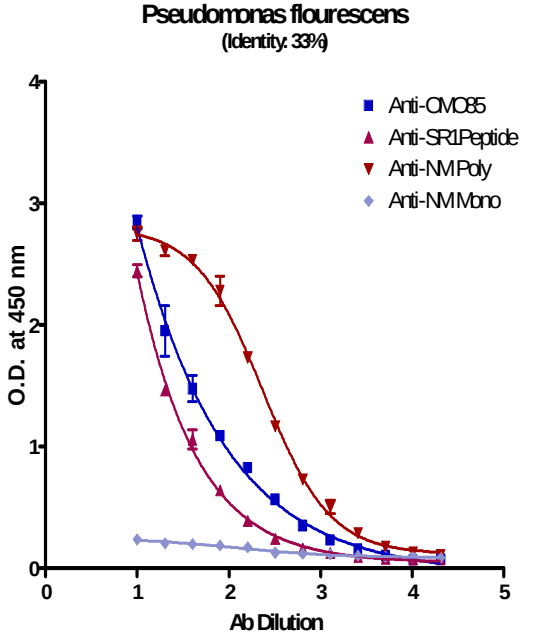
Pseudomonas flourescens
(Identity: 33%)
Anti-OMC85
Anti-SR1Peptide
Anti-NM Poly
Anti-NM Mono
O.D. at 450 nm
Ab Dilution
0
1
2
3
4
5

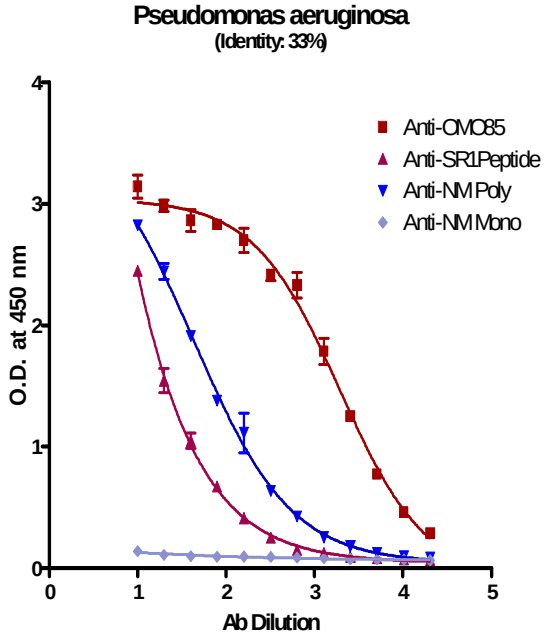
Pseudomonas aeruginosa
(Identity: 33%)
Anti-OMC85
Anti-SR1Peptide
Anti-NM Poly
Anti-NM Mono
O.D. at 450 nm
Ab Dilution
0
1
2
3
4
5

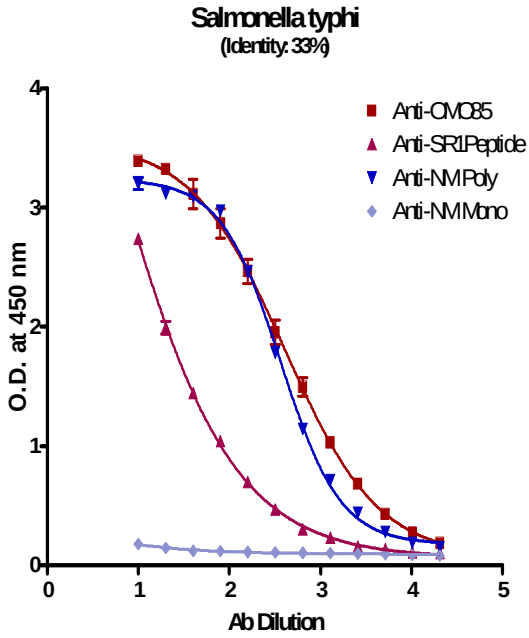
Salmonella typhi
(Identity: 33%)
Anti-OMC85
Anti-SR1Peptide
Anti-NMPoly
Anti-NMMono
O.D. at 450 nm
Ab Dilution

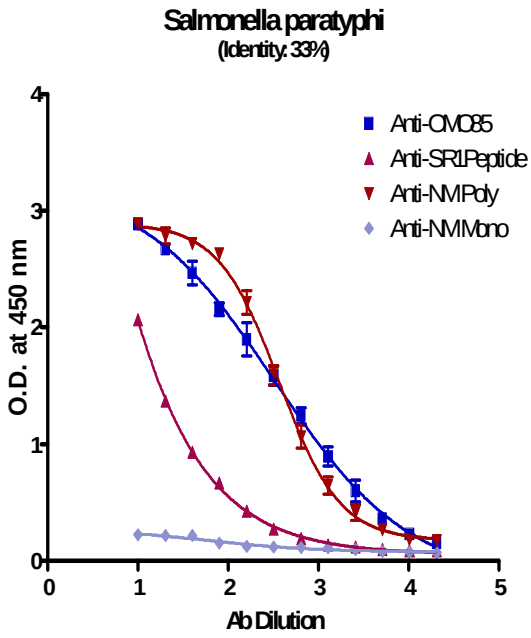
Salmonella paratyphi
(Identity: 33%)
Anti-OMC85
Anti-SR1Peptide
Anti-NMPoly
Anti-NMMono
O.D. at 450 nm
Ab Dilution

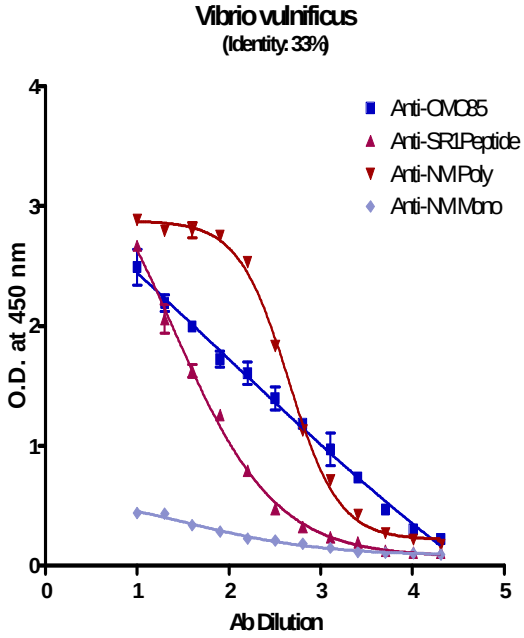
Vibrio vulnificus
(Identity: 33%)
Anti-OMC85
Anti-SR1Peptide
Anti-NMPoly
Anti-NMMono
O.D. at 450 nm
Ab Dilution

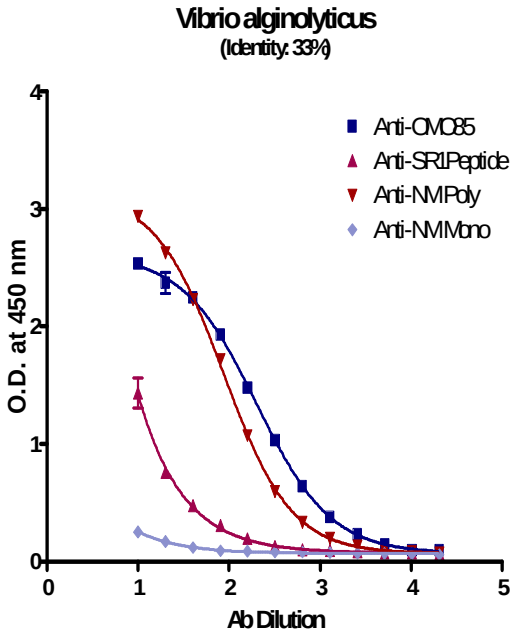
Vibrio alginolyticus
(Identity: 33%)
Anti-OMC85
Anti-SR1Peptide
Anti-NMPoly
Anti-NMMono
O.D. at 450 nm
Ab Dilution

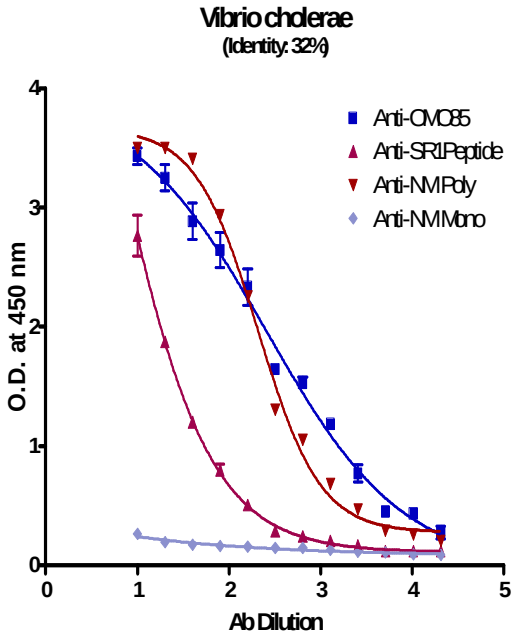
Vibrio cholerae
(Identity: 32%)
Anti-OMC85
Anti-SR1Peptide
Anti-NM Poly
Anti-NM Mono
O.D. at 450 nm
Ab Dilution

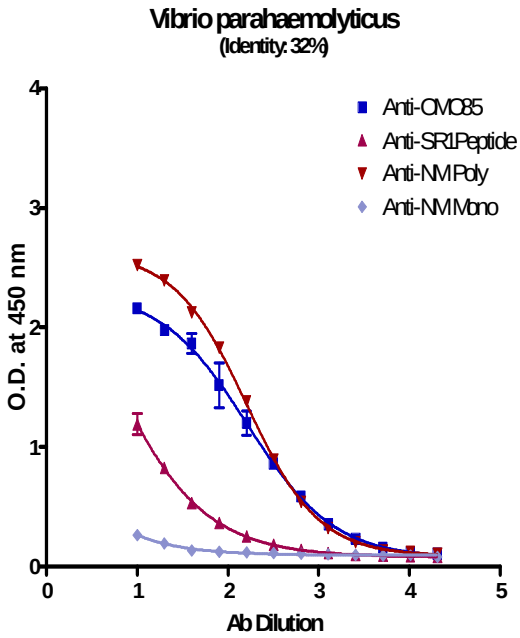
Vibrio parahaemolyticus
(Identity: 32%)
Anti-OMC85
Anti-SR1Peptide
Anti-NM Poly
Anti-NM Mono
O.D. at 450 nm
Ab Dilution

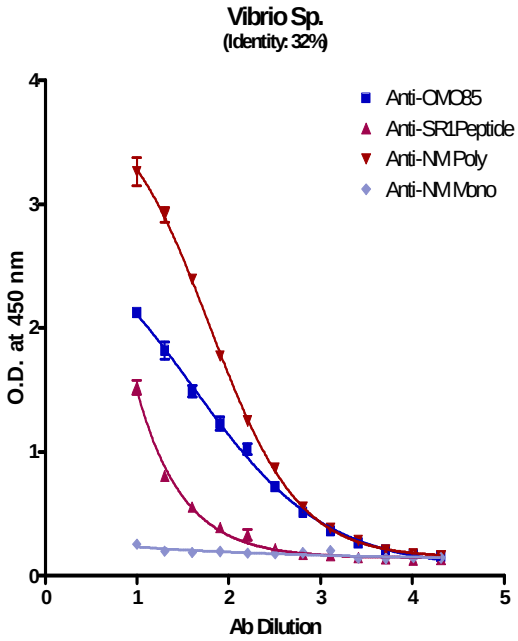
Vibrio Sp.
(Identity: 32%)
Anti-OMC85
Anti-SR1Peptide
Anti-NM Poly
Anti-NM Mono
O.D. at 450 nm
Ab Dilution

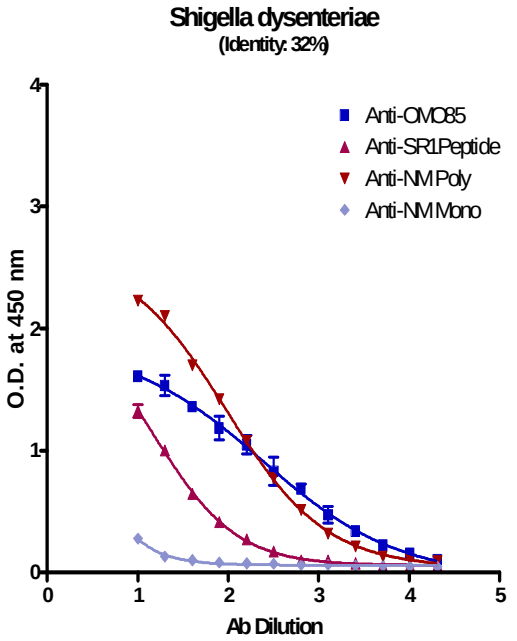
Shigella dysenteriae
(Identity: 32%)
Anti-OMC85
Anti-SR1Peptide
Anti-NM Poly
Anti-NM Mono
O.D. at 450 nm
Ab Dilution

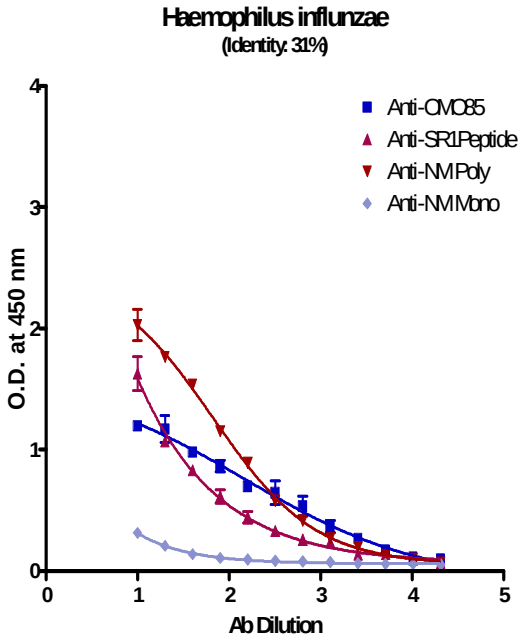
Haemophilus influnzae
(Identity: 31%)
Anti-OMC85
Anti-SR1Peptide
Anti-NMPoly
Anti-NMMono
O.D. at 450 nm
Ab Dilution

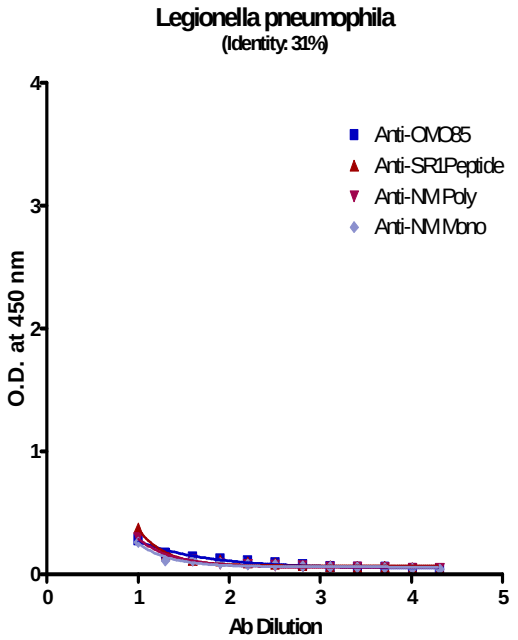
Legionella pneumophila
(Identity: 31%)
Anti-OMC85
Anti-SR1Peptide
Anti-NMPoly
Anti-NMMono
O.D. at 450 nm
Ab Dilution

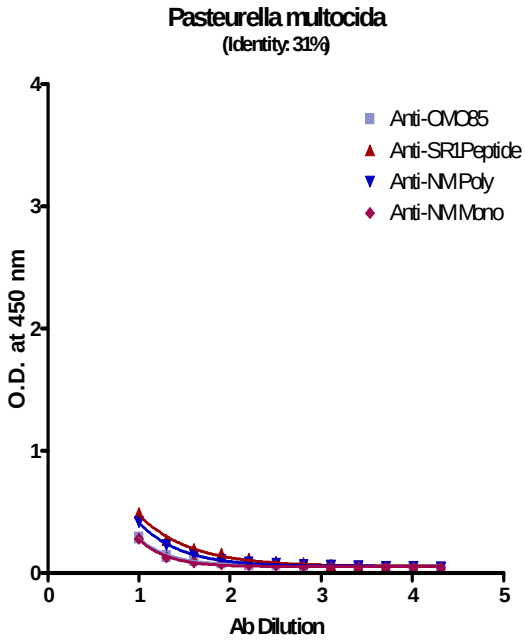
Pasteurella multocida
(Identity: 31%)
Anti-OMC85
Anti-SR1Peptide
Anti-NMPoly
Anti-NMMono
O.D. at 450 nm
Ab Dilution

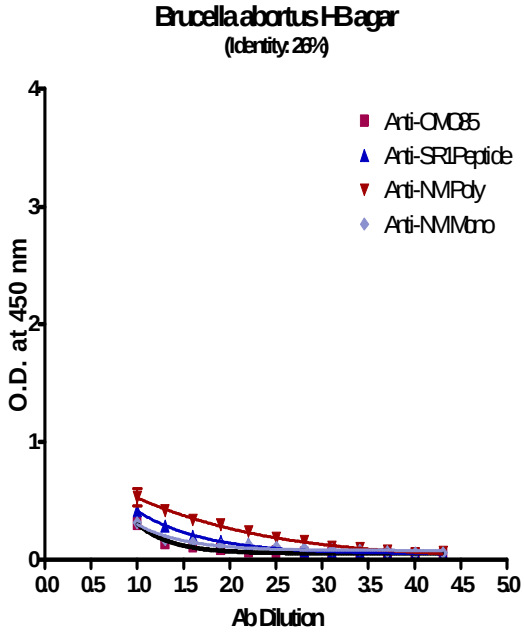
Brucella abortus HB agar
(Identity: 28%)
Anti-OMC85
Anti-SR1Peptide
Anti-NMPoly
Anti-NMMono
O.D. at 450 nm
Ab Dilution

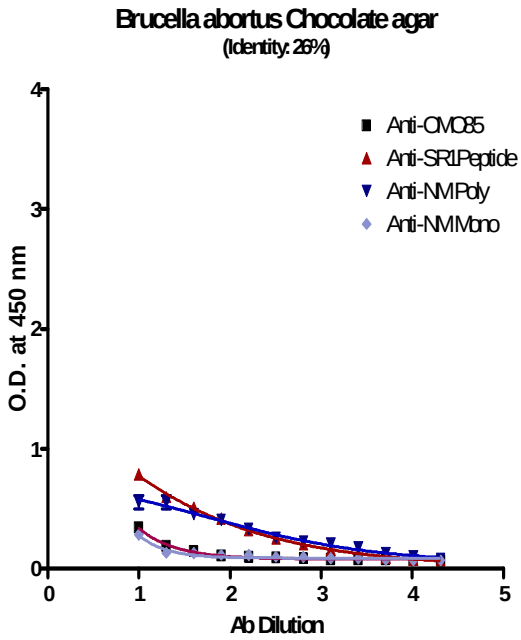

Figure 2.21. Cross reactivity with different closely related bacteria against the panel of antibodies.

	Identity With OMP 85	Anti-OMP85	Anti-SR1 Peptide	Anti-NM poly	Anti-NM mono
Neisseria meningitidis	100%	3+	2+	4+	4+
Neisseria meningitidis MC 58	99%	3+	2+	4+	4+
Neisseria gonorrhoeae	95%	2+	2+	3+	+
Chromobacterium violaceum HB Agar	50%	2+	1+	2+	+
Chromobacterium violaceum LB Agar	50%	1+	1+	2+	+
Bordetella pertussis	36%	3+	3+	3+	+
Acinetobactor Sp.	34%	+	1+	1+	+
Escherichia coli	33%	1+	3+	2+	+
Pseudomonas flourescens	33%	3+	2+	2+	+
Pseudomonas aeruginosa	33%	3+	2+	3+	+
Salmonella typhi	33%	3+	2+	3+	+
Salmonella paratyphi	33%	3+	2+	3+	+
Vibrio vulnificus	33%	2+	2+	2+	+
Vibrio alginolyticus	33%	2+	1+	2+	+
Vibrio cholerae	32%	3+	2+	4+	+
Vibrio parahaemolyticus	32%	2+	1+	2+	+
Vibrio Sp.	32%	2+	1+	3+	+
Shigella dysenteriae	32%	1+	1+	2+	+
Haemophilus influnzae	31%	1+	1+	2+	+
Legionella pneumophila	31%	+	+	+	+
Pasteurella multocida	31%	+	+	+	+
Brucella abortus HB agar	26%	+	+	+	+
Brucella abortus Chocolate agar	26%	+	+	+	+

Table 2.6. Summary of data from cross-reactivity studies: A panel of different antibodies were assessed for their cross reactivity against different bacteria. In this summary, 4+ indicates highest reactivity and + indicates least or no reactivity.

2.4.9. Protein A / Protein G sepharose purification of polyclonal antisera

All of the antibody preparations were purified by affinity column chromatography. Rabbit IgG antibodies were purified by using protein A sepharose column and the sheep IgG antibodies were purified by using protein G sepharose column using the method described in section 2.3.13. Figure 2. 22. represents the typical antibody purification experiment by immunoaffinity chromatography.

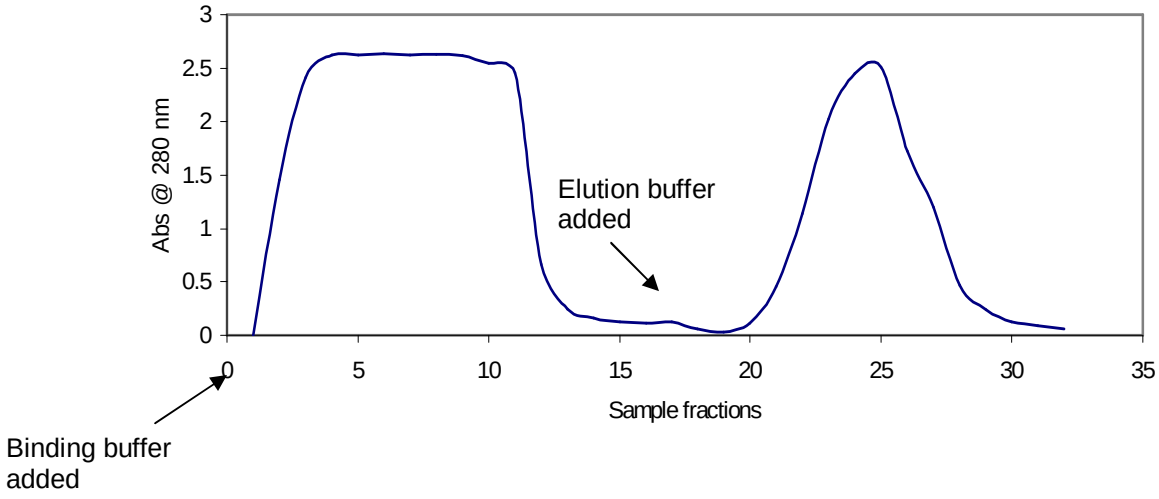

Figure 2.22. Protein G sepharose purification of sheep anti-SR1 polyclonal antiserum

2.4.10. Monospecificity of anti-SR1 antibodies

As expected, the affinity purification of SR1 specific antibodies removed the cross-reactive antibodies to make the antibody monospecific (Figure 2.23.). The purified antibody showed no cross reactive response against all of the bacteria examined except *vibrio sp.* (Figure 2.24.).

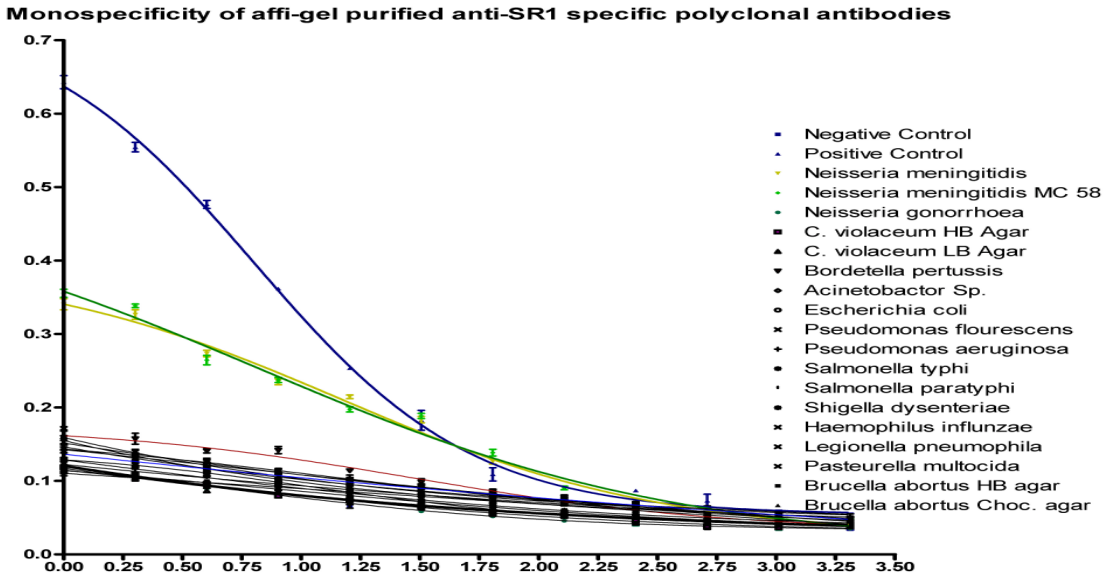

Figure 2.23. Cross-reactivity studies of anti-SR1 monospecific antibody on different species, showing no cross reactivity with bacteria which was positive before with the anti-SR1 polyclonal antisera.

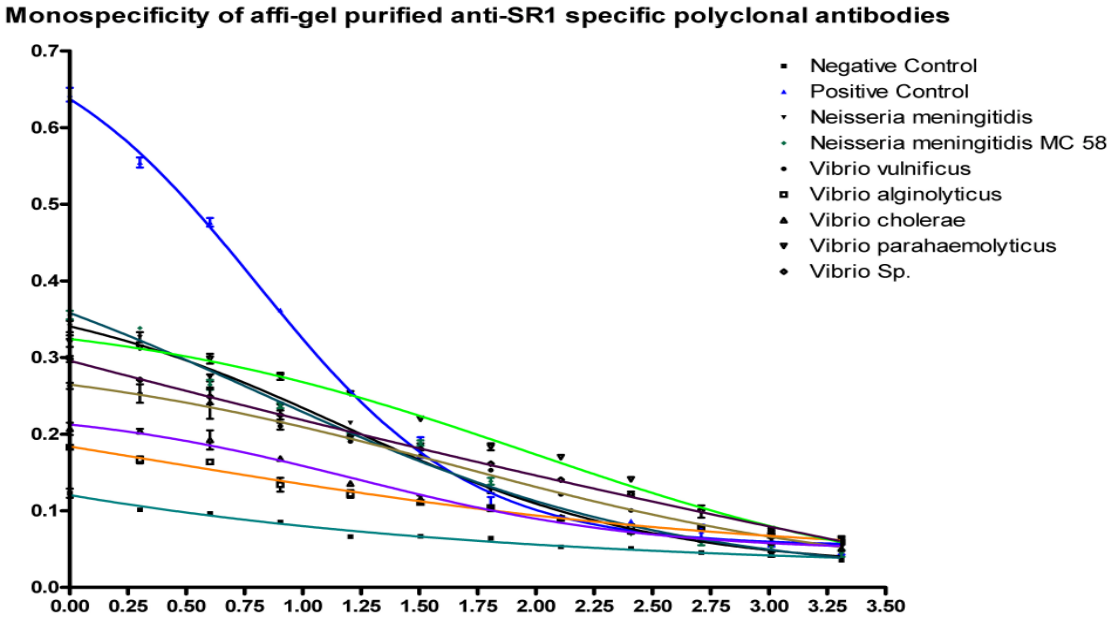

Figure 2.24. Reactivity of mono-specific anti-SR1 antibody towards different *Vibrio* bacteria.

2.4.11. Shark IgNAR phagemid library panning

After completing 4 rounds of panning the IgNAR library against the different target antigens, positive clones were picked from the ELISA experiment (Table 2.7.). IgNAR specific PCR was positive for the selected clones (Figure 2.25.). After DNA sequencing, all clones selected were identified as either non-specific or "sticky" clones.

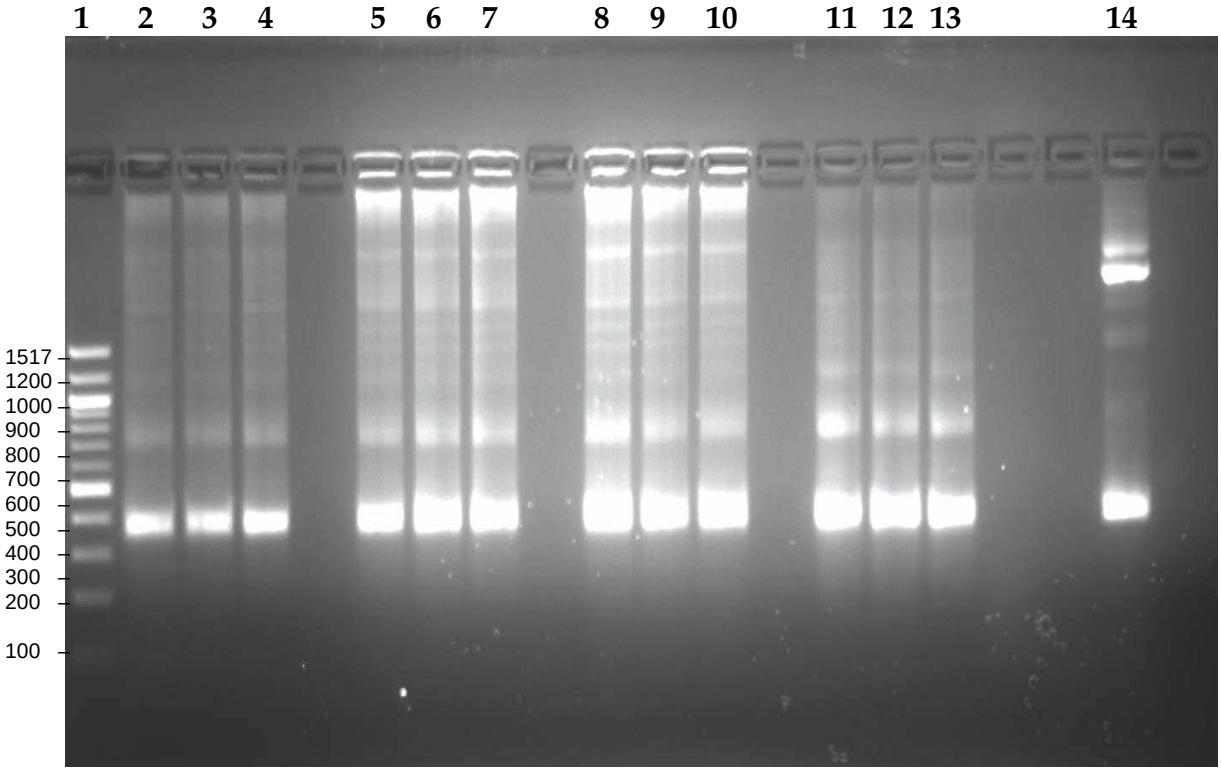

Figure 2.25. PCR reaction showing the IgNAR positive gene (non-specific clone). Lane 1: 100 bp DNA ladder, lanes 2-4: semi-pure OMP85 specific IgNAR clones, lanes 5-7: pure OMP85 specific IgNAR clones, lanes 8-10: SR1 specific IgNAR clones, lanes 11-12: capsule specific clones and lane 14 is the positive control.

Antigens Screened	Round 1 No. of Colonies	Round 2 No. of Colonies	Round 3 No. of Colonies	Round 4 No. of Colonies	IgNAR PCR +ves	Tth PCR +ves	No. of possible clones picked from ELISA	DNA Sequencing results
OMP85	0	0	2.5×10^4	2.6×10^2	100%	100%	6	Sticky and non-specific clones
SR-1 peptide	0	0	4.8×10^5	2.6×10^2	100%	100%	4	Sticky and non-specific clones
Capsule	2.4X 105	0	4.0×10^5	5.2×10^2	100%	100%	2	Sticky and non-specific clones

Table 2.7. Shark IgNAR phagemid library panning. After 4 round of panning, different clones which appeared positive from PCR were selected for ELISA. After DNA sequencing, all of the selected clones were proved to be non-specific clones.

2.5. Discussion

The recombinant OMP 85 protein, polysaccharide capsule component of the bacteria and whole bacteria were selected as target antigens. A peptide unique to *N. meningitidis* serogroup B was also synthesised using optimised t-boc chemistry. All of the antigens were prepared and their respective antibodies were purified using either protein A or protein G-sepharose affinity chromatography.

2.5.1. OMP85 and rabbit anti-OMP85 polyclonal antibodies

The recombinant OMP85 expressed with hexa-His tag was cloned, transformed and expressed in *E. coli* successfully. With Ni-NTA affinity column chromatography, other proteins were eluted along with prominent OMP85 protein. This might be due to the partial affinity of other proteins towards the Ni-NTA resin because hexa histidine does not exhibit the highest level of specificity. The use of transition metal complexes of iminodiacetic and nitrilotriacetic acid (NTA) has become commonly used for the efficient purification of hexa-His tagged proteins. NTA forms a tetravalent chelate with Ni(II) that subsequently is coordinated by basic amino acids such as histidine (Nallamsetty, Austin *et al.* 2005). Even after optimising the imidazole concentration to elute more of OMP85 and less of other proteins, the protein isolated was not homogeneous. Accordingly, modified sonic gel extraction procedure from SDS-PAGE maxi gels (16X16 cm) was followed, through which pure protein was obtained and the yield was much higher than the electro elution technique. Positive western blot

results with both crude and purified OMP85 antigen confirmed that the protein was expressed in its immunoreactive conformation.

A BLAST search revealed the presence of OMP85 homologues in the complete genome sequences of all Gram negative bacteria examined (Surana, Grass *et al.* 2004). Manning *et al.*. (Manning, Reschke *et al.* 1998) described surface cross-linking experiments that suggested as OMP85 is surface exposed and interacts with other proteins on the bacterial surface. Conservation in the amino acid sequences is observed throughout the OMP85 protein. Two highly conserved motifs are located between amino acid residues 360-395 and 643-662 of neisserial OMP85 protein (OMP85 2002). OMP85 has been suggested as a possible vaccine target, as it is highly conserved among the Gram negative bacteria and elicits an immune response (Surana, Grass *et al.* 2004). Information regarding the possible binding sites of anti OMP85-antibodies is not available but it may be postulated that the two membrane-exposed loops are targets for host antibodies (Surana, Grass *et al.* 2004).

Secondary structure prediction methods, such as PsiPred (Jones 1999) and PHD (Rost and Sander 1993), predicted the presence of at least two extracellular domains in OMP85 protein. A two-domain model for OMP85 was proposed, with a highly conserved NH2-terminal α/β periplasmic domain that includes the sequences required for secretion from the bacteria (Manning, Reschke *et al.* 1998;

Voulhoux, Bos *et al.* 2003) and a 12 stranded β–barrel domain at the COOH terminus domain consisting of β-strands and terminal phenyl alanine residue and could form a β-barrel for anchorage in the OM (Bredemeier, Schlegel *et al.* 2006). The COOH-terminal domain is referred as "surface antigen", because antibodies against this domain are protective against *Haemophilus influenzae* infection in animal models (Loosmore, Yang *et al.* 1997).

The rabbit anti-OMP 85 polyclonal antibodies showed a higher degree of cross reactivity against the range of closely related bacteria. Given that OMP85 is a conserved protein amongst Gram negative bacteria (Surana, Grass *et al.* 2004) and that the protein is expressed in *E. coli*, it would be expected that anti-OMP85 polyclonal antiserum would have high cross reactivity. There are no known commercial monoclonal antibodies available against OMP85 because of its conserved nature. Pre clearing the anti-OMP85 polyclonal antibodies with *E.coli* and other bacteria may be utilised to make them more specific to *Neisseria meningitidis* and may be useful as a capture system in ELISA or in quartz crystal microbalance (QCM) experiments.

It has been postulated that OMP 85 could be used as an alternate vaccine candidate for serogroup B (Romero and Outschoorn 1994). Being a highly conserved protein among Gram negative bacteria, the greatest limitation of OMP vaccines is the specificity (subtype and serotype) of the protection that they

induce. Consequently, they cannot be used worldwide as prevalent meningococcal strains vary from region to region (Porritt, Mercer *et al.* 2000).

2.5.2. SR1 peptide and sheep anti-SR1 polyclonal antibodies

Sequence analysis of the surface antigen domain of OMP85 from *N. meningitidis* suggests it would form a 12- stranded β-barrel structure (Voulhoux, Bos *et al.* 2003). Across the prokaryotic and eukaryotic members of the OMP85 family (fungi, plants, and animals (including humans)), there is strong sequence conservation in the regions predicting as β-strands, with variable intervening sequences that might correspond to inter-strand loops (Martelli, Fariselli *et al.* 2002; Surana, Grass *et al.* 2004). These predictors may not sufficiently be reliable to determine a valid structural model for OMP85 but, the overall predictions on the family suggest a close structural relationship that goes beyond simple sequence similarities.

Though it is a conserved protein, it still serves as a useful diagnostic marker and may be a potential vaccine candidate, since the predicted antigenic sequence between local residues 720 and 745 is unique to this organism (Judd and Manning 2003). A BLAST search of this particular sequence against the database reveals only as the sequence present in *N. meningitidis* serotype B bacteria (100% sequence identity). Also, there are five additional amino acids at the N-terminus

which distinguishes it from other related outer membrane proteins (Judd and Manning 2003). A useful approach will be to target these specific sequences as selective epitopes for immunodiagnosis of *Neisseria meningitidis*. By targeting these specific regions, OMP85 may be utilised as a more effective diagnostic marker.

The selected *N. meningitidis* specific amino acid sequence (SR1) from OMP85 protein sequence was synthesised using t-boc chemistry and confirmed by HPLC and mass spectrometry. After the synthesis, the SR1 peptide was conjugated to Keyhole Limpet Haemocyanine (KLH) as a carrier protein using SMCC as a linker molecule. Polyclonal antibodies were raised in sheep against this SR1-KLH conjugate. The antiserum was tested for high titre and specificity for the peptide, OMP85 protein and the whole cell bacteria.

Anti-SR1 peptide antibodies reacted with the peptide, the OMP85 protein and the *N. meningitidis* bacteria itself. It proved that not only the OMP85 protein, but also the peptide sequence itself also is highly immunogenic and the anti-SR1 peptide antibodies are able to identify whole bacteria. Unfortunately, in initial cross reactivity experiments, the anti-SR1 polyclonal antiserum was highly cross reactive with other closely associated Gram negative bacteria. The high degree of cross-reactivity of sheep anti-SR1 peptide antiserum might be due to the background of polyclonal antiserum and may be due to previous environmental

exposure to any of the tested organisms. Being a highly specific target against *Neisseria meningitidis*, anti-SR1 antiserum has potential to become a useful specific diagnostic marker for this organism.

Purification of monospecific anti-SR1 antibodies by the immuno-affinity chromatography removed all cross-reactivity of the anti-SR1 antibodies except the *Vibrio* species. This should not be a limiting factor as the *Vibrio* sp. is not present in the cerebrospinal fluid of the infected person (Blake, Weaver *et al.* 1980). In light of the specificity of these antibodies, it may be useful to raise monoclonal antibodies against the peptide for commercial application as a diagnostic tool for NM serogroup B.

OMP85 is an outer membrane protein that is located beneath a polysaccharide capsule (Rosenstein, Perkins *et al.* 2001). This may be a limiting factor that would affect the accessibility of diagnostic and/or therapeutic reagents that are specific to OMP85 or the SR1 peptide. During the life cycle of the *N. meningitidis,* bacteria shreds capsule and thus both capsulate and non-capsulate forms exist at different stages. Anti-SR1 antibodies against the non-capsulate bacteria form the potential base for the specific and rapid diagnosis of meningitis. Like many other virulence factors, the expression of capsular PS is phase variable (Hammerschmidt, Muller *et al.* 1996), allowing the bacteria to vary from adherent, serum sensitive, un-encapsulated phenotype to a less-adherent, serum resistant encapsulated

phenotype. Colonisation is favored by the absence of the capsule, unencapsulated mutants adhering to human buccal epithelial cells or nasopharyngeal organ cultures in greater numbers than the encapsulated parent (Stephens, Spellman *et al.* 1993). This is in strict contrast to systematic spread: encapsulation is a pre-requisite for bacterial survival in the blood. In contrast to case isolates that are frequently encapsulated, approximately 40-50% of the strains isolated from carrier patients lack the capsule and hence are not grouped serologically (Caugant, Kristiansen *et al.* 1988; Ala'Aldeen, Neal *et al.* 2000). Alternatively, when the patient sample is subjected to treatment with detergents such as SDS, NM bacteria shred the capsule under stress conditions which exposes the outer membrane proteins.

2.5.3. Capsule and anti-capsular monoclonal antibodies

With the exception of serogroup A meningococci, all disease associated serogroup B, C, Y and W135 have sialic acids in their capsular polysaccharide structures (Vogel, Hammerschmidt *et al.* 1996) and the capsule is the major virulence factor of meningococcus bacteria. The poor immunogenicity of the *Neisseria meningitidis* group B polysaccharide capsule, a homopolymer of a sialic acid, has been attributed to immunologic tolerance induced by prenatal exposure to host polysialyated glycoproteins, such as the neural cell adhesion molecules expressed in a variety of host tissues (Orskov, Orskov *et al.* 1979; Beuvery, van Rossum *et al.* 1982).

The capsular polysaccharide of *N. meningitidis* serogroup B bacteria was purified by a simple and slightly modified procedure (Section 2.3.9.). The purity was assessed by Tricine-SDS PAGE gel electrophoresis. Using Reversed phase HPLC, the capsule preparation was observed as a single peak without any impurities. Commercial anti-capsular monoclonal antibodies were equally reactive both with the bacteria and the purified capsule. The capsule was purified as an alternate target antigen for future experiments for the gold nanoparticle based experiments as described in chapter 4 and 5.

2.5.4. Cross reactivity assay and monospecificity of anti-SR1 antibodies

A panel of different antibodies were examined for cross reactivity against the range of closely associated bacteria. The anti-OMP 85 and anti-NM polyclonal antibodies showed a higher degree of cross reactivity relative to the anti-SR1 polyclonal antibodies. It is mainy that the cross-reactivity is due to the nature of polyclonal antibodies which contain a multitude of reactive antibodies against a broad range of epitopes. Being a highly conserved protein among Gram negative bacteria and that the protein was expressed in *E. coli*, explains why anti-OMP85 polyclonal antiserum showed high cross reactivity. Pre clearing the anti-OMPP85 polyclonal antibodies with *E.coli* and other bacteria may be an idea to make them more specific to *Neisseria meningitidis* and it could be used as in capture system in an ELISA or in a QCM immunosensor.

2.5.5. Shark IgNAR phagemid library panning

Screening of IgNAR library to identify OMP85 protein and other antigen specific IgNAR's (at CSIRO Health Sciences and Nutrition, Parkville) was not successful. All the psuedopositive clones were finally proven as either non-specific or sticky clones.

These target antigens and their antibodies and in particular OMP85 antigen and anti-OMP85 antibody were utilized to conjugate to the gold nanoparticles and ultimately to develop a model diagnostic assay for the rapid diagnosis of *N. meningitidis*.

Chapter 3

Gold Nanoparticles: conjugation with proteins

3.1. Introduction

For the past few decades, colloidal gold nanoparticles and their attractive and unusual solution properties have led to the development of a range of useful applications, especially in the biotechnology and nanotechnology fields (Gittins, Bethell *et al.* 2000; Bachtold, Hadley *et al.* 2001). Nano-scale particles are also referred with other names such as, clusters, colloids, hydrosols, nanoparticles and nanocrystals.

Attention was drawn to colloidal gold particles because their unique properties are very different from the bulk or the atomic state**.** Despite all the promise about the nanotechnology, the control of nanostructures and ordered assemblies of nanoparticles to develop a proper nanodiagnostic assay has so far been limited. This chapter describes the synthesis of gold nanoparticles and the conjugation of biomolecules to the nanoparticles.

For many different biotechnological applications, colloidal gold nanoparticles are conjugated with biomolecules. Before proteins can be conjugated to nanoparticles, a preliminary titration must be performed to determine the

optimum conditions for conjugation to favour protein binding to the gold particles. The optimal conjugation ratio can be determined by means of a flocculation assay.

Under normal circumstances, the monodisperse gold nanoparticles suspended in water are surrounded by a predominantly anionic double layer. This anionic coating, which is also referred to as the plane of shear, is usually measured in terms of zeta-potential (mV). This helps to stabilise the particles by the repulsive forces and can be considered as a direct measure of the stability of the colloid (Xie, Tkachenko *et al.* 2003).

However, due to induced changes in the charges by the addition of millimolar concentrations of various electrolytes, the particles can become aggregated as a result of the shielding of the repulsive double-layer charges which normally stabilise them (Xie, Tkachenko *et al.* 2003). This irreversible process changes the colour of the colloidal solution from red to blue.

Aggregation can be prevented by coating the gold nanoparticles with a protein layer as a stabiliser. The amount of stabiliser or protein needed to prevent aggregation is determined by increasing the concentration of electrolyte in various nanoparticle preparations, previously coated with distinct amounts of proteins (Xie, Tkachenko *et al.* 2003). The aggregation can be conveniently

monitored photometrically by the decrease and/or red shift of the plasmon absorption band at approximately 520 nm.

The conjugation of a protein to the gold nanoparticle surface may originate from both chemical (hydrogen bonding, polarity and charge effects) (Mann 1988) and structural (size and morphology) recognition mechanisms (Weissbuch, Addadi *et al.* 1991). Target biomolecules such as proteins, peptides and oligonucleotides which usually have a positive charge in solution near neutral pH, can be electro statically attached to the negatively charged colloidal gold nanoparticles surface for detection and localisation (Sarikaya, Tamerler *et al.* 2003). In the case of gold clusters, biomolecules are attached to nanoparticles by covalent linking.

Colloidal gold nanoparticles are often stabilised by anionic ligands such as carboxylic acid derivatives such as citrate, tartrate and lipoic acid (Keating, Kovaleski *et al.* 1998; Peng, Chen *et al.* 2007). Citrate reduced gold nanoparticles have been conjugated with immuniglobulin molececules through non-covalent electrostatic interactions at pH values that are slightly above the isoelectric point of the citrate ligand (Keating, Kovaleski *et al.* 1998). This helps in effective binding between the positively charged amino acid side chains of the protein and the negatively charged citrate groups of the colloids. In addition, colloidal gold conjugates can also be stabilised with an inert macromolecule such as bovine

serum albumin (BSA), gelatin, carbowax or polyethylene glycol to block the non-specific binding sites on the nanoparticle surface.

The adsorption of haem-containing redox enzymes on to citrate-stabilised silver nanoparticles (Broderick, Natan *et al.* 1993; Macdonald and Smith 1996) and the conjugation of basic leucine zipper proteins to lipoic acid stabilised semiconductor particles (Mattoussi, Mauro *et al.* 2000) are examples of protein conjugaton by electrostatic interactions. Biomolecules conjugated by this method may not be active and can be readily lost from the surface and thereby lose their biocatalytic or biorecognition properties. However, most proteins and enzymes have been shown to retain their native structure and activity after they were electrostatically conjugated to the nanoparticles and very few conjugations resulting in conformational changes and loss of biological activity of the protein involved (Keating, Kovaleski *et al.* 1998).

The problems of non-specific binding of proteins through electrostatic interactions may be prevented by covalent attachment of proteins to nanoparticle surfaces, thus overcoming the problems of false or background labelling (Jain 2006). Unlike conventional colloidal gold nanoparticles, gold nanocluster labels are coordination complexes and are neutral in nature. Nanoclusters can be covalently linked to specific sites or reactive group on biomolecules, for detection

and localisation. This gives the covalent linking, a range and versatility which is not available in case of ionic interaction of colloidal gold.

Gold nanoparticles can be covalently cross-linked to a specific functional group on biomolecules (Jain 2006). For example, monomaleimido-NHS and mono-*sulpho*-NHS reagents react only with thiol (sulphydryl) groups and amine groups of the proteins respectively (Gregori, Hainfeld *et al.* 1997). This site-specificity allows it to be conjugated at a position remote from the recognition site so that it does not interfere with target binding. For example, monomaleimido-gold nanoparticles binds antibody Fab' fragments specifically at the hinge region (Lee and El-Sayed 2006). The most commonly used functional targeted groups for covalent conjugation of the biological compounds to nanoparticles are amine, active ester, and maleimide groups and this is achieved by means of carbodiimide-mediated esterification and amidation reactions or through reactions with thiol groups (Niemeyer 2001).

For generation of biomolecule-nanoparticle conjugates by covalent interaction, low-molecular weight bifunctional linkers, with an anchor group for attachment to nanoparticle surfaces and a functional group for conjugation to the target biomolecules, are used (Niemeyer 2001). A wide variety of terminal functional groups such as thiols, disulphides, or phosphine ligands are available in different bifunctional linkers for the binding to Au, Ag, CdS, and CdSe nanoparticles. The

chemically modified clusters with single functional groups (e.g. active ester or amine units) on gold nanoparticles are also available (Malecki, Hsu *et al.* 2002). These structures are helpful for the covalent binding of a single target biomolecule per nanoparticle.

3.1.1. Reactions of Thiolate-stabilised gold nanoparticles

The binding of functionalised thiolated molecules, such as oligopeptides to nanoparticles is achieved by means of covalent linking (Parak, Pellegrino *et al.* 2003). In the case of proteins, thiol groups from cysteine residues that exist in the proteins can bind with the nanoparticle surface (Hayat 1991). If thiolated residues are not present in the native protein sequence, thiol groups can be incorporated by chemical means, for example, with 2-iminothiolane (Traut's reagent) (Hayat 1991) or through genetic engineering (Hong, Jiang *et al.* 1994).

Alkane thiolate stabilised gold nanoparticles are synthesised directly and also, various functional thiols could be partially incorporated into gold nanoparticles using a substitution reaction. Various other groups, labels and catalysts have been similarly introduced using this ligand-exchange reaction (Hostetler, Wingate *et al.* 1998; Li, Luk *et al.* 1999; Templeton, Wuelfing *et al.* 2000; Song and Murray 2002; Montalti, Prodi *et al.* 2003). Apart from the use of thiols and other linker molecules, there have been reports that describe the use of gold-binding peptides (for example; MHGKTQATSGTIQS) with substantially improved

binding compared with native protein binding even in the presence of a detergent and at high salt concentrations (Sarikaya, Tamerler *et al.* 2003).

Conjugate separation from unlabelled gold or free ligand is usually achieved by either centrifugation or by membrane filtration or dialysis or by gel size exclusion chromatography (SEC) using HPLC (Wolfe, Warrington *et al.* 2005). SEC is the best method for separating gold nanoparticle labelled conjugates, although membrane centrifugation is useful, especially for the labelling of very large proteins (Wolfe, Warrington *et al.* 2005). Density gradient ultracentifugation and other separation methods are also often used to separate colloidal gold conjugates from non-conjugates. Ion exchange, hydrophobic interaction, or reversed-phase chromatography may also be used, if the conjugate biomolecule is charged or has very distinct hydrophobic properties.

Gold nanoparticle-biomolecule conjugates may be visualised using native gel electrophoresis (Wang, Wu *et al.* 2006). A gold nanoparticle-labelled molecule typically runs higher on the gel due to the added weight of the gold nanoparticle, although in practice the observed gel shift may be very small.

Following purification of conjugates, the extent of labelling may be determined from analysis of the UV-Visible spectrum of the conjugate (Haiss, Thanh *et al.* 2007). Gold labelling of most proteins is best calculated using the molar absorptivity constant at 280 nm, where proteins usually absorb strongly and their

molar absorptivity constant are known, and 520 nm, where gold nanoparticles absorb strongly but most proteins do not. Most proteins do not absorb at all in the visible spectrum: therefore, the absorption at 520 nm arises solely from the gold nanoparticle (Haiss, Thanh *et al.* 2007). With antibody labelling, the calculation is simplified because these proteins do not absorb at 520 nm. The molar absorptivity constant of a typical IgG is 203,000 $cm^{-1}M^{-1}$ at 280 nm. This value may have to be determined for individual proteins.

Numerous challenges including synthesis of the nanoparticles with uniform size and shape, controlling their mineralogy, surface structures and chemistry, and predicting their spatial distribution need to be addressed before the nanoparticles can be successfully implemented for future technological materials and devices (Niemeyer 2001).

3.2. Materials and Methods

Materials

All glassware was scrupulously clean. Glass and plastic containers and stirrers were cleaned in aqua-regia and thoroughly washed in Milli Q water. Aqua regia (3:1 HCl:HNO_3) was made fresh each time. 13 nm gold nanoparticles were prepared by citrate reduction method. The larger size gold nanoparticles (30nm, 40nm, 50nm and 60nm) used in this chapter were purchased from the British Biocell Ltd., UK.

Sodium citrate, aurochloric acid ($HAuCl_4 \cdot 3H_2O$), β-mercaptoethanol, N-acetyl cysteine (NAc), mercapto succinic acid (MSA), phenylalanine, Tween-20 and SDS were purchased from Sigma-Aldrich Ltd., USA. Bio-Rad Bradford assay reagent was used for protein estimation. All reagents were of high quality analytical grade and were filtered immediately before use.

3.2.1. Synthesis of gold nanoparticles

A solution of 5.0 x 10^{-3}M $HAuCl_4$ in water was prepared. A 1.0 mL aliquot of 5.0 x 10^{-3}M $HAuCl_4$ solution was added to 18.0 mL of distilled H_2O and heated until it began to boil. Once boiling, 1.0 mL of 0.5% (w/v) sodium citrate solution was added to gold solution. The reduction of the gold ions by the citrate ions was complete after 5 min which was evident by the solution colour change to deep

red solution. The boiling was continued for further 30 min (Turkevich, Stevenson *et al.* 1951).

The solution was removed from the heating element and continued to stir until it cooled down to room temperature. The solution was topped up to 20 mL to account for any loss due to boiling. The colloidal suspension was stored at 4 °C in a bottle covered with aluminium foil. The larger size gold nanoparticles (30nm, 40nm, 50nm and 60nm) used in this chapter were purchased from the British Biocell Ltd., UK.

3.2.2. Characterisation of gold nanoparticles

3.2.2.1. UV-Vis Spectrophotometry

The synthesised gold nanoparticles were analysed using a Hitachi U2000, UV-visible absorption spectrophotometer. Each batch synthesised, including the commercial gold nanoparticles were analysed by spectral scan in the range of 400-800 nm to identify the characteristic wavelength peak and for uniform size distribution.

3.2.2.2. Transmission electron microscopy (TEM) analysis of gold nanoparticles

Citrate-reduced gold nanoparticles were characterised in terms of uniform size distribution by TEM using Philips EM400 microscope at an accelerating voltage of 80 kV). Approximately, 20 µL of gold nanoparticles were coated onto a

Formvar coated copper EM grid (200 mesh) and dried for at least 30 minutes. The suspension on the grid was observed without further treatment.

3.2.2.3. Particle Size - Light scattering

The 13 nm gold nanoparticles prepared by citrate reduction method and the commercial gold particles were analysed by dynamic light scattering (DLS) method using Brookhaven 90 Plus particle size analyser and measured with scattered 657 nm laser light at 90°. Colloidal suspensions were diluted when counts/sec were greater than 600,000 to prevent multiple photon scattering.

3.2.3. Preparation of antigen/antibody–gold nanoparticle conjugates

The 13 nm lab made citrate capped gold nanoparticles and 30, 40, 50 and 60 nm commercial gold nanoparticles from British Biocell were used for conjugation. Both the antibody and antigen were affinity purified using protein A sepharose and Ni-NTA chromatography respectively. The OMP85 and anti-OMP85 antibody were conjugated to the gold nanoparticles by identical procedures. Critical flocculation concentration (CFC) and the role of different stabilisers were evaluated to optimise the conditions for protein-gold nanoparticle conjugation. The following scheme was followed in order to determine the critical flocculation concentration (CFC) of OMP85 antigen and anti-OMP85 antibody for conjugation and stabilisation of the gold nanoparticles.

3.2.3.1. Determination of optimal NaCl concentration (CFC)

Gold nanoparticle-OMP85 protein conjugates (10 mg/mL) were prepared using the gold nanoparticle–protein conjugation protocol which is detailed in the later part of the protocol. These gold nanoparticle conjugates were dispensed in a series (100 µl each) into 96 well ELISA plate. The gold nanoparticle conjugates were then exposed in duplicates to 100 µl of different sodium chloride (NaCl) concentrations (to a final concentration of 0.001 - 2.0 M NaCl in equal volumes). The solutions were agitated for 5 minutes and observed for aggregation to determine the maximum concentration of NaCl, after which the conjugates were no longer stable. Aggregation was monitored at different wavelengths (490 nm, 595nm, 620 nm and 650 nm) in an ELISA plate reader (Bio-Rad, USA).

3.2.3.2. Optimum Protein Concentration

Gold nanoparticle-protein conjugates with varying concentrations of both OMP85 antigen and anti-OMP85 antibody (0.01-10 mg/mL) were prepared by following the gold nanoparticle – protein conjugation protocol. Having determined the optimum salt concentration in the previous experiment, a series of 100 µl aliquots of NaCl (one dilution below the optimum concentration) were dispensed into a 96 well ELISA plate.

Followed by addition of 100 µl (in duplicates) of different concentrations of gold nanoparticle-protein conjugates. Then the solutions were agitated for 5 minutes and observed for aggregation to find the minimum amount of protein required

to stabilise the particles at that particular NaCl concentration. Aggregation was again monitored at four different wavelengths 490 nm, 595 nm, 620 nm and 650 nm.

3.2.3.3. Effect of different stabilisers

Folowing the determination of the optimum salt concentration and the minimum amount of protein required for successful conjugation, the effect of different stabilisers were examined to observe their effect upon stability of the conjugates and whether the stabiliser is displacing any bound protein.

3.2.3.3A. Effect of increasing concentration of stabilisers

Gold nanoparticle-protein conjugates aliquots (100 µl) were dispensed into an ELISA plate as described before. Then, 60 µl of NaCl (to a final optimum concentration) was added to each well. At this stage, all the suspensions were red in colour.

This step was followed by the addition of 40 µl of the different stabilisers (N-acetyl cysteine, mercapto succinic acid (MSA), phenylalanine, Tween-20 and SDS) at varying concentrations. After mixing for 5 minutes, the plates were assessed for aggregation to determine the effect of different stabilisers on the stability of conjugates. The ELISA plates were centrifuged and the supernatants were collected for determination of free protein content using the Bradford assay.

3.2.3.3B. With increasing concentration of NaCl

Gold nanoparticle-protein conjugates were prepared using the optimum concentration of the protein. The conjugates were distributed (100 µl aliquots) into an ELISA plate as described previously. Then, 40 µl of the different stabilisers (N-acetyl cysteine, mercapto succinic acid (MSA), phenylalanine, Tween-20 and SDS) of predetermined concentrations were added. Every combination was performed in duplicate.

This step was followed by addition of 60 µl of NaCl (increasing from critical flocculation concentration) to each well. Following mixing for 5 minutes and observed for aggregation to find out whether the presence of any stabilisers increased/decreased the stability of conjugates. Aggregation was monitored at 620 nm wavelength in an ELISA plate reader.

3.2.3.4. Protein-gold nanoparticle Conjugation

After determining the optimum conditions required for the successful conjugation and stabilisation of proteins to the gold nanoparticles, the quantities were scaled up. Typical experimental details are described as follows (Figure 3.1).

The OMP85 antigen and the anti-OMP85 antibody solutions (1.0 µg/µl) were resuspended in 5 mM sodium carbonate buffer pH 9.4, by using 30 kDa cut-off membrane filters. It was followed by addition of the predetermined amount of

antibody/antigen (to a final concentration of 0.25 mg/mL of OMP85 and 0.5 mg/mL of anti-OMP85 antibody) solution drop wise to the gold nanoparticle suspension, while mixing gently. Mixing continued for 30 minutes followed by another 30 minutes of incubation at room temperature (without mixing).

Any exposed binding sites on the surface of the gold particles were blocked to prevent non-specific binding by addition of 100 µl of filtered 1% (w/v) BSA in 5mM sodium carbonate buffer pH 9.4 and stirred gently for 15 minutes.

3.2.3.5. Purification

The gold conjugates were purified from excess protein and nanoparticles before using for any experiment or storing. To separate any unbound protein and nanoparticles, nanoparticle conjugates were washed three times by centrifugation at 5000 to 20, 000 x g for 30-60 minutes, depending on the size of nanoparticles.

These speeds and times were optimised and determined experimentally. The conjugates were centrifuged at different x g forces according to gold particle size:

13nm	20,000 x g	for 1h @ 4 °C
20nm	16,000 x g	for 1h @ 4 °C
30nm	12,000 x g	for 1h @ 4 °C
40nm	8,000 x g	for 1h @ 4 °C
50nm	6,000 x g	for 1h @ 4 °C
60nm	5,000 x g	for 1h @ 4 °C

The final product was a loose red precipitate. The clear supernatant was separated and used to determine the amount of protein adsorbed onto the nanoparticles using the Bradford protein assay. The pellet was resuspended and stored in 10 mM sodium phosphate buffer pH 7.4 containing 1% (w/v) BSA in order to shield any exposed binding sites on the gold surface. The suspensions were stable for several months. The conjugates prepared were examined for sensitivity and specificity by ELISA against the specific antigen/antibody molecules.

Protein coated gold nanoparticle suspensions were stored in vials wrapped with aluminum foil and stored in the dark at 4 °C to protect the gold nanoparticles from oxidation and light-induced aggregation.

3.2.3.6. Conjugation efficiency

To determine the amount of OMP85 and anti-OMP85 antibody adsorbed onto the nanoparticles, 10 mM mercaptoethanol was added to reduce the sulphur – gold bond and to release all conjugated protein into solution. The amount of released protein was measured by absorbance at 280 nm and the gold particle concentration was measured by optical absorbance in the range of 520 – 535 nm according to the size.

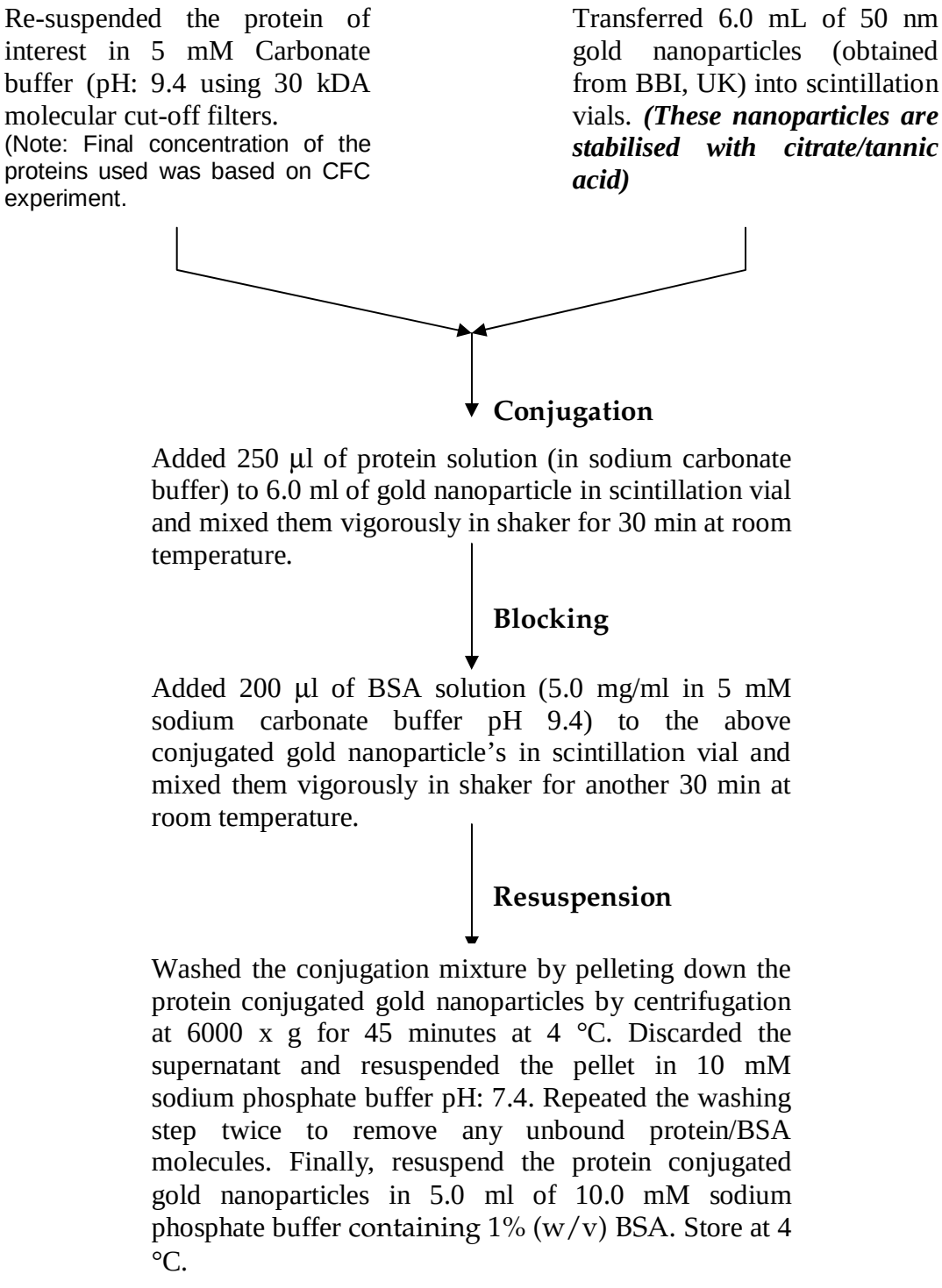

Figure 3.1. Flow chart of Gold Nanoparticle-Protein Conjugation Protocol

3.2.4. Detection of protein-conjugated gold nanoparticles by SDS-PAGE

After labelling the gold nanoparticles with proteins, unbound gold particles were removed by centrifugation. After separating the unbound proteins and nanoparticles, 20 µl of OMP85 conjugated gold nanoparticle suspension was mixed with 5.0 µl of modified SDS-PAGE sample buffer (appendix 2). With out heating, the samples were loaded in duplicates onto a 6% SDS-PAGE gel and the normal gel running procedure was followed (Section 2.3.1C).

Silver staining was performed to develop the gold nanoparticles effectively. When optimal staining was reached, further development was stopped by rinsing in distilled water. The gel was scanned to visualise the bands pattern.

3.3. Results

3.3.1. Gold nanoparticle synthesis

The 13 nm gold nanoparticles were synthesised successfully according to standard wet chemical method (Turkevich, Stevenson *et al.* 1951) using sodium citrate as a reducing agent. Figure 3. 2 show the typical reaction of formation gold nanoparticles by citrate reduction.

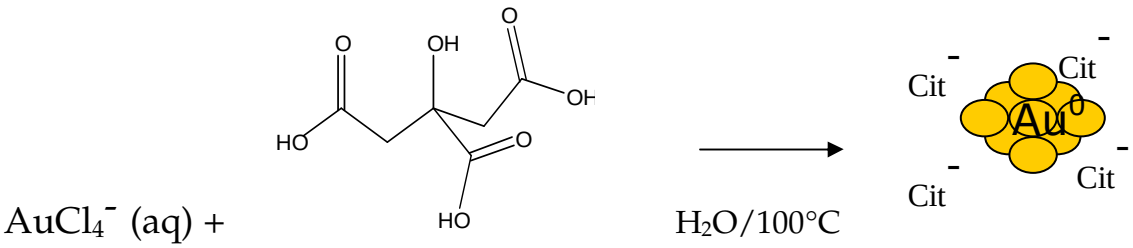

Figure 3.2. Reduction of $HAuCl_4$ by sodium citrate

3.3.2. UV-Vis spectral analysis of gold colloidal suspension

The characteristic surface plasmon band for 13 nm gold nanoparticles at 520 nm peak wavelength was observed (Figure 3. 3) in the UV-Visible spectrum, confirming the presence of gold nanoparticles.

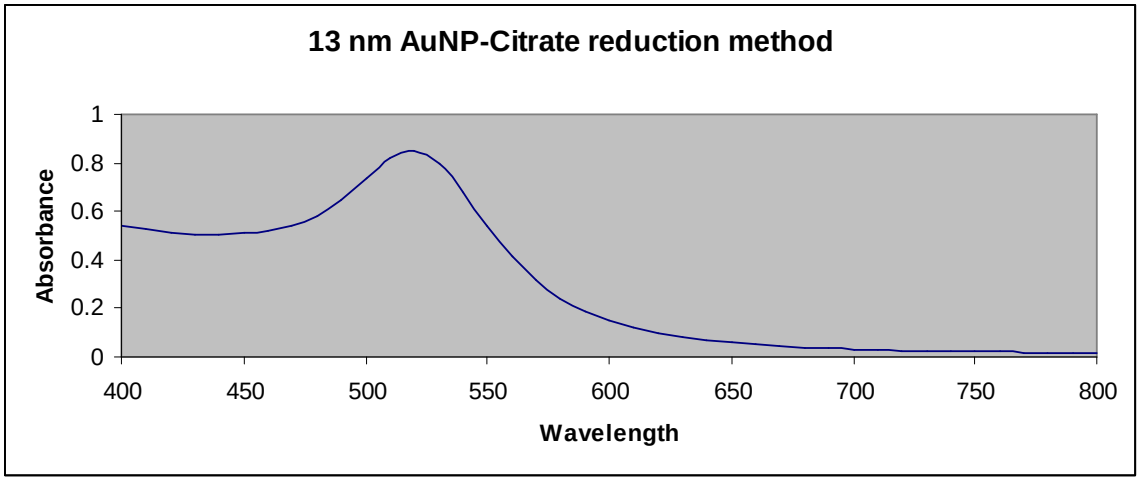

Figure 3.3. UV/Visible absorbance spectrum of 13 nm gold nanoparticles with a characteristic peak at 520 nm.

3.3.3. Transmission Electron Microscopy (TEM) analysis

Both laboratory synthesised 13 nm gold nanoparticles and the commercial 30, 40, 50 and 60 nm gold nanoparticles were analysed by transmission electron microscopy. TEM micrographs (Figure 3. 4) showed the presence of spherical gold nanoparticles of approximate size (13 nm and 50 nm) with uniform size distribution. Although the actual value of the mean size might vary slightly from each preparation, the size distribution was found to be always about 10% standard deviation. Size distribution analysis clearly showed that nearly 90% of the particles reside within their size range.

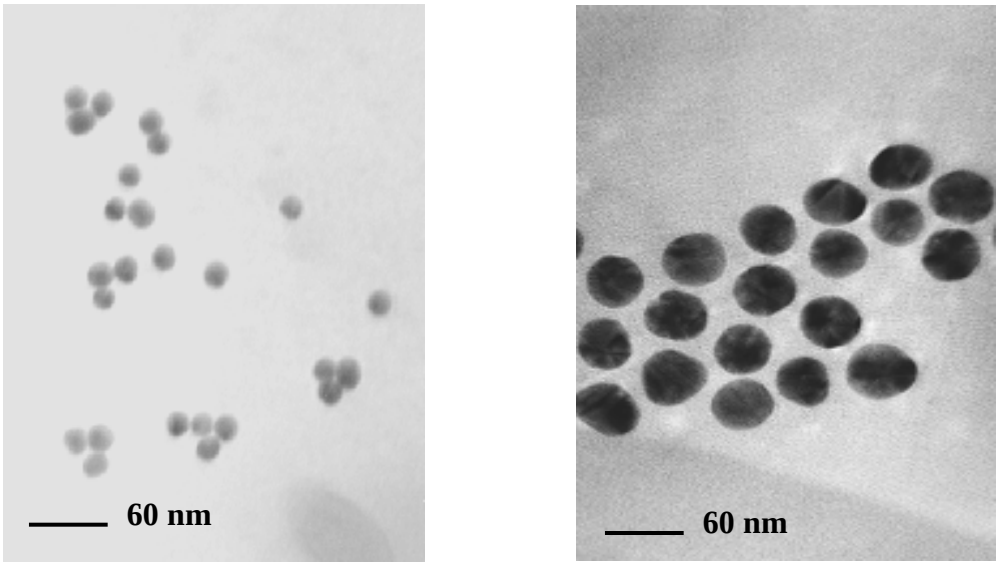

(a) (b)

Figure 3.4. TEM images of (a) 13 nm gold nanoparticles and (b) 50 nm gold nanoparticles.

3.3.4. Particle Size – Light Scattering analysis

Dynamic light scattering measurements showed the average mean diameter of the particles. Figure 3. 5 show the light scattering results of the 30nm, 40 nm and 60 nm gold nanoparticles.

(a)

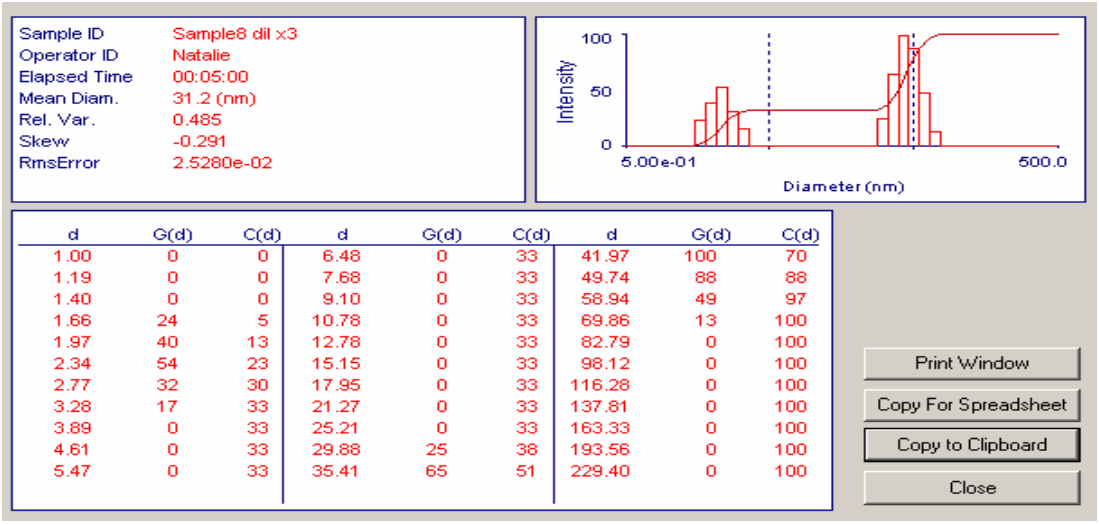

(b)

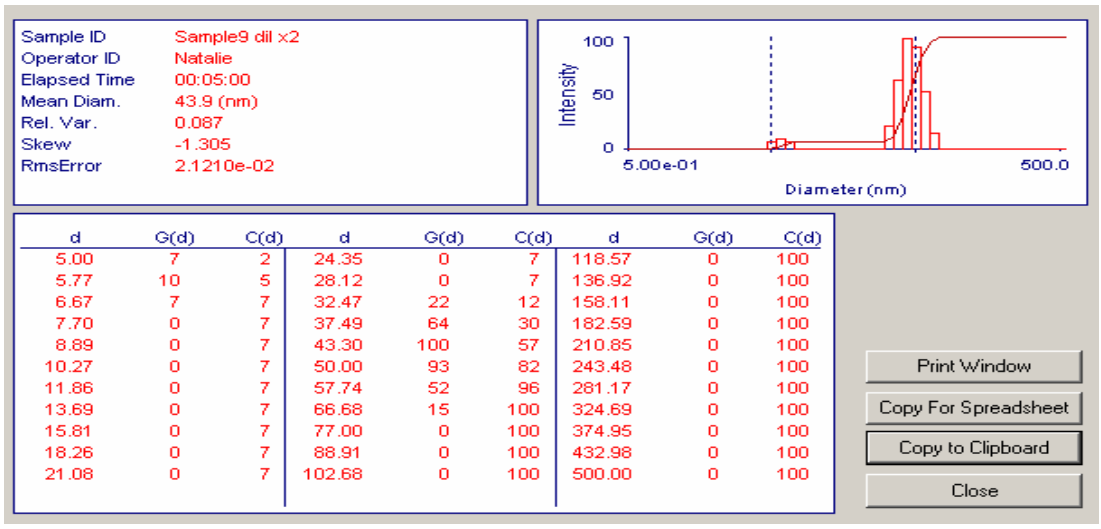

(c)

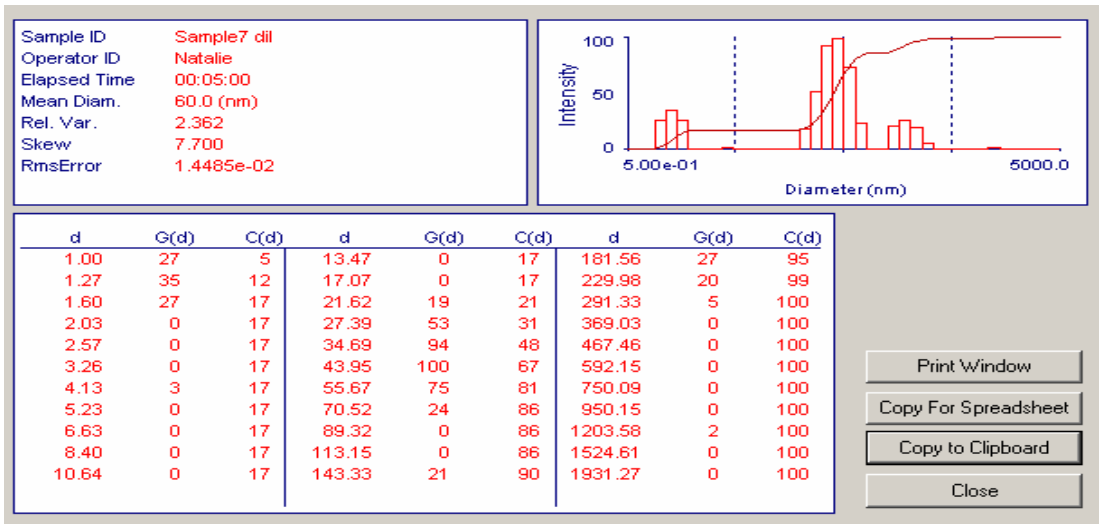

Figure 3.5. Dynamic light scattering measurements of (a) 30nm, (b) 40nm and (c) 60 nm gold nanoparticle

3.3.5. Protein-gold nanoparticle conjugation

3.3.5.1. Critical Flocculation Concentration

The NaCl solution destabilised the colloid gold nanoparticles and caused aggregation. The sample containing gold nanoparticles and no protein was destabilised immediately upon the addition of electrolytes. As the protein

concentration increased, the stability of the nanoparticles also increased which was reflected by a resistance to change from red to blue colour shift. During the flocculation assay, the aggregation was monitored photometrically by the decrease and/or red shift of the plasmon absorption band at different wavelengths of 490nm, 595 nm, 620 nm and 650 nm.

3.3.5.2. Optimum NaCl Concentration

The tube containing the minimum amount of salt to keep the particles stable was indicated by change from red to blue. In the case of both OMP85 and anti-OMP85 antibody conjugation experiments, the particles were stable up to a final concentration of 0.512 M NaCl. Nanoparticles started to aggregate with any concentration of the salt above 0.512 M NaCl (Figure 3. 6).

(a)

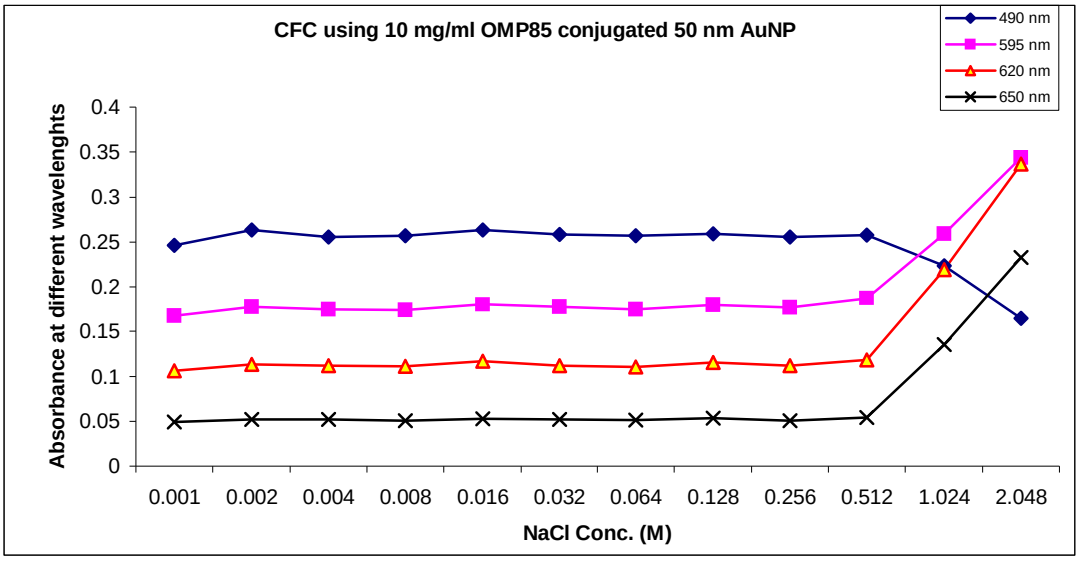

(b)

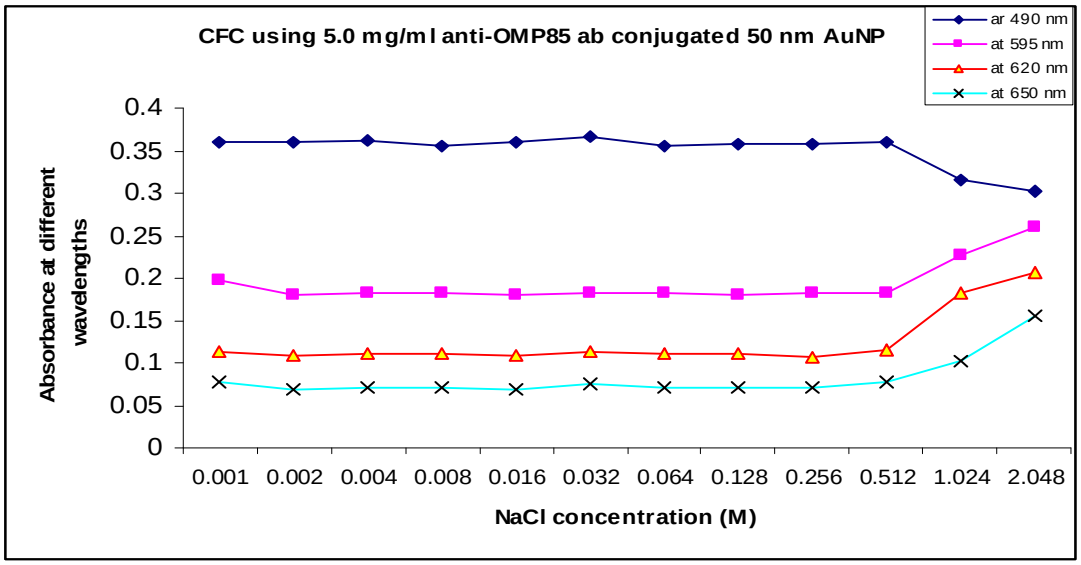

Figure 3.6. Critical flocculation concentration of 50 nm gold nanoparticles conjugated with (a) OMP 85 protein and (b) anti-OMP85 antibody. Both were stable up to a final concentration of 0.512 M NaCl

3.3.5.3. Optimum Protein Concentration

Though the optimum salt concentration of 0.512 M (from the above experiment) was observed, one dilution below that point i.e. 0.256 M NaCl concentration was used for determining the optimum protein concentration. The tube containing the minimum amount of protein required to stabilise the gold sol was indicated by the one in which the colour of the gold sol did not change from red to blue upon the addition of NaCl. In the case of both OMP85 and anti-OMP85 antibody conjugation experiments, the minimum amount of protein required to keep the particles stable was found to be 0.4 mg/mL of final concentration (Figure 3. 7). Nanoparticles started to aggregate when the protein concentration used fell below 0.3 mg/mL.

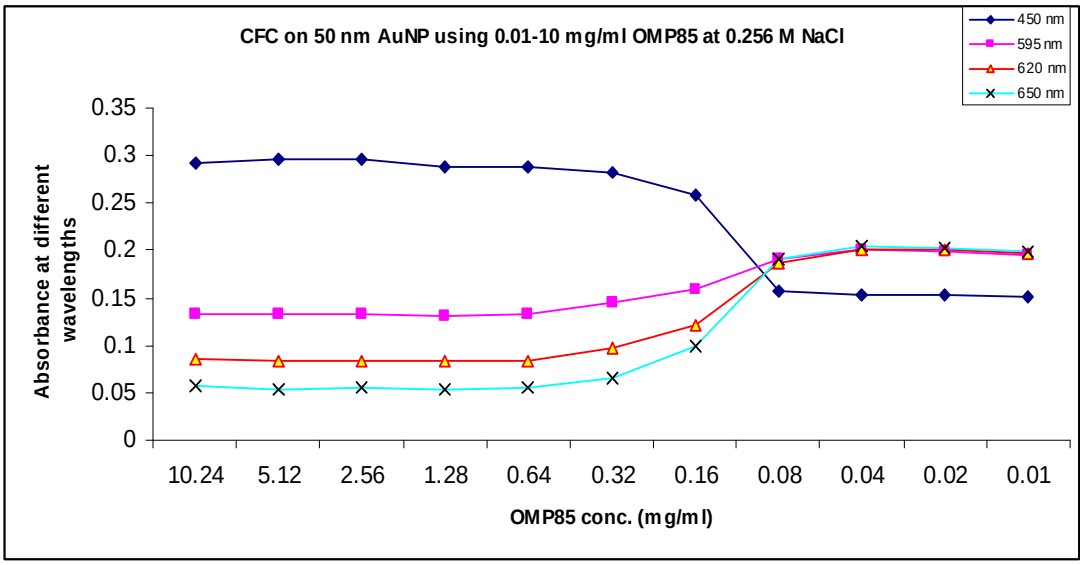

(a)

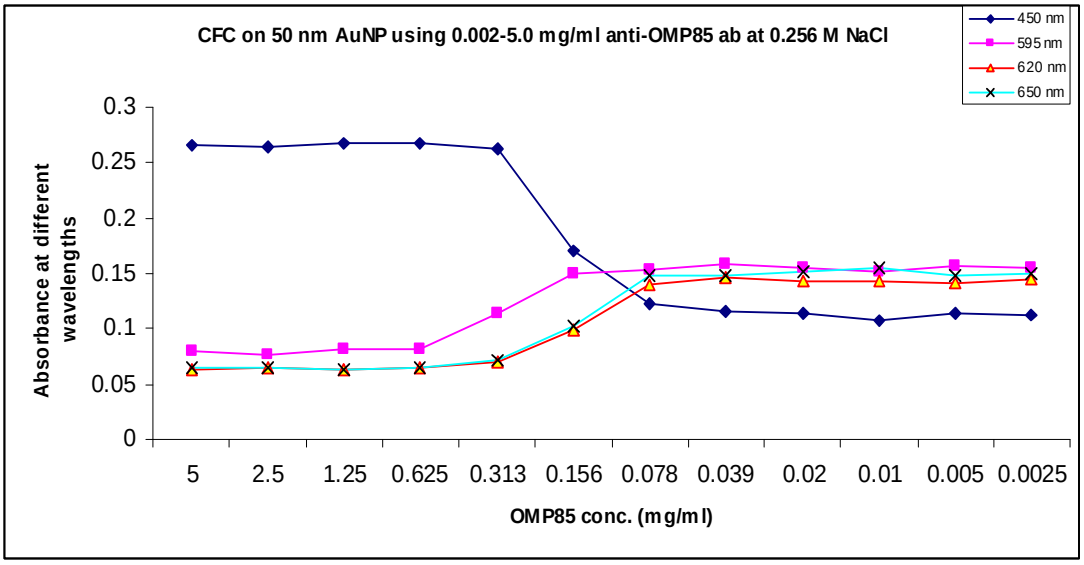

(b)

Figure 3.7. Critical flocculation conentration experiment to determine the minimum protein concentration required to stabilise the 50 nm gold nanoparticle in presence of 0.256 M NaCl. (a) OMP85 conjugated and (b) anti-OMP85 conjugated.

3.3.5.4. Effect of different stabilisers

The effect of different stabilisers on the increasing or decreasing of stability of

gold nanoparticle-protein conjugates did not produce any conclusive results.

The presence of NAc and MSA led to aggregation of the conjugates resulting in a colour change from ruby red to blue, despite the fact that analysis of the supernatants using Bradford assay showed that no protein was released or displaced from the aggregated conjugates (Figure 3.8). Addition of phenylalanine, Tween-20 and SDS resulted in no colour change of the conjugates. However, the Bradford assay on the supernatants revealed that, phenylalanine and SDS did not displace the bound protein, whereas the particle suspension containing Tween-20 appeared to have protein present in the supernatant suggesting that protein was released from the nanoparticles.

(a)

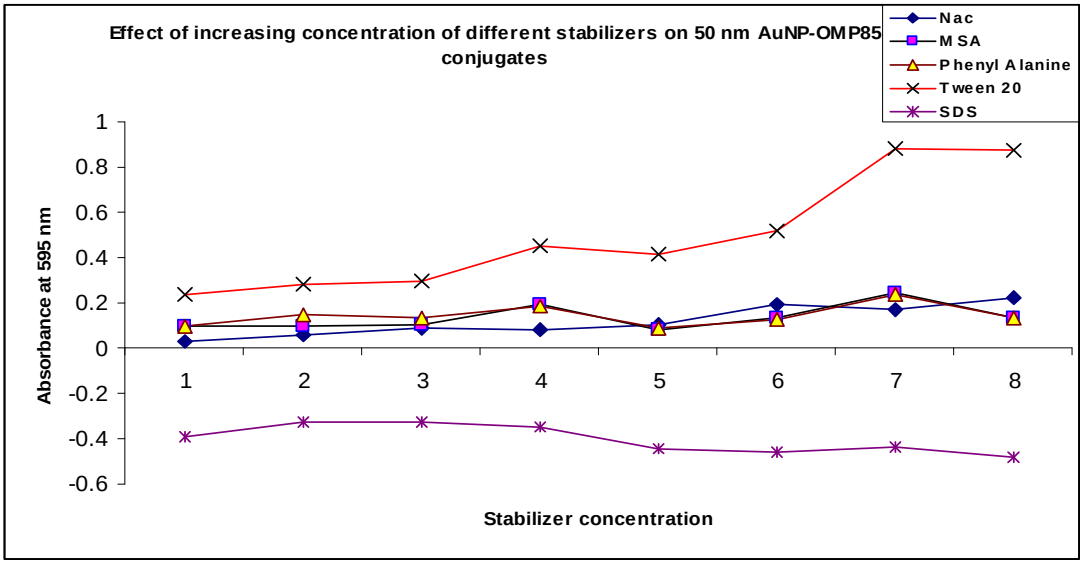

(b)

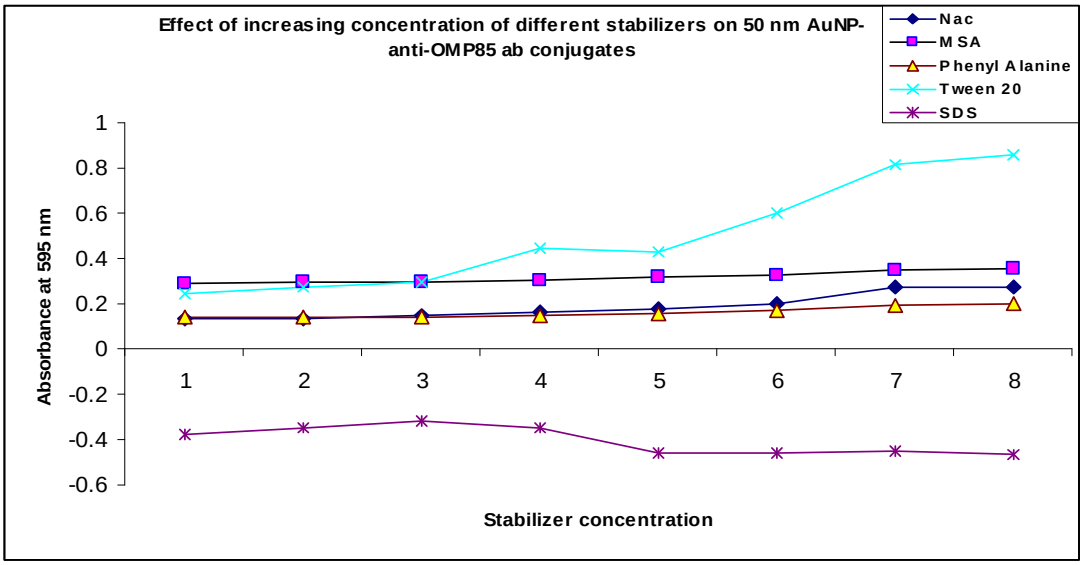

Figure 3.8. Effect of increasing concentration of different stabilisers on the 50 nm gold nanoparticle conjugated with (a) OMP85 protein and (b) anti-OMP85 antibody, in presence of 0.256 M NaCl.

3.3.5.5. Effect of Sodium Chloride concentration in presence of stabilisers

Presence of NAc and MSA did not increase the stability of the conjugates but rather, the conjugates aggregated immediately. However, the stability was increased by two fold by the addition of SDS and Tween-20. That is the stability of the particles increased from 0.256 M NaCl to 0.512 M NaCl. However, there was no change in the stability of the conjugates in the presence of phenylalanine.

Figure 3. 9. shows the image of a typical CFC experiment of conjugating OMP85 protein and anti-OMP85 antibody conjugated gold nanoparticles in the presence of increasing salt concentration.

Figure 3.9. Image of the critical flocculation experiment (CFC) experiment of 50 nm gold nanoparticle conjugated with OMP 85 protein. Similar experiment was performed with anti-OMP85 antibody conjugated 50 nm gold nanoparticles. Both were stable up to a final concentration of 0.512 M NaCl.

3.3.5.6. Gold nanoparticle-protein conjugation

Despite some initial inconsistencies with the gold nanoparticles and protein conjugation techniques, conditions were optimised for different sized gold nanoparticles to achieve successful conjugation with OMP 85 and anti-OMP 85 antibodies. Unbound proteins and nanoparticles from the nanoparticle-protein conjugates were separated by centrifugation and the conjugated nanoparticles were resuspended in 10 mM sodium phosphate buffer pH 7.4 containing 1% (w/v) BSA and they remained as a ruby red colour during storage.

A wavelength scan of the conjugated gold nanoparticles showed slight (~3-5 nm shift) or no difference from the naked gold nanoparticles (Figure 3. 10). Although conjugated gold nanoparticles are usually more stable, they were stored in a dark vial at 4°C to avoid any instability issues associated with high temperatures.

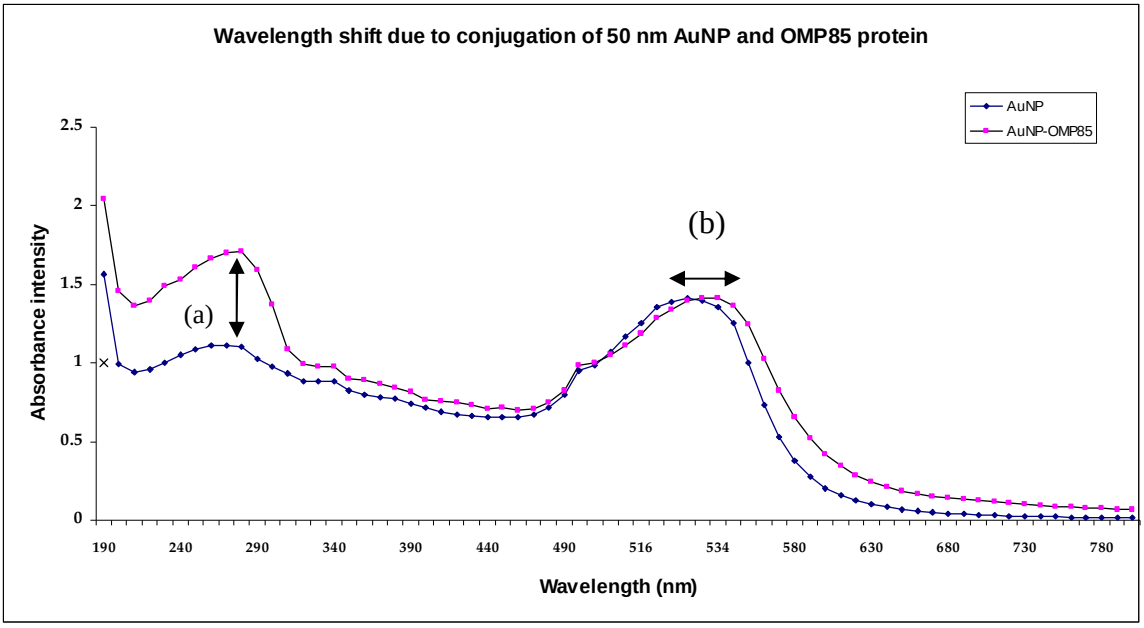

Figure 3.10. UV-visible absorbance spectrum of the 50 nm naked nanoparticles and the OMP85 conjugated gold nanoparticles. (a) Increase in absorbance at 280 nm indicating the successful conjugation of nanoparticles and OMP85 protein, (b) 5 nm red shift due to the conjugation.

Once coated and properly stabilised, the colloidal gold particles in 10mM sodium phosphate buffer containing 0.1% (w/v) BSA and 0.05% (w/v) sodium azide, did not show any sign of nonspecific agglutination. This helps to prevent bacterial contamination and also prevents the protein from adhering to the surfaces of the storage vessel.

3.3.6. Detection of protein labelled gold nanoparticles on gels

Nanoparticles were observed as a red band passing through the gel while running. Native gold nanoparticles were not stained by Coomassie blue R-250. With silver staining, proper gel shift and the difference between conjugated and

unconjugated gold nanoparticles in the gel was noticed. Detected each component separately and specifically to confirm labelling.

The molecular wt. of the 13 nm gold nanoparticles appeared to be around 80 kDa. Molecular wt. of OMP 85 is normally around 85 kDa and the molecular wt. of OMP85 conjugated nanoparticles was appeared to be in between 130 kDa to 170 kDa. Thus there was an observable gel shift (Figure 3. 11). Aggregates of the gold nanoparticles did not enter the gel and small amounts of free gold gave background staining.

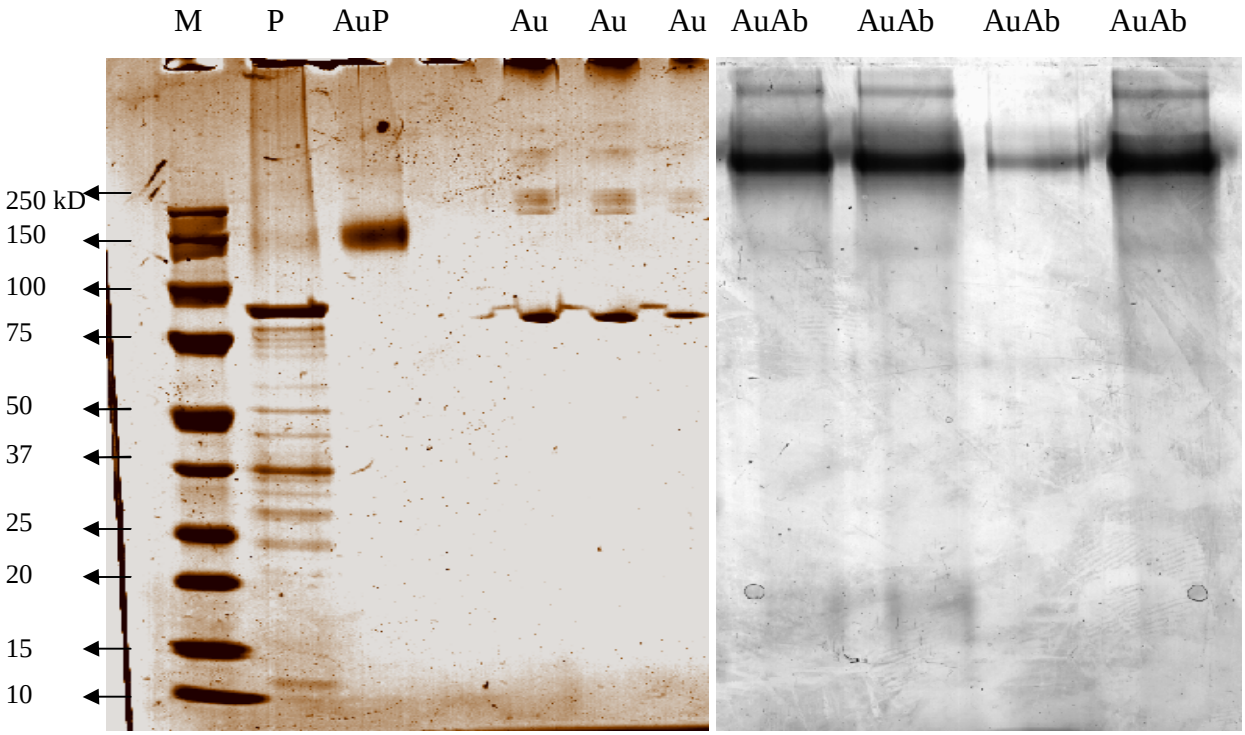

Figure 3.11. OMP85 and anti-OMP85 antibody conjugated 13 nm gold nanoparticle in ative polyacrylamide gel electrophoresis (M: Marker; P: OMP85 protein; Au: 13 nm gold nanoparticle; AuP: gold nanoparticle-OMP85 conjugates; AuAb: gold nanoparticle-anti-OMP85 antibody conjugates. Both gels were stained using different silver staining methods, resulting in differences in colour.

3.4. Discussion

The most simple method for the synthesis of gold nanoparticles was published by J. Turkevitch *et al.*. in 1951 and which was then refined by G. Frens in 1970s (Turkevich, Stevenson *et al.* 1951; Frens 1973). The sodium citrate initially acts as a reducing agent and then the negatively charged citrate ions are adsorbed onto the reduced gold nanoparticles surface. This introduced surface charge helps to repel the particles to each other and thus helps to prevent them from aggregating. It is believed that each particle has an Au^0 core and an Au^I shell as a result of incomplete reduction at the nanoparticle surface (Frens 1973). Citrate and chloride ions coordinate to the Au^I shell, and thus, each gold nanoparticle has an overall negative charge.

The citrate reduction method is generally followed to produce monodisperse spherical gold nanoparticles in the range of 10–20 nm in diameter. In this work, monodisperse gold nanoparticles with a uniform size of 13 nm were produced. These particles had a characteristic surface plasmon wavelength of 520 nm indicating that spherical particles were obtained. In general, the red colour of a colloidal gold nanoparticle suspension with diameters of 5–20 nm is due to a characteristic surface plasmon resonance peak at around 520 nm.

By varying the citrate : gold chloride ratio, larger particles can be produced, but this comes at the cost of monodispersity and shape (Haiss, Thanh *et al.* 2007). For

this reason, larger nanoparticles (30nm, 40 nm, 50 nm and 60 nm) were purchased from British Biocell and these were made using citrate/tannic acid method instead of citrate alone. These particles were fairly uniform in size and had characteristic surface plasmon wavelength peaks corresponding to their size (Haiss, Thanh *et al.* 2007).

TEM analysis of the 13 nm particles synthesised in the laboratory and the commercial larger particles confirmed the monodispersity and uniform size distribution of the nanoparticles (Daniel and Astruc 2004). To further establish the near monodispersity and sample uniformity in these materials, samples were also studied using dynamic light scattering (DLS) (Storhoff, Lazarides *et al.* 2000). Like TEM, this technique also has inherent limitations such as limited measurement range, and may not give particle diameters which are identical to the TEM observations. Nonetheless, a major advantage of DLS is that it gives a bulk measurement and thus avoids selective sampling as can occur in TEM. As such, DLS in combination with TEM and UV-visible measurements can serve as a very useful supporting technique (Mukherjee, Bhattacharya *et al.* 2007). Data obtained from DLS analysis of the larger particles supported the TEM results indicating that to make larger particles, reduction and stabilisation using citrate/tannic acid combination is better than citrate alone.

Stabilisation is an essential part of the nanoparticle synthesis process to avoid aggregation of the newly formed particles. The stability of aqueous gold nanodispersions is influenced by a number of variable factors such as salt concentration and pH (Xie, Tkachenko *et al.* 2003). In general, classical citrate-stabilised particles exhibit very poor electrostatic stability and may form aggregates in the presence of low (10 mM) concentration of electrolyte solutions. The colour of colloidal gold depends on the size and the shape of particles, as well as the composition of the surrounding medium (Underwood and Mulvaney 1994; Link and El-Sayed 1999). Aggregation of the nanoparticles shifts the peak toward longer wavelength and changes the colour of the colloidal suspension to purple to blue (Link and El-Sayed 1999). To prevent the particles from aggregating due to addition of small electrolytes, a stabilising agent that adsorbes to the nanoparticles surface is usually added. Protein adsorption stabilises the metal particles and prevents flocculation (Daniel and Astruc 2004).

The coating of colloidal gold nanoparticles with proteins was performed by an electrostatic adsorption method (Peng, Chen *et al.* 2007). Colloidal gold nanoparticles remain negatively charged over a broad pH range. The citrate ions being weakly anionic, they can be easily replaced with strong anions. So, the OMP85 antigen and anti-OMP85 antibody dissolved in sodium carbonate buffer pH 9.4, bound to the gold nanoparticles by replacing the already existing citrate ions.

Conjugation of proteins to gold nanoparticles mainly depends upon different phenomena such as, ionic attraction between the gold nanoparticles and the proteins and dative binding between the gold conducting electrons and sulphur atoms which are present in cysteine residues (if present) in the protein (Beesley 1989; Mukherjee, Bhattacharya *et al.* 2007). In some proteins the sulphydryl functionality may be in the form of a disulfide group and in other proteins sulphydryl sites may be buried within the protein structure, and therefore inaccessible to the gold nanoparticles (Mukherjee, Bhattacharya *et al.* 2007).

However, studies on peptides binding to gold predicted that the mechanism of binding of gold binding peptide (GBP) to inorganic metal surfaces mainly involve the polar side chains of serine and threonine (Braun, Sarikaya *et al.* 2002). Interestingly, most of the sequences studied didn't have cysteine, and only a few of them contained histidines, two residues known to bind to transition metal ions (Slocik, Moore *et al.* 2002). On the whole, binding between the protein and the nanoparticles may not only occur through the sulphydryl groups but also through hydrophobic and hydroxyl group-containing polar amino acids.

Successful conjugation of proteins to gold nanoparticles was established by the observed increase in stability of the conjugates in the presence of high salt concentrations. The amount of protein needed to prevent aggregation was

determined by preliminary titrations in the presence of increasing concentration of electrolyte and utilising the red to blue colour change of the various gold nanoparticle preparations previously coated with defined amounts of protein. This was established by the increased stability (no red to blue colour change) of the Au colloid in the presence of a monolayer of surface-attached proteins (Xie, Tkachenko *et al.* 2003). A single monolayer of protein attached to the surface of the nanoparticles is often sufficient to stabilise the nanoparticles (Niemeyer 2001). Thus, exposure of these protein-conjugated gold nanoparticles upto 0.256 M NaCl revealed no particle growth as shown by UV-vis absorbance spectrophotometry (Xie, Tkachenko *et al.* 2003). A separate titration to determine the protein/colloid ratio was performed with every batch of nanoparticles used.

The conjugation of biomolecules to nanoparticles is affected by several factors such as solvents, buffers, solubility of the proteins, pH, temperature, ratio of reagents etc (Sharma, Brown *et al.* 2006). It is necessary to determine the optimum pH for successful conjugation of proteins to gold nanoparticles (Peng, Chen *et al.* 2007). It is believed that pH can influence the correct orientation of the biomolecule on the particle for proper ligand recognition (Broderick, Natan *et al.* 1993; Keating, Kovaleski *et al.* 1998). It has been suggested that the conjugation is best performed at or near isoelectric point of the protein. The theoretical isoelectric point for OMP85 was predicted to be 8.5 (Swiss-Prot/TrEMBL). The optimum pH for OMP85 conjugation was determined by performing a

preliminary titration at two different pH values namely, pH 7.4 and 9.2 and examining the extent of conjugation by Bradford assay. A pH of above 9.0 was found to be more effective for successful conjugation. Whilst the optimal pH for coating usually lies around the isoelectric point of the protein, there are no general rules and adsorption interaction isotherms should be conducted in each case (Broderick, Natan *et al.* 1993; Keating, Kovaleski *et al.* 1998).

Optimising the pH also helps to target the amine group for binding (Mandal, Phadtare *et al.* 2005). The pK_a of the α-amino group of proteins and peptides at the N-terminal region is often slightly lower than that of the side-chain amine groups such as ε-NH_2 of lysine; therefore, under the right pH conditions, the proteins may be preferentially conjugated to the gold nanoparticles (Mandal, Phadtare *et al.* 2005). In order to maintain this amine group in the non-protonated form, the conjugation was performed in an alkaline buffer (pH above 9.0).

It was also observed that conjugation of proteins to nanoparticles was higher with the concentrated protein solution than diluted one. Protein conjugation efficiencies were improved by gentle agitation of the mixture after addition of the protein, since generating air bubbles by vigorous agitation may denature the protein solution or promote oxidation of thiol groups catalysed by atmospheric oxygen (Hainfeld 1988). However, once the optimal conditions were identified, the coating process was usually reproducible and was easy to scale-up.

An important goal with gold nanoparticle conjugation is isolating the labelled conjugate from unbound gold nanoparticles or from unlabelled biomolecule. This was done by centrifugation at a predetermined speed (Haiss, Thanh *et al.* 2007). Once after isolating gold nanoparticle conjugate, the extent of labelling (the number of gold nanoparticles per biomolecule) was calculated using the UV/visible absorption spectra of the gold nanoparticle conjugates. OMP85 and anti-OMP85 antibody absorb strongly at 280 nm, but have no absorbance at 520 nm. Therefore in the conjugate spectrum, while any absorbance at 520 nm must be due to gold nanoparticles, the absorbance at 280 nm contained a contribution from the conjugated protein (Haiss, Thanh *et al.* 2007).

After conjugation, only a modest shift in the surface plasmon band from 529 to 534 nm was observed. The surface plasmon resonance (SPR) peak of protein conjugated 50 nm gold nanoparticles was about 534 nm with a red shift of 5 nm compared to that of original citrate/tannic acid-stabilised gold nanoparticles (529 nm). This shift might be due to centrifugation of the protein conjugated gold nanoparticles which may affect the particle size distribution due to slight aggregation, which in turn could affect the position of the plasmon band (Hayat 1991). The centrifugation appears to decrease the intensity of the plasmon band possibly due to slight aggregation and a decrease in particle concentration. This red shift also denotes that protein molecules were adsorbed on to the gold

surface by Au–S interaction and a so-formed dielectric monolayer of protein around gold nanoparticles resulting in the red colour shift (Nath and Chilkoti 2002). These assembled protein-gold nanoparticle bioconjugates in aqueous suspension maintained their activity with enhanced stability and similar pH dependence.

Electrophoresis was perfomed to visualise the successful conjugation of protein and nanoparticles. During SDS-PAGE gel electrophoresis, gold nanoparticle conjugates may degrade upon exposure to thiols such as β-mercaptoethanol or dithiothreitol (DTT) (Beesley 1989). Based on these observations, a non-reducing gel was used in these studies. Samples were not heated to avoid any degradation of nanoparticle conjugates when heated above 50°C.

Gold nanoparticle-labelled molecules may be separated using gel electrophoresis, but one should be cautious in interpreting the results, as gel shifts alone are frequently not found to be good indicators of successful conjugation (Beesley 1989). Two-thirds of the gold nanoparticle is comprised of very dense gold atoms and thus the molecule is actually smaller than a protein or other macromolecule of the same weight (Rao, Kulkarni *et al.* 2000). In gel electrophoresis, the gold nanoparticles travel similarly to a protein of smaller molecular weight. A gold nanoparticle-labelled molecule typically runs higher on the gel due to the added weight of the gold nanoparticle. Conjugates were

visualised by usual gel stains (Coomassie and gel silver stains) which detected protein present in the samples.

From the gel electrophoresis analysis, the apparent molecular weight of the 13 nm gold nanoparticles was found to be around 80 kDa based on the assumption that these particles had a shape similar to an unfolded globular protein. A band around around 160 kDa on the gel, suggested the successful conjugation of OMP85 protein (85 kDa) with the 13 nm gold nanoparticles (80 kDa). Another band above 200 kDa possibly suggested the presence of 13nm gold nanoparticle-anti-OMP85 antibody conjugates.

A series of five water-soluble stabiliser ligands with different solubility i.e., N-acetyl cysteine (NAc)(Gautier and Burgi 2005), phenylalanine (Shao, Jin *et al.* 2004), mercaptosuccinic acid (MSA) (Li, Chen *et al.* 2006) and surfactants like Tween-20 (Paciotti, Myer *et al.* 2004) and sodium dodecyl sulfate (SDS) (Mafune 2004) were used to enhance the stability of the protein stabilised nanoparticle conjugates. The stability of OMP85 and anti-OMP85 antibody conjugated gold nanoparticles toward both salt concentration and displacement of the bound proteins was investigated. Addition of some of the stabilisers was found to be useful in particular applications, as discussed below.

For particles stabilised with Tween-20 and SDS, the stability of the preparations toward salt concentration was found to increase significantly as the surfactants form a monolayer around the particles. However, nanoparticles treated with NAc and MSA didn't show any increase in stability but rather led to aggregation of the previously stabilised particles. The conjugate suspension in presence of MSA was aggregated which is likely due to hydrogen bonding formation between the carboxylic acid and amino acid group (Figure 3. 12) (Choi, Lee *et al.* 2003). Presence of phenylalanine as a stabiliser made no difference to the stability of the particles. This may be due to the reason that phenylalanine might not be binding with the gold surface. This effect may be primarily due to the end group rather than variations in total ligand molecular weight, even though the molar masses for this series of ligands were not all identical. It is not clear at this stage whether this difference in results is due to the mode of binding to the gold surface or the fact that Tween-20 and SDS form a micelle structure around the nanoparticles.

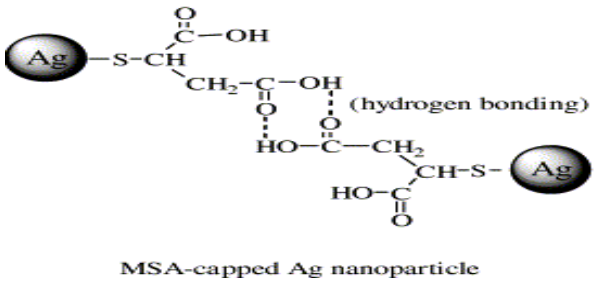

MSA-capped Ag nanoparticle

Figure 3.12. Structure of the precipitated MSA capped Ag colloids (Choi, Lee *et al.* 2003).

Once stabilised, the gold nanoparticle-protein conjugates were stable to wide ranges of pH and ionic strength. Although gold nanoparticles are usually stable, under some conditions labelled conjugates may not be stable at higher temperatures (<50 °C) and therefore stored at 4 °C until used.

Chapter 4

The assembly and validation of the diagnostic assay: A colour shift assay based on Surface plasmon resonance

4.1. Introduction

Colloid gold has a long history of safe use in clinical applications (Faraday 1857; Mulvaney 2003). The use of biomolecules such as proteins and nucleic acids with nanoparticles for developing nanotechnology devices has led to the development of hybrid nanomaterials (Sarikaya, Tamerler *et al.* 2003). Novel devices may become available by tuning the spectroscopic, fluorescence, luminescence, and electrochemical characteristics of gold nanoparticles with those of substrates including DNA, carbohydrates and other biological molecules or systems.

Although bulk gold is well known for being inert, the reactivity of the gold nanoparticles has recently proven very useful in developing recognition systems based on their optical properties. Gold nanoparticles exhibit a specific optical property called Surface Plasmon Resonance (SPR), which is responsible for the deep red colour of the suspension (Mie 1908; Link and El-Sayed 2000). The aggregation of gold nanoparticles leads to the red shift of the absorption band from 520nm to longer wavelengths in the range of 600-800 nm, as a result of

electric dipole-dipole interaction and coupling between the plasmons of neighboring particles in the formed aggregates. A better understanding of the surface plasmon resonance properties of the gold nanoparticles can prove fruitful to develop the most sensitive reagents and technology for detecting biological molecules.

Major parameters that control the formation of extended nanoparticle aggregates include, the size, size distribution, shape (Mock, Barbic *et al.* 2002), and chemical composition of the nanoparticle building blocks, the length and stability of the particle linker molecules (Mucic, Storhoff *et al.* 1998). Ordered or disordered assembly of nanoparticles in aggregates is possible by incorporating complementary receptor-substrate sites on the surface of the nanoparticles which permits the recognition-driven assembly of nanoparticles (Daniel and Astruc 2004). The antibodies and antigens can be utilised as candidate molecules for the controlled assembly of nanoparticles in suspension (Mann, Shenton *et al.* 2000). By utilising the specific recognition properties of the coupling molecules, novel materials with controlled growth have been generated (Niemeyer 2001; Sun and Xia 2002; Djalali, Chen *et al.* 2003). Gold nanoparticles may be utilised to design an ideal colorimetric assay, based on the their extremely high extinction coefficients and the strongly distance-dependent optical properties (Liu and Lu 2004).

The combination of the surface plasmon absorption property of gold nanoparticles with biology and medicine has already been demonstrated by using complementary DNA oligonucleotides attached to the surfaces of gold nanoparticles. Earlier work by Mirkin (Mirkin, Letsinger *et al.* 1996) and Alivisatos (Alivisatos, Johnsson *et al.* 1996) showed that complementary DNA oligonucleotides could be used to self-assemble nanoparticles. Mirkin *et al.*. (Mirkin, Letsinger *et al.* 1996) described a method for reversible assembly of 13 nm colloidal gold nanoparticles into macroscopic aggregates by utilising the DNA specific interactions. Excellent specificity in base pairing, and its ability to address at the nanoscale makes DNA an ideal candidate for applications in biosensing and bionanotechnology.

The inter-particle distance dependent colour change of colloidal gold due to aggregation has been used by Mirkin and co-workers to design a sensor capable of determining single-base mismatches in DNA hybridisation, (Elghanian, Storhoff *et al.* 1997; Storhoff, Elghanian *et al.* 1998). Selective colorimetric polynucleotide detection with the gold nanoparticle probes resulted in the formation of aggregates with an ultimate red to purple colour change in suspension (Storhoff, Elghanian *et al.* 1998).

A highly sensitive and selective colorimetric biosensor has been designed based on DNAzyme-directed assembly of gold nanoparticles resulting in red to blue

colour shift (Liu and Lu 2003) and it has been reported that this can be used for a broad range of analytes. The DNAzyme catalyses specific cleavage of the substrate strand in the presence of lead. This ultimately disrupted the formation of the nanoparticle assembly, and resulted in red-coloured individual nanoparticles. The application of this particular sensor in lead detection in lead-based paints was also demonstrated (Liu and Lu 2003; Liu and Lu 2004). This red shift based on the surface plasmon resonance of the gold nanoparticles, has been observed in other non–oligonucleotide-based strategies (Brust, Fink *et al.* 1995; Grabar, Smith *et al.* 1996; Storhoff, Mucic *et al.* 1997; Bao, Peng *et al.* 2005).

However, protein-based recognition systems offer some additional advantages over oligonucleotides with a large number of complementary systems and a wide range of free energies of association (Mann, Shenton *et al.* 2000). To test the possibility of using antibody-antigen interactions in programmable nanoparticle self-assembly, Shenton *et al.*., (Shenton, Davis *et al.* 1999) described a study based on the interaction between a bivalent antigen molecule, DNP (bis-N-2,4-dinitrophenyloctamethylenediamine) and anti-DNP IgE antibodies, conjugated with 12 nm gold nanoparticles. A macroscopic purple precipitate and a clear supernatant were evident after incubating overnight at 4 °C. TEM examination of the aggregates established the presence of large disordered three dimensional networks of discrete gold nanoparticles. The biomolecular specificity of the ligand-induced recognition was confirmed by a control experiment in which the

DNP antigen was added to a sol of Au nanoparticles conjugated with anti-biotin IgG antibodies. In this case, no precipitate was observed (Shenton, Davis *et al.* 1999; Mann, Shenton *et al.* 2000).

Streptavidin (STV)-biotin binding is an ideal model for studies on nanoparticle aggregation based on protein-ligand interactions. Being a small ligand, the complex is extremely stable over a wide range of temperature and pH (Mann, Shenton *et al.* 2000). Connolly and Fitzmaurice (Connolly and Fitzmaurice 1999) and Mann *et al.*. (Mann, Shenton *et al.* 2000) have used the STV-biotin interaction to organise an ordered assembly of nanoparticles. The immediate change of the suspension colour from red to blue was indicative of the formation of recognition driven assembly of nanoparticle networks. Studies by dynamic light scattering (DLS), showed that the average radius of all particles in suspension rapidly increased due to the STV-directed assembly (Niemeyer 2001). Analysing the aggregates by TEM revealed clusters of nanoparticles with an average of 20 interconnected particles that were separated by about 5 nm. This inter-particle distance correlates with the diameter of an STV molecule. The results were also confirmed by Small Angle X-ray scattering (SAXS) technique.

Using protein coated gold nanoparticles; a simple colorimetric sensor was also designed for studying the conformational changes in a protein. The conformational changes in the yeast iso-1-cytochrome c due to pH changes

caused measurable shifts in the colour of the respective protein coated gold nanoparticle suspensions, and it was detected by UV-Vis absorption spectroscopy (Chah, Hammond *et al.* 2005).

The versatility of using gold nanoparticles in association with the antigen-antibody recognition system should make it possible to produce a wide range of nanoparticle aggregates involving specific cross-linked structures, compositions and macroscopic architectures (Shenton, Davis *et al.* 1999). Such nanoparticle-based receptors may generate novel probes for the recognition of various biomolecular specific ligands, and thus may provide novel tools for immunoassays and biosensors (Niemeyer 2001). This chapter mainly deals with an attempt made to utilize the surface plasmon resonance property of gold nanoparticles using the OMP85 antigen and anti-OMP85 antibody system.

4.2. Materials and Methods

Materials

All glassware was scrupulously clean. Glass and plastic containers and stirrers were cleaned in aqua-regia and thoroughly washed in Milli Q water. Aqua regia (3:1 HCl:HNO_3) was made fresh each time. 13 nm gold nanoparticles were prepared by citrate reduction method. The larger size gold nanoparticles (30nm, 40nm, 50nm and 60nm) used in this chapter were purchased from the British Biocell Ltd., UK. Molecular cut-off filters were obtained from Millipore Ltd., USA. Lysozyme and anti-lysozyme antibody were obtained from Sigma-Aldrich Ltd., USA. Bio-Rad Bradford assay reagent was used for protein estimation. All reagents were of high quality analytical grade and were filtered using 0.45µ nylon membrane filter, immediately before use.

4.2.1. Conjugation of OMP85 and anti-OMP85 antibody molecules to different size gold nanoparticles

Antibodies and antigens were attached to the surfaces of Au nanoparticles by identical procedures described in Chapter 3. The OMP 85 protein purified by sonic extraction method (Chapter 2) and protein A purified rabbit anti-OMP 85 polyclonal antibody were re-suspended in 5 mM sodium carbonate buffer pH 9.4, using 30 kDa molecular cut-off filters separately to achieve a final concentration of the protein of 5mg/mL as determined by Bradford assay.

To separate glass vials containing 6.0 mL of each size nanoparticles suspension (13, 30, 40, 50 and 60 nm) of gold nanoparticles (BBI, UK), 250 µl of protein solution (in carbonate buffer) was added and mixed gently on a shaker for 30 minutes at room temperature. To block the unbound sites on the gold nanoparticles surface, 250 µl of 5 mg/mL BSA in 5 mM sodium carbonate buffer pH 9.4, was added to the above conjugated gold nanoparticle suspensions and mixed gently on a shaker for another 30 minutes at room temperature.

Excess protein and gold nanoparticles were removed from the individual size nanoparticles conjugation mixture by centrifugation at at 5000 to 20, 000 x g for 45 minutes, at 4 °C, depending on the size of nanoparticles. The supernatant liquid was discarded and the pellet resuspended in low ionic strength 10 mM sodium phosphate buffer pH: 7.4. The washing step was repeated twice to remove any traces of unbound protein and BSA. Finally, the protein conjugated gold nanoparticles were resuspended in 5.0 mL of 10.0 mM sodium phosphate buffer pH 7.4.

The optical absorption spectra of these systems were acquired using Hitachi U-2000 dual-beam spectrophotometer using 1 cm path length quartz cuvettes. The absorbance of the supernatants was also measured in order to establish any presence of free protein or gold. To prevent light induced aggregation, all colloidal gold conjugations were stored in glass vials or polypropylene

centrifuge tubes in the dark at 4 °C. The suspensions were stable for several months.

4.2.2. Coupling of nanoparticle-protein conjugates

To verify the antigen and antibody mediated gold nanoparticle coupling of surface plasmons, 250 µl of anti-OMP85 antibody conjugated 13-60 nm gold nanoparticles in 10 mM sodium phosphate buffer pH 7.4 and 250 µl of OMP85 conjugated 13-60 nm gold nanoparticles in 10 mM sodium phosphate buffer pH 7.4 were added in a 48 well plate. All the combinations were carried out in triplicate.

OMP85-conjugated gold nanoparticles (500 µl) and 500 ul of anti-OMP 85 antibody conjugated gold nanoparticles were added to separate wells as controls. Native gold nanoparticles of each size (500 µl) were also added to separate wells as controls. They were mixed gently and then 100 µl of varying NaCl concentration were added (to a final concentration in the range from 2.0 mM to 256 mM) to each combination of nanoparticles. They were mixed gently at room temperature.

The colour shift was observed visually in specific combinations. The absorbance change at 620 nm was also measured within 5 minutes in a Hitachi U2000 UV-vis

absorption spectrophotometer. The schematic representation of the coupling procedure is given in the following Figure 4.1.

Control system was tested using lysozyme/anti-lysozyme antibody conjugated 13 nm gold nanoparticles without the addition of salt.

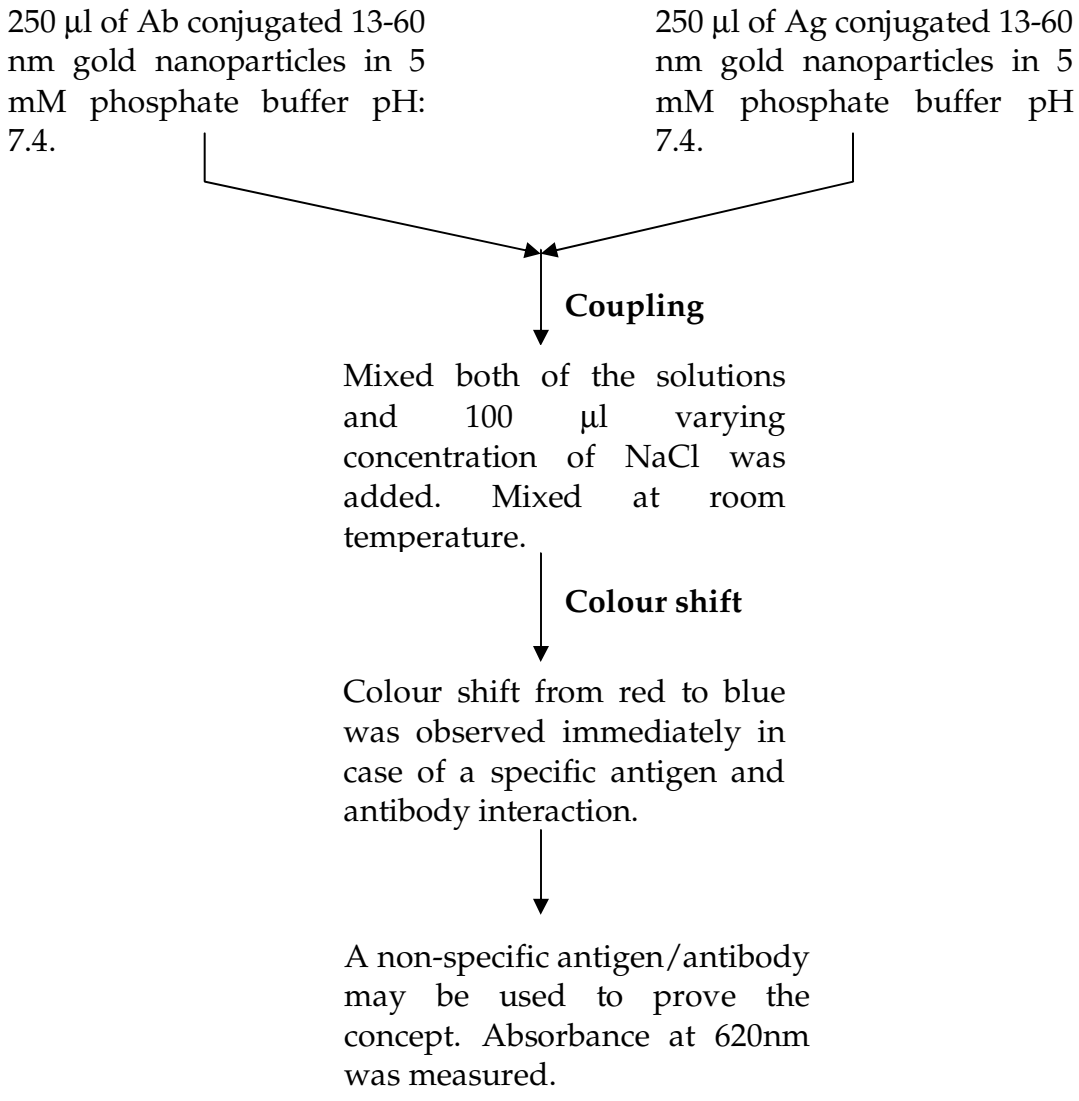

Figure 4.1. Schematic representation of antigen and antibody mediated gold nanoparticle coupling of surface plasmon resonance.

4.3. Results

4.3.1. Gold nanoparticle Conjugation

Different size fractions of gold nanoparticles were successfully conjugated with OMP 85 and anti-OMP 85 antibodies. After separating the unbound proteins from the bound proteins, conjugated nanoparticles were resuspended in 10 mM sodium phosphate buffer pH 7.4 and the suspension appeared in ruby red colour. The absorbance at around 520 nm of the conjugated gold nanoparticles revealed slight or no difference in the absorbance in comparison to the native gold nanoparticles. After successful conjugation, the colloidal gold particles did not show any sign of non-specific aggregation. Reagent preparations stored at 4°C for approximately 6 months were evaluated and shown to have no substantial loss in reactivity.

4.3.2. Coupling of nanoparticle conjugates

The coupling of surface plasmons of individual gold nanoparticles due to binding of OMP 85 and anti-OMP 85 antibodies in the presence of salt and subsequent colour shift from red to blue was studied. In presence of increasing NaCl concentration (to a final concentration in the range 2 mM to 256 mM NaCl), there was no observable colour shift in 13, 30, 40 and 60 nm size gold nanoparticles conjugated with OMP 85 and anti-OMP 85 antibodies. The absorbance at 620 nm of coupled nanoparticles remained below or identical to the individual conjugated nanoparticles. Plain gold nanoparticles of all sizes

aggregated immediately with salt addition and the suspension colour turned blue.

However, in the case of coupling of 50 nm gold nanoparticles conjugated with OMP 85 and anti-OMP 85 antibody, the colour changed from red to blue and thus a change in absorbance at 620 nm as seen in Figure 4.2. Wavelength scans from 190-800 nm (Figure 4.3.) showed a significant difference in absorbance in the range 600-800 nm in case of OMP85 and anti-OMP85 antibody coupling in comparision to the absorbance of individual conjugated nanoparticles in the presence of same salt concentration. Colour changed from red to blue immediately in a specific antigen-antibody interaction, but no colour shift was observed in the controls with BSA conjugated 50 nm gold nanoparticles and anti-OMP85 antibody conjugated 50 nm gold nanoparticles.

It was found that, coupling of the 50 nm OMP85 conjugated gold nanoparticles with the anti-OMP85 antibody conjugated nanoparticles and subsequent spectral shift was not reproducible (6 out of 23 times) under identical conditions. Figure 4.4. shows images of the colour shift experiment and their corresponding TEM images of the nanoparticle assemblies.

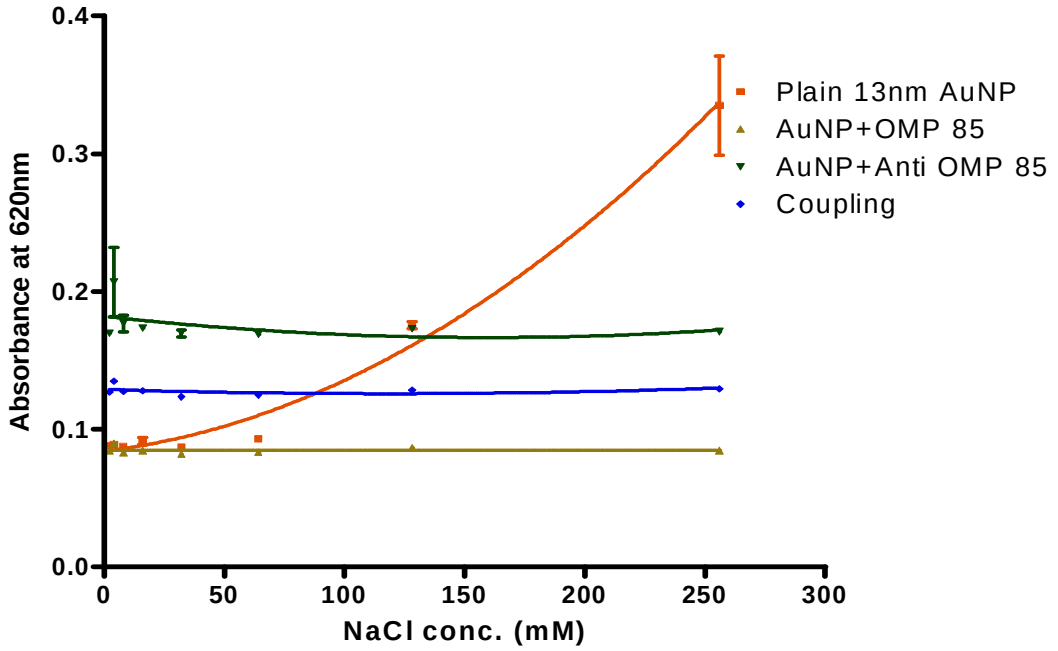

(a) 13 nm gold nanoparticle spectral change with variable NaCl concentrations.

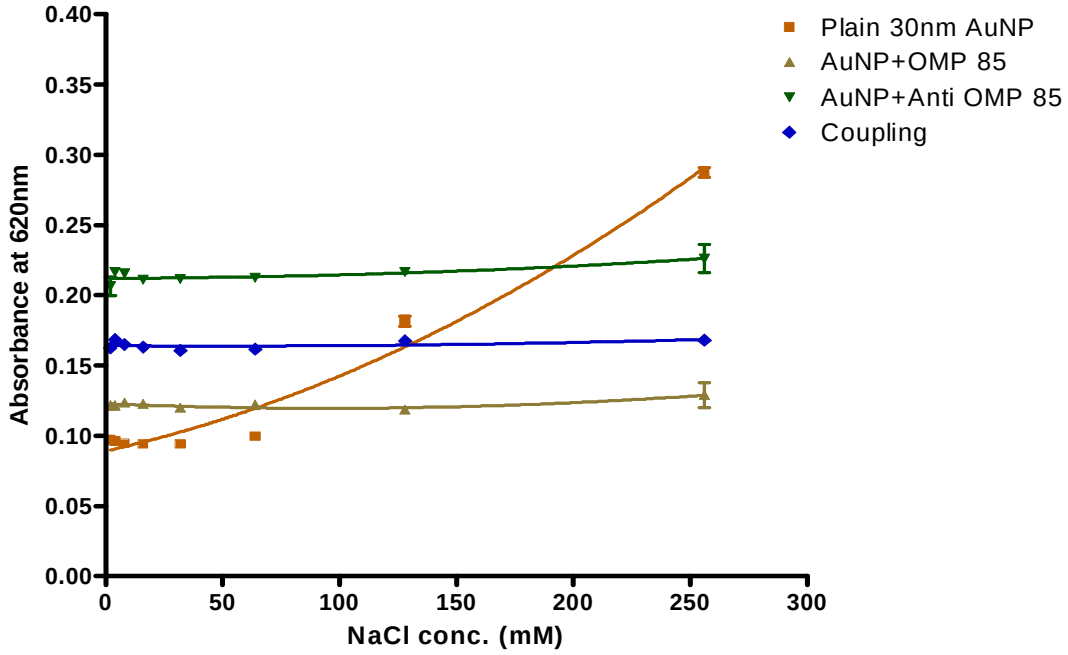

(b) 30 nm gold nanoparticle spectral change with variable NaCl concentrations.

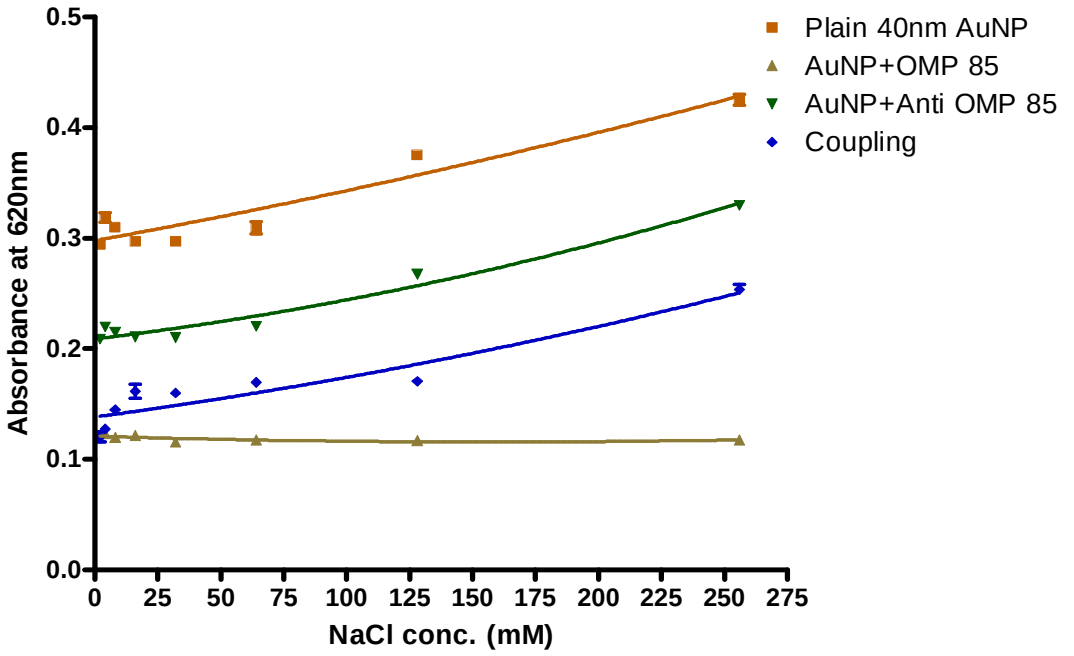

(c) 40 nm gold nanoparticle spectral change with variable NaCl concentrations.

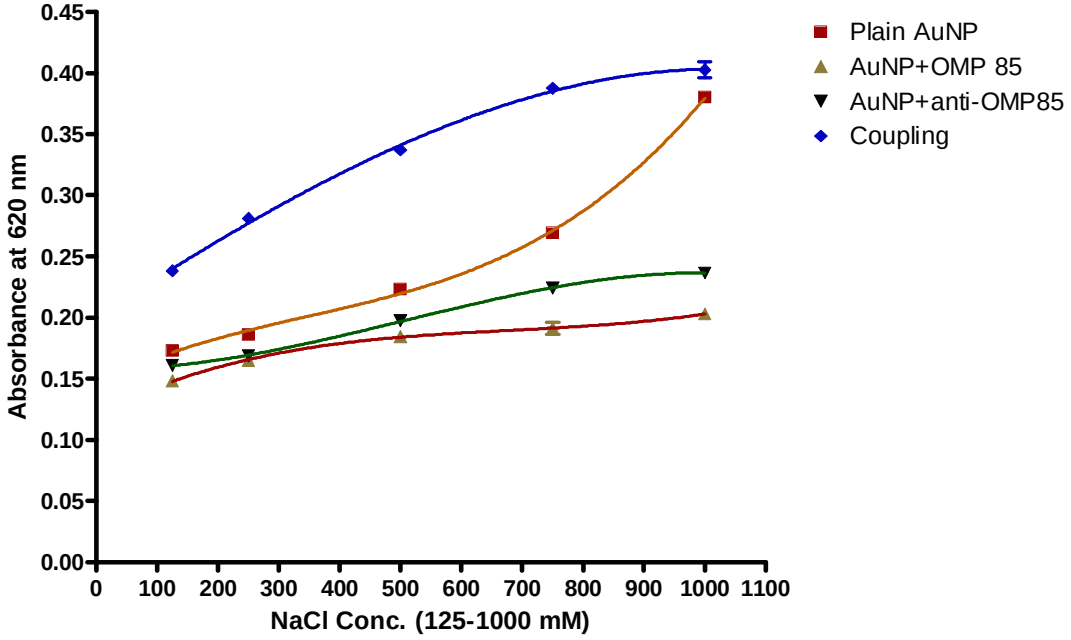

(d) 50 nm gold nanoparticle spectral change with variable NaCl concentrations.

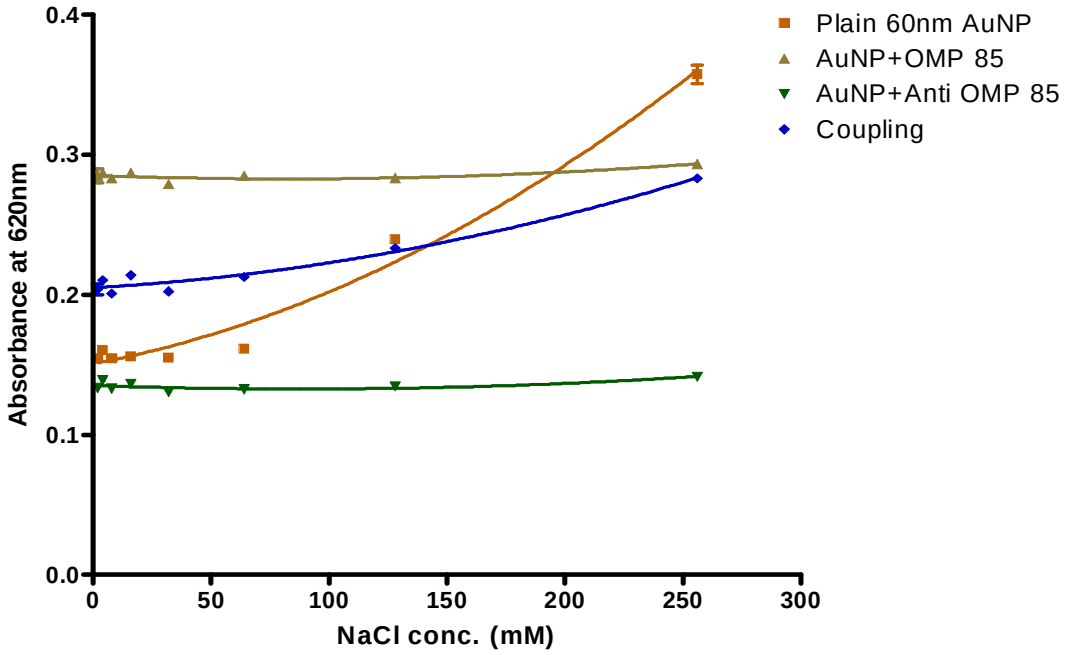

(e) 60 nm gold nanoparticle spectral change with variable NaCl concentrations.

Figure 4.2. Red shift of gold nanoparticles and nanoparticle-protein conjugates to 600-800 nm due to coupling of surface plasmon resonance induced by specific interaction of OMP85 and anti-OMP85 antibody conjugated gold nanoparticles of different sizes. (a) 13 nm, (b) 30 nm, (c) 40 nm, (d) 50 nm and (e) 60 nm colloidal gold nanoparticles.

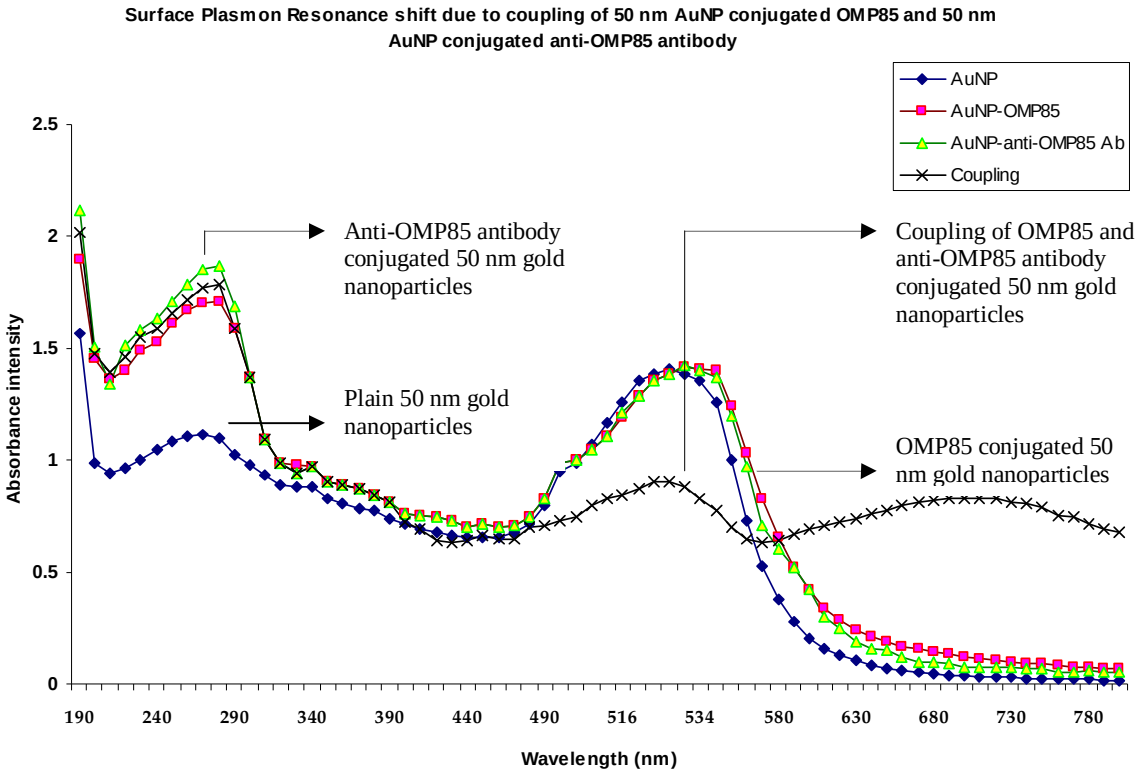

Figure 4.3. Absorption spectra of the OMP85 and anti-OMP85 antibody conjugated 50 nm colloidal gold nanoparticles. Mixing the two conjugates resulted in a red shift of the wavelength to 600-800 nm which resulted in colour shift from red to blue.

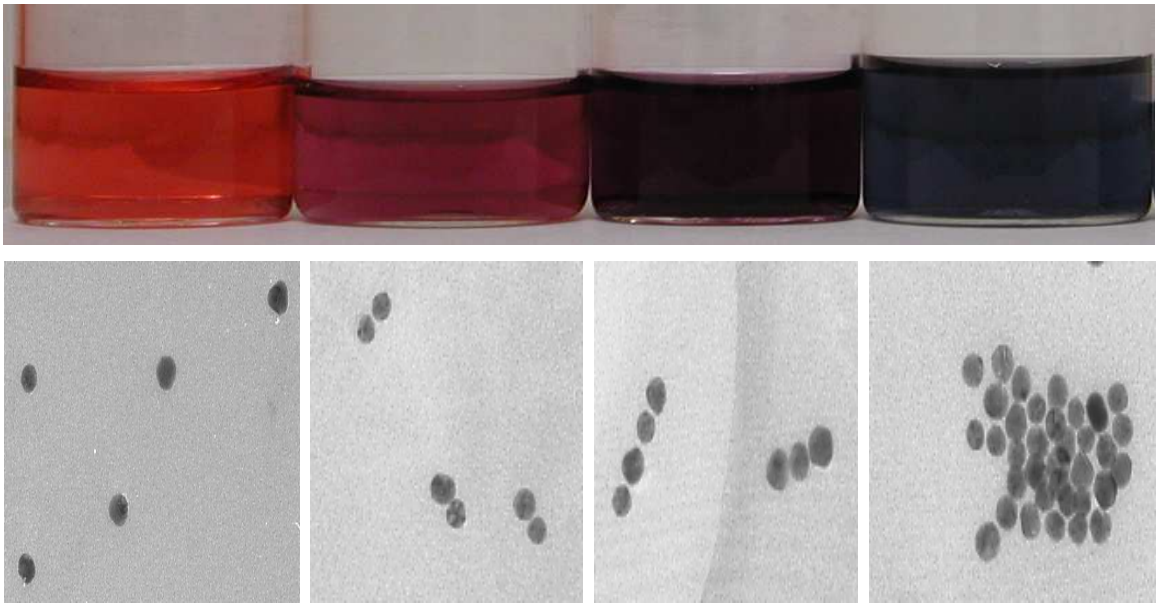

Figure 4.4. Images of red to blue colour shift experiment using OMP85 antigen and anti-OMP85 antibody conjugated 50 nm gold nanoparticles (with 0.512M NaCl) and their corresponding TEM images.

4.3.3. Lysozyme and anti-lysozyme antibody coupling

The coupling of surface plasmons of individual gold nanoparticles (13 nm) due to binding of lysozyme and anti-lysozyme antibodies and subsequent colour shift from red to blue was also studied as a model system. The colour changed from red to blue indicating a change in absorbance at 620 nm. There was a significant difference in absorbance at 620 nm in the case of lysozyme and anti-lysozyme antibody coupling in comparison to the absorbance of individual conjugated nanoparticles (Figure 4.5.). No colour shift was observed in the controls with BSA conjugated 13 nm gold nanoparticles and anti-lysozyme Ab conjugated 13 nm gold nanoparticles.

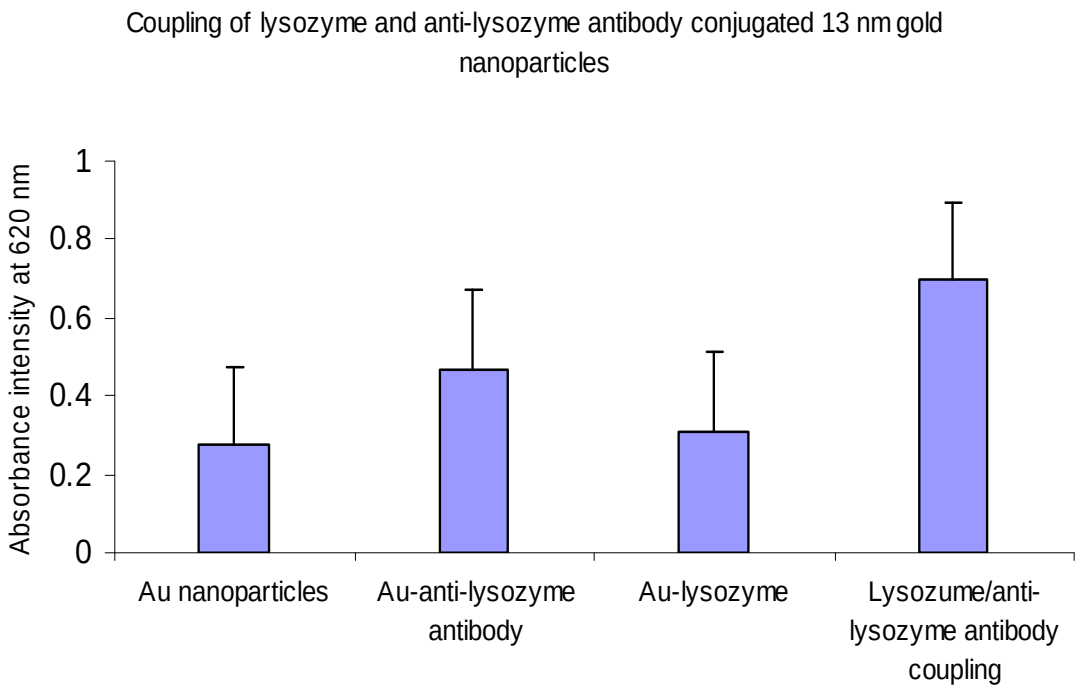

Figure 4.5. Proof of concept experiment using lysozyme and anti-lysozyme antibody conjugated 13 nm colloidal gold nanoparticles (n=0.2).

4.4. Discussion

In this chapter, the distance-dependent optical properties of gold nanoparticles are evaluated as a novel method for detecting a *N. meningitidis* specific antigen as aggregated gold nanoparticles conjugated with specific antigens and antibodies. The capacity of colloidal gold to undergo a chromic transition upon aggregation makes possible its use as reporter agents for immunodiagnostic applications where it can provide a visible range of detection. Aggregation of gold nanoparticles by utilising OMP 85 and anti-OMP 85 antibody systems was used to demonstrate that gold nanoparticle aggregates could be directed by biomolecular recognition.

The potential of a rapid diagnostic assay for *N. meningitidis* by utilising the specific interaction of OMP 85 and anti-OMP 85 antibody conjugated to gold nanoparticles was evaluated as a model system. It was postulated that specific interaction of OMP85 and anti-OMP85 antibody coated nanoparticles leads to coupling of surface plasmons and thus readily observable colour shift occurs.

Following the detailed biochemical characterisation of both the OMP85 antigen and the anti-OMP85 antibody receptors, they were conjugated by simple electrostatic adsorption to gold nanoparticles of different sizes in the range 13 – 60 nm and tested for their ability to bind with resulting colour shifts due to SPR effects. It has been reported previously that, in order to observe the aggregation

induced colour shift, the gap between the nanoparticles should be less than the average diameter of the individual gold nanoparticles (Kreibig, Schmitz *et al.* 1987; Elghanian, Storhoff *et al.* 1997). In that case, the size of the nanoparticles is related to the size of the biomolecules. This was evaluated in a model system with the lysozyme and anti-lysozyme interaction, where a red shift was observed with 13 nm gold nanoparticles. In order to verify the optimum size range of the nanoparticles to achieve such a colour shift, OMP85 and anti-OMP85 antibody molecules were conjugated with 13, 30, 40, 50 and 60 nm gold nanoparticles.

The optimal pH and the minimum amount of OMP85 antigen and anti-OMP85 antibody required for optimal coating of the particles by charge adsorption were determined by a series of concentration-dependent experiments and by isothermal titration. A critical flocculation concentration assay, based on the red to blue colour change of the native gold nanoparticles in the presence of high salt concentrations, were used to determine the optimum protein-colloidal gold ratio required for effective surface coverage for increased stability (as indicated by no red to blue colour change). The colloidal aggregation observed under these conditions for the uncoated colloid was arrested due to the adsorbed protein molecules.

The optical spectrum of a suspension of gold nanoparticles conjugated with OMP85 or anti-OMP85 antibody did not significantly deviate from the

absorption spectrum of the bare gold nanoparticle suspension not showing a broadening of the spectrum or formation of a new absorption band. With all size fractions of nanoparticles after conjugation, a 3-5 nm shift of the plasmon peak was observed compared to that of the original gold nanoparticles. The probable reasons responsible for this shift were explained in Chapter 3 (Hayat 1991; Nath and Chilkoti 2002). These assembled protein-gold nanoparticle bioconjugates in aqueous suspension maintained their activity with enhanced stability and similar pH dependence. This clearly indicates that the protein conjugated gold nanoparticles have a high dispersivity in suspension without aggregation and in addition showed long-term stability at 4°C.

During the coupling experiment in the presence of a particular salt concentration, no colour shift was observed with different size nanoparticle combinations except in the case of 50 nm gold nanoparticles. With the coupling of 50 nm gold nanoparticles conjugated with OMP85 and anti-OMP85, a broadening of the spectrum and the formation of a new absorption band at wavelengths longer than 600 nm was observed, indicating particle aggregation. Binding resulted in an immediate change in the SPR signal, which was observed as a colour shift, indicating directly the presence of a specific interaction. No colour shift was observed in case of the controls which occurred with only either gold nanoparticle-OMP85 conjugates or gold nanoparticle-anti-OMP85 antibody

conjugates demonstrating that the aggregation was due to the OMP85-anti-OMP85 antibody specific interaction.

In the case of plain gold nanoparticles, the addition of electrolytes caused flocculation as a result of the shielding of the repulsive double-layer charges which normally stabilise them. Whereas, the presence of a minimal quantity (CFC) of electrolytes in the protein-conjugated nanoparticle suspensions may help to keep the conjugated proteins in flexible conformation rather than as a rigid mass. This may provide better access of the antigen to the antibody. It has been reported that nearly 20% of the attached protein molecules are not available for coupling. This is most likely to be caused by steric hindrance effects, which prevents some of the adsorbed proteins from binding to targets. Thus presence of low levels of electrolytes can increase the probability of specific antigen-antibody interaction, when conjugated to gold nanoparticles.

The SPR effect becomes negligible when the gap between the nanoparticles is larger than about 2.5 times the short-axis length (Su, Wei *et al.* 2003). As the spacing between particles was reduced by less than their average diameter, the surface plasmon resonance peak was shifted to higher wavelength and this shift is well described as an exponential function of the gap between the two particles (Sidhaye, Kashyap *et al.* 2005). Because the colour change depends on the nanoparticle spacing, the size of the nanoparticles is a defining characteristic of

the system considering the size of the proteins and antibodies. Thus, smaller nanoparticles with an average diameter much lesser than the size of the protein are likely to be ineffective in yielding a colour shift. This is indicative of the reason why the colour shift was observed only in the case of 50 nm gold nanoparticles. The average diameter of the 60 nm gold nanoparticles may be greater than the distance between the nanoparticles brought about by the coupling of OMP 85 and anti-OMP 85 antibody and hence the colour shift was not observed.

Liu *et al*.. used nanoparticles with larger sizes, to accelerate the rate of colour change (Liu and Lu 2004). It is known that the optical properties of a nanoparticle aggregate are dominated by their size, rather than the number of nanoparticles in the aggregate. Therefore, a lower degree of aggregation would be required to give the same spectral shift with larger nanoparticles, and the time required for the colour change should be decreased (Liu and Lu 2004). This was indeed what was observed. The colour change approached completion in less than 10 min for 50nm nanoparticles. Formation of large aggregates, which changes the proximity of colloidal gold nanoparticles in suspension cause large changes in the absorbance spectrum of the colloidal suspension due to long-range coupling of surface plasmons.

During the antigen-antibody induced aggregation process of gold nanoparticles, the change in visible absorbance, and shift toward longer wavelengths, is proportional to the concentration of ligand involved and occurs according to the kinetics of the interaction process. Such quantitative results may be obtained by monitoring the ratio of extinction at the plasmon peak (532 nm) to the 600-800 nm. This ratio was higher with separated nanoparticles of red colour, while a lower ratio was associated with aggregated nanoparticles of blue colour.

The combination of OMP85 and anti-OMP85 antibody affinity binding detection system shows the advantages such as, a very short procedure time, no fading of the signal and high spatial resolution. Therefore, this new approach potentially offers an addition to other methods for the diagnosis of meningitis. Nevertheless, it was noted that the assay, as conducted at room temperature was not completely reproducible, even from the same batch of conjugate preparation.

There may be different factors responsible for affecting the reproducibility of the system. The aggregation rate depends primarily on the collision frequency of the particles, which is directly related to the concentration of gold nanoparticle conjugates within the analyte solution. Ligand-conjugated gold nanoparticles need to maintain good dispersion and long-term stability for use as signal amplification probes. Several methods have been used to improve the dispersivity in aqueous suspension by controlling the ligand density on the

surface of the gold nanoparticles and by utilizing surfactants like Tween-20 have definitely increased the stability of the particles.

Gold nanoparticle aggregation depends on the coverage of the monolayer formed on the colloidal gold surface and that the antigen/antibody concentration used for conjugation was the critical concentration to observe specific aggregation of gold nanoparticles in this system. There is thus a critical surface concentration for each protein, at which the gold nanoparticles may be appropriately stabilised with room available for the coupling of surface plasmons to occur between the particles.

Nanoparticles may also be covalently cross-linked to a specific functional group on a targeted biomolecule (Li, He *et al.* 2007) such that this site-specificity allows it to be conjugated at a position remote from the binding site so that it does not interfere with substrate binding. Specific peptides in place of proteins and Fab' fragments in place of whole antibodies may also be used with small size nanoparticles (Lee, Oh *et al.* 2006). Consequently, a single connection between two particles could produce differences in the antigen-binding affinities of the remaining uncoupled surface-attached antibodies, depending on their proximity to the interparticle cross-link (Shenton, Davis *et al.* 1999). The ability to fabricate the nanoparticle aggregates with controlled connectivity requires a specific design approach of the antibody-antigen interface. Indeed, the versatility of

using gold nanoparticles in association with antigen-antibody engineering may ultimately make it possible to assemble a wide range of nanoparticle-based diagnostic assays against different pathogens.

Chapter 5

Quartz Crystal Microbalance as an Immunosensor

5.1. Introduction

The combination of highly specific recognition properties of biological macromolecules and the sensitivity of various transducers, such as optical, thermal, gravimetric, electrochemical and surface acoustic wave sensors, has led to the development of sensitive and selective biosensors as valuable tools in analytical biochemistry. Acoustic wave sensors based on the piezoelectric properties of materials such as quartz crystal resonators demonstrate a linear relationship between mass adsorbed on to the surface and the resonant frequency of the crystal in air or a vacuum (Vidal, Garcia-Ruiz *et al.* 2003).

When an electrical field is applied through the quartz crystal, the inner dipoles are reorientated to create a mechanical strain. In 1920, Cady used the reverse piezoelectric effect in which case, mechanical vibrations of the crystal were observed due to deformation under an alternate electric field. The degree of deformation in a piezoelectric quartz crystal depends on the applied potential (Shana and Josse 1994). When the applied potential is altered, an oscillatory motion is generated, which then forms an acoustic wave in the material. It was found that, when this arrangement was included in an appropriate electronic

circuit, the measured oscillation frequency was close to the resonant frequency of the quartz crystal and this generated the maximum wave amplitude. Ultrasonic waves are also generated when the quartz crystal is vibrating near its resonant frequency. Thus, a modification of the mass or the thickness of the resonator, led to a resonant frequency variation. In biosensors, mass changes occuring on the crystal surface due to the various biomolecular interactions, are measured.

A biosensor is an analytical tool consisting of two components: a receptor and a detector. The receptor is responsible for the selectivity of the sensor and the biorecognition elements that act as receptors include antibodies, enzymes (Bentley, Atkinson *et al.* 2001) or whole living cells (Nomura and Okuhara 1982). The transducer translates the biophysical or biochemical signal into an electrical signal, which is measured by the detector. Thus, similar principle applies to a H-electrode, an oxygen electrode or a piezoelectric crystal (Figure 5.1.).

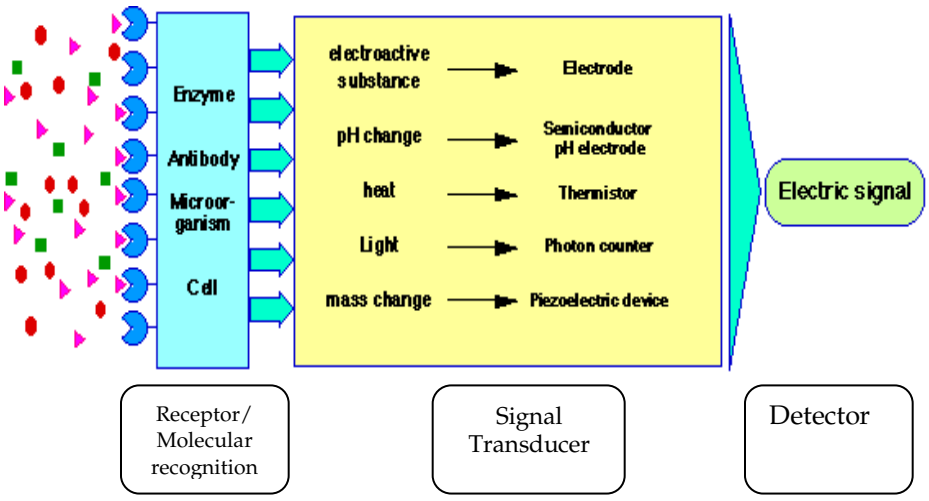

Figure 5.1. Schematic for a general Biosensor (Bogdan 2005)

One promising simple form of a detector that fits the above criteria is the Quartz Crystal Microbalance (QCM). The QCM is a piezoelectric mass-sensing device that detects changes in frequency of the crystal due to changes in mass on the surface of the crystal.

Application of biosensors to biological samples became possible only after suitable oscillator circuits which could operate in liquids were developed (Suleiman and Guilbault 1991). The selectivity provided by the biological coatings together with the intrinsic sensitivity of the piezoelectric (PZ) devices and the ability to oscillate the crystal in liquid medium have induced a rising interest in this class of sensors (Castillo, Gaspar *et al.* 2004). Biosensors are being used in a variety of different fields, ranging from pesticides to biological weapons.

As mentioned earlier, biosensors based on acoustic wave propagation utilize a piezoelectric material such as quartz crystal. Depending on the cut-angle of the quartz mother crystal, different resonator types may be obtained with frequencies ranging from 5×10^{2} to 3×10^{8} Hz. Acoustic waves cover a frequency range of 14 orders of magnitude, starting from 10^{-2} Hz (seismic waves) and extending to 10^{12} Hz (thermoelastic excited phonons). The acoustic resonators generally oscillate in a narrow frequency range of 10^{6}-10^{9} Hz. The four common

types of acoustic resonators are surface-acoustic-wave (SAW) resonator, acoustic-plate-mode (APM) resonator, flexural-plate-wave (FPW) resonator and thickness-shear-mode (TSM) resonator, also known as the quartz-crystal microbalance (Martin, Frye *et al.* 1994). Here, only TSM resonators are discussed as it is relevant to the study.

5.1.1. Thickness-Shear-Mode (TSM) Sensors (Quartz-Crystal Microbalances)

TSM resonators are also referred as bulk-acoustic-wave (BAW) resonators or as quartz-crystal microbalances (QCMs) (Buttry and Ward 1992). TSM devices work due to the acoustic wave propagation inside a quartz plate.

The active element of a QCM is formed by a thin round plate of AT-cut quartz crystal (cut with an angle of 35.25° to the *z*-axis or 35° 10′ with respect to the optical axis) with two gold electrodes deposited on the two opposite sides. These electrodes allow an alternating electrical field to be applied and the quartz crystal oscillates near its resonant frequency or at an overtone. When a mass is added or removed, this is considered as an increase or a decrease of the crystal's thickness (Sauerbrey 1959) and thus as a result, the resonance frequency decreases (Turner 2000). In general, the classical working frequencies for QCM range between 5 MHz to 10 MHz.

QCM can measure the mass and the thickness of an analyte bound in real time. Many platforms based on TSM sensors, have been developed for the analysis of binding specificities, affinities, kinetics and conformational changes associated with a molecular recognition event (Buttry and Ward 1992). Even though flexural-plate-wave (FPW) or surface-acoustic-wave (SAW) sensors are more sensitive in comparison to TSM resonators, TSM sensors are widely preferred due to their robust nature, availability, and affordable electronics.

5.1.2. The QCM Operating Principle

Lostis (Lostis 1958), Sauerbrey (Sauerbrey 1959) and Stockridge (Stockbridge 1965) all derived equations to explain the relationship between the resonant frequency of an oscillating piezoelectric crystal and the mass loaded on the crystal surface (Kumar 2000). Although, each one of them followed a different path and came to a similar conclusion, the Sauerbrey equation is most widely accepted equation to describe this relationship between mass and frequency change (Sauerbrey 1959).

$$\Delta f = \frac{-2\Delta m f_0^2}{A\sqrt{\rho_q \mu_q}} = -\frac{2f_0^2}{A\ \rho_q v_q}\Delta m$$

where Δf is the frequency change in oscillating crystal in Hz, and

Δm is the mass of deposited film in g

f_0 is the resonant frequency of the crystal or the initial standing wave,

A is the active area of the crystal surface in cm^2 (between electrodes),

ρ_q is the density of quartz,

μ_q is the shear modulus of quartz, and

v_q is the shear wave or oscillation wave velocity with in the quartz crystal.

Studies of the spatial distribution of the differential mass sensitivity on the QCM crystal have found that the sensitivity is maximum in the centre of the quartz crystal and decreases towards the borders of the crystal (Sauerbrey 1959; Buttry and Ward 1992). However, if the thickness of the electrodes is too thin (usually less than 500 Å), the resonant frequencies and thus the mass sensitivities of the entire crystal surface is very similar. The frequency shift obtained can be corrected to minimize these bulk effects (Schumacher, Borges *et al.* 1985; Urbakh and Daikhin 1994).

5.1.2.1. Sauerbrey relationship limitations

The equation is valid only when the following conditions are fulfilled: (i) the resonator is operated either in air or vaccum, (ii) the adsorbed mass is distributed evenly over the crystal. (iii) Δm is much smaller than the mass of the crystal itself (less than 1%), (Lu and Lewis 1972; Bandey, Martin *et al.* 1999) and (iv) the adsorbed mass is rigidly attached, with no slip or inelastic deformation in the added mass due to the oscillatory motion.

The Sauerbrey equation is valid only for thin, rigid, uniform and purely elastic added layers. The deposition of the layer is thus treated as a thickening of the crystal mass (Muratsugu, Ohta *et al.* 1993) and thus is assumed that the added layer possessing the same acoustic properties. It does not apply for thick films, viscous liquids, elastic solids, and viscoelastic bodies, since the density would change and viscous coupling would change. These limitations are in general due to a non-ideal behaviour of the added film.

Biomolecules bound to a sensor surface cannot be considered completely rigid because biological systems operate in liquid environments and also the biomolecules coordinate with water which will enhance the sensor signal. Due to high damping with liquid loads, the development of special oscillator circuits was necessary to operate in liquids (Ward and Delawski 1991; Josse, Lee *et al.* 1998). The amplitude of vibration is usually 10-20 nm in air and is reduced in water to a mere 1-2 nm (Cooper and Singleton 2007).

However, using radio-isotope labelling methods, Muratsugu and coworkers have shown that under a liquid environment, the linear relationship between mass and frequency response will persist with a coefficient of about 4 maintaining the frequency-to-mass relationship (Muramatsu, Tamiya *et al.* 1988).

This was then further developed by Kanazawa (1997), who expanded the model to Newtonian (viscous and lossy) liquids. The following equation describes the frequency shift for liquid- loaded sensor surface in which the liquid is defined by its density ρ_l and viscosity η_l:

$$\Delta f_l = -\sqrt{f_0^3 \frac{\eta_l \rho_l}{\pi \mu_q \rho_q}} = -f_0^{\frac{3}{2}} \sqrt{\frac{\eta_l \rho_l}{\pi \mu_q \rho_q}}$$

in which μ_q is the shear modulus in x-direction and ρ_q is the density of the crystal. This equation can be derived by calculation of an effective mass loading based on the penetration depth of the transversal wave propagated from the crystal surface into the liquid.

5.1.2.2. Dissipation factor

For systems operating under vacuum, in gas or in liquid, energy is lost, that is dissipated, during oscillation (Buttry and Ward 1992). For example, energy is lost in liquids due to frictional losses within the liquid as well as between the adsorbate and the liquid (Uttenthaler, Kolinger *et al.* 1998).

Kasemo and co-workers first described the quartz crystal microbalance with dissipation (QCM-D) technique, that measures the mechanical properties of an adsorbate, such as viscosity, elasticity, density and thickness. This QCM-D technique allows the resonance frequency and dissipation factor to be monitored

simultaneously (Buttry and Ward 1992; Rodahl, Hook *et al.* 1997). In this technique a quartz plate is excited with a frequency generator and the free decay of the oscillation is recorded by switching off the source and the procedure is repeated each second. The dissipation factor together with the resonance frequency is obtained by a curve fit. The Quality factor, Q is simply the inverse of D and sometimes this Q factor, Q, is used instead of dissipation.

Other factors which affect the frequency of the crystal include, the surface roughness (Martin, Granstaff *et al.* 1991; Yang and Thompson 1993), water trapped in surface cavities (Buttry and Ward 1992) etc. The frequencies shifts obtained could be corrected to minimize these bulk affects.

5.1.3. Applications

The first analytical application of a PZ detector was reported by King in 1964 (King 1964). The initial applications of the piezosensors were limited to measurement in the gas phase, because of the common belief at the time that stable oscillations could not be obtained in the liquid phase. However, with the development of new powerful oscillator circuits, it was shown that quartz crystals can oscillate in contact with solution (Martin and Hager 1989) and that enabled this technique to be introduced into bioanalytical applications. Since then, there has been a growing interest in the design of biosensors capable of detection in the areas of health eg. clinical diagnosis and environmental

monitoring eg. food and water-quality control. Although there is an extensive literature on the applications of QCM in various fields, the application only relevant to this present study is discussed.

5.1.3.1. Analysis of protein-protein interactions using QCM technique

QCM has been employed for the study of a range of protein-protein interactions. To continuously monitor the frequency during protein-protein interactions, a continuous liquid-phase piezoelectric biosensor for kinetic immunoassay was developed by Davis and Leary (Davis and Leary 1989), facilitating the observation of both the extent and the kinetics of these interactions. A number of protein-protein interactions have been studied such as, specific interactions of proinsulin C and engineered anti-C peptide antibodies (Caruso, Rodda *et al.* 1997) and the affinity of myocardial infarction marker troponin T for α-tropomyosin (Salvay, Grigera *et al.* 2003). The QCM technique has also been used to study the influence of cations, anions and solvent on protein–protein interactions (Wang, Jiang *et al.* 1998).

5.1.3.2. Piezoimmunosensors

Despite the established ELISA technique (Engvall 1980), the development of rapid, simple and label-free immunosensors based on piezoelectric transducers has been widely investigated due to their attractive applications in mass sensitive detection (Suleiman and Guilbault 1994). Such immunosensors are valued because, if there is an antibody against a particular analyte, an immunosensor

may be developed to recognize it. The piezoelectric immunosensor, as one of the most sensitive analytical instruments developed to date.

5.1.3.2A. Immobilization

In general, the immobilization of proteins is accomplished by a range of methods including, (a) simple physisorption (Voros 2004), or (b) by electrostatic interaction (Zhi and Haynie 2004), or (c) by covalently linking through amines (Melles, Anderson *et al.* 2005), or (d) using thiol-containing compounds (Zhu, Bilgin *et al.* 2001), or (e) attachment by affinity interactions. The recent immobilization methods use materials such as a silanized layer (Babacan, Pivarnik *et al.* 2000), sol–gel matrices (Unen, Engbersen *et al.* 2001), polymer membrane (Su and Li 2004), Langmuir-Blodgett film (Walter, Bussow *et al.* 2000), or self-assembled monolayer (SAM) (Angenendt, Glokler *et al.* 2003). However, simple nonspecific immobilization techniques on flat surfaces utilize soft membranes such as PVDF (Walter, Bussow *et al.* 2000) and nitrocellulose membrane (Joos, Schrenk *et al.* 2000) or poly(L-lysine).

Antibody immobilization is a very important step for successful fabrication of a piezoelectric immunosensor. Antibodies immobilized on a solid-phase surface usually show less binding activity than that of soluble antibodies (Sokoll and Chan 1999), likely due to a combination of steric-hindrance effects of the molecules on the solid-phase (Kele, Nagy *et al.* 2006) and the random orientation

of the antibody molecules on solid-phase surface (Herr, Throckmorton *et al.* 2005). Thus, there is a requirement to develop improved methods for the immobilization of antibodies in a highly oriented manner with increased binding activity.

Affinity tag based immobilization techniques include, such as biotin, hexa-His tag, or glutathione S-transferase (GST), avidin coated surfaces, (Schäferling, Riepl *et al.* 2003) Ni-NTA-coated (Zhu, Bilgin *et al.* 2001), and glutathione coated surfaces (Kawahashi, Doi *et al.* 2003), Protein A or Protein G coated surfaces to immobilize immunoglobulin G (IgG) (Byung-Keun, Young-Kee *et al.* 2003), respectively.

5.1.3.2B. Immunosensing in the gaseous phase

Coating of a PZ crystal with an antigen was first demonstrated by Shons *et al.* (Shons, Dorman *et al.* 1972) on a surface precoated with a low surface energy plastic coating, nyebar C (30% solution in 1-3 di [trifluoromethyl] benzene), providing a layer capable of forming hydrophobic bonds with proteins such as BSA. An improved indirect assay method for the determination of antigens was reported by Oliveira *et al.* (Oliveira and Silver 1980). A method for determination of both the type of antibody subclass and the concentration of antibody present was patented by Rice (Rice 1980; Rice 1982). The detection of gaseous substrates

by PZ immunosensors was first reported by Guilbault and co-workers (Ngeh-Ngwainbi, Foley *et al.* 1986).

5.1.3.2C. Immunoassay in the liquid phase

The detection of analytes in solution reported before have been carried out by comparing the resonant frequency of the crystal before and after exposure to the test sample and the frequency measurement were subsequently carried in the gas phase. However, in 1982, Nomura and Okuhara (Nomura and Okuhara 1982) were the first to design a device capable of operating in fluids, which became the starting point for the development of a new class of bioanalytical tools.

The first online detection of antibody-antigen reactions in aqueous solutions originally started with the work of Roederer and Bastiaans on SAW sensors (Roederer and Bastiaans 1983; Roederer and Bastiaans 1988) to detect human IgG in solution. Thompson *et al.* (Thompson, Arthur *et al.* 1986) evaluated the response of a AT-cut quartz plate device, applied for the the detection of IgG in solution under various conditions including stationary and flowing water, change of interfacial chemistry, and different aqueous viscosities.

Unlike the above mentioned findings, Muramatsu *et al.* (Muramatsu, Dicks *et al.* 1987) demonstrated that an immobilized layer of protein A placed on the surface of crystals modified with (ϒ-aminopropy1)triethoxy-silane could be successfully

utilized to determine the concentration of IgG and its subclass in solution. Piezoimmunosensors have also been used for the quantitative detection of antigen present in sample solution, in a number of studies including tumour necrosis factor (Liu, Tang *et al.* 2004) and human and rabbit IgG (Zhang, Mao *et al.* 2004). A QCM-based immunoassay for the detection of HSA, an early indicator of renal disease in diabetic patients have been reported (Sakti, Lucklum *et al.* 2001). Assays for detection of disease-associated antibodies have also been developed for Schistosoma japonicum (Wang, Wang *et al.* 2002), Toxoplasma gondii (Wang, Li *et al.* 2004) and anti-sperm antibodies (Shen, Tan *et al.* 2006).

Specific clinical markers can also be analyzed using QCM including plasma vitellogenin (Oshimaa, Nakajimaa *et al.* 2005), cholinesterase (Halámeka, Tellera *et al.* 2006), α-fetoprotein (Chou, Hsu *et al.* 2002), human ferritin (Chou, Hsu *et al.* 2002) and ceruloplasmin (Wang, Li *et al.* 2004). QCM-D also has also been utilized for studying antigen and antibody interactions (Lu, Morimoto *et al.* 2003) and hemocompatibility of biomaterials (Ebersole, Miller *et al.* 1990; Fawcett, Craven *et al.* 1998).

5.1.3.3. QCM-based detection of microorganisms

Piezoelectric immunosensors haven also been used for direct detection of bacteria. Generally, primary or capture antibodies are immobilized onto gold coated AT-cut quartz crystal and the specific binding of bacteria onto the

immobilized antibodies ultimately results in decrease of the sensor's resonant frequency.

A number of piezoelectric immunosensors have been developed for rapid detection of bacteria including *Salmonella typhimurium* (Muramatsu, Kajiwara *et al.* 1986), *S. paratyphi* (Bao, Deng *et al.* 1996), *E. coli* O157:H7 (Suleiman and Guilbault 1994; Ben-Dov, Willner *et al.* 1997; Ivnitski, Abdel-Hamid *et al.* 1999; Dmitri Ivnitski 2000)., *E. coli* K12, *Chlamydia trachomatis, Yersisinia pestis, Candida albicans* (Sato, Endo *et al.* 1995; Sato, Serizawa *et al.* 1998), *Shigella dysenteriae*, *Staphylococcus epidermidis* (Hengerer, Decker *et al.* 1999) etc. and this has been summarized in several reviews (Bizet, Gabrielli *et al.* 1995). These immunosensors generally have a detection limit of 10^5–10^7 CFU/mL and show minimum or no cross reactivity towards related species.

As an alternative to whole cell capture-based assays, Su *et al.*. (2001) developed a test for *Salmonella enteritidis* by immobilizing the bacteria to detect the corresponding antibodies in 1/100 diluted chicken serum and egg-white samples, with a clinical specificity of 100 and 92.9%, respectively (Su, Low *et al.* 2001). Direct screening using QCM and virus-specific antibodies has been applied to human serum from patients with dengue fever virus infection (Wu, Su *et al.* 2005).

The detection of bovine ephemeral fever virus was demonstrated in minutes, potentially leading to a rapid diagnostic technique (Lee and Chang 2005). Amounts as low as 1 ng of two orchid viruses was detected acoustically by immobilizing specific virus antibodies on the sensor surface (Eun, Huang *et al.* 2002). Other viral immunoassays reported include those for *Tobacco Mosaic Virus* (TMV) (Rice 1980) herpes simplex type I (HSV1) (Cooper, Dultsev *et al.* 2001), and influenza (Amano and Cheng 2005). A sensitive technique for analyzing phage libraries within a short time by using a flow injection system, was also achieved by the quartz-crystal microbalance (Tian, Wei *et al.* 2004).

5.1.4. Amplification of the QCM signal

Besides the unique optical properties of the gold nanoparticles, the particles also have been applied as signal enhancers for QCM based detection (Kim, Baek *et al.* 2007). DNA-conjugated nanoparticles have been used to enhance the signal produced upon hybridization to a surface-bound single-stranded template (Taton, Mirkin *et al.* 2000; Wang, Xu *et al.* 2001; Ha, Kim *et al.* 2004; He and Liu 2004; Liu, Tang *et al.* 2004). They were also used to increase the surface area available to immobilize the DNA template on a sensor (Liu, Li *et al.* 2005). Detection sensitivity is generally around 10^{-15}–10^{-16} M, however, Mo *et al.*. reported zeptomolar (10^{-21} M) sensitivity for the detection of specific nucleic acid (Mo, Wang *et al.* 2005). Different size nanoparticles were used in the range 10-60nm however, it has been shown that 20 nm is the optimal particle size for

maximal sensitivity. The larger particles were found to suffer from weaker binding to the surface and are therefore lost on exposure to flow across the sensor surface (Tao, Jian *et al.* 2003).

A unique strategy using gold nanoparticles as signal amplification probes for the high-sensitive detection of the streptavidin–biotin interaction on a QCM device has been reported (Kim, Baek *et al.* 2007). Recently, amplification schemes similar to sandwich ELISA have been reported (Kolinger, Uttenthaler *et al.* 1995). Two approaches using an amplified mass immunosorbent assay (AMISA) concept and a reusable polyvinyl-ferrocene (PV-FC) film coated on the crystal, have been described for the detection of adenosine 5'-phosphosulfate (APS) reductase and human chorionic gonadotropin (hCG) respectively.

A method designated as latex piezoelectric immunoassay (LPEIA), was developed for immunoassay of C-reactive protein (CRP), a marker for acute inflammation (Kurosawa, Tawara *et al.* 1990). In this method, the amplification of the frequency shift was observed using antibody-coated latex without any film on the crystal. Antibody-coated latex beads were also employed in an assay for identification of degradation products of fibrinogen and fibrin (Aizawa, Kurosawa *et al.* 2003). Thus, acoustic sensor technology is thus regarded as a highly interdisciplinary and has added advances and improvements ranging from from electrical engineering to cell biology.

5.2. Materials and Methods

5.2.1. Materials

Monodisperse suspensions of gold nanoparticles with an average 50 nm particle diameter were obtained from British Biocell (UK), while bovine serum albumin (BSA), N,N-dimethyl formamide (DMF) and absolute ethanol and methanol were obtained from Sigma-Aldrich, USA. Casein was obtained from Ajax chemicals Ltd, PVDF membrane (0.45 μm) from Millipore, USA and the 5 MHz gold coated QCM sensors were obtained from Maxtek Inc., USA.

The working buffer used in these experiments was 0.1M phosphate buffer (PB) pH 7.4. Piranha solution (1:3 H_2O_2 (30% v/v) : conc. H_2SO_4), 0.1N NaOH, 0.1N HCl were all prepared using analytical reagent grade chemicals. In all instances, high purity deionized water was used as a diluent.

5.2.2. QCM instrumentation

The RQCM Quartz crystal microbalance (Maxtek Inc., USA) allows simultaneous measurement of crystal frequency and crystal resistance. The RQCM was used with a standard 25 mm diameter polished AT-cut quartz crystal wafer with circular electrodes on both sides and coated by gold disc-shaped films deposited on chromium underlayers (Figure 5.2.). The electrode area was approximately 133 mm^2 (Maxtek model No. 149211-2). The crystals were mounted in a Maxtek

CHT-100 crystal holder which was connected to a flow cell to create a 100 µl flow cell.

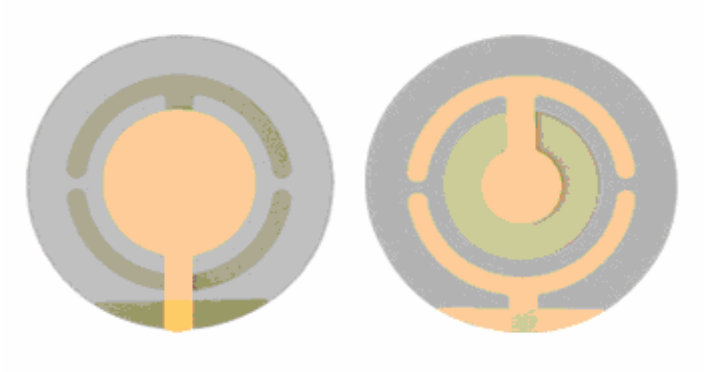

Figure 5.2. The images of gold coated QCM crystals used in this study.

A high performance phase lock oscillator circuit of the system initiates the oscillation of the crystal by a voltage pulse and the crystal is then driven at its resonance frequency to achieve the series resonance. The frequency of the vibrating crystal was monitored by a multifunction frequency counter. This circuit is capable of supporting heavily loaded crystals, up to 5,000 Ohms resistance. This circuit also incorporates a potentiometer to adjust the crystal capacitance cancellation thus reducing errors caused by stray capacitance of the system. This is is essential for accurate measurements in lossy films. This has enabled to measure frequency and crystal resistance to a high degree of accuracy over wide operating conditions. A software program (RQCM data log program) facilitated remote operation and the data acquisition.

5.2.3. QCM crystal pre-treatment

The fabrication of the immunoassay system on 5 MHz AT-cut quartz crystals commenced with cleaning the crystals by the following chemical treatment. The crystals were pre-treated with 1M NaOH for 10 min, 1M HCl for 10 min, and then with Piranha etch solution, in sequence, to obtain a clean gold surface. After pre-treatment, the crystals were rinsed with ethanol and water successively and dried at room temperature under a nitrogen atmosphere prior to use.

5.2.4. Operation of flow-cell

After the pre-treatment, the 5 MHz AT-cut quartz crystal was mounted in an acrylic crystal holder between two O-ring seals inserted in a Teflon cell with leads, so that only the gold surface of the crystal was in contact with the liquid. The crystal surface was exposed to a 100 µl chamber which was connected to a syringe pump (Razel, USA; Model No. A-99.EZ) through 1/16" Teflon tubing (Upchurch Scientific Inc., USA). The sample solutions were injected through a manually controlled six-way valve (VICI, Cheminert, USA; Model No. 06S-0373L). All fittings and connectors were obtained from FIA Lab Instruments Inc., USA.

The crystal holder was placed at an angle of 30° and sealed to air in order to remove the potential of air bubbles remaining on the crystal after filling from the dry state and to allow air bubbles in the liquid phase to pass out without

adhering to the crystal. This placement of the crystal holder also alters the liquid meniscus in order to avoid reflection of induced longitudinal waves at the air-liquid interface which in turn influence the resonant frequency of the quartz crystal. A constant flow rate of 3.0 mL $hour^{-1}$ was maintained through out the experiment.

5.2.5. Preparation of the Self Assembled Monolayer (SAM)-based immunosensor

Rabbit anti-OMP85 polyclonal antibodies purified by protein A sepharose chromatography were used (Chapter 2) in these studies. Anti-OMP85 antibodies were immobilized by direct adsorption onto the gold surface of the crystals. Anti-OMP85 antibody solution (200 µl of 0.5 mg/mL) in PB was spread over the entire Au electrode surface and incubated at 4 °C overnight. The excess antibody was removed by rinsing with PB. The antibody-modified crystals were then saturated with 1% (w/v) Casein dissolved in PB for at least 1 h to block unreacted and nonspecific binding sites on the crystal surface. After rinsing with PB, the crystals were dried under nitrogen. The crystals were then mounted into a crystal holder and washed with PB until a steady/stable base line was achieved. OMP85 conjugated 50 nm gold nanoparticle suspension (Chapter 3) was then injected and resulting frequency changes were monitered.

5.2.6. Deposition of PVDF film on QCM crystal by spin coating

PVDF solution was prepared by dissolving 75 mg of PVDF membrane (Millipore, USA) in 1.0 mL N,N-dimethyl formamide at 60 °C for 5 minutes. A 100 µl aliquot of the PVDF solution was then spin coated on to the surface of a QCM electrode, using a Laurell Technologies model WS-400A-6NPP spin coater, at increasing speed in the range of 0-5000 rpm at an acceleration of 50 rpm/sec for 2 minutes. The spinning process was repeated twice. The crystal was removed from the spin coater and then washed thoroughly with double distilled water to remove any residual DMF and dried in a vacuum oven at 60 ºC for 30 – 60 minutes. The deposited PVDF film was uniform and dried during the spin coating procedure. The film on other parts of the crystal apart from the gold surface was manually removed, so that only the gold surface was coated with PVDF. The coated crystals were stored at room temperature in a clean chamber until used.

5.2.7. Surface characterisation of PVDF coating

The PVDF film coating on the QCM crystal surface was characterized by the following techniques:

5.2.7.1. Scanning Electron Microscopy (SEM) studies

SEM was performed on the PVDF film coating using a Philips XL30 microscope, to obtain the information about the structural morphology of the deposition. PVDF coated QCM crystals were affixed to aluminium pegs with carbon tape

and sputter coated with gold for 60 sec at 0.016 mA (Agron plasma) using a SPI-Module Sputter Coater (SPI Supplied Division of Structure Probe, Inc).

Then, the crystal was placed inside the microscope's vacuum column through an air-tight door. Emitted from a tungsten source, the high energy electron beam which typically has an energy ranging from a few hundred eV to 30 keV is focused into a very fine focal spot sized 0.4 nm to 5 nm. As the electron beam hits each spot on the sample, due to the energy exchange between the electron beam and the sample, secondary electrons are deflected from its surface. A detector counts these electrons and sends the signals to an amplifier. The final image is built up from the number of electrons emitted from each spot on the sample.

This scanning electron microscope has a magnification range from 15x to 200,000x and a resolution of 5 nanometers. The resulting images were scanned on a digital imaging system by computer enhancement. Images of fresh PVDF film coating were taken before and after using the crystal multiple times. Also, an approximate estimation of the film thickness was obtained from the SEM cross section images at 25,000X magnification.

5.2.7.2. Atomic Force Microscopy (AFM) studies

The Atomic Force Microscopy (AFM) (Binnig *et al.*. 1986) measurements were performed with a Nanoscope IIIa Multimode scanning probe microscope (Digital

Instruments Inc., Santa Barbara, CA, USA) in order to achieve information about the surface morphology of the PVDF coated QCM surfaces. The images were scanned in tapping mode (Martin *et al.*. 1987, Zhong *et al.*. 1993) in air with a sharp tip attached to a cantilever (Vecco, USA). Rectangular phosphorus doped silicone tips (0.5-2.0 ohm-cm) with a spring constant of 40N/m were used in the frequency range of 100-500kHz. The thickness of the cantilever was 4 micrometer with back side coating of 40nm aluminium. Tip region of contact (ROC) was <10nm with tipROC max of 12.5 nm, front and back and side angles of the tip were 15°, 25° and 17.5° respectively. Scan speed was varied depending on the scan size without affecting the quality of the image. When a laser beam is directed onto the cantilever, the deflection of the cantilever is detected with a photo detector. Both the height and roughness profiles of the PVDF surface and the attachment of the whole cell NM bacteria on the sensor surface were analysed.

5.2.7.3. Network analyzer studies

An Agilent E5100A Netwrok analyzer was used to study the impedance profile of the crystal before and after coating with PVDF layer. A Pi-network test fixture was used in the data acquition process. The dissipation change was measured by periodically switching off the driving power to the thickness-shear-mode oscillation of the sensor crystal and recording the decay of the damped oscillation.

5.3. Results

In these studies, the use of QCM was explored to develop a real time immunoassay for OMP85 antigen and to assess the applicability for the development of a biosensor for detection of *Neisseria meningitidis.*

5.3.1. Self Assembled Monolayer (SAM) based Immunosensor

The clean gold surface on the QCM crystal coated with anti-OMP85 antibodies was washed in situ with 0.1M PB pH 7.4. The excess anti-OMP85 antibody and casein molecules were removed by PB wash and a stable base line was achieved. Introduction of OMP85 antigen conjugated with 50 nm gold nanoparticle, on the QCM crystal surface resulted in frequency changes, corresponding to the antigen concentration. Figure 5.3 shows the time and concentration dependent frequency changes upon the exposure of the anti-OMP85 antibody layer to 6.25 μg/mL OMP85-conjugated to 50 nm gold nanoparticle. The frequency change for the same amount of antigen without the gold nanoparticles was not measurable in this QCM system (data not shown).

However, the frequency shifts due to the specific antigen-antobody interactions were varied and sometimes unobservable. For reasons not clear, the system was not stable and the measured frequency change was variable with high noise levels. In order to address these issues with stability and noise, a PVDF film with protein A layer on QCM was utilized as an alternate approach.

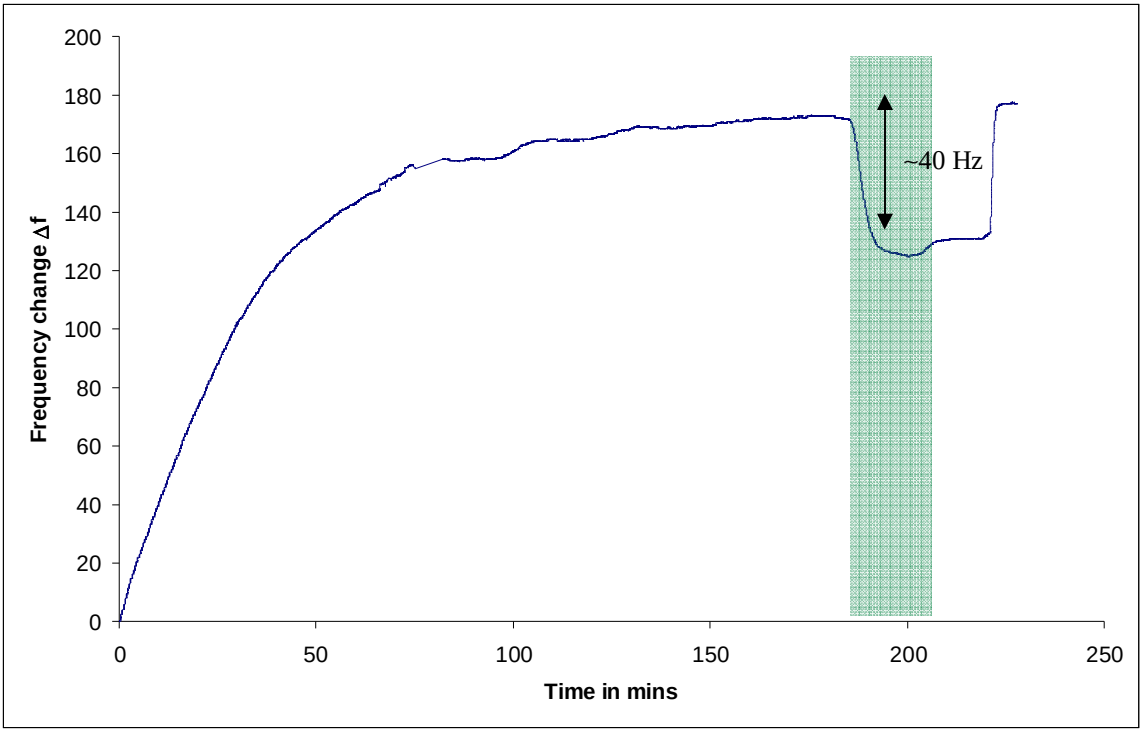

Figure 5.3. Changes in frequency as a function of time following the sequential exposure of the antibody coated quartz crystal to the OMP85 conjugated 50 nm gold nanoparticles. The grey area indicates the OMP85 and anti-OMP85 antibody binding event and resulting frequency change.

5.3.2. Real-time measurements using a PVDF coated QCM immunosensor

A method for the preparation of preparation of a PVDF solution was developed and used to spin coat the QCM crystals. This method was desribed in section 5.2.6.

5.3.2.1. Real time analysis of the in situ preparation of a Immunosensor

Before an experiment, the RQCM instrument was warmed up for at least two and half hours with or without a crystal in the holder. The PVDF-coated 5 MHz AT-cut quartz crystal was mounted in an acrylic crystal holder between two O-

ring seals, so that only the coated surface of the crystal was in contact with the liquid. Analytical grade methanol was injected for 3 minutes to pre-wet the PVDF membrane. After wetting the PVDF film with methanol for 5 minutes, 0.1M PB pH 7.4 was passed through the chamber to remove the methanol and obtain a stable base line. The crystal resistance was observed in the range of 500-600 Ohms. Similar resistances were recorded following the application of subsequent film coatings. If necessary, capacitance cancellations were carried out to lock the crystal frequency. The frequency shift was recorded as a function of time at an interval of 5 s using the RQCM data log program on a computer.

The detection of OMP85 target antigen molecules using this approach was as follows: The PVDF coating was washed using 0.1M phosphate buffer pH 7.4 until a steady baseline was achieved overnight. Following the observation of a steady baseline, a layer of protein A was first adsorbed on the PVDF coated Au surface of the QCM electrode by passing a solution of 100 ug/mL protein A at a flow rate of 3.0 mL $hour^{-1}$. After the protein A baseline was stabilised (shift less than 1 Hz min^{-1}), excess protein A was removed by washing with 0.1M PB (pH 7.4). The PB wash was continued until another stable baseline was observed for 5-10 minutes. Subsequent blocking of unbound sites using 1% (w/v) casein in PB on the sensing interface was then carried out at a similar flow rate. Excess casein solution was removed with PB until a baseline was achieved for a further 5-10 minutes.

Following the stabilisation of the QCM response, the protein A - sepharose purified anti-OMP85 antibody solution (100 µg/mL) was then injected for binding to the surface immobilized protein A molecules and allowed to bind until a stable base line was observed. After rinsing with PB to remove the excess antibodies, finally the cognate antigen, OMP85 was allowed to specifically bind with the anti-OMP85 antibodies by passing 20 µg/mL OMP85 antigen over the crystal surface at the same flow rate. After achieving the stable baseline frequency, excess OMP85 antigen was flushed with PB to obtain a steady baseline (Figure 5.4.).

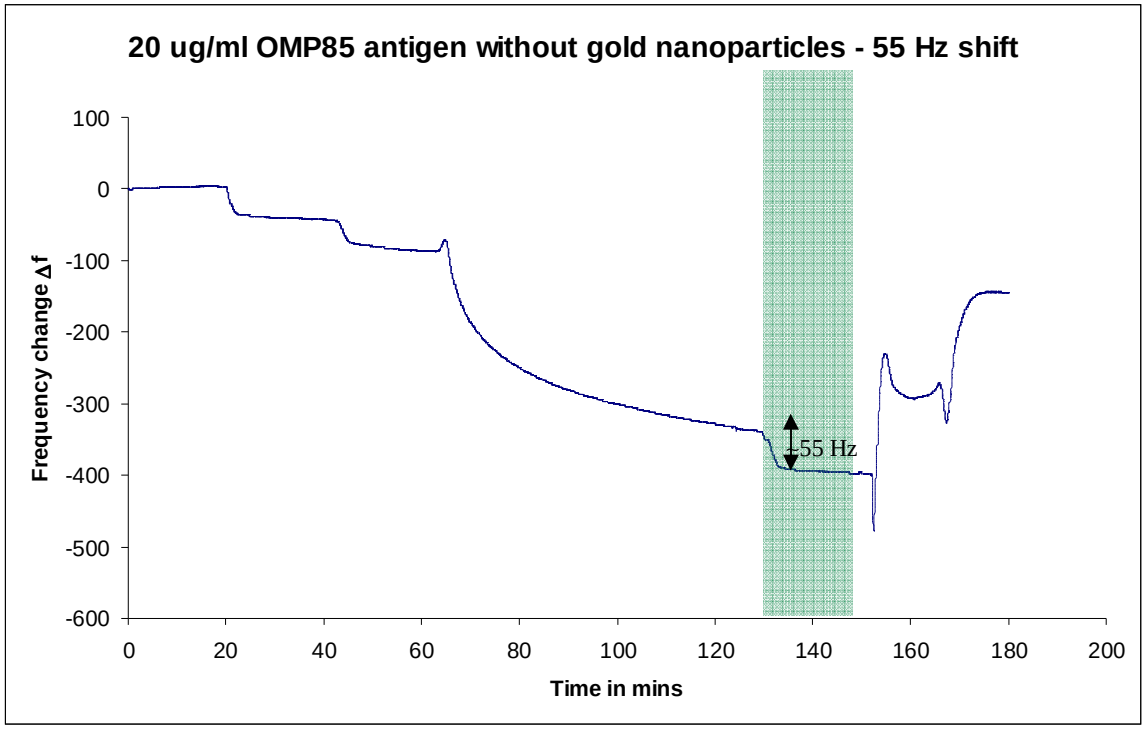

Figure 5.4. Changes in frequency following sequential exposure of the PVDF coated quartz crystal to the OMP85 antigen alone.

5.3.3. Enhancement of mass sensitivity using gold nanoparticles

The gold nanoparticles were used to enhance the mass sensitivity and 50 nm gold nanoparticles conjugated with OMP85 antigen was passed over the protein A immobilized anti-OMP85 antibody layer and the frequency change was monitored. When the antigen was added without gold nanoparticles at 20 μg/mL OMP85 concentration, a ~55 Hz frequency shift was observed (Figure 5.4.), whereas, at 300 ng/mL concentration, the temporal response curves could not be distinguished from the baseline of the negative control curve. For example, with 5 μg/mL OMP85-gold nanoparticle suspension (as measured by Bradford assay) injected in the QCM cell, a large decrease of the microbalance frequency, Δf = 130 Hz, was observed (Figure 5.5.). For the same amount of antigen without gold nanoparicles, a frequency shift of 22 Hz was observed. For the entire range of concentrations analyzed (300ng-20μg/mL OMP85), a five fold increase in the sensitivity was observed with the use of 50nm gold nanoparticles (Table 5.1.).

OMP85 Conc. (μg/mL)	Δf with gold nanoparticle	Δf without gold nanoparticle
20	250	55
10	185	32
5	130	22
2.5	90	15
1.25	65	10
0.625	40	6
0.312	12	4

Table 5.1. QCM response for various concentrations of OMP85 antigen both with and without gold nanoparticles.

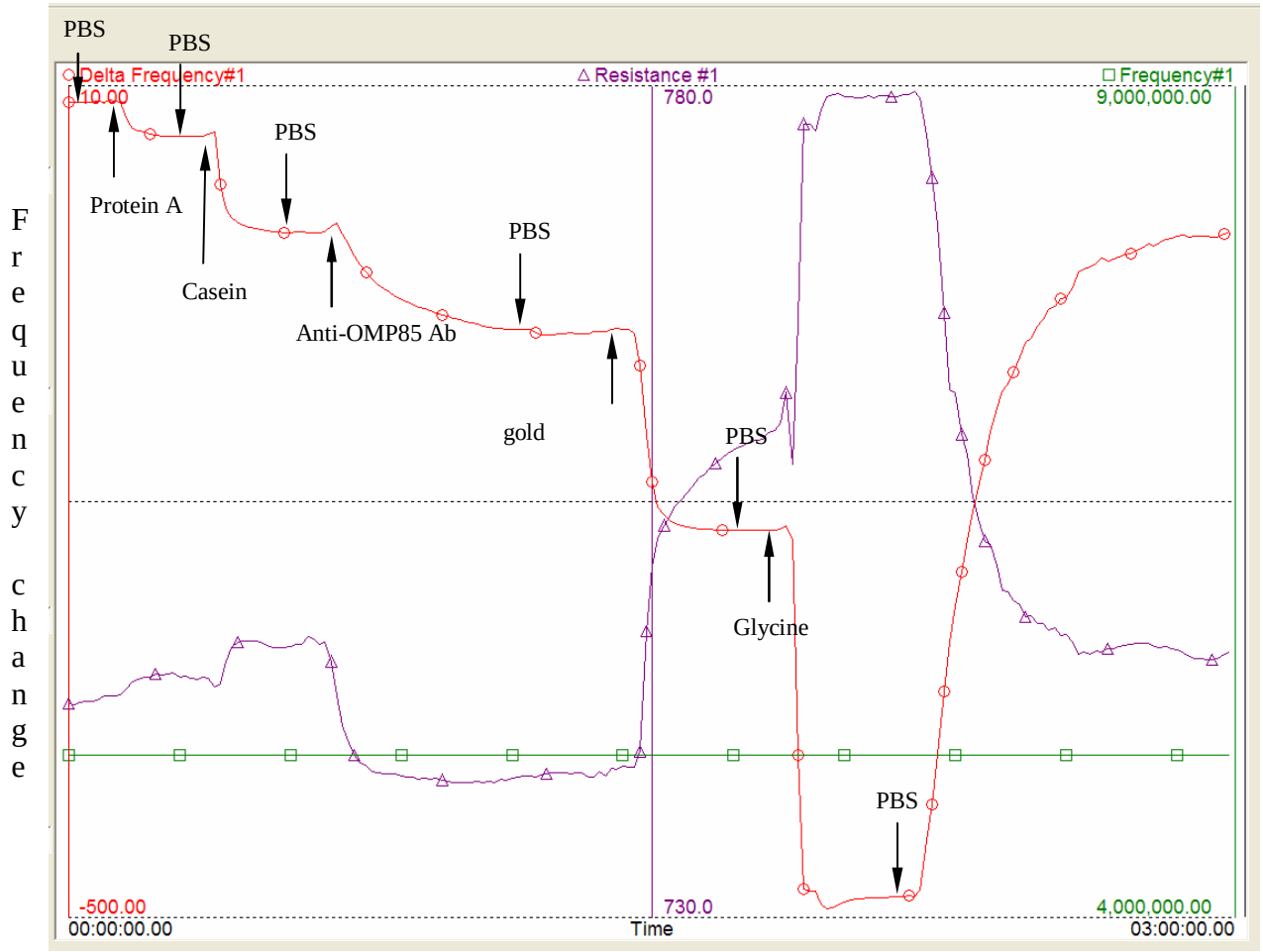

Figure 5.5. A flow through experiment showing detected frequency changes in response to sequential addition of protein A (100 µg/mL), casein (0.1%), anti-OMP85 antibody (100 µg/mL) and 50 nm gold nanoparticle conjugated OMP85 antigen (5 µg/mL).

All frequency changes due to different binding events were monitored step by step in real time (Figure 5.5. and 5.6.). In every step, the frequency change reached a plateau after a variable period of time which indicated no further change in the mass on the crystal surface. Once a stable base line was established

at each step, replacement of the protein solution by buffer solution (PB) did not produce any noticeable change in the frequency response. This indicates that the possible effect of variations in bulk density and viscosity due to fluid exchange were negligible. Except for the antibody step, the resonant frequency of the crystal reached a baseline very quickly in all other steps and the stable frequencies obtained at different times were almost identical. A prolonged baseline, stable over few hours with a noise level less than ± 1 Hz when PB was flowing across the crystal surface at 3.0 mL/hour was also demonstrated.

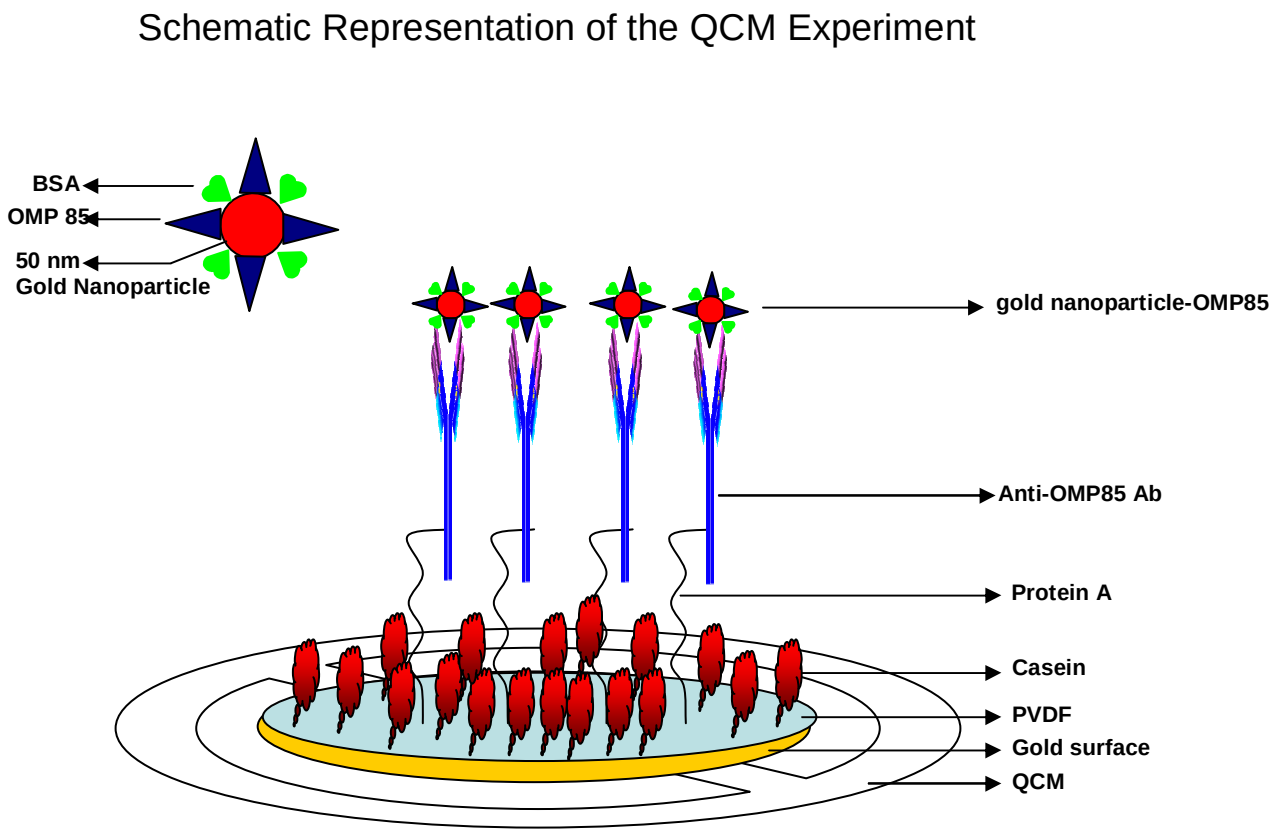

Figure 5.6. A schemtatic representation of a piezoelectric immunosensor used in these studies in the order of addition of different layers of biomolecules.

To test the reproducibility of the immunosensor, the QCM response to different concentrations of OMP85 antigen, was determined in duplicates. An inter-assay variation of 5-10Hz was observed with the various concentrations. This result indicates that the proposed piezoimmunosensor could provide reproducible determination of OMP85 antigen.

5.3.4. Dose–response curves

It can be seen that for the entire OMP85 working concentration range of 300 ng–20 μg/mL, the higher the concentration, the greater the sensor responses (Figure 5.7a., 5.7b. and 5.7c.), and a nonlinear relationship between frequency change and amount of OMP85-gold nanoparticle conjugate was observed (Table 5.1.).

(a) 20 µg/mL OMP 85 antigen – 250 Hz Frequency shift

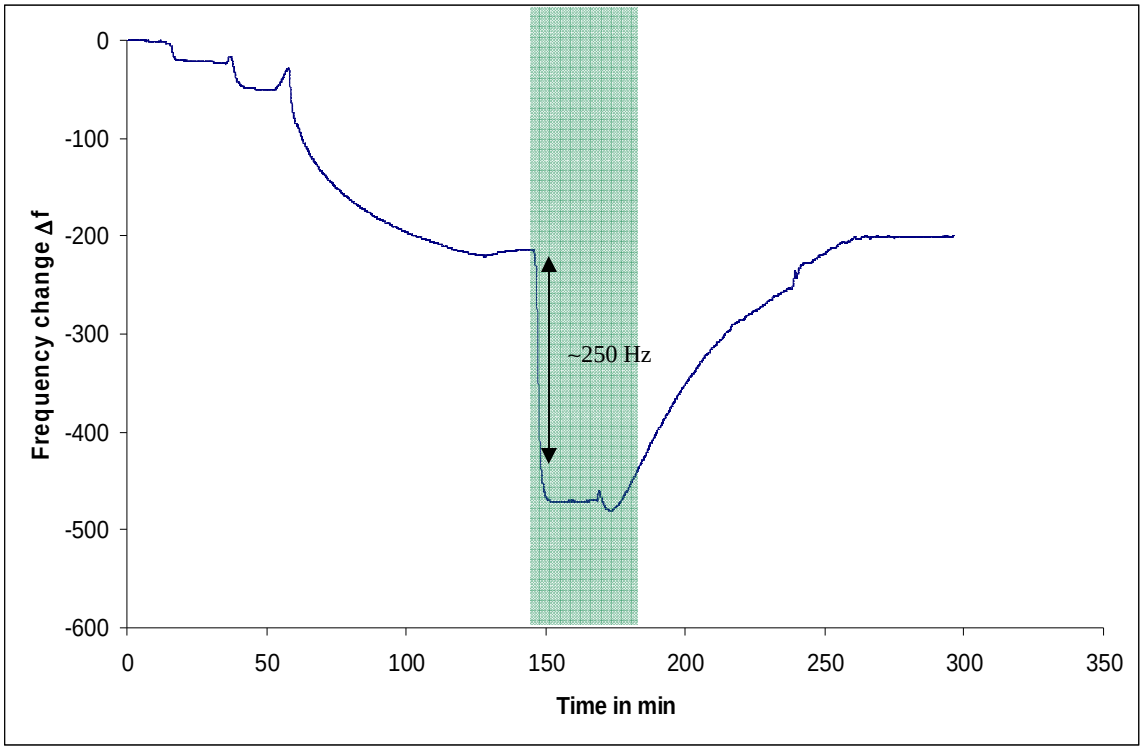

(b) 2.5 µg/mL OMP 85 antigen – 130Hz Frequency shift

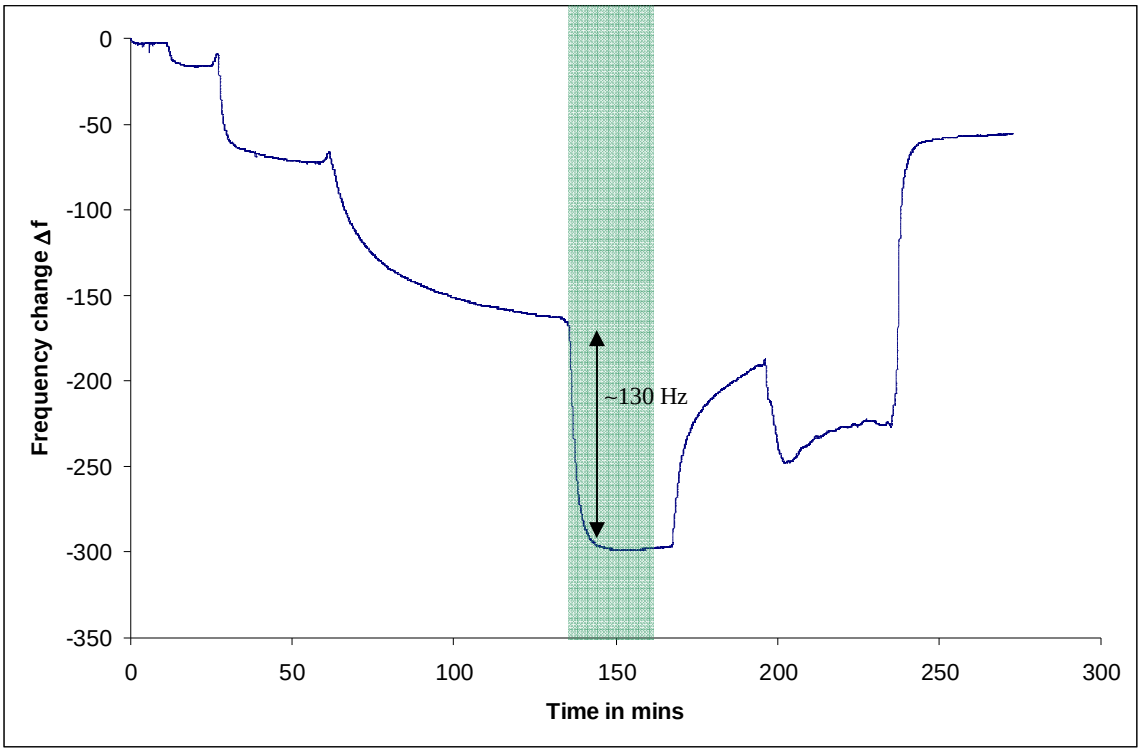

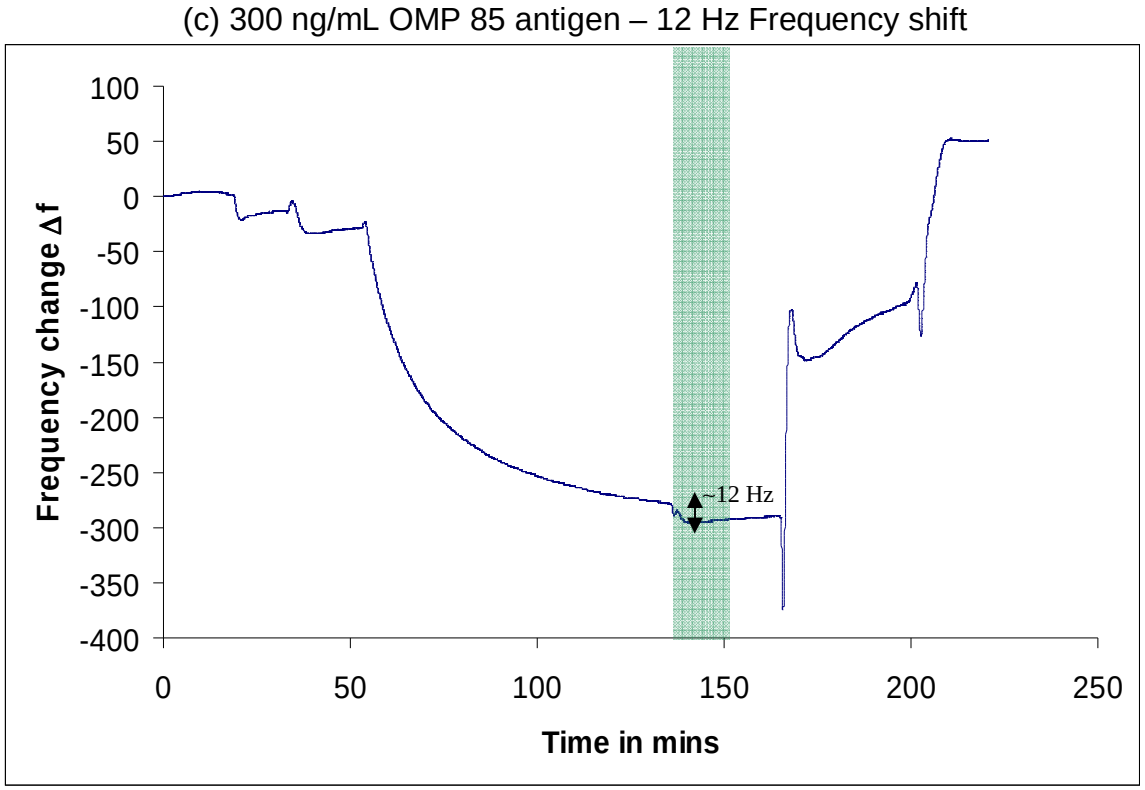

Figure 5.7. Changes in frequency as a function of time following the sequential exposure of the PVDF coated quartz crystal to OMP85 protein conjugated to 50 nm gold nanoparticle. (a) 20 µg/mL, (b) 2.5 µg/mL and (c) 300 ng/mL. The grey area indicates the gold nanoparticle-OMP85 and anti-OMP85 antibody binding event and subsequent frequency change. All the responses after the Ag-Ab binding event are the washing steps.

The specificity of biosensor was assessed using BSA conjugated gold nanoparticles as a non-specific antigen. No non-specific interaction was observed using upto 20 µg/mL BSA-gold nanoparticle conjugate, illustrating the specificity of the sensor (Figure 5.8a.). The dip immediately after the introduction of the BSA coated nanoparticle suspension might have occurred due to the

viscosity difference between the solutions. The microbalance frequency remained constant when neat 50 nm gold nanoparticle suspensions were injected onto the QCM surface coated with protein A/anti-OMP85 antibodies (Figure 5.8b.). Nanoparticles were blocked with casein to prevent non-specific Au-protein binding.

(a) 20 µg/mL BSA antigen – 0 Hz shift

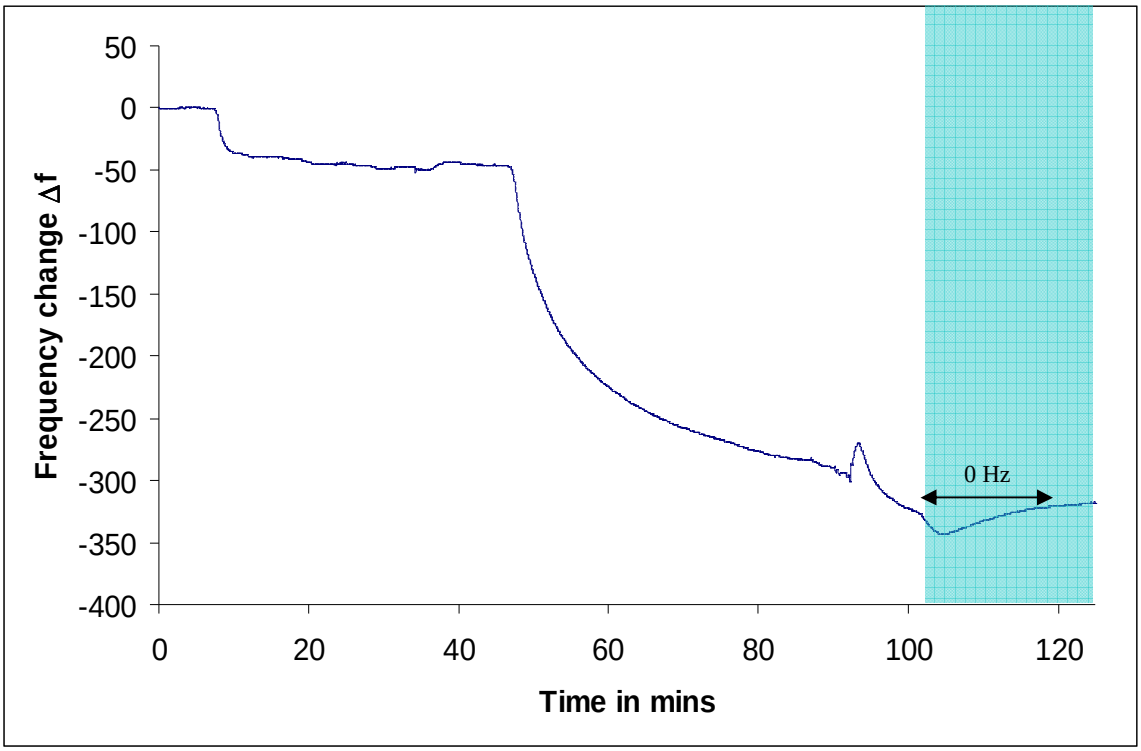

(b) Neat gold nanoparticles - 0 Hz Frequency shift

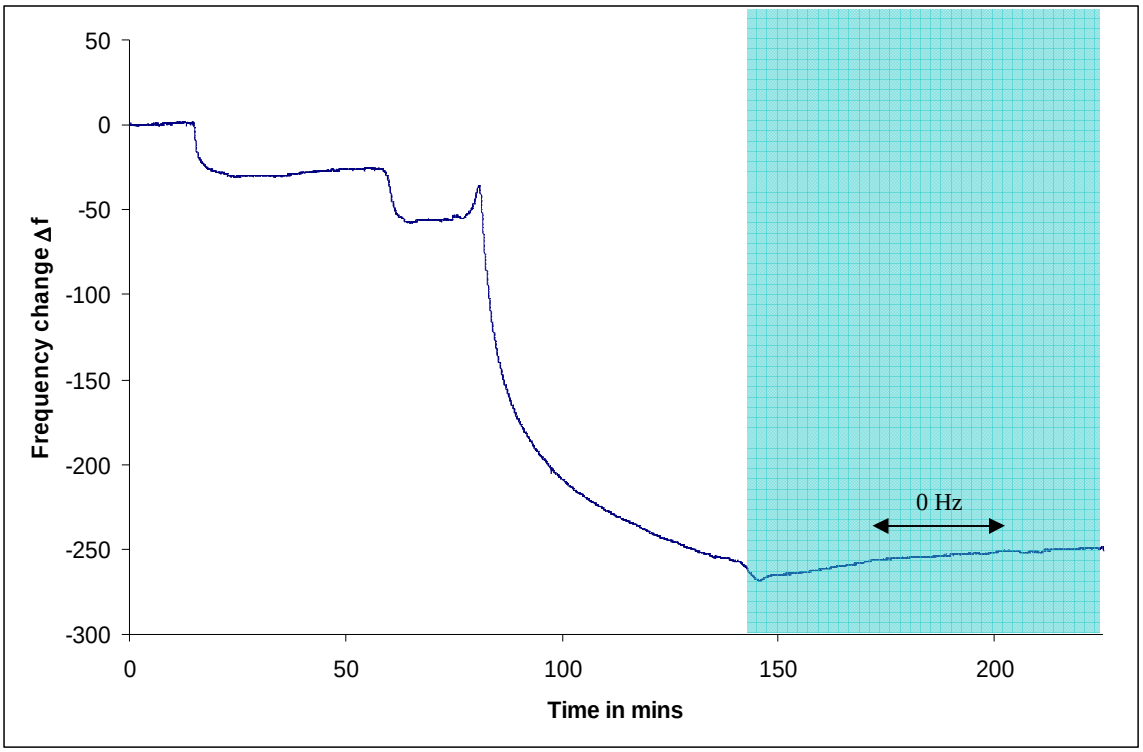

Figure 5.8. Changes in frequency following the exposure of the PVDF coated quartz crystal with protein A and anti-OMP85 antibody to (a) BSA conjugated 50 nm gold nanoparticles and (b) neat gold nanoparticles. No change in frequency was observed. The grey area indicates the injection of neat/BSA conjugated gold nanoparticles and subsequent elution without binding to the immobilised anibodies.

5.3.5. Calibration curve for the detection of OMP85

A calibration curve was constructed using OMP85 antigen at different concentrations in the range of 300 ng - 20 μg/mL on the antibody-coated crystals, which resulted in differing frequencies accordingly, all significantly distinguishable from the background noise. Calibration curves were obtained for both gold nanoparticle-OMP85 conjugates and OMP85 alone on the sensor.

The calibration curve determined from the net frequency changes showed significant linearity over a range from 300 ng/mL to 20 µg/mL of OMP85 target molecule (5.9a. and 5.9b.) These experiments clearly indicate that gold nanoparticles can be used to enhance the detection limits of the conventional QCM detection systems.

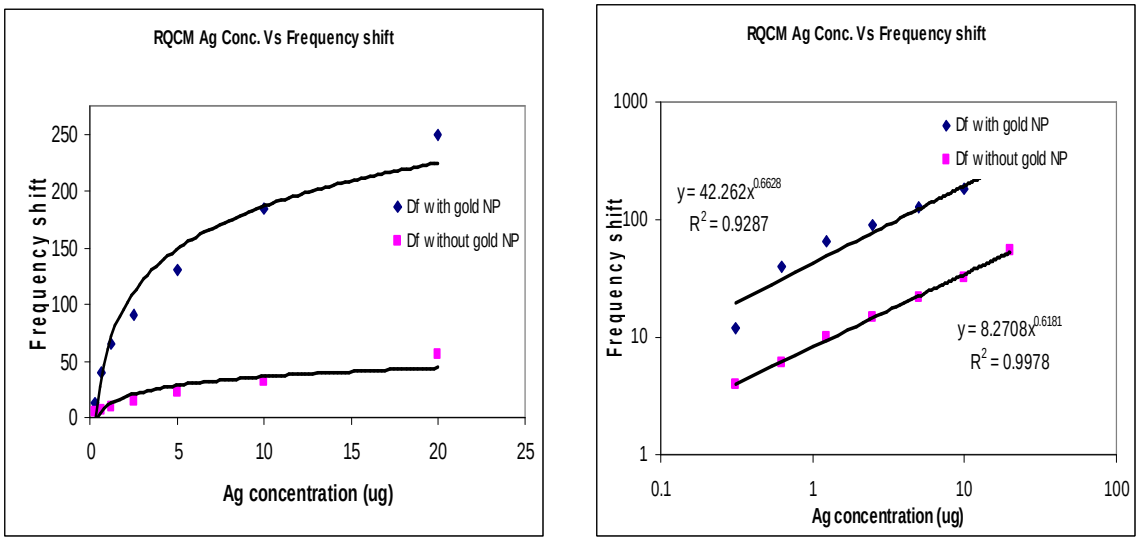

Figure 5.9. The calibration curve determined from the net frequency changes upon OMP85 and anti-OMP85 antibody interactions and the difference in frequency measured with and without conjugation with gold nanoparticles. The concentration of OMP85 target molecules ranged from 300 ng/mL to 20 µg/mL resulting frequency changes were in the range from 10 to 250 Hz. (a). The calibration curve determined from the net frequency changes by OMP85 target molecules with different concentrations and additional frequency changes due to OMP85 conjugated gold nanoparticles. (b) The calibration graph of frequency decrease vs. logarithm of antigen concentration is linear within the same detection range.

5.3.6. Regeneration of immunosensor

After each run, the used QCM crystals were regenerated by injecting the elution buffer solution (0.1 M Glycine-HCl, pH 3.0) to release antigen–antibody complexes from the protein A layer. Washing continued until return to the original protein A baseline was observed. The glycine solution removed all biological layers except the protein A and casein layers, which could be seen from the frequency base line. Finally methanol was applied to remove the protein A and casein layers as well and followed by PB wash until the initial baseline was achieved. The crystal was reused for the subsequent experiments.

Using this regeneration method, the coated crystals were reused up to 25 times without significant loss of protein binding activity. One important observation was that the crystal base resistance increased with each use. After 20-25 uses, the PVDF film from the crystal surface was removed with an acetone wash and re-coated with a fresh PVDF solution to regenerate the PVDF layer.

5.3.7. Analysis of whole cell NM bacteria by the immunosensor

To evaluate the designed sensor for the detection of whole cell bacteria with and without Au nanoparticles attachment, sheep anti-NM polyclonal antibody were immobilized using protein G on the sensor surface. Formalin treated *N. meningitides* cell suspension at a concentration of 300×10^6 cfu L^{-1} were prepared.

Figure 5.10. indicates a 7 Hz frequency shift upon attachment of the 100 cfu/mL cells. However with PBS wash, the frequency change was reduced to 4 Hz net change. For the same concentration of bacteria conjugated with 50 nm gold nanoparticles, significant frequency shift (17 Hz) was observed but notably this occurred in the opposite direction (Figure 5.11.). Similar response in the opposite direction was observed with large number of bacteria (3 x 10^4 cfu/ml) injected onto the sensor surface.

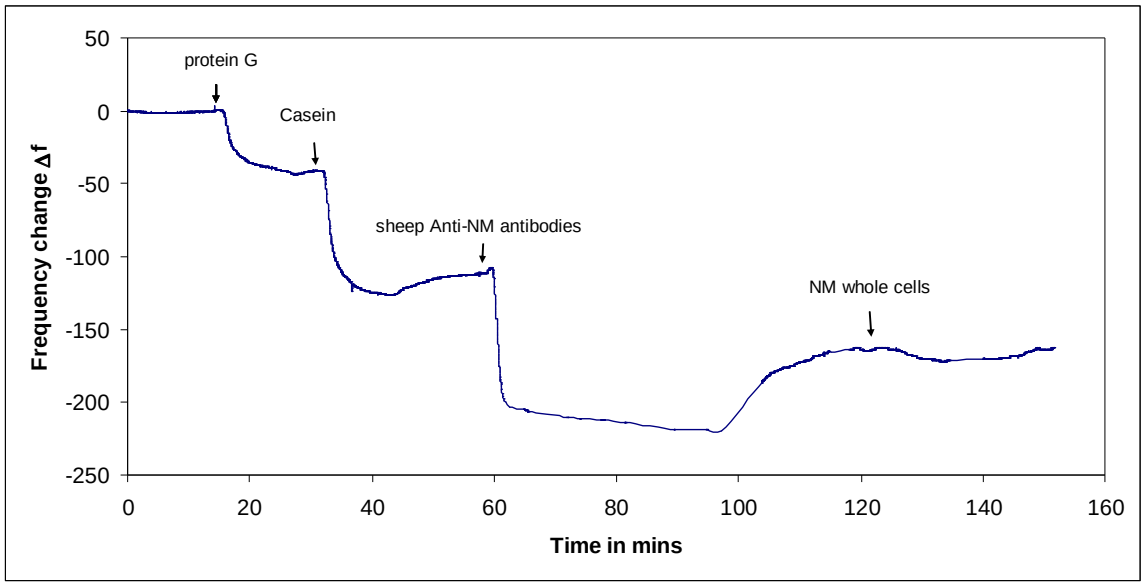

Figure 5.10. Changes in frequency following the exposure of the PVDF coated quartz crystal to *N. meningitidis* whole cells. A net frequency shift of 4 Hz was observed for 100 cfu/mL bacteria.

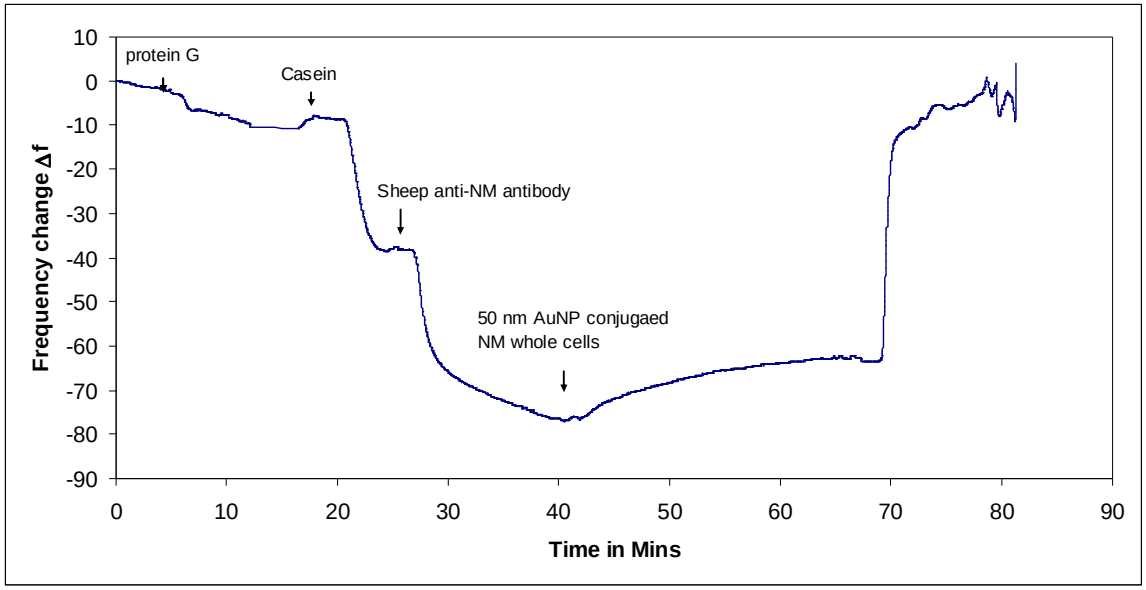

Figure 5.11. Changes in frequency following the exposure of the PVDF coated quartz crystal to *N. meningitidis* whole cells conjugated with 50 nm gold nanoparticles. A net frequency shift of 17 Hz was observed in the opposite direction for 100 cfu/mL bacteria.

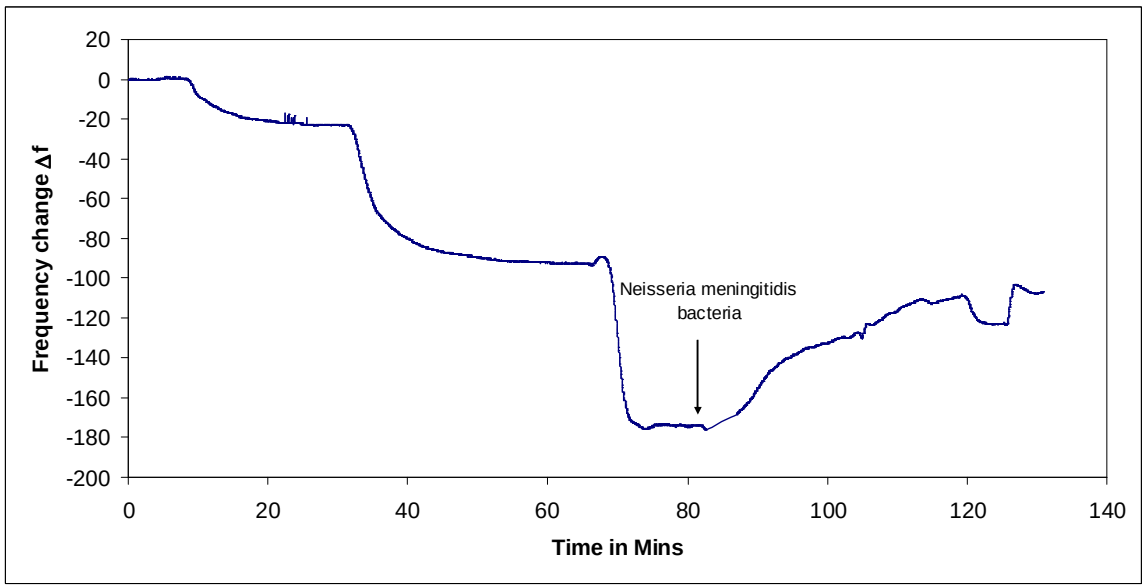

Figure 5.12. Changes in frequency following the exposure of the PVDF coated quartz crystal to *N. meningitidis* whole cells. For a total of 2 x 10^4 cfu/mL, a frequency shift was observed in the opposite direction with the response reaching the pre-antibody attachment base-line.

5.3.8. Surface characterisation of PVDF coating

5.3.8.1. Scanning Electron Microscopy (SEM) studies

SEM images clearly showed the uniform distribution of the polymer. PVDF formed a thin, porous, rough and rigid structure on the QCM surface (Figure 5.13a. and 5.13b). These pores are predicted to be hydrophobic pockets based on the structural similarity to the pores in the PVDF membrane (Figure 5.14.), which also indicates that dissolution conditions didn't alter the structural features of the PVDF membrane. A distorted structure of the film after multiple uses was observed as seen in Figure 5.15. An estimation of the film thickness was found to be less than 1 μm, as measured from the cross section of the film (Figure 5.16.).

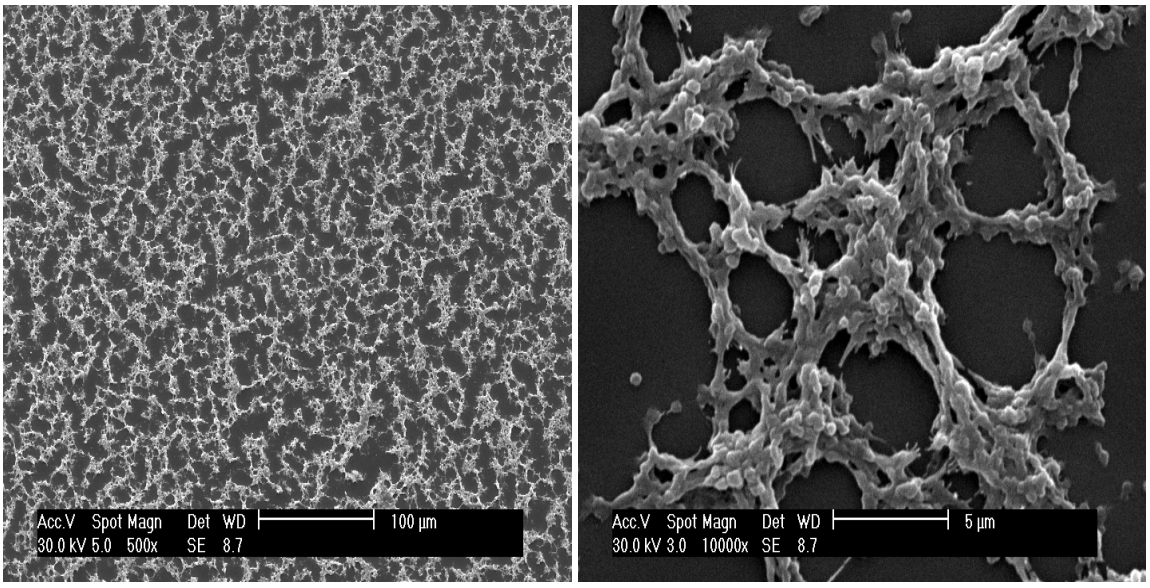

(a) (b)

Figure 5.13. PVDF film distribution on the QCM magnification at (a) 500x and (b) 10000X.

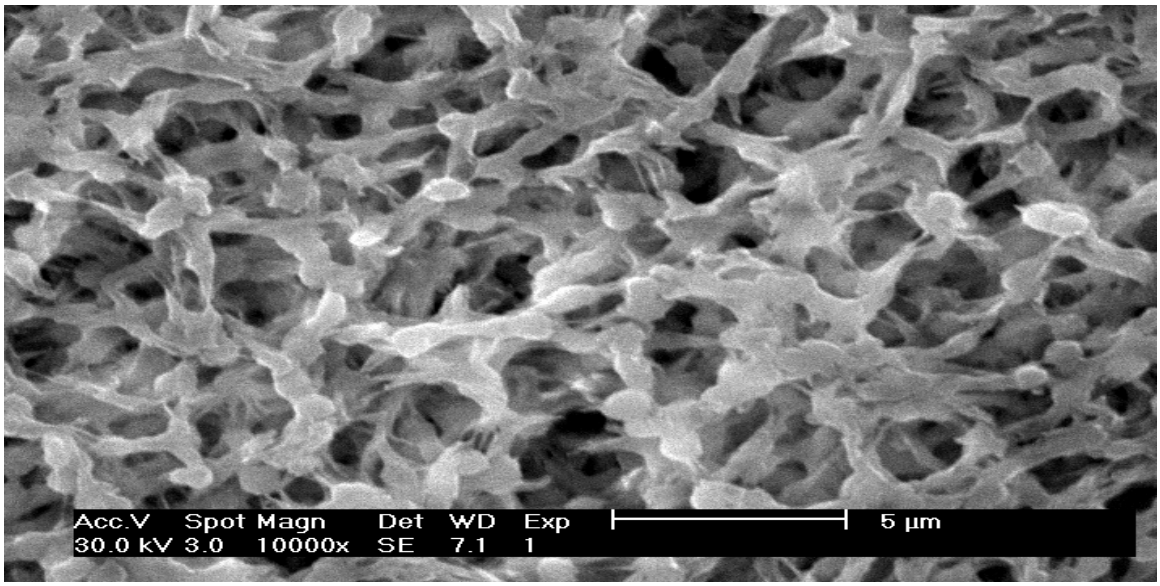

Figure 5.14. PVDF membrane structure at 10000X magnification.

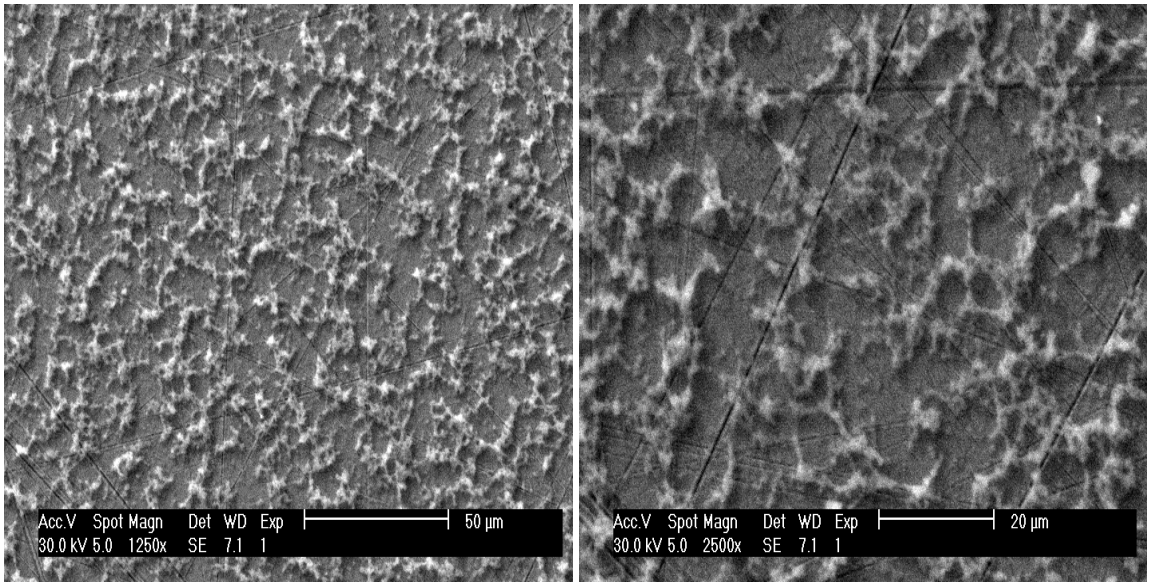

Figure 5.15. Distorted PVDF film structure after multiple runs on the same film.

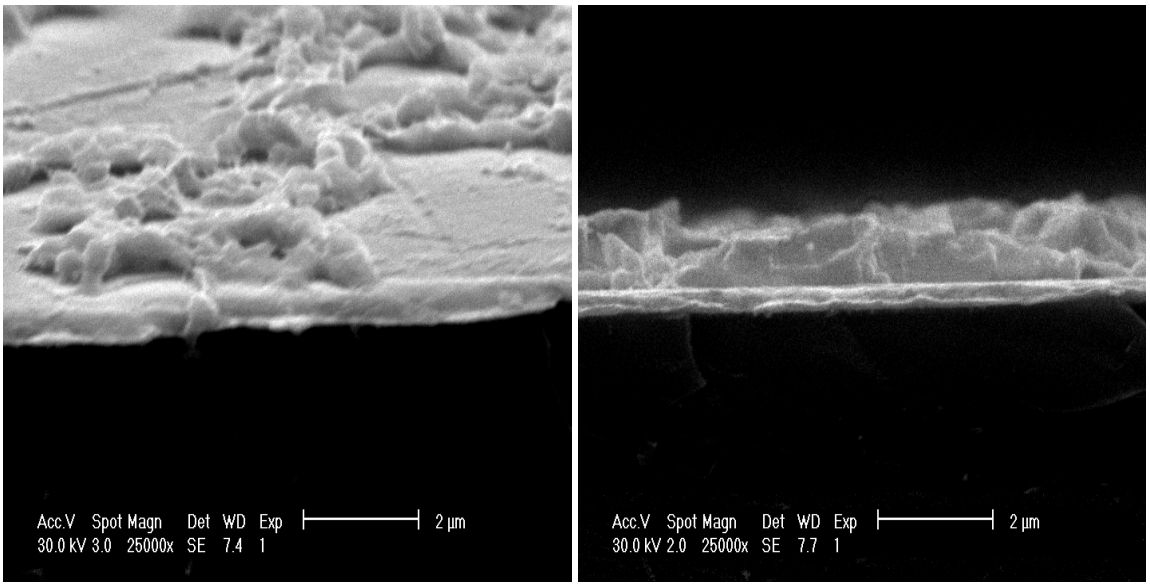

Figure 5.16. The cross sectional view of the PVDF film coated on the QCM crystal showing the thickness of the film.

5.3.8.2. Network analysis

A network analyzer was used to monitor the frequency shift and the acoustic damping of admittance at the crystal resonance frequency after film deposition (Figure 5.17 and Figure 5.18). The film quality was quantified by calculating the Q factor of the crystal, which represents the rate at which an oscillating system dissipates its energy. The higher the Q factor, the better the quality of the QCM resonator, and the lower the dissipation of oscillation energy in the resonating system.

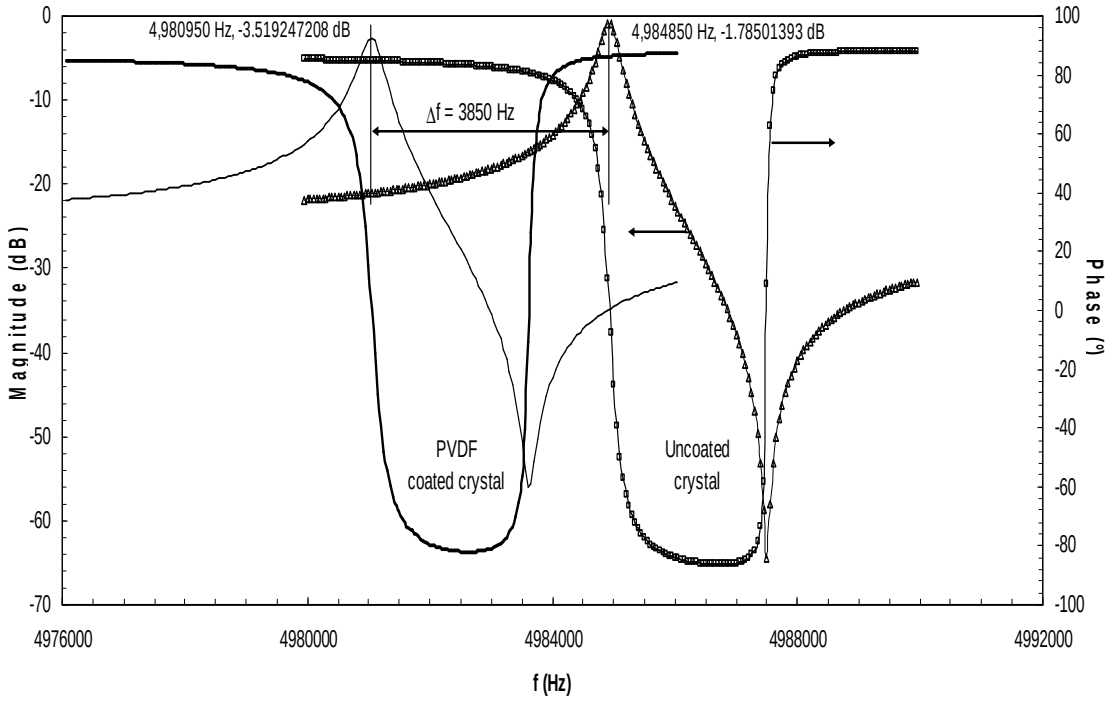

Figure 5.17. The impedance behavior of 5 MHz quartz in the presence and absence of the PVDF film coating. An alternating electric field was applied to the crystal causing an oscillary motion. As the field is switched off, the amplitude of the oscillation declines. The rate at which it declines depends on the energy dissipation.

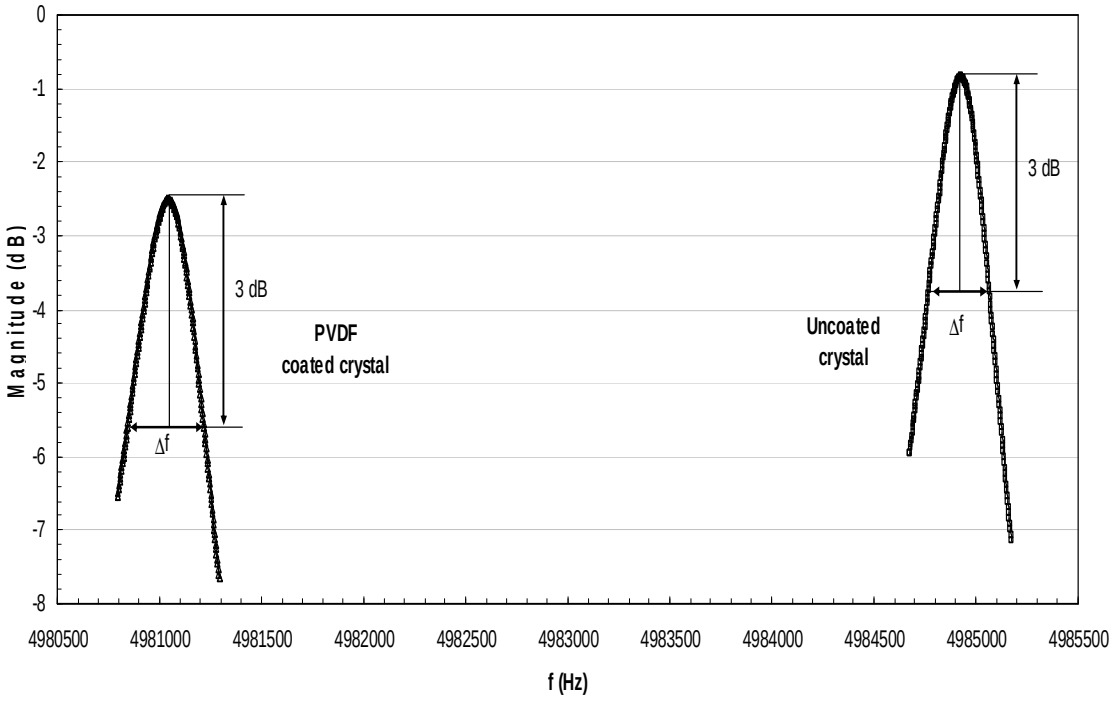

Figure 5.18. Changes in energy dissipation as a function of time obtained from the QCM measurements for the same sequence of events as displayed in Figure 5.14.

5.3.8.3. Atomic Force Microscopy studies

The surface profile of the PVDF film on the quartz crystal was also monitered by AFM. Tapping mode was used, in order to avoid the sample deformation when imaging polymeric materials such as PVDF presents. An atomic force microscopy image of the PVDF modified crystal surface is presented in Figure 5.16., which was similar to the image obtained from SEM. The polymer distribution was rough and the root mean square roughness (RMS) of the coating was found to be 247.99 nm, respectively, which can be seen in Figure 5.19. The 3D image of the roughness distribution profile can be seen in Figure 5.20. The

contrast between the AFM images of a plain gold surface area and the area covered by PVDF film allows the rough estimation of the thickness of the film to be approximately 79.68 nm (Figure 5.21.). AFM images (Figure 5.22. and Figure 5.23.) of the bacteria attached QCM sensor confirmed the presence of bacteria.

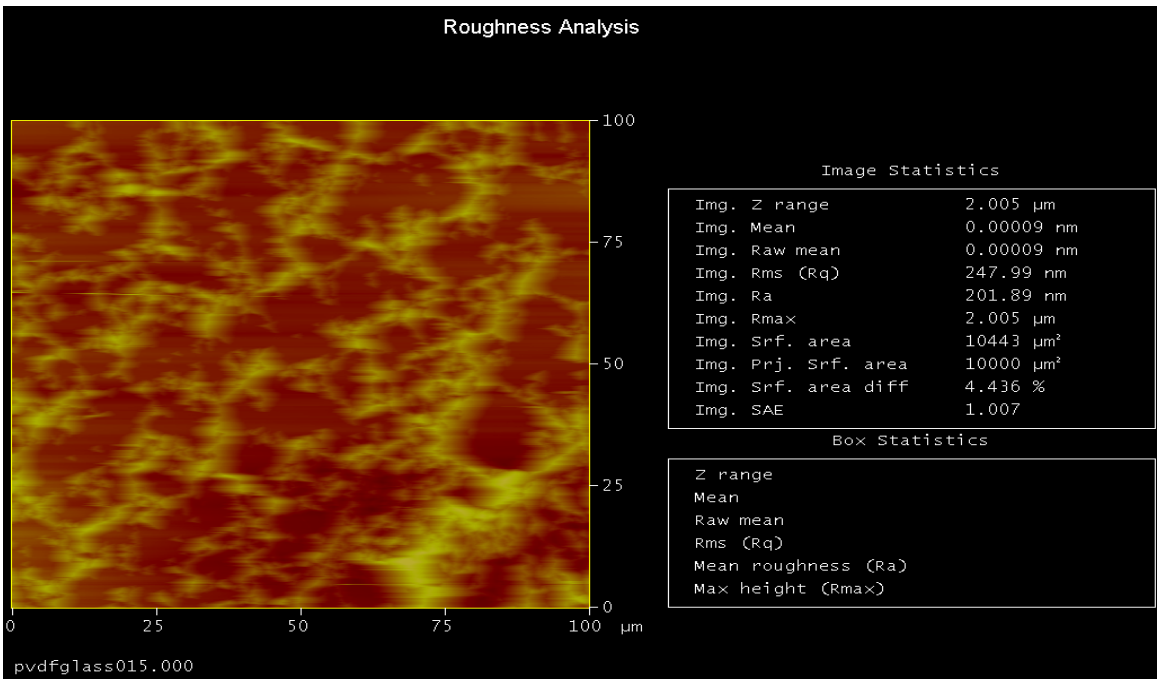

Figure 5.19. AFM image of the PVDF film coating on the QCM surface.

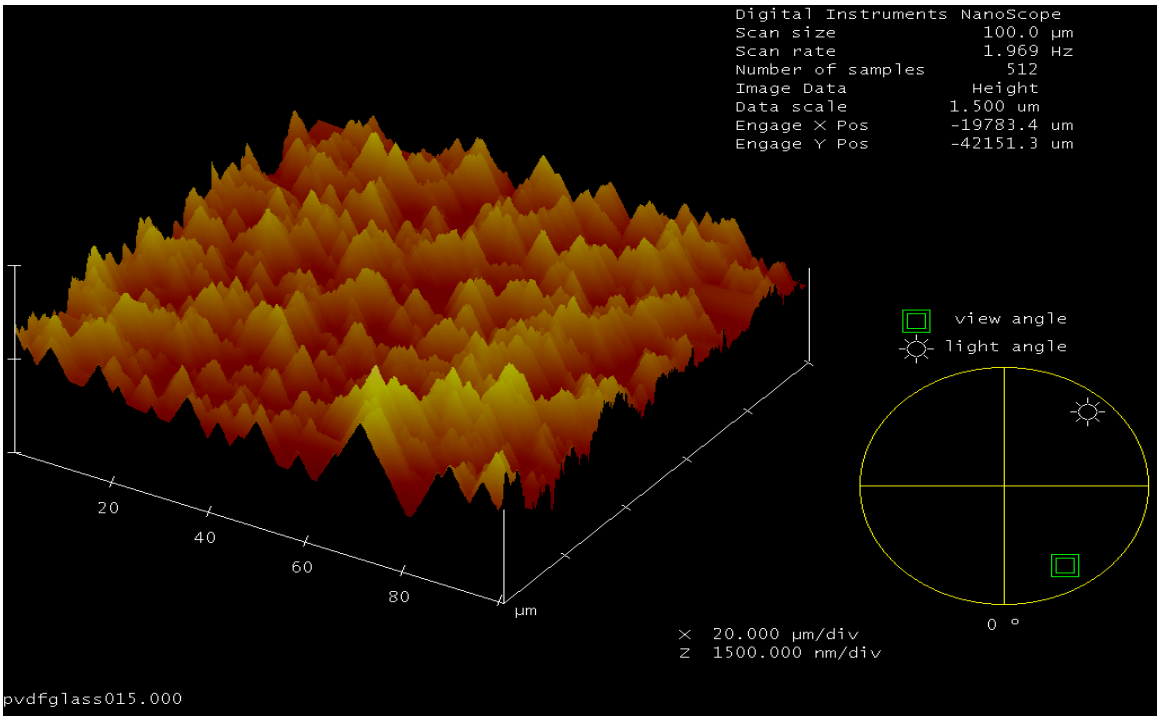

Figure 5.20. AFM image showing the roughness distribution of the PVDF film coating on the QCM surface

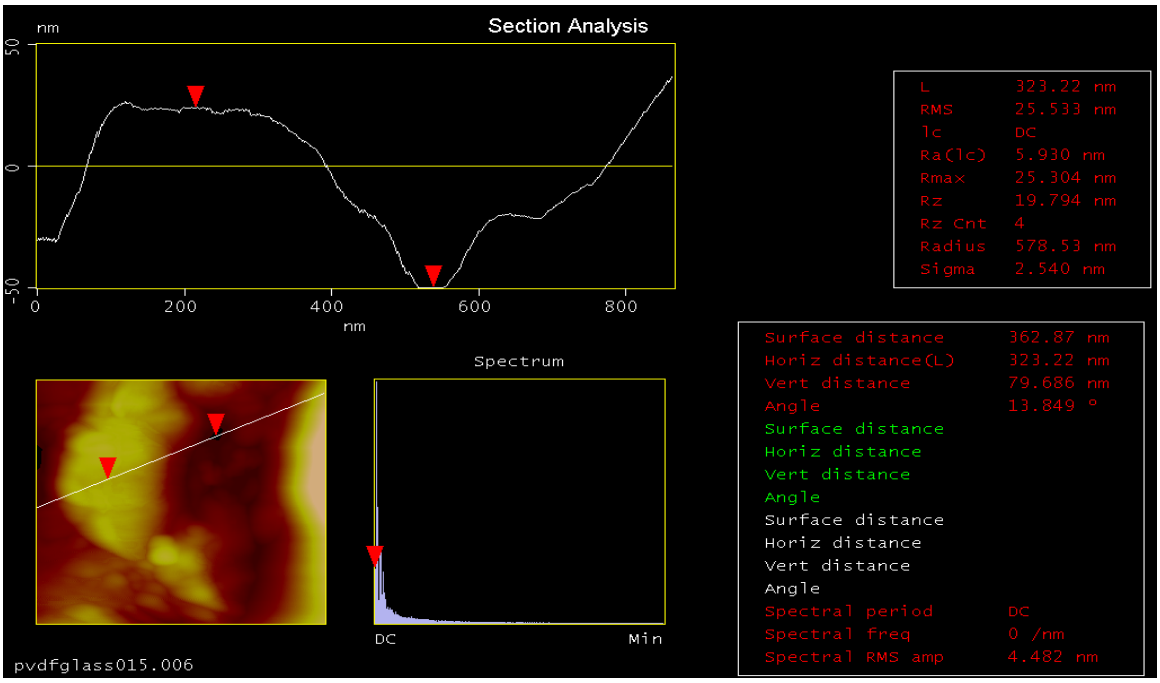

Figure 5.21. Height analysis of the PVDF film by atomic forece microscopy to determine the approximate thickness of the layer.

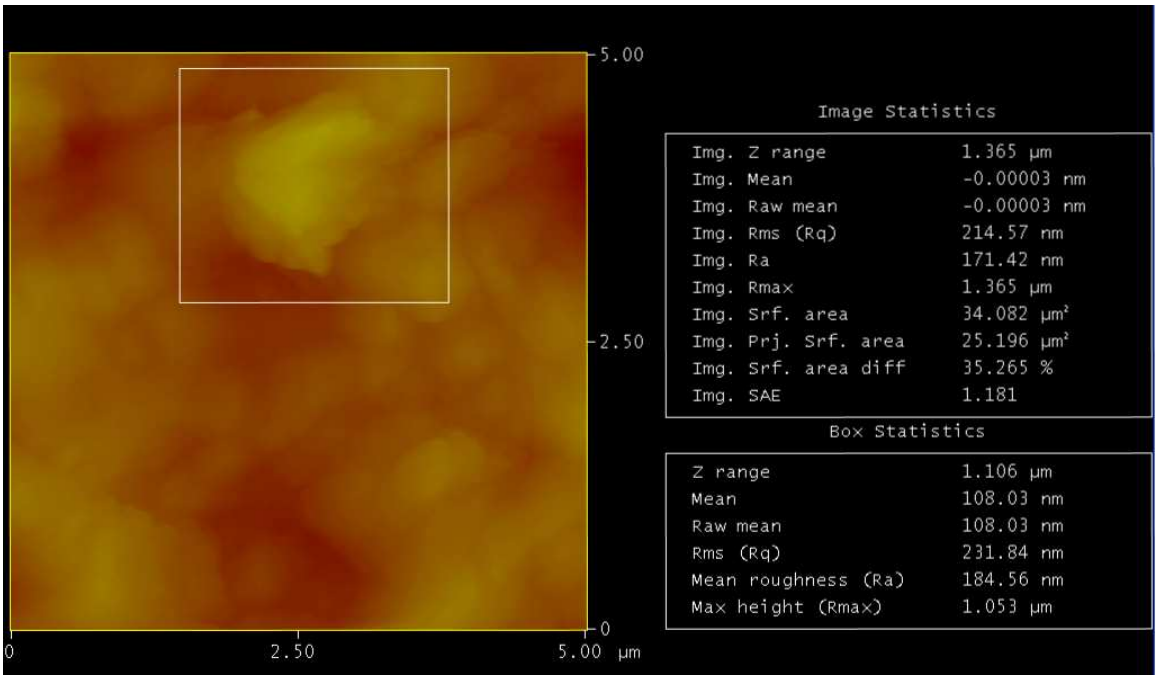

Figure 5.22. AFM image of a *N. meningitides* bacterium attached to the sensor surface through protein G and anti-NM antibody immobilization.

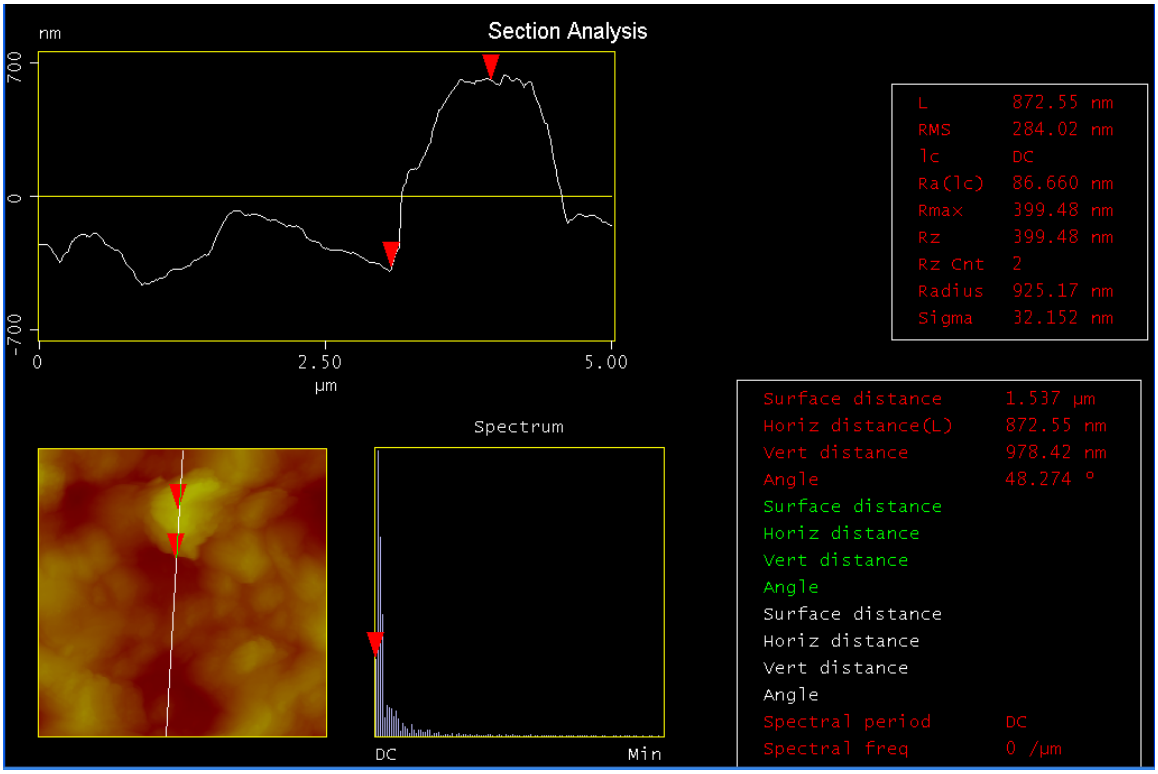

Figure 5.23. Height and section analysis of the QCM sensor surface also indicates the presence of attached bacteria (approximately 1 µm size).

5.4. Discussion

The piezoelectric crystal sensor is becoming a very powerful analytical tool because of the established relationship for the change in frequency to the analyte concentration with high sensitivity. Being a label free assay, piezoelectric immunosensing methods, offer an alternative to existing conventional methods. In this chapter, a highly selective QCM based immunosensor was designed for the rapid diagnosis of meningococcal meningitis using OMP85 and anti-OMP85 antibody as a model system.

AT cut crystals with polished surface are very popular in QCM techniques because of their excellent frequency versus temperature characteristics (low df/dt) over a wide range of temperatures and they are specially designed for operation in liquids. The mass sensitivity of a 5 MHz quartz crystal is approximately 0.057 Hz cm^2 ng^{-1}, which is approximately 100 times higher than that of an electronic fine-balance which has a sensitivity of 0.1 μg. Thus, it is ideal to choose a coating that will undergo highly selective chemical or physical binding with the analyte to be detected.

The flow-through QCM biosensors have drawn increasing attention due to their ease for automation of the process (Rickert, Brecht *et al.* 1997). After fixing the crystal in the crystal holder, capacity cancellations were done to lock the crystal frequency in the system. Proper capacitance cancellations are required to assure

true series resonance operation of the crystal oscillator, and to eliminate frequency and resistance errors.

Antibody immobilization is a vital step in successful development of a piezoelectric immunosensor. Apart from affiinity based and chemical immobilization methods, antigens or antibodies are frequently immobilized by the simple physisorption on clean gold surfaces (Sargent and Sadik 1998). The stability of those immobilized molecules does not differ significantly from the covalently coupled ones. However, problems arising from these immobilization techniques are the nondirectional orientation of the molecules on the surface and thus some of the antigen or antibody molecules are not accessible for binding. In this study, the frequency shift observed for the binding of a particular concentration of OMP85 antigen, was much less in comparision to the frequency shift observed for the same amout of antigen bound on the PVDF coated crystal with protein A bound antibody. This reflects the importance of using protein A and the directional orientation of the antibody molecues for maximum sensitivity.

PVDF (average molecular weight, $M_w = 530{,}000$) transfer membrane is a naturally hydrophobic, unsupported transfer membrane. Its exceptional tensile strength and high binding capacity make these membranes ideal for use in Western blots, immunoblotting, protein sequencing, MS analysis and solid phase

assays. PVDF membranes are also used in various detection systems which includes, radioactive, chromogenic, chemiluminescent, fluorescent, and chemifluorescent techniques. Its high binding capacity, prevents protein from passing through the membrane, and has a low background that provides an excellent signal-noise ratio. Also, PVDF film exhibits piezoelectric, pyroelectric and ferroelectric properties and which all have been utilized in sensors and actuators including modal transducers, electromechanical transducers, biomedical photoacoustic imaging arrays, infrared imaging arrays, and fingerprint sensors.

Deposition of uniform ultrathin film on a quartz crystal is a crucial point to achieve stable and reproducible results each time. Interpretation of adsorption phenomena is strongly influenced by the surface roughness of quartz resonators (Beck, Pittermann *et al.* 1992; Martin, Frye *et al.* 1993). Hence, smooth surfaces are required when operating in fluids so as to avoid frequency shifts arising from changes in surface energies (Martin, Frye *et al.* 1993). There are various methods for depositing PVDF films on a substrate such as casting, spray, sputtering, spin, self-assembling, evaporation and the Langmuir–Blodgett technique. Each method has its strengths and shortcomings. For example, with the casting method it is possible to deposit a thicker polymeric film, but there is a poor control on the amount of material deposited.

Spin coating is a simple and fast technique to prepare thin films of best uniformity in a repeatable manner. The film formation, its thickness and roughness can be controlled by varying parameters such as solution concentration, solvent properties, spinning speed, acceleration and spinning time (Emir, Zhong *et al.* 2006). In this work, PVDF film coating on QCM crystal surface was ahieved by spincoating of a PVDF solution prepared as described in section 5.2.6. The primary aim was to obtain sufficiently smooth and fully covered films of PVDF, which would work in the RQCM instrument.

After careful trials, the PVDF concentration was optimized (75 mg/mL) to achieve the same resistance (500-600 Ohms) each time. The spinning was repeated twice to yield a more compact structure following drying of the membrane. The film on the silica surface surrounding the electrode was manually peeled off so that only the film remains on the gold surface. This was done principally to reduce the mass load on the crystal and so that the crystal frequency could be locked in the system. An interesting observation was that the film was loosely bound on the silica surface, where as on the gold surface it was tightly bound and hence there was not slip against the electrode surface of the quartz crystal during oscillation. PVDF coated crystals may be stored dry for long periods of time at room temperature. Prior to use, dried membrane coated crystals must be wet by soaking in 100% methanol.

PVDF is an inherently hydrophobic polymer, so aqueous buffers cannot penetrate the pore structure. It has been generally considered that the pore structure must be made accessible by a prewetting step with methanol so that proteins can interact with the PVDF membrane. Methanol also assists in removing any complexed SDS from the protein molecules (Mozdzanowski and Speicher 1992) and thereby increases the probability that a protein molecule will bind to the membrane. Once the membrane is wetted, protein binding may be achieved by simply bringing the protein into contact with the membrane. Because binding occurs throughout the depth of the membrane, the binding capacity is determined by the internal surface area of the pores (Mansfield, 1994). Complete wetting with methanol was evident by a change in the membrane's appearance from opaque to semi-transparent.

Due to the hydrophobic character and the steric constraints of the surrounding PVDF layer, the physical adsorption of antibody molecules directly within the PVDF polymer may induce a marked loss of their recognition activity. Also, the antibody molecules buried in the porous structures may drastically reduce the accessibility to the immobilized antibody molecules. Such limitations may hinder the formation of specific antigen– antibody bonding.

Although many immobilization methods have been studied and applied to piezoelectric immunosensor developments, it is usually necessary to determine a

suitable immobilization method for each biological material in a particular application (Blonder, Ben-Dov *et al.* 1997). In clinical immunoassays, it is preferable that antibodies are immobilized with highly controlled orientation and the steric-hindrance effect must be reduced (Sokoll and Chan 1999) so as to maximize their antigen-binding efficiency and attain ultimate sensitivity and selectivity of immunoassay (Lee and Chang 2005). Protein A is a polypeptide isolated from *Staphylococcus aureus* that binds specifically to immunoglobulin molecules, especially IgG antibodies, through the Fc domain without interacting at the antigen site. Protein A layer might also be serving as an intervening "spacer" matrix to extend the immobilized antibodies away from the surface and makes them more accessible to the antigens. This property permits the formation of tertiary complexes consisting of protein A, antibody and antigen.

Protein A has been widely utilized for oriented immobilization of antibodies and constructions of piezoelectric immunosensors (Muramatsu, Dicks *et al.* 1987; Konig and Gratzel 1994; Babacan, Pivarnik *et al.* 2000). It was shown that Protein A-based piezoelectric immunosensor was more favorable than the polyethylenimine-glutaraldehyde method in detecting *S. typhimurium* due to its stability and better reproducibility of the immobilization layers (Babacan, Pivarnik *et al.* 2000). A Protein-A based SPR immunosensor has been developed for detection of *E. coli* O157:H7 (Fratamico, Strobaugh *et al.* 1998). The

immobilization of Protein A caused a highly insulating layer, and the insulation was further improved by antibody immobilization and protein binding.

Blocking any unbound or non-specific sites on the layer to maximize the signal-to-noise ratio was was necessary because of the inherent affinity of the polymeric surface for proteins. Also interstitial places between hydrophobic pores might have been filled with protein A and Casein molecules as a result of their smaller size.

After washing with phosphate buffer to remove any excess casein from the transducer surface, anti-OMP85 antibody solution was injected. Being a directional coupling between protein A and antibody molecules, this particular step took more than an hour to reach the base line. As the hydrophobic pores in the PVDF film were filled with protein A and casein molecules, antibodies should only bind to the protein A molecules. On the other hand, without protein A molecules, antibodies would have penetrated into the porous structure of the membrane and only those antibody molecules on the very top layer of the surface may actually be available for antigen binding. Antibody molecules embedded within the pore structure may not participate in the overall reaction.

After washing with PB to clear any excess antibody, OMP85 antigen conjugated with 50 nm colloidal gold nanoparticles was introduced. It is shown that, the

resonant frequency of the sensor decreased over time due to the binding of OMP85 antigen onto the immobilized antibodies, and the time to reach a plateau ranged from 5 to 15 minutes. The total mass of macromolecules deposited onto the electrode was directly proportional to the frequency change of the QCM. When the different molecules were bound onto the crystal surface, the roughness range of the crystal was decreased and thus the resistance.

It is well known that the behavior of a piezoelectric sensor in solution is much different to that in air. In solution, in addition to surface mass change due to specific or nonspecific adsorption, variation of surface viscoelasticity and solution density and viscosity can all result in a frequency change of the quartz crystal (Martin, Granstaff *et al.* 1991). Other important parameters that influence the resonant frequency of the quartz crystal in solution are the ionic strength and dielectric constant of the electrolyte. To avoid the possible error resulting from different additions of solutions or samples, the frequency changes of each step were monitored with PB wash for more than 5 minutes (after the achieving the base line for each sample) until equilibrium was reached. When it was equilibrated with the phosphate buffer, the crystal could reach a new equilibrium generally within 3 min after replacement injection, and the baseline was stable over many hours with a noise level less than ±1 Hz.

The maximum frequency increase due to washing with PB was less than 1.0 Hz, which was negligible when compared to multilayer frequency shifts when protein solutions were added. Further addition of PB after the protein layers have been resulted in no change total frequency of the crystal, indicating that specific adsorption of the protein layer has occurred.

For small biomolecule detection at low concentrations, it may be quite difficult to obtain observable and direct signals. This is mainly due to the lack of mass sensitivity of the commonly used QCM instruments, as they generally employ 5 to 10 MHz quartz crystals (Zhang, Feng *et al.* 1997). Besides their use in colorimetric assays, gold nanoparticles can be used in mass detection techniques to amplify the mass of analytes thereby increasing the sensitivity of the assay, as noted previously. The conjugation of colloidal gold nanoparticles to macromolecules can retain the activity of biomolecules and enhance the immobilized amount of biomolecules (Chu, Zhao *et al.* 2006; Tripathi, Kandimalla *et al.* 2006).

This sensitivity was sufficient to directly detect the binding event between the OMP85 alone and the specific antibody layer. Conjugated gold nanoparticles were used as signal amplification probes for high-sensitive detection of target antigen at very low concentrations. First, in contrast to the direct binding of antigen with immobilized antibody on bulk gold surfaces, OMP antigen was

bound on gold nanoparticle surfaces. Second, the high surface-to-volume ratio of the assembled gold nanoparticles may greatly enhance the immobilization density of bound proteins. The OMP85 antigen was then detected directly by the frequency change observed as it bound to the specific antibodies. The present immunoassay system exhibited the analytical performance such as sensitivity, precision, accuracy, analytical time, stability and reproducibility needed for quantification of the OMP85 antigen.

To ensure that the frequency change was due to the OMP85 and anti-OMP85 antibody interaction, neat gold nanoparticles without antigen were injected onto the PVDF coated crystal containing protein A and anti-OMP85 antibodies. No frequency change was observed and this observation led to the following conclusions: (a) the interactions between anti-OMP85 antibody and OMP85 antigen was specific as reflected by the frequency change, (b) neat nanoparticles didn't bind to the either PVDF or antibody coated QCM crystal and (c) changes due to solution viscosity were negligible as the measurable signal was constant when the nature of the solution was modified. Moreover, 90 % of the signal was obtained within 10 minutes.

Stability and regeneration of immunosensors are crucial to consider for the development of practical immunosensors. Commonly, the regeneration of immunosensors is achieved by releasing the antigen–antibody complexes

adsorbed electrostatically from the sensing surface with a strong base and high ionic strength salt (NaOH+NaCl). Janshoff *et al.* (Janshoff, Steinem *et al.* 1996) used proteases to regenerate the sensor surfaces. In this study, 0.1M glycine-HCl, pH 2.3 solution was used to release antigen–antibody complexes from the biorecognition surface to regenerate the active surface. An erratic response was observed with 0.1M glycine pH 3.0 solution and this might be due to a difference in viscosity of the solutions and changes in temporal excess flow pressure on the crystal. Final treatment with methanol not only removed the protein A and casein layers, but also wetted the membrane for the next experiment.

Evidence of restoration of the initial resonance frequencies revealed that the dissociation of the antigen–antibody complex was successfully attained. Up to 20-25 repetitive assays were achieved without significant loss of detection sensitivity, showing high reusability and stability in the successive assays. After reusing for more than 25 times, then, the sensitivity of the immunosensor declined very sharply. This was performed twice with consistent results.

Typical calibration curves of the immunosensor for 50 nm gold nanoparticle conjugated with different concentrations of OMP85 were obtained and the frequency shift was directly proportional to the antigen concentration. To clarify the amplification characteristics of the gold nanoparticle conjugation, the calibration curves of the frequency responses without nanoparticle conjugation

were also obtained for each concentration of OMP85 anigen. The calibration curve was linear over the same OMP85 concentration range. After comparing the difference in the frequency shifts between the OMP85–gold nanoparticle conjugates and the nanoparticles alone, it was found that there was five fold increase in the sensitivity with nanoparticle conjugation.

The developed immunosensor was able to detect the whole cell NM bacteria. At low numbers (100 cfu/mL) normal frequency shift with 4 Hz net response was observed. Initial 7 Hz shift was reduced to 4 Hz after PB wash, which might be due to the removel of unbound bacteria from the sensor surface. After PB wash, when bacteria were re-injected, 3 Hz frequency shift was observed, and with the subsequent PB wash, response had gone back to the initial base line. This suggests that, excess or unbound bacteria were removed from the sensor surface with PB wash.

However, with the same concentration of bacteria attached with gold nanoparticles and also with excess number of bacteria, there was a significant frequency response but notably this occurred in the opposite direction. It was observed that with a 6×10^4 cfu/mL, the frequency trace rises to the frequency which is equivalent to the initiation of the antibody attachment. This suggests that, under the shear force of the oscillating QCM crystal and the high surface to volume ratio of the bacteria, might be removing the specifically bound antibodies

from the surface as indicated by the frequency returning to the initial pre-Ab attachment state. Previous QCM studies have employed cell detachment as a detection mechanism. Dultsev *et al.*. (2001) showed that specifically adsorbed bacteriophage could be detected by breaking the interaction between proteins displayed on a phage coat and ligands on the surface of a QCM (Dultsev, Speight *et al.* 2001). Gryte *et al.*. (1993) used 5 MHz QCM crystal to monitor the attachment and detachment of anchorage-dependent mammalian cells on a surface (Gryte, Ward *et al.* 1993). In both cases the frequency rose upon detachment following immunorecognition. Future experimentation with small gold nanoparticles with lower inertial shear force and determining the optimum dilution of bacteria may produce continuous attachment and frequency changes in the same direction as the initial case.

As a control experiment, protein A was used instead of protein G for binding with sheep IgG. This resulted in no binding of sheep IgG to the protein A layer and subsequently, NM cells were shown not to bind to this protein A layer. Indirectly, it shows that, bacteria do not adhere to the surface non-specifically under flow conditions. Perhaps, a more valid alternative control experiment would be to test the immunosensor with binding of NM cells to a control antibody (IgG) of the same species.

The QCM resonator system can be considered as an electric or electromechanical system. The Q factor of the QCM as an electric resonating system represents the resistance of the system, but as an electromechanical resonator, the Q factor represents the level of mechanical friction that causes the decay of the oscillation energy. An increase of the QCM surface roughness causes a higher frequency shift and a higher mechanical friction and thus damping of the oscillation energy. There are three factors that must be optimized in order to produce a polymer coated QCM with a high Q factor, suitable for use in the PLL oscillator system in a liquid medium. They are: (i) the mass load, (ii) the film uniformity (mass distribution and uniform morphology), and (iii) the surface roughness.

In order to measure the dissipation factor of the crystal due to PVDF coating, an impedance analysis was performed in the range of the resonance frequencies of the quartz. The observed significant dissipation changes suggest that the PVDF layer adsorbed on the Au electrode forms a compact structure, being elongated outward from the sensing surface. Network analysis revealed that the motional resistance R, which is indicative of energy loss, changes in the same fashion as the serial resonance frequency (Figure 5.17 and Figure 5.18). A lower mass load, and uniform film thickness, improved the coating quality and caused less damping of the QCM oscillation energy, whilst maintaining a sufficiently high Q factor of the resonating crystal.

To study surface morphology of thin films on a micro-scale, the films were characterized by atomic force microscope (AFM). The results showed that the polymer distribution was uniform and the roughness may be attributed to the porous nature of the polymer. To reduce the surface roughness of the coating, an extra layer for PVDF may be applied to the QCM. But, if the porous stuructures in the film become too deep, the protein A and anti-OMP85 antibody layers may be buried, which will result in a decrease of the sensitivity. Similar results were obtained from different scanning regions, which indicated the uniform distribution of the polymer film. AFM studies on the sensor surface utilized for the detection of bacteria, revealed that the bacteria was attached to the antibody (Figure 2.22. and Figure 2.23.).

The PVDF film coating on the QCM was analyzed by SEM to study the morphology and thickness of the coating. Though the actual PVDF membrane used to make the film had a thickness of 140-250 μm, on the QCM it formed a thin layer that may be due to its self-limiting growth. The pore size formed in the film was comparable to the pore size in the actual membrane. After using the same crystal multiple times, the sensitivity of the crystal was drastically reduced which was evident by the SEM pictures which shows the distorted structure (Figure 5.12.).

This work advances the design and evaluation of a QCM based model biosensor for the rapid diagnosis of meningococcal meningitidis. In this study using the real-time QCM measurements, a novel strategy has been developed for the high-sensitivity detection of target biomolecules with very low concentrations on a quartz crystal microbalance (QCM) device using gold nanoparticles as signal amplification probes. The protein A/protein G affinity-based approach preserved the access of the antigen to the oriented immobilized antobody and facilitated macromolecular interactions. Without protein A/ptotein G based immobilization, owing to the severe steric hindrance of three-dimensional network of the polymer, the antibodies may not have been so accessible to the antigen.

The QCM method used in this work is operationally attractive because of its simplicity and suitability for in situ measurement. The results show the specificity of the QCM immunosensor and the determination of OMP85 antigen and the whole cell bacteria based on gold nanoparticle conjugation is practically free of interference from nonspecific binding events. This has shown that the use of PVDF modified QCM crystals can successfully and reproducibly be employed in the detection of protein antigens as well as whole cell bacteria.

Direct measurements are attractive when compared with classical colorimetric tests, such as ELISA, where several steps are necessary to obtain an optimal

signal, which are, of course, time consuming. QCM detection of the analyte can occur online and is label-free within minutes to specifically detect any macromolecule. However, the obtained sensitivity of piezoimmunosensors is lower than that of an ELISA assay. The sensitivity of the flow-through immunosensor could possibly be further improved by decreasing flow rate and/or increasing sample running time although reducing analytical speed. The sensitivity of the QCM immunosensor, however, might be improved by using 10 MHz or higher frequency crystals (Uttenthaler, Schraml *et al.* 2001), at the same time, noise levels should be reduced.

The results presented in this chapter suggest that the use of gold nanoparticle protein conjugates in this immunosensor allow for the determination of OMP85 antigen down to 300 ng/mL and the bacteria to 100 cfu/mL. Previous studies on QCM immunosensor have reported similar findings. Piezoelectric immunoassays for the detection of human serum albumin, have been reported with the sensitivity in the clinically relevant range, 20-200 µg/mL (Sakti, Lucklum *et al.* 2001). Using the SAM based method on 10 MHz crystal, Tsai *et al.*, (2005) reported about the development of an immunosensor for the detection of α-fetoprotein, with an observable 10 Hz frequency shift for 500 ng/mL protein concentrations (Tsai and Lin 2005). With a 27 MHz quartz crystal, Bizet *et al.* had reported a frequency shift of 150 Hz for 5 µg/mL antibody concentration (Bizet, Gabrielli *et al.* 1999). Where as, with 5 MHz QCM crystal using gold

nanoparticles as signal amplification probes, Kim *et al.* had achieved 3.3 Hz frequency shift for a 50 ng/mL biotin concentration (Kim, Baek *et al.* 2007). Amplification of the 10 MHz QCM response by back-filling immobilization of nanogold on biorecognition surface was reported with a detection range of 3.0-50 ng/mL protein concentration.

All the previously published reports claims to have detected the bacteria in the concentration range of 10^5–10^7 CFU/mL (Muramatsu, Kajiwara *et al.* 1986; Suleiman and Guilbault 1994; Sato, Endo *et al.* 1995; Bao, Deng *et al.* 1996; Ben-Dov, Willner *et al.* 1997; Sato, Serizawa *et al.* 1998; Hengerer, Decker *et al.* 1999; Ivnitski, Abdel-Hamid *et al.* 1999; Dmitri Ivnitski 2000). However, a tremendous improvement in terms of sensitivity has been achieved with this designed immunosensor where, a significant QCM response was observed with bacterial concentration as low as 100 cfu/mL. Furthermore, direct measurements without time-consuming sample preparation are possible in complex matrices such as body fluids. The sensor configuration meets the sensitivity, selectivity, and response time requirements of such a platform technology. This QCM methodology provides a valuable contribution to both qualitatively and quantitatively identify the meningococcal antigen and to demonstrate the potential power of QCM technique both as a research and a diagnostic tool.

Chapter 6

Summary and Conclusion

The traditional techniques used for the diagnosis of meningococcal meningitis are slow, expensive, need skilled operators, and require additional steps of sample pre-treatment that will increase the time and cost of these tests. Thus, there is a clear need for rapid, accurate and affordable detection techniques for meningococcal meningitis to ensure prompt treatment.

The primary aim of this project was to develop a model immunodiagnostic assay for the rapid, specific and sensitive detection of meningitis, using a highly conserved OMP85 antigen and its cognate receptor, anti-OMP85 antibody as model system. Two individual approaches were tested in this regard, both utilising gold nanoparticle-protein conjugates, but with different applicability. Conjugation of the proteins to gold nanoparticles resulted in increased stability of the nanoparticles, but also retained the native protein structure as reflected by maintenance of the specific recognition capabilities of the colloid-bound antigen and antibodies.

6.1. Surface Plasmon Resonance based colour shift assay

The surface plasmon resonance based colour shift experiment due to coupling of gold nanoparticles mediated by the specific interaction of OMP85 and anti-

OMP85 antibody molecules, demonstrated that the nanoparticles can be potentially used as molecular labels for detection of *N. meningitidis* infection. The relationship between the size of nanoparticles, the size of the proteins and the occurrence of the surface plasmon resonance based colour shift was established in this study. Also, the importance of the presence of electrolytes for the coupling process was identified. The coupling behaviour of gold nanoparticles was investigated by UV-visible absorption spectrophotometry and TEM analysis. However, for reasons that are not clear, this colour shift assay method was not reproducible. The major problem observed was, at times the particles were either too stable or else they tended to aggregate in the presence of the same electrolyte concentration. Once these problems are overcome, this method has many desirable features including rapid detection, a colorimetric response, good selectivity and little or no required instrumentation. The results obtained from these studies take our understanding of nanoparticle-based diagnostics one step further towards developing detection methods that may eventually be used as point of care diagnostic tests.

6.2. Quartz Crystal Microbalance as an immunosensor

Due to the problems associated with the reproducibility of the colour shift assay, QCM was chosen as an alternative approach towards developing a working model assay for the rapid diagnosis of meningococcal infection. The development of the QCM based immunosensor included the highly successful

novel immobilisation composite architecture which consisted of PVDF film coating on the QCM crystal surface and the directional orientation of antibodies using protein A molecules. This allowed the fabrication of a QCM immunosensor with control over selectivity, sensitivity and functionality with gold nanoparticles as signal amplification probes to improve the detection limit that may equal or surpass those achieved by more widely accepted optical techniques. Additional features of this technique include a rapid response time, a requirement for only a single analyte-specific antibody, less interference from non-analyte components, and kinetic data is obtained with high resolution and real time monitoring of all events. These results in this study offer a real alternative approach for the clinical diagnosis of meningococcal infection without the need for sample preparation.

6.3. Future directions of the surface plasmon resonance based colour shift assay

There are currently no known commercial diagnostic tests for pathogens available that are based on this concept of coupled gold nanoparticles-induced colour shift. The major problem with the technique is reproducibility which may be addressed by fine tuning of the conjugation process to determine optimum concentration of the protein required which stabilise the gold nanoparticles with sufficient space available between the particles for the resulting SPR induced colour shift.

As a future development, new probes can be engineered so that the gold nanoparticle label can be positioned away from the binding site so it does not interfere with binding. For example, specific peptides instead of whole antigens and Fab' fragments instead of whole antibody, labelled to gold nanoparticles may have several advantages over whole protein labelling. These advantages include the requirement of smaller nanoparticles over large ones, great control over the conjugation process and the smaller protein molecules more likely to be in their native conformation. Once established, this technique may be expanded for development of sensitive and rapid medical diagnostic assays for a range of pathogens.

6.4. Future Direction of the QCM-based immunosensor

The use of coated piezoelectric devices as immunochemical sensors for the detection of meningococcal infection is very promising and should be considered as a viable alternative to other immunodetection methods. In future work based on this study, other types of nanoparticles and of various sizes may be studied as signal enhancement probes for high sensitivity detection. To improve the stability of the device, all electronic oscillator components could be thermostatically controlled and better shielded from external environmental influnces. In order to further increase the sensitivity for minor component analysis, crystals with operational frequency of greater than or equal to 10 MHz with higher mass sensitivity and optimised noise levels may be used.

Polymers used as sensor coatings enable a variety of modifications of composition and functionality, enabling optimum adaptation of the sensitive surface to the analyte. Besides their selectivity and low cost, QCM immunosensors can be easily automated and developed as simple portable devices, which would allow a rapid detection of meningococcal infection at the point of care setting. This raises an exciting possibility of using quartz crystal arrays for high throughput screening of a range of different from a clinical sample at one time.

Instead of CSF, serum samples may be analysed for detection of anti-OMP85 and anti-capsular antibodies. The detection of the antigen in blood could constitute a more convenient method of screening high-risk populations. Monoclonal antibodies against the SR1 peptide may be used as target receptors with high specificity for *N. meningitidis* serogroup B bacteria. Based on the insights achieved through these studies, and following further characterisation studies, SR1 could be used as a versatile molecular marker and open new avenues in the diagnostic as well as therapeutic management of meningitis.

Thus, the results of this study demonstrate that it is feasible to detect meningococcal meningitis rapidy with a great control over sensitivity and selectivity. Moreover, there is scope for the development of a hybrid technique

with enhanced sensitivity for example, by combining the quartz-crystal microbalance with other detection techniques. It envisaged that once optimised, these techniques would serve as prototypes for more generic tests for the rapid diagnosis of a range of bacterial and viral pathogens. However, this step from research to product development and commercial availability remains a significant one.

References

Aiyer, H. N., V. Vijayakrishnan, et al. (1994). "Investigations of Pd clusters by the combined use of HREM, STM, high-energy spectroscopies and tunneling conductance measurements." Surface Science **313**(3): 392-398.

Aizawa, H., S. Kurosawa, et al. (2003). "Conventional detection method of fibrinogen and fibrin degradation products using latex piezoelectric immunoassay." Biosensors and Bioelectronics **18**: 765-771.

Ala'Aldeen, D. A. A., K. R. Neal, et al. (2000). "Dynamics of Meningococcal Long-Term Carriage among University Students and Their Implications for Mass Vaccination." J. Clin. Microbiol. **38**(6): 2311-2316.

Alivisatos, A. P., K. P. Johnsson, et al. (1996). "Organization of 'nanocrystal molecules' using DNA." Nature **382**(6592): 609-611.

Amano, Y. and Q. Cheng (2005). "Detection of influenza virus: traditional approaches and development of biosensors." Analytical and Bioanalytical Chemistry **381**(1): 156-164.

Angenendt, P., J. Glokler, et al. (2003). "Next generation of protein microarray support materials:: Evaluation for protein and antibody microarray applications." Journal of Chromatography A **1009**(1-2): 97-104.

Arend, S. M., A. P. Lavrijsen, et al. (2006). "Prospective controlled study of the diagnostic value of skin biopsy in patients with presumed meningococcal disease." Eur J Clin Microbiol Infect Dis **25**(10): 643-9.

Atherton, M. Gait, et al. (1979). "Polyamide method of solid-phase peptide and oligonucleotide synthesis " BioOrganic Chemistry **8**(3): 351-370.

Augustine, J. (2005). ""Mom, I think I'm really sick"." Emerg Med Serv **34**(10): 34, 37.

Babacan, S., P. Pivarnik, et al. (2000). "Evaluation of antibody immobilization methods for piezoelectric biosensor application." Biosensors and Bioelectronics **15**(11-12): 615-621.

Bachtold, A., P. Hadley, et al. (2001). "Logic circuits with carbon nanotube transistors." Science **294**(5545): 1317-20.

Balasubramanian, R., B. Kim, et al. (2002). "Dispersion and Stability Studies of Resorcinarene-Encapsulated Gold Nanoparticles." Langmuir **18**(9): 3676-3681.

Band, J. D., M. E. Chamberland, et al. (1983). "Trends in meningococcal disease in the United States, 1975-1980." J Infect Dis **148**(4): 754-8.

Bandey, H. L., S. J. Martin, et al. (1999). "Modeling the Responses of Thickness-Shear Mode Resonators under Various Loading Conditions." Anal. Chem. **71**(11): 2205-2214.

Bao, H., Z. Peng, et al. (2005). "Size-dependent aggregates of gold nanoparticles induced by a "molecular fork"." New Journal of Chemistry **29**: 1004-1006.

Bao, L., L. Deng, et al. (1996). "Determination of microorganisms with a quartz crystal microbalance sensor." Analytica Chimica Acta **319**(1-2): 97-101.

Beck, R., U. Pittermann, et al. (1992). "Influence of the Surface Microstructure on the Coupling Between a Quartz Oscillator and a Liquid." Journal of The Electrochemical Society **139**(2): 453-461.

Beek, D. v. d., J. d. Gans, et al. (2004). "Clinical features and prognostic factors in adults with bacterial meningitis." N Engl J Med **351**(18): 1849-59.

Beesley, J. (1989). "Colloidal Gold. A new perspective for cytochemical marking", Oxford Science Publications. Oxford University Press.

Ben-Dov, I., I. Willner, et al. (1997). "Piezoelectric Immunosensors for Urine Specimens of Chlamydia trachomatis Employing Quartz Crystal Microbalance Microgravimetric Analyses." Anal. Chem. **69**(17): 3506-3512.

Bentley, A., A. Atkinson, et al. (2001). "Whole cell biosensors -- electrochemical and optical approaches to ecotoxicity testing." Toxicology in Vitro **15**(4-5): 469-475.

Beuvery, E. C., F. van Rossum, et al. (1982). "Comparison of the induction of immunoglobulin M and G antibodies in mice with purified pneumococcal type 3 and meningococcal group C polysaccharides and their protein conjugates." Infect. Immun. **37**(1): 15-22.

Bharathi, S., N. Fishelson, et al. (1999). "Direct Synthesis and Characterization of Gold and Other Noble Metal Nanodispersions in Sol-Gel-Derived Organically Modified Silicates." Langmuir **15**(6): 1929-1937.

Bianco, A., K. Kostarelos, et al. (2005). "Applications of carbon nanotubes in drug delivery." Curr Opin Chem Biol **9**(6): 674-9.

Bicanic, T. and T. S. Harrison (2004). "Cryptococcal meningitis." Br Med Bull **72**: 99-118.

Bizet, K., C. Gabrielli, et al. (1999). "Biosensors based on piezoelectric transducers." ANALUSIS **27**: 609-619.

Bizet, K., C. Gabrielli, et al. (1995). "La microbalance a quartz electrochimique: perspectives d'application en biologie medicale." Immuno-analyse & Biologie Specialisee **10**(4): 205-211.

Blake, P. A., R. E. Weaver, et al. (1980). "Diseases of Humans (Other than Cholera) Caused by Vibrios." Annual Review of Microbiology **34**(1): 341-367.

Blatchford, C. G., J. R. Campbell, et al. (1982). "Plasma resonance -- enhanced raman scattering by absorbates on gold colloids: The effects of aggregation." Surface Science **120**(2): 435-455.

Blonder, R., I. Ben-Dov, et al. (1997). "Photochemically-activated electrodes: application in design of reversible immunosensors and antibody patterned interfaces." Biosensors and Bioelectronics **12**(7): 627-644.

Bogdan, D. (2005). The Quartz Crystal Microbalance (QCM) as a Biosensor. New York, Clarkson University**:** 13.

Bovin, J. O. and J. O. Malm (1991). "Atomic resolution electron microscopy of small metal clusters." Zeitschrift für Physik D Atoms, Molecules and Clusters **19**(1): 293-298.

Bradford, M. M. (1976). "A rapid and sensitive method for the quantitation of microgram quantities of protein utilizing the principle of protein-dye binding." Anal Biochem **72**: 248-54.

Bradley, J., G. Schmid, et al. (2005). Syntheses and Characterizations: 3.2 Synthesis of Metal Nanoparticles. Nanoparticles. S. Prof. Dr. Günter**:** 185-238.

Bradley, J. S. (1994). The Chemistry of Transition Metal colloids. Clusters and Colloids: From Theory to Applications. G. Schmid. New York, VCH: Weinheim**:** 459-544.

Braun, R., M. Sarikaya, et al. (2002). "Genetically engineered gold-binding polypeptides: structure prediction and molecular dynamics." J Biomater Sci Polym Ed **13**(7): 747-57.

Bredemeier, R., T. Schlegel, et al. (2006). "Functional and phylogenetic properties of the pore forming beta -barrel transporters of the Omp85 family." J Biol Chem.

Broderick, J. B., M. J. Natan, et al. (1993). "Evidence for retention of biological activity of a non-heme iron enzyme adsorbed on a silver colloid: a surface-enhanced resonance Raman scattering study." Biochemistry **32**(50): 13771-6.

Bronska, E., J. Kalmusova, et al. (2006). "Dynamics of PCR-based diagnosis in patients with invasive meningococcal disease." Clin Microbiol Infect **12**(2): 137-41.

Bronstein, L., D. Chernyshov, et al. (1999). "Laser Photolysis Formation of Gold Colloids in Block Copolymer Micelles." Langmuir **15**(1): 83-91.

Brown, D. H. and W. E. Smith (1980). "The Chemistry of the Gold Drugs Used in the Treatment of Rheumatoid Arthritis." Chemical Society Reviews **9**: 217-240.

Brown, K. R., D. G. Walter, et al. (2000). "Seeding of Colloidal Au Nanoparticle Solutions. 2. Improved Control of Particle Size and Shape." Chem. Mater. **12**(2): 306-313.

Brust, M., J. Fink, et al. (1995). "Synthesis and reactions of functionalised gold nanoparticles." Journal of the Chemical Society, Chemical Communications 1655 - 1656.

Brust, M., J. Fink, et al. (1995). "Synthesis and reactions of functionalised gold nanoparticles." Journal of Chemical Society, Chemical Communication(16): 1655 - 1656.

Brust, M., M. Walker, et al. (1994). "Synthesis of thiol-derivatised gold nanoparticles in a two-phase Liquid–Liquid system." Journal of the Chemical Society, Chemical Communications 801 - 802.

Brust, M., M. Walker, et al. (1994). "Synthesis of thiol-derivatised gold nanoparticles in a two-phase Liquid–Liquid system." Journal of Chemical Society, Chemical Communication(7): 801 - 802.

Burda, C., X. Chen, et al. (2005). "Chemistry and Properties of Nanocrystals of Different Shapes." Chem. Rev. **105**(4): 1025-1102.

Buttry, D. A. and M. D. Ward (1992). "Measurement of interfacial processes at electrode surfaces with the electrochemical quartz crystal microbalance." Chem. Rev. **92**(6): 1355-1379.

Byung-Keun, O., K. Young-Kee, et al. (2003). "Immunosensor for detection of Legionella pneumophila using surface plasmon resonance." Biosensors and Bioelectronics **18**(5-6): 605-611.

Carrot, G., J. C. Valmalette, et al. (1998). "Gold nanoparticle synthesis in graft copolymer micelles." Colloid & Polymer Science **276**(10): 853-859.

Caruso, F., E. Rodda, et al. (1997). "Quartz Crystal Microbalance Study of DNA Immobilization and Hybridization for Nucleic Acid Sensor Development " Analytical Chemistry, **69**(11): 2043 -2049.

Castaneda, M. T., A. Merkoci, et al. (2007). "Electrochemical genosensors for biomedical applications based on gold nanoparticles." Biosens Bioelectron **22**(9-10): 1961-7.

Casterman, C. H., T. Atarhouch, et al. (1993). "Naturally occurring antibodies devoid of light chains." Nature **363**: 446 - 448.

Castillo, J., S. Gaspar, et al. (2004). "Biosensors for life quality: Design, development and applications." Sensors and Actuators B: Chemical **102**(2): 179-194.
Caugant, D. A. (1998). "Population genetics and molecular epidemiology of Neisseria meningitidis." Apmis **106**(5): 505-25.
Caugant, D. A., B. E. Kristiansen, et al. (1988). "Clonal diversity of Neisseria meningitidis from a population of asymptomatic carriers." Infect. Immun. **56**(8): 2060-2068.
CDCP. (1998). "Laboratory Methods for the Diagnosis of Meningitis Caused by Neisseria meningitidis, Streptococcus pneumonia e and Haemophilus influenzae." Retrieved 03 March 2006, 1998, from http://www.cdc.gov/ncidod/DBMD/diseaseinfo/files/menigitis_manual.pdf.
Chadwick, D. R. (2005). "Viral meningitis." Br Med Bull **75-76**: 1-14.
Chah, S., M. R. Hammond, et al. (2005). "Gold Nanoparticles as a Colorimetric Sensor for Protein Conformational Changes." Chemistry & Biology **12**(3): 323-328.
Chan, W. C. W. and S. Nie (1998). "Quantum Dot Bioconjugates for Ultrasensitive Nonisotopic Detection." Science **281**(5385): 2016-2018.
Chanteau, S., S. Dartevelle, et al. (2006). "New Rapid Diagnostic Tests for Neisseria meningitidis Serogroups A, W135, C, and Y." PLoS Medicine **3**(9): e337.
Chechik, V. and R. M. Crooks (1999). "Monolayers of Thiol-Terminated Dendrimers on the Surface of Planar and Colloidal Gold." Langmuir **15**(19): 6364-6369.
Chen, F., G.-Q. Xu, et al. (2003). "Preparation and assembly of colloidal gold nanoparticles in CTAB-stabilized reverse microemulsion." Materials Letters **57**(21): 3282-3286.
Choi, S.-H., S.-H. Lee, et al. (2003). "Interaction between the surface of the silver nanoparticles prepared by [gamma]-irradiation and organic molecules containing thiol group." Radiation Physics and Chemistry **67**(3-4): 517-521.
Chou, S.-F., W.-L. Hsu, et al. (2002). "Determination of {alpha}-Fetoprotein in Human Serum by a Quartz Crystal Microbalance-based Immunosensor." Clin Chem **48**(6): 913-918.
Chou, S. F., W. L. Hsu, et al. (2002). "Development of an immunosensor for human ferritin, a nonspecific tumor marker, based on a quartz crystal microbalance." Analytica Chimica Acta **453**: 181-189.
Chow, M. K. and C. F. Zukoski (1994). "Gold Sol Formation Mechanisms: Role of Colloidal Stability." Journal of Colloid and Interface Science **165**(1): 97-109.
Chu, X., Z. L. Zhao, et al. (2006). "Quartz crystal microbalance immunoassay with dendritic amplification using colloidal gold immunocomplex." Sensors and Actuators B. **114**(2): 696-704.
Connolly, M. and N. Noah (1999). "Is group C meningococcal disease increasing in Europe? A report of surveillance of meningococcal infection in Europe 1993-6. European Meningitis Surveillance Group." Epidemiol Infect **122**(1): 41-9.
Connolly, S. and D. Fitzmaurice (1999). "Programmed Assembly of Gold Nanocrystals in Aqueous Solution." Advanced Materials **11**(14): 1202-1205.
Cooper, M. A., F. N. Dultsev, et al. (2001). "Direct and sensitive detection of a human virus by rupture event scanning." Nat Biotech **19**(9): 833-837.

Cooper, M. A. and V. T. Singleton (2007). "A survey of the 2001 to 2005 quartz crystal microbalance biosensor literature: applications of acoustic physics to the analysis of biomolecular interactions." Journal of Molecular Recognition **20**(3): 154-184.

Creighton, J. A. and D. G. Eadon (1991). "Ultraviolet–visible absorption spectra of the colloidal metallic elements." Journal of the Chemical Society, Faraday Transactions **87**: 3881 - 3891.

Csaki, A., R. Moller, et al. (2002). "Gold nanoparticles as novel label for DNA diagnostics." Expert Review of Molecular Diagnostics **2**(2): 187-193.

Cushing, B. L., V. L. Kolesnichenko, et al. (2004). "Recent Advances in the Liquid-Phase Syntheses of Inorganic Nanoparticles." Chem. Rev. **104**(9): 3893-3946.

D'Alessandro, M. P. (2006). "Virtual Pediatric Hospital." Retrieved 21st June 2006, 2007, from http://www.vh.org/adult/provider/internalmedicine/AdultCriticalCare/FM/Overview.html.

Dai, X., Y. Tan, et al. (2002). "Formation of Gold Nanoparticles in the Presence of o-Anisidine and the Dependence of the Structure of Poly(o-anisidine) on Synthetic Conditions." Langmuir **18**(23): 9010-9016.

Daniel, M. C. and D. Astruc (2004). "Gold Nanoparticles: Assembly, Supramolecular Chemistry, Quantum-Size-Related Properties, and Applications toward Biology, Catalysis, and Nanotechnology." Chem. Rev. **104**(1): 293-346.

Daniel, M. C. and D. Astruc (2004). "Gold nanoparticles: assembly, supramolecular chemistry, quantum-size-related properties, and applications toward biology, catalysis, and nanotechnology." Chem Rev **104**(1): 293-346.

Davis, K. A. and T. R. Leary (1989). "Continuous liquid-phase piezoelectric biosensor for kinetic immunoassays." Anal. Chem. **61**(11): 1227-1230.

Dawson, A. and P. V. Kamat (2000). "Complexation of Gold Nanoparticles with Radiolytically Generated Thiocyanate Radicals." J. Phys. Chem. B **104**(50): 11842-11846.

de Filippis, I., C. R. do Nascimento, et al. (2005). "Rapid detection of Neisseria meningitidis in cerebrospinal fluid by one-step polymerase chain reaction of the nspA gene." Diagn Microbiol Infect Dis **51**(2): 85-90.

Diaz, M., A. S. Greenberg, et al. (1998). "Somatic hypermutation of the new antigen receptor gene (NAR) in the nurse shark does not generate the repertoire: Possible role in antigen-driven reactions in the absence of germinal centers." PNAS **95**(24): 14343-14348.

Djalali, R., Y. F. Chen, et al. (2003). "Au nanocrystal growth on nanotubes controlled by conformations and charges of sequenced peptide templates." J Am Chem Soc **125**(19): 5873-9.

Dmitri Ivnitski, I. A.-H. P. A. E. W. S. S. (2000). "Application of Electrochemical Biosensors for Detection of Food Pathogenic Bacteria." Electroanalysis **12**(5): 317-325.

Donna, P.-B., R.-G. Melanie, et al. (2004). "Iron Transport Systems in Neisseria meningitidis." Microbiol. Mol. Biol. Rev. **68**(1): 154-171.

Dooley, H., M. F. Flajnik, et al. (2003). "Selection and characterization of naturally occurring single-domain (IgNAR) antibody fragments from immunized sharks by phage display." Molecular Immunology **40**(1): 25-33.

Dultsev, F. N., R. E. Speight, et al. (2001). "Direct and Quantitative Detection of Bacteriophage by "Hearing" Surface Detachment Using a Quartz Crystal Microbalance." Anal. Chem. **73**(16): 3935-3939.

Dunbar, S. A., R. A. Eason, et al. (1998). "Microscopic examination and broth culture of cerebrospinal fluid in diagnosis of meningitis." J Clin Microbiol **36**(6): 1617-20.

Ebersole, R. C., J. A. Miller, et al. (1990). "Spontaneously Formed Functionally Active Avidin Monolayers on Metal Surfaces: A Strategy for Immobilizing Biological Reagents and Design of Piezoelectric Biosensors." Journal of American Chemical Society **112**: 3239.

Edwards, E. A. (1971). "Immunologic investigations of meningococcal disease. I. Group-specific Neisseria meningitidis antigens present in the serum of patients with fulminant meningococcemia." J Immunol **106**(2): 314-7.

Elghanian, R., J. J. Storhoff, et al. (1997). "Selective Colorimetric Detection of Polynucleotides Based on the Distance-Dependent Optical Properties of Gold Nanoparticles." Science **277**(5329): 1078-1081.

Emir, G. S. V., CA, US) , T. S. C. Zhong, CA, US) , et al. (2006). Method of uniformly coating a substrate. Free patents online. U. patent. USA. **7018943**.

Englebienne, P. (1999). "Synthetic materials capable of reporting biomolecular recognition events by chromic transition." Journal of Material Chemistry **9**: 1043-1054.

Engvall, E. (1980). "Enzyme immunoassay ELISA and EMIT." Methods Enzymol **70**(A): 419-39.

Epifani, M., C. Giannini, et al. (2000). "Sol-Gel Synthesis and Characterization of Ag and Au Nanoparticles in SiO2, TiO2, and ZrO2 Thin Films." Journal of the American Ceramic Society **83**(10): 2385-2393.

Esumi, K., T. Hosoya, et al. (2000). "Spontaneous Formation of Gold Nanoparticles in Aqueous Solution of Sugar-Persubstituted Poly(amidoamine)dendrimers." Langmuir **16**(6): 2978-2980.

Eun, A. J. C., L. Huang, et al. (2002). "Detection of two orchid viruses using quartz crystal microbalance (QCM) immunosensors." Journal of Virological Methods **99**: 71-79.

Faraday, M. (1857). "The Bakerian Lecture: Experimental Relations of Gold (and Other Metals) to Light " Philosophical Transactions of the Royal Society of London **147**: 145-181.

Faraday, M. (1857). " "Experimental relations of gold (and other metals) to light."" Pholosophical Transactions of The Royal Society, London **147**: 145-181.

Fawcett, N. C., R. D. Craven, et al. (1998). "QCM Response to Solvated, Tethered Macromolecules " Analytical Chemistry **70**(14): 2876 -2880.

Fecondo, J. V., Mansell, A. S. & Boyd, A. W. (1996). Development of Simplified and Efficient Synthesis Cycles for the Applied Biosystems 431A Peptide Synthesiser. 24th European Peptide Symposium, Edinburgh, Scotland.

Feinberg, R. S. and R. B. Merrifield (1975). "Modification of peptides containing glutamic acid by hydrogen fluoride-anisole mixtures. Gamma-acylation of anisole or the glutamyl nitrogen." J Am Chem Soc **97**(12): 3485-96.

Fernandez-Rodriguez, A., J. A. Vazquez, et al. (2005). "Latex agglutination for bacterial antigens and meningococcus PCR: two useful tools in legal sudden deaths." Forensic Sci Int **147**(1): 13-20.

Feynman, R. P. (1959). There's Plenty of Room at the Bottom. A. P. Society. California.

Fields, G. B., R. H. Angeletti, et al. (1994). "Variable Success of Peptide-Resin Cleavage and Deprotection Following Solid-Phase Synthesis." Techniques in Protein Chemistry V: 501-507.

Fischer, E. and E. Fourneau (1901). Berichte **34**: 2868.

Fischler, M. and U. Simon (2007). DNA-Based Assembly of Metal Nanoparticles: Structure and Functionality. Charge Migration in DNA**:** 263-282.

Fisseha, M., P. Chen, et al. (2005). "Characterization of Native Outer Membrane Vesicles from lpxL Mutant Strains of Neisseria meningitidis for Use in Parenteral Vaccination." Infect. Immun. **73**(7): 4070-4080.

Fitch, M. T. and D. v. d. Beek (2007). "Emergency diagnosis and treatment of adult meningitis." Lancet Infect Dis **7**(3): 191-200.

Fitzpatrick, D. A. and J. O. McInerney (2005). "Evidence of positive Darwinian selection in Omp85, a highly conserved bacterial outer membrane protein essential for cell viability." J Mol Evol **60**(2): 268-73.

Flexner, S. (1913). "The results of the serum treatment in thirteen hundred cases of epidemic meningitis." J. Exp. Med. **17**(5): 553-576.

Fox, A. J., M. K. Taha, et al. (2007). "Standardized nonculture techniques recommended for European reference laboratories." FEMS Microbiol Rev **31**(1): 84-8.

Francisci, A. (1618). Panacea Aurea-Auro Potabile. Hamburg, Bibliopolio Frobeniano.

Frankamp, B. L., A. K. Boal, et al. (2002). "Controlled Interparticle Spacing through Self-Assembly of Au Nanoparticles and Poly(amidoamine) Dendrimers." J. Am. Chem. Soc. **124**(51): 15146-15147.

Fratamico, P. M., T. P. Strobaugh, et al. (1998). "Detection of Escherichia coli 0157:H7 using a surface plasmon resonance biosensor." Biotechnology Techniques **12**(7): 571-576.

Frens, G. (1973). ""Controlled Nucleation for the Regulation of Particle Size in Monodisperse Gold Solutions," " Nature Physical Science **241.**: 20-22.

Frens, G. (1973). "Controlled Nucleation for the Regulation of Particle Size in Monodisperse Gold Solutions." Nature Physical Science **241.**: 20-22.

Frens, G. (1973). "Controlled nucleation of the regulation of the particle size in monodisperse gold solutions." Nature, Phys. Sci. **241**: 20-22.

Frosch, M., I. Gorgen, et al. (1985). "NZB Mouse System for Production of Monoclonal Antibodies to Weak Bacterial Antigens: Isolation of an IgG Antibody to the Polysaccharide Capsules of Escherichia coli K1 and Group B Meningococci." Proceedings of the National Academy of Sciences **82**(4): 1194-1198.

Frosch, M. and U. Vogel (2006). Structure and Genetics of the Meningococcal Capsule. Handbook of Meningococcal Disease. P. D. M. C. J. M. Prof Dr Matthias Frosch**:** 145-162.

Fulhame, M. (1794). An Essay on Combustion with a View to a New Art of Dying and Painting. London, J. Cooper.

Gans, R. (1915). "Über die Form ultramikroskopischer Silberteilchen." Annalen der Physik **352**(10): 270-284.

Garci, M. B. G., C. F. Sanchez, et al. (2000). "Colloidal gold as an electrochemical label of streptavidin–biotin interaction." Biosensors and Bioelectronics **15**(5-6): 315-321.

Garcia, M. B. G. and A. C. Garcia (2000). "Silver electrodeposition catalyzed by colloidal gold on carbon paste electrode: application to biotin-streptavidin interaction monitoring." Biosens Bioelectron **15**(11-12): 663-70.

Gautier, C. and T. Burgi (2005). "Vibrational circular dichroism of N-acetyl-l-cysteine protected gold nanoparticles." Chem Commun (Camb)(43): 5393-5.

Genevrois, S., L. Steeghs, et al. (2003). "The Omp85 protein of Neisseria meningitidis is required for lipid export to the outer membrane." The EMBO Journal **22**(8): 1780–1789.

Gentle, I., K. Gabriel, et al. (2004). "The Omp85 family of proteins is essential for outer membrane biogenesis in mitochondria and bacteria." J. Cell Biol. **164**(1): 19-24.

Gentle, I. E., L. Burri, et al. (2005). "Molecular architecture and function of the Omp85 family of proteins." Mol Microbiol **58**(5): 1216-25.

Giersig, M. and P. Mulvaney (1993). "Preparation of ordered colloid monolayers by electrophoretic deposition." Langmuir **9**(12): 3408-3413.

Gittins, D. I., D. Bethell, et al. (2000). "A nanometre-scale electronic switch consisting of a metal cluster and redox-addressable groups." Nature **408**(6808): 67-9.

Gittins, D. I. and F. Caruso (2002). "Biological and Physical Applications of Water-Based Metal Nanoparticles Synthesised in Organic Solution." Chemphyschem **3**(1): 110-113.

Glode, M. P., A. Sutton, et al. (1977). "Pathogenesis of neonatal Escherichia coli meningitis: induction of bacteremia and meningitis in infant rats fed E. coli K1." Infect Immun. **16**(1): 75–80.

Goia, D. V. and E. Matijevi (1998). "Preparation of monodispersed metal particles." New Journal of Chemistry **22**: 1203 - 1215.

Goldschneider, I., E. C. Gotschlich, et al. (1969). "Human immunity to the meningococcus. I. The role of humoral antibodies." J Exp Med **129**(6): 1307-26.

Grabar, K. C., P. C. Smith, et al. (1996). "Kinetic Control of Interparticle Spacing in Au Colloid-Based Surfaces: Rational Nanometer-Scale Architecture." J. Am. Chem. Soc. **118**(5): 1148-1153.

Graham, T. (1861). "Liquid Diffusion Applied to Analysis." Philosophical Transactions of the Royal Society of London **151**: 183-224.

Granoff, D. M., A. Bartoloni, et al. (1998). "Bactericidal Monoclonal Antibodies That Define Unique Meningococcal B Polysaccharide Epitopes That Do Not Cross-React with Human Polysialic Acid." J Immunol **160**(10): 5028-5036.

Gray, B. M. (1979). "ELISA methodology for polysaccharide antigens: Protein coupling of polysaccharides for adsorption to plastic tubes." Journal of Immunological Methods **28**(1-2): 187-192.

Greenberg, A. S., D. Avila, et al. (1995). "A new antigen receptor gene family that undergoes rearrangement and extensive somatic diversification in sharks." Nature **374**(6518): 168-173.

Gregori, L., J. F. Hainfeld, et al. (1997). "Binding of Amyloid beta Protein to the 20S Proteasome." J. Biol. Chem. **272**(1): 58-62.

Gryte, D. M., M. D. Ward, et al. (1993). "Real-time measurement of anchorage-dependent cell adhesion using a quartz crystal microbalance." Biotechnol Prog **9**(1): 105-8.

Gunawan, J., D. Simard, et al. (2005). "Structural and Mechanistic Analysis of Sialic Acid Synthase NeuB from Neisseria meningitidis in Complex with Mn2+, Phosphoenolpyruvate, and N-Acetylmannosaminitol." J. Biol. Chem. **280**(5): 3555-3563.

Ha, T. H., S. Kim, et al. (2004). "Influence of liquid medium and surface morphology on the response of QCM during immobilization and hybridization of short oligonucleotides." Biosensors and Bioelectronics **20**(2): 378-389.

Hainfeld, J. F. (1988). "Gold cluster-labelled antibodies." Nature **333**(6170): 281-282.

Hainfeld, J. F. (1992). "Site-specific cluster labels." Ultramicroscopy **46**(1-4): 135-144.

Hainfeld, J. F. and F. R. Furuya (1992). "A 1.4-nm gold cluster covalently attached to antibodies improves immunolabeling." J. Histochem. Cytochem. **40**(2): 177-184.

Haiss, W., N. T. K. Thanh, et al. (2007). "Determination of Size and Concentration of Gold Nanoparticles from UV-Vis Spectra." Anal. Chem. **79**(11): 4215-4221.

Halámeka, J., C. Tellera, et al. (2006). "EQCN based cholinesterase biosensors." Electrochimica Acta **51**(24): 5174-5181.

Hammerschmidt, S., A. Muller, et al. (1996). "Capsule phase variation in Neisseria meningitidis serogroup B by slipped-strand mispairing in the polysialyltransferase gene (siaD): correlation with bacterial invasion and the outbreak of meningococcal disease." Molecular Microbiology **20**(6): 1211-1220.

Han, M., X. Gao, et al. (2001). "Quantum-dot-tagged microbeads for multiplexed optical coding of biomolecules." Nat Biotechnol **19**(7): 631-5.

Hauser, E. A. (1952). "Aurum Potabile." Journal of Chemical Education **29**: 456-458.

Hayat, M. A. (1991). Colloidal Gold: Principles, Methods, and Applications. San Diego, CA., Academic Press.

He, F. and S. Liu (2004). "Detection of P. aeruginosa using nano-structured electrode-separated piezoelectric DNA biosensor." Talanta **62**(2): 271-277.

Helcher, H. H. (1718). Aurum Potabile oder Gold Tinstur. Breslau and Leipzig.

Hengerer, A., J. Decker, et al. (1999). "Quartz crystal microbalance (QCM) as a device for the screening of phage libraries." Biosensors and Bioelectronics **14**(2): 139-144.

Henriques, A. W. S., E. Jessouroun, et al. (2006). "Capsular polysaccharide production by Neisseria meningitidis serogroup C: Optimization of process variables using response surface methodology." Process Biochemistry **41**(8): 1822-1828.

Herr, A. E., D. J. Throckmorton, et al. (2005). "On-chip native gel electrophoresis-based immunoassays for tetanus antibody and toxin." Anal Chem **77**(2): 585-90.

Hirai, H., Y. Nakao, et al. (1978). "Preparation of Colloidal Rhodium in Poly(vinyl Alcohol) by Reduction with Methanol." Journal of Macromolecular Science, Part A **12**(8): 1117 - 1141.

Hirst, R. A., B. Gosai, et al. (2003). "Streptococcus pneumoniae damages the ciliated ependyma of the brain during meningitis." Infect Immun **71**(10): 6095-100.

Hone, D. C., P. I. Walker, et al. (2002). "Generation of Cytotoxic Singlet Oxygen via Phthalocyanine-Stabilized Gold Nanoparticles: A Potential Delivery Vehicle for Photodynamic Therapy." Langmuir **18**(8): 2985-2987.

Hong, H. G., M. Jiang, et al. (1994). "Cysteine-specific surface tethering of genetically engineered cytochromes for fabrication of metalloprotein nanostructures." Langmuir **10**(1): 153-158.
Hoogenboom, H. R. and P. Chames (2000). "Natural and designer binding sites made by phage display technology." Immunology Today **21**(8): 371-378.
Hostetler, M. J., J. E. Wingate, et al. (1998). "Alkanethiolate Gold Cluster Molecules with Core Diameters from 1.5 to 5.2 nm: Core and Monolayer Properties as a Function of Core Size." Langmuir **14**(1): 17-30.
Hövel, H., S. Fritz, et al. (1993). "Width of cluster plasmon resonances: Bulk dielectric functions and chemical interface damping." Physical Review B **48**(24): 18178.
Hsieh, S. M., C. C. Hung, et al. (1996). "Concomitant human immunodeficiency virus infection and syphilitic meningitis." J Formos Med Assoc **95**(2): 166-9.
Hubert, B., L. Watier, et al. (1992). "Meningococcal disease and influenza-like syndrome: a new approach to an old question." J Infect Dis **166**(3): 542-5.
Hughes, J. H., D. J. Biedenbach, et al. (1993). "E test as susceptibility test and epidemiologic tool for evaluation of Neisseria meningitidis isolates." J Clin Microbiol **31**(12): 3255-9.
Hunter, R. J. (1993). Introduction to Modern Colloid Science, Oxford Science Publications.
Hutter, E. and M. P. Pileni (2003). "Detection of DNA Hybridization by Gold Nanoparticle Enhanced Transmission Surface Plasmon Resonance Spectroscopy." J. Phys. Chem. B **107**(27): 6497-6499.
Hwang, W.-M., C.-Y. Lee, et al. (2003). "Separation of Nanoparticles in Different Sizes and Compositions by Capillary Electrophoresis." Bull. Korean Chem. Soc. **24**(5).
Hyning, V. D. L. and C. F. Zukoski (1998). "Formation Mechanisms and Aggregation Behavior of Borohydride Reduced Silver Particles." Langmuir **14**(24): 7034-7046.
Institute, C. a. L. S. (2005). Performance standards for antimicrobial susceptibility testing M100-S15., Clinical and Laboratory Standard Institute: Wayne, Pennsylvania;.
Ivnitski, D., I. Abdel-Hamid, et al. (1999). "Biosensors for detection of pathogenic bacteria." Biosensors and Bioelectronics **14**(7): 599-624.
Jain, K. K. (2006). "Nanoparticles as targeting ligands." Trends in Biotechnology **24**(4): 143-145.
Janshoff, A., C. Steinem, et al. (1996). "Specific binding of peanut agglutinin to GM1-doped solid supported lipid bilayers investigated by shear wave resonator measurements." European Biophysics Journal **25**(2): 105-113.
Jiang, W., B. Y. Kim, et al. (2007). "Advances and challenges of nanotechnology-based drug delivery systems." Expert Opin Drug Deliv **4**(6): 621-633.
Jianrong, C., M. Yuqing, et al. (2004). "Nanotechnology and biosensors." Biotechnol Adv **22**(7): 505-18.
Jin, L. and R. V. Lloyd (1997). "In situ hybridization: Methods and applications." Journal of Clinical Laboratory Analysis **11**(1): 2-9.
Jones, D. T. (1999). "Protein secondary structure prediction based on position-specific scoring matrices." Journal of Molecular Biology **292**(2): 195-202.
Joos, T. O., M. Schrenk, et al. (2000). "A microarray enzyme-linked immunosorbent assay for autoimmune diagnostics." Electrophoresis **21**(13): 2641-2650.

Jordens, J. Z. and J. E. Heckels (2005). "A novel porA-based real-time PCR for detection of meningococcal carriage." J Med Microbiol **54**(Pt 5): 463-6.

Josse, F., Y. Lee, et al. (1998). "Analysis of the Radial Dependence of Mass Sensitivity for Modified-Electrode Quartz Crystal Resonators." Anal. Chem. **70**(2): 237-247.

Judd, R. C. F., MT, US) and D. S. M. Manning, MT, US) (2002). Omp85 proteins of neisseria gonorrhoeae and neisseria meningitidis, compositions containing same and methods of use thereof Free Patents Online. U. Patents. United States. **424/184.1**.

Judd, R. C. F., MT, US) and D. S. M. Manning, MT, US) (2003). OMP85 protein of neisseria meningitidis, compositions containing the same and methods of use thereof. Free Patents Online. U. S. Patent. United States. **424/250.1**.

Kahn, R. L. (1928). Serum Diagnosis for Syphilis. In Colliodal Chemistry, Vol. II. J. Alexander, Ed. New York, The Chemical Catalog Co. **II:** 757.

Kamata, K., Y. Lu, et al. (2003). "Synthesis and Characterization of Monodispersed Core-Shell Spherical Colloids with Movable Cores." J. Am. Chem. Soc. **125**(9): 2384-2385.

Katz, E. and I. Willner (2004). "Integrated Nanoparticle-Biomolecule Hybrid Systems: Synthesis, Properties, and Applications." Angewandte Chemie International Edition **43**(45): 6042-6108.

Kawahashi, Y., N. Doi, et al. (2003). "In vitro protein microarrays for detecting protein-protein interactions: Application of a new method for fluorescence labeling of proteins." Proteomics **3**(7): 1236-1243.

Keating, C. D., K. M. Kovaleski, et al. (1998). "Protein:Colloid Conjugates for Surface Enhanced Raman Scattering: Stability and Control of Protein Orientation." J. Phys. Chem. B **102**(47): 9404-9413.

Kele, P., K. Nagy, et al. (2006). "The Development of Conformational-Dynamics-Based Sensors." Angew Chem Int Ed Engl **45**(16): 2565-2567.

Kent, S. and I. Clark-Lewis (1985). Modern methods for the chemical synthesis of biologically active peptides. In Synthetic Peptides in Biology and Medicine. K. Alitalo, Partanen, P. & Vaheri, A., Elsevier, Amsterdam.

Kim, C. K., R. K. Rajamohan, et al. (2006). "Gold-nanoparticle-based miniaturized laser-induced fluorescence probe for specific DNA hybridization detection: studies on size-dependent optical properties." Nanotechnology **17**: 3085-3093.

Kim, N. H., T. J. Baek, et al. (2007). "Highly Sensitive Biomolecule Detection on a Quartz Crystal Microbalance Using Gold Nanoparticles as Signal Amplification Probes." Analytical Sciences **23**(2): 177.

King, W. H. (1964). "Piezoelectric Sorption Detector." Anal. Chem. **36**(9): 1735-1739.

Kolinger, C., E. Uttenthaler, et al. (1995). "Comparison of the QCM and the SPR method for surface studies and immunological applications." Sensors and Actuators B: Chemical **24**(1-3): 107-112.

Konig, B. and M. Gratzel (1994). "A novel immunosensor for herpes viruses." Anal Chem **66**(3): 341-4.

Krasteva, N., R. Krustev, et al. (2003). "Vapor Sorption in Self-Assembled Gold Nanoparticle/Dendrimer Films Studied by Specular Neutron Reflectometry." Langmuir **19**(19): 7754-7760.

Kreibig, U. and C. v. Fragstein (1969). "The limitation of electron mean free path in small silver particles." Zeitschrift für Physik A Hadrons and Nuclei **224**(4): 307-323.

Kreibig, U., B. Schmitz, et al. (1987). "Separation of plasmon-polariton modes of small metal particles." Physical Review B **36**(9): 5027 LP - 5030.

Kreibig, U. and M. Vollmer (1995). Optical Properties of Metal Clusters. Berlin, Springer.

Kumar, A. (2000) "Biosensors Based on Piezoelectric Crystal Detectors: Theory and Application." Journal of the Minerals, Metals and Materials Society **Volume**, DOI:

Kunckels, J. (1676). Nuetliche Observationes oder Anmerkungen von Auro und Argento Potabili. Hamburg.

Kurosawa, S., E. Tawara, et al. (1990). "Latex piezoelectric immunoassay: detection of agglutination of antibody-bearing latex using a piezoelectric quartz crystal." Chem Pharm Bull (Tokyo) **May; 38**(5): 1117-20.

Lapeyssonnie, L. (1963). "La méningite cérébro-spinale en Afrique." Bull. W. H. O. **28**(3): 114.

Lee, B. E. and H. D. Davies (2007). "Aseptic meningitis." Curr Opin Infect Dis **20**(3): 272-7.

Lee, K. S. and M. A. El-Sayed (2006). "Gold and Silver Nanoparticles in Sensing and Imaging: Sensitivity of Plasmon Response to Size, Shape, and Metal Composition." J. Phys. Chem. B **110**(39): 19220-19225.

Lee, O., L. D. Cromwell, et al. (2005). "Carcinomatous meningitis arising from primary nasopharyngeal carcinoma." Am J Otolaryngol **26**(3): 193-7.

Lee, W., B.-K. Oh, et al. (2006). "Signal Enhancement of Surface Plasmon Resonance Based on Gold Nanoparticle-Antibody Complex for Immunoassay." Journal of Nanoscience and Nanotechnology **6**: 3521-3525.

Lee, Y.-G. and K.-S. Chang (2005). "Application of a flow type quartz crystal microbalance immunosensor for real time determination of cattle bovine ephemeral fever virus in liquid." Talanta **65**(5): 1335-1342.

Leff, D. V., L. Brandt, et al. (1996). "Synthesis and Characterization of Hydrophobic, Organically-Soluble Gold Nanocrystals Functionalized with Primary Amines." Langmuir **12**(20): 4723-4730.

Leuenberger, D., S. Curran, et al. (2005). Mitochondrial Biogenesis. The Biogenesis of Cellular Organelles**:** 138-163.

Lewis, L. N. (1993). "Chemical catalysis by colloids and clusters." Chem. Rev. **93**(8): 2693-2730.

Li, C., X. Chen, et al. (2006). "A facile approach for synthesis of high-stable CdS nanoparticles." Chinese Science Bulletin **51**(10): 1266-1268.

Li, D., Q. He, et al. (2007). "Immobilization of glucose oxidase onto gold nanoparticles with enhanced thermostability." Biochemical and Biophysical Research Communications **355**(2): 488-493.

Li, H., Y. Y. Luk, et al. (1999). "Catalytic Asymmetric Dihydroxylation by Gold Colloids Functionalized with Self-Assembled Monolayers." Langmuir **15**(15): 4957-4959.

Li, J., X. Chu, et al. (2005). "A colorimetric method for point mutation detection using high-fidelity DNA ligase." Nucl. Acids Res. **33**(19): e168-.

Lin, C. C., Y. C. Yeh, et al. (2002). "Selective Binding of Mannose-Encapsulated Gold Nanoparticles to Type 1 Pili in Escherichia coli." J. Am. Chem. Soc. **124**(14): 3508-3509.

Lin, F. Y. H., M. Sabri, et al. (2005). "Development of a Nanoparticle-Labeled Microfluidic Immunoassay for Detection of Pathogenic Microorganisms." Clin. Diagn. Lab. Immunol. **12**(3): 418-425.

Lin, S. T., M. T. Franklin, et al. (1986). "Nonaqueous colloidal gold. Clustering of metal atoms in organic media. 12." Langmuir **2**(2): 259-260.

Link, S. and M. A. El-Sayed (1999). "Size and Temperature Dependence of the Plasmon Absorption of Colloidal Gold Nanoparticles." J. Phys. Chem. B **103**(21): 4212-4217.

Link, S. and M. A. El-Sayed (1999). "Spectral Properties and Relaxation Dynamics of Surface Plasmon Electronic Oscillations in Gold and Silver Nanodots and Nanorods." J. Phys. Chem. B **103**(40): 8410-8426.

Link, S. and M. A. El-Sayed (2000). "Shape and size dependence of radiative, non-radiative and photothermal properties of gold nanocrystals." International Reviews in Physical Chemistry **19**(3): 409-453.

Link, S., Z. L. Wang, et al. (1999). "Alloy Formation of Gold-Silver Nanoparticles and the Dependence of the Plasmon Absorption on Their Composition." J. Phys. Chem. B **103**(18): 3529-3533.

Lisiecki, I. and M. P. Piled (1995). "Copper Metallic Particles Synthesized “in Situ” in Reverse Micelles: Influence of Various Parameters on the Size of the Particles." Journal of Physical Chemistry **99**: 5077-5082.

Liu, J. and Y. Lu (2003). "A colorimetric lead biosensor using DNAzyme-directed assembly of gold nanoparticles." J Am Chem Soc **125**(22): 6642-3.

Liu, J. and Y. Lu (2004). "Accelerated Color Change of Gold Nanoparticles Assembled by DNAzymes for Simple and Fast Colorimetric Pb^{2+} Detection." J. Am. Chem. Soc. **126**(39): 12298-12305.

Liu, J. and Y. Lu (2004). "Colorimetric biosensors based on DNAzyme-assembled gold nanoparticles." J Fluoresc **14**(4): 343-54.

Liu, S.-f., J.-R. Li, et al. (2005). "Surface modification of platinum quartz crystal microbalance by controlled electroless deposition of gold nanoparticles and its enhancing effect on the HS-DNA immobilization." Colloids and Surfaces A: Physicochemical and Engineering Aspects **257-258**: 57-62.

Liu, S., D. o. n. Leech, et al. (2003). "Application of Colloidal Gold in Protein Immobilization, Electron Transfer, and Biosensing." Analytical Letters **36**(1): 1 - 19.

Liu, T., J. Tang, et al. (2004). "The enhancement effect of gold nanoparticles as a surface modifier on DNA sensor sensitivity." Biochemical and Biophysical Research Communications **313**: 3-7.

Liu, T., J. a. Tang, et al. (2004). "The enhancement effect of gold nanoparticles as a surface modifier on DNA sensor sensitivity." Biochemical and Biophysical Research Communications **313**(1): 3-7.

Loosmore, S. M., Y. P. Yang, et al. (1997). "Outer membrane protein D15 is conserved among Haemophilus influenzae species and may represent a universal protective antigen against invasive disease." Infect. Immun. **65**(9): 3701-3707.

Lostis, M. (1958). Relationship between the resonant frequency of an oscillating piezoelectric crystal and the mass deposited on the crystal surface Faculty of Science, University of Paris. **Ph.D. dissertation**.

Love, J. C., L. A. Estroff, et al. (2005). "Self-Assembled Monolayers of Thiolates on Metals as a Form of Nanotechnology." Chem. Rev. **105**(4): 1103-1170.

Lu, C.-S. and O. Lewis (1972). "Investigation of film-thickness determination by oscillating quartz resonators with large mass load." Journal of Applied Physics **43**(11): 4385-4390.

Lu, Q.-W., S. Morimoto, et al. (2003). "Cardiac troponin T mutation R141W found in dilated cardiomyopathy stabilizes the troponin T-tropomyosin interaction and causes a Ca2+ desensitization." Journal of Molecular and Cellular Cardiology **35**(12): 1421-1427.

Lyon, L. A., M. D. Musick, et al. (1998). "Colloidal Au-Enhanced Surface Plasmon Resonance Immunosensing." Anal. Chem. **70**(24): 5177-5183.

Lyon, L. A., M. D. Musick, et al. (1999). "Surface plasmon resonance of colloidal Au-modified gold films." Sensors and Actuators B: Chemical **54**(1-2): 118-124.

Macdonald, I. D. G. and W. E. Smith (1996). "Orientation of Cytochrome c Adsorbed on a Citrate-Reduced Silver Colloid Surface." Langmuir **12**(3): 706-713.

Mafune, F. (2004). "Structure diagram of gold nanoparticles in solution under irradiation of UV pulse laser." Chemical Physics Letters **397**(1-3): 133-137.

Mafune, F., J. y. Kohno, et al. (2002). "Full Physical Preparation of Size-Selected Gold Nanoparticles in Solution: Laser Ablation and Laser-Induced Size Control." J. Phys. Chem. B **106**(31): 7575-7577.

Maiden, M. C. (2004). "Dynamics of bacterial carriage and disease: lessons from the meningococcus." Adv Exp Med Biol **549**: 23-9.

Malecki, M., A. Hsu, et al. (2002). "Molecular immunolabeling with recombinant single-chain variable fragment (scFv) antibodies designed with metal-binding domains." PNAS **99**(1): 213-218.

Mallick, K., Z. L. Wang, et al. (2001). "Seed-mediated successive growth of gold particles accomplished by UV irradiation: a photochemical approach for size-controlled synthesis." Journal of Photochemistry and Photobiology A: Chemistry **140**(1): 75-80.

Manchanda, V., S. Gupta, et al. (2006). "Meningococcal disease: History, epidemiology, pathogenesis, clinical manifestations, diagnosis, antimicrobial susceptibility and prevention." Indian Journal of Medical Microbiology **24**(1): 7-19.

Mandal, S., S. Phadtare, et al. (2005). "Interfacing biology with nanoparticles." Current Applied Physics **5**(2): 118-127.

Mangeney, C., F. Ferrage, et al. (2002). "Synthesis and Properties of Water-Soluble Gold Colloids Covalently Derivatized with Neutral Polymer Monolayers." J. Am. Chem. Soc. **124**(20): 5811-5821.

Manimaran, M. and N. R. Jana (2007). "Detection of protein molecules by surface-enhanced Raman spectroscopy-based immunoassay using 2-5 nm gold nanoparticle lables." Journal of Raman Spectroscopy **38**(10): 1326-1331.

Mann, S. (1988). "Molecular recognition in biomineralization." Nature **332**(6160): 119-124.

Mann, S., W. Shenton, et al. (2000). "Biologically Programmed Nanoparticle Assembly." Advanced Materials **12**(2): 147-150.

Manning, D. S., D. K. Reschke, et al. (1998). "Omp85 proteins ofNeisseria gonorrhoeaeandNeisseria meningitidisare similar toHaemophilus influenzaeD-15-Ag andPasteurella multocidaOma87." Microbial Pathogenesis **25**(1): 11-21.

Marchiafava, E. and A. Celli (1884). "Spra i micrococchi della meningite cerebrospinale epidemica." Gazz degli Ospedali **5**: 59.

Marinac, J. S. (1992). "Drug- and chemical-induced aseptic meningitis: a review of the literature." Ann Pharmacother **26**(6): 813-22.

Martelli, P. L., P. Fariselli, et al. (2002). "Prediction of the disulfide bonding state of cysteines in proteins with hidden neural networks." Protein Eng. **15**(12): 951-953.

Martin, B. A. and H. E. Hager (1989). "Flow profile above a quartz crystal vibrating in liquid." Journal of Applied Physics **65**(7): 2627-2629.

Martin, S. J., G. C. Frye, et al. (1993). "Effect of surface roughness on the response of thickness-shear mode resonators in liquids." Analytical Chemistry (Washington) ; Vol/Issue: 65:20; DOE Project: Pages: 2910-2922.

Martin, S. J., G. C. Frye, et al. (1994). "Dynamics and Response of Polymer-Coated Surface Acoustic Wave Devices: Effect of Viscoelastic Properties and Film Resonance." Anal. Chem. **66**(14): 2201-2219.

Martin, S. J., V. E. Granstaff, et al. (1991). "Characterization of a quartz crystal microbalance with simultaneous mass and liquid loading." Anal. Chem. **63**(20): 2272-2281.

Masson, L. and B. E. Holbein (1983). "Physiology of sialic acid capsular polysaccharide synthesis in serogroup B Neisseria meningitidis." J. Bacteriol. **154**(2): 728-736.

Mattoussi, H., J. M. Mauro, et al. (2000). "Self-Assembly of CdSe-ZnS Quantum Dot Bioconjugates Using an Engineered Recombinant Protein." J. Am. Chem. Soc. **122**(49): 12142-12150.

Mauel, J. (1982). "Effector and escape mechanisms in host-parasite relationships." Prog Allergy **31**: 1-75.

Maye, M. M., S. C. Chun, et al. (2002). "Novel Spherical Assembly of Gold Nanoparticles Mediated by a Tetradentate Thioether." J. Am. Chem. Soc. **124**(18): 4958-4959.

Mayer, A. B. R. and J. E. Mark (1998). "Colloidal gold nanoparticles protected by water-soluble homopolymers and random copolymers." European Polymer Journal **34**(1): 103-108.

McNeil, G. and M. Virji (1997). "Phenotypic variants of meningococci and their potential in phagocytic interactions: the influence of opacity proteins, pili, PilC and surface sialic acids." Microb Pathog **22**(5): 295-304.

Melles, E., H. Anderson, et al. (2005). "Electroimmobilization of proinsulin C-peptide to a quartz crystal microbalance sensor chip for protein affinity purification." Analytical Biochemistry **341**(1): 89-93.

Merrifield, R. B. (1963). "Solid Phase Peptide Synthesis. I. The Synthesis of a Tetrapeptide." J. Am. Chem. Soc. **85**(14): 2149-2154.

Mie, G. (1908). "Beiträge zur Optik trüber Medien, speziell kolloidaler Metallösungen." Annalen der Physik **330**(3): 377-445.

Milonovich, L. M. (2007). "Meningococcemia: epidemiology, pathophysiology, and management." J Pediatr Health Care **21**(2): 75-80.
Mirkin, C. A., R. L. Letsinger, et al. (1996). "A DNA-based method for rationally assembling nanoparticles into macroscopic materials." Nature **382**(6592): 607-609.
Miyazaki, A. and Y. Nakano (2000). "Morphology of Platinum Nanoparticles Protected by Poly(N-isopropylacrylamide)." Langmuir **16**(18): 7109-7111.
Mo, Z., H. Wang, et al. (2005). "Highly reproducible hybridization assay of zeptomole DNA based on adsorption of nanoparticle-bioconjugate." Analyst **130**(12): 1589-94.
Mock, J. J., M. Barbic, et al. (2002). "Shape effects in plasmon resonance of individual colloidal silver nanoparticles." The Journal of Chemical Physics **116**(15): 6755-6759.
Montalti, M., L. Prodi, et al. (2003). "Kinetics of Place-Exchange Reactions of Thiols on Gold Nanoparticles." Langmuir **19**(12): 5172-5174.
Moore, P. S., M. W. Reeves, et al. (1989). "Intercontinental spread of an epidemic group A Neisseria meningitidis strain." Lancet **2**(8657): 260-3.
Morley, S. L. and A. J. Pollard (2001). "Vaccine prevention of meningococcal disease, coming soon?" Vaccine **20**(5-6): 666-87.
Mothershed, E. A., C. T. Sacchi, et al. (2004). "Use of real-time PCR to resolve slide agglutination discrepancies in serogroup identification of Neisseria meningitidis." J Clin Microbiol **42**(1): 320-8.
Moxon, E. R. and P. A. Murphy (1978). "Haemophilus influenzae bacteremia and meningitis resulting from survival of a single organism." Proc Natl Acad Sci U S A **75**(3): 1534-6.
Mozdzanowski, J. and D. W. Speicher (1992). "Efficient electroblotting and on-membrane proteolysis at high sensitivity for sequence analysis." Analytical Biochemistry **207**: 11-18.
Mucic, R. C., J. J. Storhoff, et al. (1998). "DNA-Directed Synthesis of Binary Nanoparticle Network Materials." Journal of American Chemical Society **120**: 12674-12675.
Mukherjee, P., R. Bhattacharya, et al. (2007). "Potential therapeutic application of gold nanoparticles in B-chronic lymphocytic leukemia (BCLL): enhancing apoptosis." Journal of Nanobiotechnology **5**(1): 4.
Mulvaney, P. (2003). The beauty and elegance of Nanocrystals: How invisibly small particles will colour and shape our future. M. University. Melbourne, University of Melbourne. **12**.
Muramatsu, H., J. M. Dicks, et al. (1987). "Piezoelectric crystal biosensor modified with protein A for determination of immunoglobulins." Anal. Chem. **59**(23): 2760-2763.
Muramatsu, H., K. Kajiwara, et al. (1986). "Piezoelectric immuno sensor for the detection of candida albicans microbes." Analytica Chimica Acta **188**: 257-261.
Muramatsu, H., E. Tamiya, et al. (1988). "Computation of equivalent circuit parameters of quartz crystals in contact with liquids and study of liquid properties." Anal. Chem. **60**(19): 2142-2146.

Muratsugu, M., F. Ohta, et al. (1993). "Quartz crystal microbalance for the detection of microgram quantities of human serum albumin: relationship between the frequency change and the mass of protein adsorbed." Anal. Chem. **65**(20): 2933-2937.

Nadel, S. and J. S. Kroll (2007). "Diagnosis and management of meningococcal disease: the need for centralized care." FEMS Microbiol Rev **31**(1): 71-83.

Nallamsetty, S., B. P. Austin, et al. (2005). "Gateway vectors for the production of combinatorially-tagged His6-MBP fusion proteins in the cytoplasm and periplasm of Escherichia coli." Protein Sci **14**(12): 2964-2971.

Nath, N. and A. Chilkoti (2002). "A Colorimetric Gold Nanoparticle Sensor To Interrogate Biomolecular Interactions in Real Time on a Surface." Anal. Chem. **74**(3): 504-509.

Neiman, B., E. Grushka, et al. (2001). "Use of Gold Nanoparticles To Enhance Capillary Electrophoresis." Anal. Chem. **73**(21): 5220-5227.

Ngeh-Ngwainbi, J., P. H. Foley, et al. (1986). "Parathion antibodies on piezoelectric crystals." J. Am. Chem. Soc. **108**(18): 5444-5447.

Nickel, U., A. z. Castell, et al. (2000). "A Silver Colloid Produced by Reduction with Hydrazine as Support for Highly Sensitive Surface-Enhanced Raman Spectroscopy." Langmuir **16**(23): 9087-9091.

Niemeyer, C. M. (2001). "Nanoparticles, Proteins, and Nucleic Acids: Biotechnology Meets Materials Science." Angewandte Chemie International Edition **40**(22): 4128-4158.

Niemeyer, C. M. and B. Ceyhan (2001). "DNA-Directed Functionalization of Colloidal Gold with Proteins." Angewandte Chemie International Edition **40**(19): 3685-3688.

Nomura, T. and M. Okuhara (1982). "Frequency shifts of piezoelectric quartz crystals immersed in organic liquids." Analytica Chimica Acta **142**: 281-284.

Nuttall, S. D., U. V. Krishnan, et al. (2002). "A naturally occurring NAR variable domain binds the Kgp protease from Porphyromonas gingivalis." FEBS Letters **516**(1-3): 80-86.

Nuttall, S. D., U. V. Krishnan, et al. (2001). "Isolation of the new antigen receptor from wobbegong sharks, and use as a scaffold for the display of protein loop libraries." Molecular Immunology **38**(4): 313-326.

Oliveira, J. R. and S. F. Silver (1980). U. patent. US. **424096**.

OMP85. (2002). "OMP85-Supporting Online Material." Retrieved 12/02/2006, 2006, from http://www.sciencemag.org/cgi/data/299/5604/262/DC1/1.

Orskov, F., I. Orskov, et al. (1979). "Form variation in Escherichia coli K1: determined by O-acetylation of the capsular polysaccharide." J. Exp. Med. **149**(3): 669-685.

Oshimaa, K., H. Nakajimaa, et al. (2005). "Quartz crystal microbalance assay for determination of plasma vitellogenin." Sensors and Actuators B: Chemical **105** (2): 473-478.

Ostwald, W. (1915). Die Welt der Vernachlässigten Dimensionen. Dresden,, Steinkopf.

Otsuka, H., Y. Akiyama, et al. (2001). "Quantitative and Reversible Lectin-Induced Association of Gold Nanoparticles Modified with α-Lactosyl-ω-mercapto-poly(ethylene glycol)." J. Am. Chem. Soc. **123**(34): 8226-8230.

Paap, C. M. and J. A. Bosso (1992). "Treatment options for the pharmacological therapy of neonatal meningitis." Drugs **43**(5): 700-12.
Paciotti, G. F., L. Myer, et al. (2004). "Colloidal Gold: A Novel Nanoparticle Vector for Tumor Directed Drug Delivery." Drug Delivery **11**(3): 169 - 183.
Parak, W. J., T. Pellegrino, et al. (2003). "Conformation of Oligonucleotides Attached to Gold Nanocrystals Probed by Gel Electrophoresis." Nano Lett. **3**(1): 33-36.
Peng, Z., Z. Chen, et al. (2007). "A novel immunoassay based on the dissociation of immunocomplex and fluorescence quenching by gold nanoparticles." Analytica Chimica Acta **583**(1): 40-44.
Perez-Camarero, E. R., M. Escalante-Boleas, et al. (2000). "[Staphylococcus aureus-related meningitis]." Rev Neurol **31**(4): 397.
Phadtare, S., V. P. V. Kausik, et al. (2004). "Immobilization and biocatalytic activity of fungal protease on gold nanoparticle-loaded zeolite microspheres." Biotechnology and Bioengineering **85**(6): 629-637.
Phadtare, S., A. Kumar, et al. (2003). "Direct Assembly of Gold Nanoparticle "Shells" on Polyurethane Microsphere "Cores" and Their Application as Enzyme Immobilization Templates." Chem. Mater. **15**(10): 1944-1949.
Pol, V. G., A. Gedanken, et al. (2003). "Deposition of Gold Nanoparticles on Silica Spheres: A Sonochemical Approach." Chem. Mater. **15**(5): 1111-1118.
Popovic, T., G. Ajello, et al. (1999). "Laboratory methods for the diagnosis of meningitis caused by Neisseria meningitidis, Streptococcus pneumoniae, and Haemophilus influenzae." Communicable Disease Surveillance and Response, from http://www.who.int/csr/resources/publications/meningitis/whocdscsredc997.pdf.
Porritt, R. J., J. L. Mercer, et al. (2000). "Detection and serogroup determination of Neisseria meningitidis in CSF by polymerase chain reaction (PCR)." Pathology **32**(1): 42-5.
Prevention, C. f. D. C. a. (1998). "Laboratory Methods for the Diagnosis of Meningitis Caused by Neisseria meningitidis, Streptococcus pneumonia e and Haemophilus influenzae." 1998, from http://www.cdc.gov/ncidod/DBMD/diseaseinfo/files/menigitis_manual.pdf.
Pumera, M., J. Wang, et al. (2001). "Gold Nanoparticle-Enhanced Microchip Capillary Electrophoresis." Anal. Chem. **73**(22): 5625-5628.
Qiagen (2000). Ni-NTA Spin Handbook, Qiagen.
Qin, W. J. and L. Y. L. Yung (2007). "Nanoparticle-based detection and quantification of DNA with single nucleotide polymorphism (SNP) discrimination selectivity." Nucl. Acids Res. **35**(17): e111-.
Quagliarello, V. J. and W. M. Scheld (1997). "Treatment of Bacterial Meningitis." N Engl J Med **336**(10): 708-716.
Rao, C. N. R., G. U. Kulkarni, et al. (2000). "Metal nanoparticles and their assemblies." Chemical Society Reviews **29**: 27 - 35.
Rast, J. P., M. K. Anderson, et al. (1997). "[α], [β], [γ], and [δ] T Cell Antigen Receptor Genes Arose Early in Vertebrate Phylogeny." Immunity **6**(1): 1-11.
Rast, J. P. and G. W. Litman (1994). "T-Cell Receptor Gene Homologs are Present in the Most Primitive Jawed Vertebrates." PNAS **91**(20): 9248-9252.
Reetz, M. T. and W. Helbig (1994). "Size-Selective Synthesis of Nanostructured Transition Metal Clusters." J. Am. Chem. Soc. **116**(16): 7401-7402.

Reetz, M. T., W. Helbig, et al. (1995). "Visualization of Surfactants on Nanostructured Palladium Clusters by a Combination of STM and High-Resolution TEM." Science **267**(5196): 367-369.

Reyerson, L. H. (1939). "Inorganic Colloid Chemistry. Vol. III. The Colloidal Salts. By H. B. Weiser." J. Phys. Chem. **43**(6): 818-819.

Rice, T. K. (1980). Method for the assay of classes of antigen-specific antibodies Patent storm. U. patents. US. **4236893**.

Rice, T. K. (1982). "Sandwich Immunoassay Using Piezoelectric Oscillator," U. S. Patent. **4,314,821**

Richardson, D. C., L. Louie, et al. (2003). "Evaluation of a rapid PCR assay for diagnosis of meningococcal meningitis." J Clin Microbiol **41**(8): 3851-3.

Rickert, J., A. Brecht, et al. (1997). "QCM Operation in Liquids: Constant Sensitivity during Formation of Extended Protein Multilayers by Affinity." Anal. Chem. **69**(7): 1441-1448.

Riordan, F. A. I., O. Marzouk, et al. (1995). "The changing presentations of meningococcal disease." European Journal of Pediatrics **154**(6): 472.

Rodahl, M., F. Hook, et al. (1997). "Simultaneous frequency and dissipation factor QCM measurements of biomolecular adsorption and cell adhesion." Faraday Discuss(107): 229-46.

Roederer, J. E. and G. J. Bastiaans (1983). "Microgravimetric immunoassay with piezoelectric crystals." Anal. Chem. **55**(14): 2333-2336.

Roederer, J. E. and G. J. Bastiaans (1988). Sensor having piezoelectric crystal for microgravimetric immunoassays U. Patent. **4735906**.

Romero, J. D. and I. M. Outschoorn (1994). "Current status of meningococcal group B vaccine candidates: capsular or noncapsular?" Clin. Microbiol. Rev. **7**(4): 559-575.

Rosenstein, N. E. and B. A. Perkins (2000). "Update on Haemophilus influenzae serotype b and meningococcal vaccines." Pediatr Clin North Am **47**(2): 337-52, vi.

Rosenstein, N. E., B. A. Perkins, et al. (2001). "Meningococcal disease." N Engl J Med **344**(18): 1378-88.

Rost, B. and C. Sander (1993). "Prediction of Protein Secondary Structure at Better than 70% Accuracy." Journal of Molecular Biology **232**(2): 584-599.

Roux, K. H., A. S. Greenberg, et al. (1998). "Structural analysis of the nurse shark (new) antigen receptor (NAR): Molecular convergence of NAR and unusual mammalian immunoglobulins." PNAS **95**(20): 11804-11809.

Roux, K. H., A. S. Greenberg, et al. (1998). "Structural analysis of the nurse shark (new) antigen receptor (NAR): molecular convergence of NAR and unusual mammalian immunoglobulins." Proc Natl Acad Sci U S A **95**(20): 11804-9.

Sakti, S. P., R. Lucklum, et al. (2001). "Disposable TSM-biosensor based on viscosity changes of the contacting medium." Biosensors and Bioelectronics **16**: 1101-1108.

Salvay, A. G., J. R. Grigera, et al. (2003). "The Role of Hydration on the Mechanism of Allosteric Regulation: In Situ Measurements of the Oxygen-Linked Kinetics of Water Binding to Hemoglobin." Biophys. J. **84**(1): 564-570.

Sargent, A. and O. A. Sadik (1998). "Pulsed electrochemical technique for monitoring antibody-antigen reactions at interfaces." Analytica Chimica Acta **376**(1): 125-131.

Sarikaya, M., C. Tamerler, et al. (2003). "Molecular biomimetics: nanotechnology through biology." Nat Mater **2**(9): 577-585.

Sarin, V. K., S. B. H. Kent, et al. (1981). "Quantitative monitoring of solid-phase peptide synthesis by the ninhydrin reaction." Analytical Biochemistry **117**(1): 147-157.

Sato, T., M. Endo, et al. (1995). "The influence of serum for spreading of tumor cells on synthetic glycolipid films." J Biomater Sci Polym Ed **7**(7): 587-99.

Sato, T., T. Serizawa, et al. (1998). "Quantitative measurements of the interaction between monosialoganglioside monolayers and wheat germ agglutinin (WGA) by a quartz-crystal microbalance." Biochimica et Biophysica Acta (BBA) - General Subjects **1380**(1): 82-92.

Sau, T. K., A. Pal, et al. (2001). "Size Controlled Synthesis of Gold Nanoparticles using Photochemically Prepared Seed Particles." Journal of Nanoparticle Research **3**(4): 257-261.

Sauerbrey, G. (1959). "Verwendung von Schwingquarzen zur Wägung dünner Schichten und zur Mikrowägung." Zeitschrift für Physik A Hadrons and Nuclei **155**(2): 206-222.

Savage, G. (1973). Glass and Glassware. London,, Octopus / Mayflower.

Schäferling, M., M. Riepl, et al. (2003). "Functionalized Self-Assembled Monolayers on Gold as Binding Matrices for the Screening of Antibody-Antigen Interactions." Microchimica Acta **142**(4): 193-203.

Schmid, G. (1992). "Large clusters and colloids. Metals in the embryonic state." Chem. Rev. **92**(8): 1709-1727.

Schmid, G., A. Lehnert, et al. (1991). "Ligand-Stabilized Bimetallic Colloids Identified by HRTEM and EDX." Angewandte Chemie International Edition in English **30**(7): 874-876.

Schnolzer, M., Alewood, P., Jones, A., Alewood, D., Kent, S.B. (1992). "In situ neutralization in Boc-chemistry solid phase peptide synthesis. Rapid, high yield assembly of difficult sequences. ." Int. J. Pept. Protein Res. **40**(180): 193.

Schnolzer, M. and S. B. Kent (1992). "Constructing proteins by dovetailing unprotected synthetic peptides: backbone-engineered HIV protease." Science **256**(5054): 221-225.

Schumacher, R., G. Borges, et al. (1985). "The quartz microbalance: A sensitive tool to probe surface reconstructions on gold electrodes in liquid." Surface Science **163**(1): L621-L626.

Schwartz, B., P. S. Moore, et al. (1989). "Global epidemiology of meningococcal disease." Clin Microbiol Rev **2**: 118-124.

Shana, Z. A. and F. Josse (1994). "Quartz Crystal Resonators as Sensors in Liquids Using the Acoustoelectric Effect." Anal. Chem. **66**(13): 1955-1964.

Shao, Y., Y. Jin, et al. (2004). "Synthesis of gold nanoplates by aspartate reduction of gold chloride." Chem Commun (Camb)(9): 1104-5.

Sharma, P., S. Brown, et al. (2006). "Nanoparticles for bioimaging." Advances in Colloid and Interface Science **123-126**: 471-485.

Shelley, E. J., D. Ryan, et al. (2002). "Dialkyl Sulfides: Novel Passivating Agents for Gold Nanoparticles." Langmuir **18**(5): 1791-1795.

Shen, G., S. Tan, et al. (2006). "Electrochemical and piezoelectric quartz crystal detection of antisperm antibody based on protected Au nanoparticles with a mixed monolayer for eliminating nonspecific binding." J Immunol Methods **313**(1-2): 11-9.

Shenton, W., S. A. Davis, et al. (1999). "Directed Self-Assembly of Nanoparticles into Macroscopic Materials Using Antibody-Antigen Recognition." Advanced Materials **11**(6): 449-452.

Shi Kam, N. W., M. O'Connell, et al. (2005). "Carbon nanotubes as multifunctional biological transporters and near-infrared agents for selective cancer cell destruction." Proceedings of the National Academy of Sciences **102**(33): 11600-11605.

Shons, A., F. Dorman, et al. (1972). "An immunospecific microbalance." Journal of Biomedical Materials Research **6**(6): 565-570.

Sibbald, M. S., G. Chumanov, et al. (1996). "Reduction of Cytochrome c by Halide-Modified, Laser-Ablated Silver Colloids." J. Phys. Chem. **100**(11): 4672-4678.

Sidhaye, D. S., S. Kashyap, et al. (2005). "Gold Nanoparticle Networks with Photoresponsive Interparticle Spacings." Langmuir **21**(17): 7979-7984.

Singh, J. and A. C. Arrieta (2004). "Management of meningococcemia." Indian J Pediatr **71**(10): 909-13.

Slocik, J. M., J. T. Moore, et al. (2002). "Monoclonal Antibody Recognition of Histidine-Rich Peptide Encapsulated Nanoclusters." Nano Letters **2**(3): 169-173.

Smetana, A. B., K. J. Klabunde, et al. (2005). "Synthesis of spherical silver nanoparticles by digestive ripening, stabilization with various agents, and their 3-D and 2-D superlattice formation." Journal of Colloid and Interface Science **284**(2): 521-526.

Sokoll, L. J. and D. W. Chan (1999). "Clinical analyzers. Immunoassays." Anal Chem **71**(12): 356R-362R.

Song, Y. and R. W. Murray (2002). "Dynamics and Extent of Ligand Exchange Depend on Electronic Charge of Metal Nanoparticles." J. Am. Chem. Soc. **124**(24): 7096-7102.

Spinelli, S., L. Frenken, et al. (1996). "The crystal structure of a llama heavy chain variable domain." Nat Struct Mol Biol **3**(9): 752-757.

Spinosa, M. R., C. Prodiga, et al. (2007). "Neisseria meningitidis capsule is important for intracellular survival in human cells." Infect. Immun.: IAI.01945-06.

Spinosa, M. R., C. Progida, et al. (2007). "The Neisseria meningitidis Capsule Is Important for Intracellular Survival in Human Cells." Infect. Immun. **75**(7): 3594-3603.

Stephens, D. S. (1999). "Uncloaking the meningococcus: dynamics of carriage and disease." Lancet **353**(9157): 941-2.

Stephens, D. S., P. A. Spellman, et al. (1993). "Effect of the (alpha 2-->8)-linked polysialic acid capsule on adherence of Neisseria meningitidis to human mucosal cells." J Infect Dis **167**(2): 475-9.

Stephens, S. D., K. S. Gudlavalleti, et al. (2006). Neisseria meningitidis serogroup a capsular polysaccharide acetyltransferase, methods and compositions Free Patents Online. U. S. Patent. United States. **424/249.1**.

Stockbridge, C. D. (1965). "Effects of gas pressure on quartz crystal microbalances,". Vacuum Microbalance Techniques. Proceedings of the Princeton Conference, Princeton.

Storhoff, J. J., R. Elghanian, et al. (1998). "One-Pot Colorimetric Differentiation of Polynucleotides with Single Base Imperfections Using Gold Nanoparticle Probes." J. Am. Chem. Soc. **120**(9): 1959-1964.

Storhoff, J. J., A. A. Lazarides, et al. (2000). "What Controls the Optical Properties of DNA-Linked Gold Nanoparticle Assemblies?" J. Am. Chem. Soc. **122**(19): 4640-4650.

Storhoff, J. J., R. C. Mucic, et al. (1997). "Strategies for Organizing Nanoparticles into Aggregate Structures and Functional Materials." Journal of Cluster Science **8**(2): 179-216.

Su, K. H., Q. H. Wei, et al. (2003). "Interparticle Coupling Effects on Plasmon Resonances of Nanogold Particles." Nano Lett. **3**(8): 1087-1090.

Su, X.-L. and Y. Li (2004). "A self-assembled monolayer-based piezoelectric immunosensor for rapid detection of Escherichia coli O157:H7." Biosensors and Bioelectronics **19**(6): 563-574.

Su, X., S. Low, et al. (2001). "Piezoelectric quartz crystal based veterinary diagnosis for Salmonella enteritidis infection in chicken and egg." Sensors and Actuators B: Chemical **75**: 29-35.

Suleiman, A. A. and G. G. Guilbault (1991). "Piezoelectric (PZ) Immunosensors and Their Applications." Analytical Letters **24**(8): 1283 - 1292.

Suleiman, A. A. and G. G. Guilbault (1994). "Recent developments in piezoelectric immunosensors. A review." Analyst **119**(11): 2279-82.

Sun, Y. and Y. Xia (2002). "Shape-controlled synthesis of gold and silver nanoparticles." Science **298**(5601): 2176-9.

Surana, N. K., S. Grass, et al. (2004). "Evidence for conservation of architecture and physical properties of Omp85-like proteins throughout evolution." Proc Natl Acad Sci U S A **101**(40): 14497-502.

Swartley, J. S., A. A. Marfin, et al. (1997). "Capsule switching of Neisseria meningitidis." Proc Natl Acad Sci U S A **94**(1): 271-6.

Taha, M. K., J. M. Alonso, et al. (2005). "Interlaboratory comparison of PCR-based identification and genogrouping of Neisseria meningitidis." J Clin Microbiol **43**(1): 144-9.

Takahashi, Y., A. L. Sandberg, et al. (1997). "A specific cell surface antigen of Streptococcus gordonii is associated with bacterial hemagglutination and adhesion to alpha2-3-linked sialic acid-containing receptors." Infect Immun **65**(12): 5042-51.

Takizawa, T., K. Suzuki, et al. (1998). "Correlative Microscopy Using FluoroNanogold on Ultrathin Cryosections: Proof of Principle." J. Histochem. Cytochem. **46**(10): 1097-1102.

Tan, Y., X. Dai, et al. (2003). "Preparation of gold, platinum, palladium and silver nanoparticles by the reduction of their salts with a weak reductant–potassium bitartrate." J. Mater. Chem. **13**: 1069 - 1075.

Tan, Y., Y. Li, et al. (2002). "Fabrication of Gold Nanoparticles Using a Trithiol (Thiocyanuric Acid) as the Capping Agent." Langmuir **18**(8): 3392-3395.

Tao, L., T. Jian, et al. (2003). "Surface modification of nanogold particles in DNA detection with quartz crystal microbalance." Chinese Science Bulletin **48**(9): 873–875.

Tarentino, A. L., A. W. Phelan, et al. (1993). "2-Iminothiolane: a reagent for the introduction of sulphydryl groups into oligosaccharides derived from asparagine-linked glycans." Glycobiology **3**(3): 279-285.

Taton, T. A., C. A. Mirkin, et al. (2000). "Scanometric DNA Array Detection with Nanoparticle Probes." Science **289**(5485): 1757-1760.

Taylor, C. E., P. W. Stashak, et al. (1983). "Activation of antigen-specific suppressor T cells by B cells from mice immunized with type III pneumococcal polysaccharide." J. Exp. Med. **158**(3): 703-717.

Templeton, A. C., W. P. Wuelfing, et al. (2000). "Monolayer-Protected Cluster Molecules." Acc. Chem. Res. **33**(1): 27-36.

Thanh, N. T. K. and Z. Rosenzweig (2002). "Development of an Aggregation-Based Immunoassay for Anti-Protein A Using Gold Nanoparticles." Anal. Chem. **74**(7): 1624-1628.

Theron, S., S. Andronikou, et al. (2006). "Localized basal meningeal enhancement in tuberculous meningitis." Pediatr Radiol **36**(11): 1182-5.

Thompson, M., C. L. Arthur, et al. (1986). "Liquid-phase piezoelectric and acoustic transmission studies of interfacial immunochemistry." Anal. Chem. **58**(6): 1206-1209.

Thompson, R. H. and L. W. Swanson (1998). "Organization of inputs to the dorsomedial nucleus of the hypothalamus: a reexamination with Fluorogold and PHAL in the rat." Brain Res Brain Res Rev **27**(2): 89-118.

Tian, L., W. Wei, et al. (2004). "Kinetic studies of the interaction between antitumor antibiotics and DNA using quartz crystal microbalance." Clinical Biochemistry **37**(2): 120-127.

Tirelli, N. (2006). "(Bio)Responsive nanoparticles." Current Opinion in Colloid & Interface Science **11**(4): 210-216.

Todar, K. (2006). "Meningococcal Meningitis." Ken Todar's Microbial World, from http://www.bact.wisc.edu/themicrobialworld/homepage.html.

Tone, T. (2005). Neisseria Trevisan 1885, 105 AL. Bergey's Manual® of Systematic Bacteriology**:** 777-798.

Toshima, N. and T. Yonezawab (1998). "Bimetallic nanoparticlesÈnovel materials for chemical and physical applications." New Journal of Chemistry **22**(11): 1179-1201.

Tripathi, V. S., V. B. Kandimalla, et al. (2006). "Preparation of ormosil and its applications in the immobilizing biomolecules " Sensors and Actuators B: Chemical **114** (2): 1071-1082.

Tsai, K.-L. and J. L. Dye (1991). "Nanoscale Metal Particles by Homogeneous Reduction with Alkalides or Electrides." J. Am. Chem. Soc. **113**: 1650-1652.

Tsai, W.-C. and I. C. Lin (2005). "Development of a piezoelectric immunosensor for the detection of alpha-fetoprotein." Sensors and Actuators B: Chemical **106**(1): 455-460.

Tsang, R. S. W., D. K. S. Law, et al. (2001). "Detection of the lst gene in different serogroups and LOS immunotypes of Neisseria meningitidis." FEMS Microbiology Letters **199**(2): 203-206.

Turkevich, J., P. Stevenson, et al. (1951). "A study of the nucleation and growth processes in the synthesis of colloidal gold." Discussions of the Faraday Society **11**: 55 - 75.

Turkevich, J., P. C. Stevenson, et al. (1951). "A study of the nucleation and growth processes in the synthesis of colloidal gold." Discussions of the Faraday Society **11**: 55 - 75.

Turner, A. P. F. (2000). "BIOCHEMISTRY: Biosensors-Sense and Sensitivity." Science **290**(5495): 1315-1317.

Tzhayik, O., P. Sawant, et al. (2002). "Xanthate Capping of Silver, Copper, and Gold Colloids." Langmuir **18**(8): 3364-3369.

Underwood, S. and P. Mulvaney (1994). "Effect of the Solution Refractive Index on the Color of Gold Colloids." Langmuir **10**(10): 3427-3430.

Unen, D.-J. v., J. F. J. Engbersen, et al. (2001). "Sol-gel immobilization of serine proteases for application in organic solvents." Biotechnology and Bioengineering **75**(2): 154-158.

Urbakh, M. and L. Daikhin (1994). "Influence of the Surface Morphology on the Quartz Crystal Microbalance Response in a Fluid." Langmuir **10**(8): 2836-2841.

Uttenthaler, E., C. Kolinger, et al. (1998). "Quartz crystal biosensor for detection of the African Swine Fever disease." Analytica Chimica Acta **362**(1): 91-100.

Uttenthaler, E., M. Schraml, et al. (2001). "Ultrasensitive quartz crystal microbalance sensors for detection of M13-Phages in liquids." Biosensors and Bioelectronics **16**: 735-743.

van Deuren, M., P. Brandtzaeg, et al. (2000). "Update on Meningococcal Disease with Emphasis on Pathogenesis and Clinical Management." Clin. Microbiol. Rev. **13**(1): 144-166.

van Deuren, M., B. J. van Dijke, et al. (1993). "Rapid diagnosis of acute meningococcal infections by needle aspiration or biopsy of skin lesions." Bmj **306**(6887): 1229-32.

Vazquez, J. A. (2007). "Resistance testing of meningococci: the recommendations of the European Monitoring Group on Meningococci." FEMS Microbiology Reviews **31**(1): 97-100.

Velev, O. D. and E. W. Kaler (1999). "In Situ Assembly of Colloidal Particles into Miniaturized Biosensors." Langmuir **15**(11): 3693-3698.

Vidal, J.-C., E. Garcia-Ruiz, et al. (2003). "Recent Advances in Electropolymerized Conducting Polymers in Amperometric Biosensors." Microchimica Acta **143**(2): 93-111.

Vipond, C., J. Suker, et al. (2006). "Proteomic analysis of a meningococcal outer membrane vesicle vaccine prepared from the group B strain NZ98/254." Proteomics **6**(11): 3400-3413.

Virji, M., K. Makepeace, et al. (1995). "Opc- and pilus-dependent interactions of meningococci with human endothelial cells: molecular mechanisms and modulation by surface polysaccharides." Molecular Microbiology **18**(4): 741-754.

Vogel, G. (2003). "Infectious disease. Shortage of meningitis vaccine forces triage in Burkina Faso." Science **299**(5612): 1499-501.
Vogel, U., S. Hammerschmidt, et al. (1996). "Sialic acids of both the capsule and the sialylated lipooligosaccharide of Neisseria meningitis serogroup B are prerequisites for virulence of meningococci in the infant rat." Med Microbiol Immunol **185**(2): 81-7.
Voros, J. (2004). "The Density and Refractive Index of Adsorbing Protein Layers." Biophys. J. **87**(1): 553-561.
Voulhoux, R., M. P. Bos, et al. (2003). "Role of a highly conserved bacterial protein in outer membrane protein assembly." Science **299**(5604): 262-5.
Voulhoux, R. and J. Tommassen (2004). "Omp85, an evolutionarily conserved bacterial protein involved in outer-membrane-protein assembly." Research in Microbiology **155**(3): 129-135.
Walter, G., K. Bussow, et al. (2000). "Protein arrays for gene expression and molecular interaction screening." Current Opinion in Microbiology **3**(3): 298-302.
Wang, A., C. J. Wu, et al. (2006). "Gold Nanoparticle-Assisted Protein Enrichment and Electroelution for Biological Samples Containing Low Protein Concentration-A Prelude of Gel Electrophoresis." J. Proteome Res. **5**(6): 1488-1492.
Wang, C., H. Wang, et al. (2002). "A piezoelectric immunoassay based on self-assembled monolayers of cystamine and polystyrene sulfonate for determination of Schistosoma japonicum antibodies." Analytical and Bioanalytical Chemistry **373**(8): 803-809.
Wang, H., D. Li, et al. (2004). "A reusable piezo-immunosensor with amplified sensitivity for ceruloplasmin based on plasma-polymerized film." Talanta **62**: 199-206.
Wang, H., J. Li, et al. (2004). "Novel immunoassay for Toxoplasma gondii-specific immunoglobulin G using a silica nanoparticle-based biomolecular immobilization method." Analytica Chimica Acta **501**: 37-43.
Wang, J., M. Jiang, et al. (1998). "Dendritic nucleic acid probes for DNA biosensors." Journal of the American Chemical Society **120**(32): 8281-8282.
Wang, J., K. G. Neoh, et al. (2001). "Preparation of Nanosized Metallic Particles in Polyaniline." Journal of Colloid and Interface Science **239**(1): 78-86.
Wang, J., D. Xu, et al. (2001). "Metal Nanoparticle-Based Electrochemical Stripping Potentiometric Detection of DNA Hybridization." Anal. Chem. **73**(22): 5576-5581.
Ward, M. D. and E. J. Delawski (1991). "Radial mass sensitivity of the quartz crystal microbalance in liquid media." Anal. Chem. **63**(9): 886-890.
Wasier, A. P., L. Chevret, et al. (2005). "Pneumococcal meningitis in a pediatric intensive care unit: prognostic factors in a series of 49 children." Pediatr Crit Care Med **6**(5): 568-72.
Weissbuch, I., L. Addadi, et al. (1991). "Molecular Recognition at Crystal Interfaces." Science **253**(5020): 637-645.
WHO (1997). "Response to epidemic meningitis in Africa, 1997." Wkly Epidemiol Rec **72**(42): 313-8.
WHO (1998). "Control of epidemic meningococcal disease. WHO practical

guidelines. 2nd edition." Emerging and other Communicable Diseases, Surveillance and Control **2**(WHO/EMC/BAC/98.3): 1-84.
WHO (2005). "Weekly epidemiological record -Relevé épidémiologique hebdomadaire." Weekly Epidemiological Record **80**(20): 177-180.
Williams, A. F. and A. N. Barclay (1988). "The Immunoglobulin Superfamily x2014;Domains for Cell Surface Recognition." Annual Review of Immunology **6**(1): 381-405.
Winter, G., A. D. Griffiths, et al. (1994). "Making Antibodies by Phage Display Technology." Annual Review of Immunology **12**(1): 433-455.
Wolfe, C. L., J. A. Warrington, et al. (2005). "A Three-dimensional Working Model of the Multienzyme Complex of Aminoacyl-tRNA Synthetases Based on Electron Microscopic Placements of tRNA and Proteins." J. Biol. Chem. **280**(46): 38870-38878.
Wu, S. M., X. Zhao, et al. (2006). "Quantum-dot-labeled DNA probes for fluorescence in situ hybridization (FISH) in the microorganism Escherichia coli." Chemphyschem **7**(5): 1062-7.
Wu, T. Z., C. C. Su, et al. (2005). "Piezoelectric immunochip for the detection of dengue fever in viremia phase." Biosens Bioelectron **21**(5): 689-95.
Xiao, Y., H.-X. Ju, et al. (1999). "Hydrogen peroxide sensor based on horseradish peroxidase-labeled Au colloids immobilized on gold electrode surface by cysteamine monolayer." Analytica Chimica Acta **391**(1): 73-82.
Xie, H., A. G. Tkachenko, et al. (2003). "Critical Flocculation Concentrations, Binding Isotherms, and Ligand Exchange Properties of Peptide-Modified Gold Nanoparticles Studied by UV-Visible, Fluorescence, and Time-Correlated Single Photon Counting Spectroscopies." Anal. Chem. **75**(21): 5797-5805.
Yáñez-Sedeño, P. and J. M. Pingarrón (2005). "Gold nanoparticle-based electrochemical biosensors." Analytical and Bioanalytical Chemistry **382**(4): 884-886.
Yang, M. and M. Thompson (1993). "Surface morphology and the response of the thickness-shear mode acoustic wave sensor in liquids." Langmuir **9**(8): 1990-1994.
Yang, T.-M., C.-H. Lu, et al. (2005). "Cninical characteristics of adult *Escherichia coli* meningitis." Japanese journal of infectious diseases **58**(3): 168-170.
Yee, C. K., R. Jordan, et al. (1999). "Novel One-Phase Synthesis of Thiol-Functionalized Gold, Palladium, and Iridium Nanoparticles Using Superhydride." Langmuir **15**(10): 3486-3491.
Yu, C. J., C. L. Su, et al. (2006). "Separation of Acidic and Basic Proteins by Nanoparticle-Filled Capillary Electrophoresis." Anal. Chem. **78**(23): 8004-8010.
Zhang, B., Q. Mao, et al. (2004). "A novel piezoelectric quartz micro-array immunosensor based on self-assembled monolayer for determination of human chorionic gonadotropin." Biosensors and Bioelectronics **19**: 711-720.
Zhang, C., G. Feng, et al. (1997). "Development of a new kind of dual modulated QCM biosensor." Biosensors and Bioelectronics **12**(12): 1219-1225.
Zharov, V. P., V. Galitovsky, et al. (2003). "Photothermal detection of local thermal effects during selective nanophotothermolysis." Applied Physics Letters **83**(24): 4897-4899.

Zhi, Z. and D. T. Haynie (2004). "Direct Evidence of Controlled Structure Reorganization in a Nanoorganized Polypeptide Multilayer Thin Film." Macromolecules **37**(23): 8668-8675.

Zhu, H., M. Bilgin, et al. (2001). "Global Analysis of Protein Activities Using Proteome Chips." Science **293**(5537): 2101-2105.

Zollinger, W. and J. Boslego (1997). Immunologic methods for diagnosis of infections by gram-negative cocci. Manual of clinical laboratory immunology. C. d. M. E. Rose NR, Folds JD, Lane HC, Nakamura RM. Washington DC, ASM Press**:** 473-83.

Zsigmondy, R. A. (1926). Properties of colloids.

Appendix 1: List of Gram negative bacteria used for cross-ractive studies and the disease caused by the respective bacteria

Bacteria		Pathogenesis
Neisseria meningitidis		Meningitis
Neisseria meningitidis MC58		Meningitis
Neisseria meningitidis serogroup A strain		Meningitis
Neisseria gonorrhoeae		Gonorrhoea
Chromobacterium violaceum		Human infection caused by *Chromobacterium violaceum* is rare, but when it occurs it is associated with a high mortality rate. Human infections are reported from several continents, particularly Australia, South America, and Southeast Asia where the typical disease presentation includes cutaneous inflammation, sepsis, liver abscesses and ocular infections. Currently there are no vaccines.
Bordetella pertussis		Causes whooping cough
Acinetobacter sp. ADP1		can cause hospital acquired infections
Escherichia coli		one of the foremost causes of food poisoning
Pseudomonas fluorescens		Commensal bacteria have emerged as an important disease factor in human Crohn's disease (CD) and murine inflammatory bowel disease (IBD) models. Many *pseudomonas* live in a commensal relationship with plants. *P. fluorescens* Pf-5 provides a framework for future studies to understand the biological basis of biocontrol as an alternative to the use of chemical pesticides for control of insects of public health importance.
Pseudomonas aeruginosa		is a leading cause of opportunistic infection among persons with compromised immune systems

Salmonella enterica subsp. enterica serovar Typhi str. CT18		causes typhoid fever and is a leading cause of human gastroenteritis and is used as a mouse model of human typhoid fever
Salmonella enterica subsp. enterica serovar Paratyphi A str.		is a cause of Enteric fever
Vibrio alginolyticus		V. alginolyticus is one of many Gram-negative bacteria of marine origin with worldwide distribution, having been isolated from Europe, Australia, Japan,Hawaii, and North America. Recent exposure to seawater usually antedates the isolation of V. alginolyticus from humans. *V alginolyticus* is a halophilic *Vibrio* first recognized as being pathogenic in humans in 1973. Wound infections account for 71% of *V alginolyticus* infections. Ear infections are also seen with this organism. Gastroenteritis was thought to be a rare presentation of *V alginolyticus* infection, but it accounted for 12% of infections in one series. Other clinical syndromes reported in association with *V alginolyticus* infection include chronic diarrhoea in a patient with AIDS, conjunctivitis, and post-traumatic intracranial infection. Infections of the ear (otitis media and otitis externa) are another important source of isolates of V. alginolyticus. V. alginolyticus has rarely been recovered from sputum and an eye socket. Ocular infection due to this organism is extremely rare.
Vibrio vulnificus		Causes potentially fatal food poisoning
Vibrio cholerae		Causes Cholera
Vibrio parahaemolyticus		Causes food-borne gastroenteritis
Vibrio sp. Ex25		Causes Cholera
Shigella dysenteriae		The illness caused by *Shigella* (shigellosis- bacillary dysentery) accounts for less than 10% of the reported outbreaks of food borne illness in this country. *Shigella*

		rarely occurs in animals; principally a disease of humans except other primates such as monkeys and chimpanzees. The organism is frequently found in water polluted with human feces.
Haemophilus influenzae		Naturally-acquired disease caused by *Haemophilus influenzae* seems to occur in humans only. It was mistakenly thought to be the cause of the disease influenza, and it was named accordingly. *Haemophilus influenzae* is highly adapted to its human host. It is present in the nasopharynx of approximately 75 percent of healthy children and adults. It is rarely encountered in the oral cavity and it has not been detected in any other animal species. In infants and young children (under 5 years of age), *Haemophilus influenzae* type b causes bacteraemia and acute bacterial meningitis Occasionally, it causes epiglottitis (obstructive laryngitis), cellulitis, osteomyelitis, and joint infections. Nontypable *H. influenzae* causes ear infections (otitis media) and sinusitis in children. Initially *H. influenzae* invades the nasopharyngeal mucosa before spreading to the lower respiratory tract where the organism invades and destroys the mucous membranes producing bronchiolitis, peribronchiolitis, and/or interstitial lesions and is associated with respiratory tract infections (pneumonia).
Legionella pneumophila		Causes Legionnaires' disease
Pasteurella multocida		is a pathogenic bacteria causing many serious diseases in humans and animals. This bacterium is the causative agent of fowl cholera in chickens and turkeys, hemorrhagic septicaemia in cattle, atrophic rhinitis in pigs, and infections in humans from dog and cat bites. Patients tend to exhibit swelling, cellulitis and bloody

		drainage at the wound site. Infection may move to nearby joints where it can cause swelling and arthritis.
Brucella abortus		causes Brucellosis (spontaneous abortion in cattle and undulant fever in humans). Brucellosis is passed on to humans by drinking infected unpasteurised milk or from contact with discharges from cattle or goats that abort their foetus. It is unlikely that this disease would be spread from person to person. Symptoms include intermittent or irregular fever of variable duration, headache, weakness, profuse sweating, chills, weight loss and generalized aching. Antibiotic treatment will cure the condition.

Appendix 2: Buffers and Reagents

10X PAGE Running Buffer. Tris Base (3% w/v), Glycine (14.4% w/v) and SDS (1% w/v) was dissolved in dH_2O, pH 8.3. Dilution of 1X was used for electrophoresis.

Acrylamide/bisacrylamide solution: A 40% (w/v) solution was prepared containing 38.67% (w/v) ultra pure acrylamide and 1.33% (w/v) bisacrylamide (Bio-Rad, USA)

Ammonium Persulfate (10%). Ammonium Persulfate (100 mg) was dissolved in 1 mL of dH_2O and filter sterilised through a 0.22 µM syringe filter. The solution was stored at 4°C wrapped in foil for up to 3 months.

Ampicillin. Ampicillin (500 mg/vial) was dissolved in 5 mL of sterile water, giving a stock solution of 100 mg/mL. One mL aliquots were stored frozen at –20°C. The ampicillin was added to media or other solution at the final concentration of 100 µg/mL.

Blocking Solution. Skim milk (5%) was dissolved in TBS.

Coomassie Destaining Reagent. Ethanol (10% v/v) and Acetic Acid (10% v/v) was diluted in dH_2O.

Coomassie Stain. Coomassie Brilliant Blue R-250 (0.05% w/v) was dissolved in methanol (250 mL) and Acetic Acid (50 mL). After the Coomassie Brilliant Blue had dissolved, the solution was diluted to 500 mL with dH_2O (Final concentration 50% Methanol, 10% Acetic Acid).

ELISA Substrate Solution. Equal volumes of reagent A and reagents B of TMB substrate was mixed immediately before use.

Elution buffer (50 mM Tris-HCl, 150 mM NaCl and 0.1 mM EDTA; pH 7.5)

Elution Buffer pH: 8.0. 50 mM Na_2HPO_4 pH 7.8, 300 mM NaCl, 250 mM Imidazole, 0.05 % Tween 20 / 0.2% Triton X-100. Adjust pH to 8.0 using NaOH.

Extraction / Solubilization buffer 50 mM Tris-HCl pH 7.5, 8 M urea, 1 mM DTT, 2 mM reduced Glutathione, 0.2 mM oxidized Glutathione, 1 mM PMSF* *PMSF is instable in aqeous solutions and added to the buffer at he point described in the protocol.

Folding buffer 50mM HEPES pH7.5, 0.2M NaCl, 1mM DTT, 1M NDSB256

Horse Blood Agar Trypticase Soya Broth (3% w/v) and Bacteriological Agar (1% w/v) were dissolved in deionised H_2O and autoclaved at standard conditions. After the agar had cooled, Horse blood (5% w/v) was added to the agar and the medium poured into petri dishes.

Isoproply-β-D thiogalactopyranoside (IPTG) (0.1 M) Stock Solution. IPTG (1.2 g) was dissolved in 50 mL of sterile water, filter sterilised and stored at 4°C

Kanamycin. Kanamycin was made up as a stock solution of 50 mg/mL in sterile water and stored in 1 mL aliquots at -20°C. The working concentration of Kanamycin was 50 µg/mL.

Luria Bertoni Broth Tryptone (1% w/v), Yeast Extract (0.5% w/v), and NaCl (0.5% w/v) was dissolved in deionised H_2O and autoclaved at standard conditions.

Lysis Buffer (for enzymatic lysis) 20 mM Tris-HCl pH 8.0, 200 mM NaCl, 5mM DTT, 5% Glycerol, 0.35mg/ml lysozyme, 1% Triton X-100, 1mM PMSF (Add just before doing experiment)

Lysis buffer (for sonication) 50 mM Tris-HCl pH 7.5, 200 mM NaCl, 5 mM DTT and 1mM PMSF

Modified SDS-PAGE sample buffer for gold nanoparticle analysis. 0.6 mL of 0.1M Tris-HCL (pH 6.8), 5.0 mL 50% glycerol, 2.0 mL 10% SDS, 1.0 mL 1% bromophenol blue and 1.4 mL H_20

PBS. 0.01 M phosphate buffer, 0.0027 M potassium chloride and 0.137 M sodium chloride, pH 7.4.

PBS/T. Phosphate buffer (0.01 M), 0.0027 M potassium chloride and 0.137 M sodium chloride, pH 7.4, autoclaved at standard conditions. Tween 20® (0.05% v/v) was then added.

Renaturation buffer 2 mM reduced glutathione and 0.2 mM oxidized glutathione

SDS-PAGE Sample Buffer. Tris-HCl (125 mM, pH 6.8), SDS (2% w/v), β-mercaptoethanol (5% w/v), Bromophenol blue (0.02% w/v) and glycerol (25% v/v) in dH_2O.

Solubilisation/Extraction buffer (50 mM Tris-HCl pH 7.5 containing 8 M urea, 1 mM DTT, 2 mM reduced Glutathione, 0.2 mM oxidised Glutathione, 1 mM PMSF)

Solubilization buffer 50mM HEPES-NaOH pH7.5, 6M guanidine HCl, 25mM DTT

Stock solutions 1 mg/ml DNase and in water, 100 mM PMSF (phenylmethylsulfonyl fluoride) in isopropanol, 1M $MgCl_2$, 1% Triton X-100, 5 mM sodium carbonate buffer pH 9.4, 10 mM sodium phosphate buffer pH 7.4, 1% bovine serum albumin (BSA), 0.1% sodium azide

TBS. Tris Base (10 mM) and NaCl (500 mM) was dissolved in deionised H_2O, pH 7.4, then autoclaved at standard conditions.

TBS/Tween. Tween 20 (0.05% (v/v)) was added to TBS.

Wash buffer (pH: 8.0) 50 mM Na_2HPO_4 pH 7.8, 300 mM NaCl, 20 mM Imidazole, 0.05 % Tween 20 / 0.2% Triton X-100

SDS-PAGE Resolving gel (12.5%).

Reagents	Volume
Water	4.22 mL
1.5 M Tris (pH 8.8)	2.5 mL
10% SDS	0.1 mL
Bis-Acrylamide (40%)	3.135 mL
10% Ammonium persulfate	0.05 mL
TEMED	0.01 mL
Total volume	10 mL

SDS-PAGE Stacking gel (4%).

Reagent	Volume
Water	3.580 mL
0.5 M Tris (pH 6.8)	1 mL
10% SDS	0.04 mL
Bis-Acrylamide (40%)	0.375 mL
10% Ammonium persulfate	0.01 mL
TEMED	0.0005 mL
Total	5 mL

SDS-PAGE loading buffer was added to samples to be analysed in a 4:1 sample to buffer ratio. Prepared samples were then heated to 100°C for 10 min in a heat block. SDS-PAGE gel wells were loaded with 20 µL of sample using a syringe. SDS-PAGE was performed at 80 V for 30 min then 180 V for 50 min.